STUDIES ON THE SULFONATED CARBON NANOTUBES CATALYST AND MEMBRANE REACTOR FOR BIODIESEL PRODUCTION

SHUIT SIEW HOONG

UNIVERSITI SAINS MALAYSIA

2015

STUDIES ON THE SULFONATED CARBON NANOTUBES CATALYST AND MEMBRANE REACTOR FOR BIODIESEL PRODUCTION

by

SHUIT SIEW HOONG

Thesis submitted in fulfillment of the requirements for the degree of Doctor of Philosophy

2015

ACKNOWLEDGEMENT

First of all, I would like to express my deepest and most heart-felt gratitude to my beloved parents and siblings for their endless love and encouragement throughout my entire study.

I would like to give my sincere thanks to my dedicated supervisor Assoc. Prof. Dr. Tan Soon Huat and co-supervisor Prof. Dr. Lee Keat Teong for their excellent supervision and enormous effort spent in guiding and helping me throughout my studies. My accomplishment of this research project is a direct reflection of high quality supervision works from both of my supervisors.

Next, I would like to express my gratitude to the administrative staff of School of Chemical Engineering, Universiti Sains Malaysia especially our respected dean, Prof. Dr. Azlina Harun @ Kamaruddin, deputy deans, office staffs and technicians for giving me full support throughout my research work.

In addition, I would to show my deepest gratitude and thanks to all my beloved friends and colleagues: Man Kee, Wei Ming, Zhi Hua, Choon Ming, Peck Loo, Qi Hwa, Hui Yen, Eng Yew, Jibrail, Gaik Tin, Lee Muei, Stephanie, Swee Pin, Jing Yao, Huei Peng, Hui Xin, Qian Wen, Sim Siong, Susan, Chuan Chun, Dinie and Muaz for their unparalleled help, kindness and moral support towards me. Last but not least, the financial support given by Ministry of Higher Education Malaysia (MyPhD fellowship) is gratefully acknowledged.

SHUIT SIEW HOONG

March 2015

TABLE OF CONTENTS

LIST OF TABLES

LIST OF FIGURES

LIST OF ABBREVIATIONS

ASTM	American Society for Testing and Materials
ATR	Attenuated total reflectance
BET	Brunauer-Emmer-Teller
BJH	Barrett-Joyner-Halenda
$(CH_3\text{-}CO)_2O$	Acetic anhydride
CNTs	Carbon nanotubes
COOH	Carboxyl
DABA	3,5-diaminobenzoic acid
DI	Deionised
FAME	Fatty acid methyl ester
6FDA	4,4’-(hexafluroisopropylidene) diphthalic anhydride
6FDA-NDA/DABA	Copoly(1,5-naphthalene/3,5-benzoicacid-2,2’-bis(3,4-dicarboxyphenyl) hexafluoropropanedimide
FFA	Free fatty acid
FID	Flamed ionized detector
FTIR	Fourier transform infrared
GC	Gas Chromatography
HNO_3	Nitric acid
H_2SO_4	Sulfuric acid
IS	Internal standard
MWCNTs	Multi-walled carbon nanotubes

s-MWCNTs	Sulfonated multi-walled carbon nanotubes
MWCNTs-COOH	Purified and treated multi-walled carbon nanotubes
NDA	1,5-naphthalene diamine
NH_3-TPD	Ammonia-temperature programmed desorption
NaSS	Sodium 4-styrenesulfonate
$(NH_4)_2S_2O_8$	Ammonium persulphate
$(NH_4)_2SO_4$	Ammonium sulfate
NMP	N-methyl-pyrrolidone
PFAD	Palm fatty acid distillate
PID	Proportional-Integral-Derivative
SEM	Scanning electron microscopy
SO_3H	Sulfonic group
TCD	Thermal conductivity detector
TEM	Transmission electron microscopy
TGA	Thermogravimetric analysis
THF	Tetrahydrofuran
UV-Vis	Ultraviolet-visible spectroscopy
XRD	X-ray diffraction analysis

LIST OF SYMBOLS

A_1	Pre-exponential or frequency factors for the forward reaction rate constant
A_e	Pre-exponential or frequency factors for the equilibrium constant
θ	Molar ratio of methanol to PFAD
C_{IS}	Concentration of IS (g/L)
DF	Dilution factor
E_1	Activation energy of the forward reaction
E_e	Activation energy for the equilibrium reaction
k_1	Forward reaction rate constant
k_2	Backward reaction rate constant
k_e	Equilibrium rate constant
R	Ideal constant
R_f	Ratio of peak area of individual methyl ester to peak area of IS in standard reference
R_s	Ratio of peak area of individual methyl ester to peak area of IS in the sample
T	Reaction temperature
V	Volume of oil (mL)
x	Conversion of PFAD
x_e	PFAD conversion at equilibrium

KAJIAN DALAM SULFONAT TIUB-NANO KARBON PEMANGKIN DAN REAKTOR MEMBRAN UNTUK PENGHASILAN BIODIESEL

ABSTRAK

Tumpuan kajian ini ialah penghasilan biodiesel dengan menggunakan sulfonat tiub-nano karbon dinding berlapis (s-MWCNTs) sebagai pemangkin dan reaktor membran jenis pervaporasi sebagai teknologi pertukaran. Pada mulanya, s-MWCNTs disintesis dan diguna untuk menukar sulingan asid lemak sawit (PFAD) kepada biodiesel. Hasilan biodiesel yang dicapai oleh s-MWCNTs yang disediakan melalui rawatan haba dengan asid sulfurik pekat, in-situ pempolimeran asetik anhydride dan asid sulfurik, penguraian haba ammonium sulfat ($(NH_4)_2SO_4$) dan in-situ pempolimeran poli(natrium4-stirenasulfonat) ialah masing-masing 78.1 %, 85.8 %, 88.0 % dan 93.4 %. Penguraian haba $(NH_4)_2SO_4$ ialah kaedah yang paling sesuai dalam penyediaan s-MWCNTs kerana ia adalah satu kaedah yang mudah dan bebas asid. Seterusnya, kesan kepekatan larutan $(NH_4)_2SO_4$ dan tempoh ultrasonikasi MWCNTs dalam larutan $(NH_4)_2SO_4$ dikaji dan dioptimumkan. Prestasi s-MWCNTs yang terbaik boleh diperolehi dengan ultrasonik campuran MWCNTs tulen dalam 10 % berat larutan $(NH_4)_2SO_4$ selama 10 minit dan dipanaskan pada suhu 235 °C selama 30 minit. s-MWCNTs yang disediakan melalui cara ini memaparkan kestabilan haba dan penyebaran di dalam metanol yang baik serta mempunyai kawasan permukaan Brunauer-Emmett-Teller (BET) dan diameter liang yang besar. Kemudian, s-MWCNTs yang telah dioptimumkan diguna untuk kajian proses, kajian kinetik, penggunaan dan penjanaan semula

pemangkin untuk menunjukkan potensi s-MWCNTs sebagai pemangkin dalam penghasilan biodiesel. Kajian proses termasuk nisbah metanol kepada PFAD (8 – 30), pemuatan pemangkin (1 – 3 % berat), suhu tindak balas (80 – 200 ºC) dan masa bertindak balas (1 – 5 jam). Hasilan biodiesel setinggi 93.5 diperolehi pada nisbah metanol kepada PFAD 20, 3 % berat pemangkin, suhu 170 ºC dan masa bertindak balas selama 2 jam. s-MWCNTs menunjuk aktiviti pemangkinan yang baik dengan hasilan biodiesel melebihi 75 % walaupun selepas penggunaan kelima. Penjanaan s-MWCNTs (setelah 5 kitaran) dengan asid sulfurik berjaya memulih aktiviti pemangkinan s-MWCNTs ke paras asalnya. Model kinetik pseudo-homogen bagi esterifikasi PFAD dengan metanol diterbit berdasarkan keputusan eksperimen. Faktor praeksponen, haba molar dan tenaga pengaktifan untuk tindak balas esterifikasi ialah 1.9×10^2 L $mol^{-1}min^{-1}$, 84.1 kJ mol^{-1} and 45.8 kJ mol^{-1} masing-masing. Seterusnya, poliimeda, kopoli(1,5-naftalena/3,5-asidbenzoik-2,2'-bis(3,4-dikarboksifenil) heksafluoropropanadimeda (6FDA-NDA/DABA) disintesis dan diubah-suai dengan perangkaian silang pasa suhu tinggi untuk dijadikan membran dalam reaktor membran. Dalam masa tindak balas selama 10 jam, membran polyimide 6FDA-NDA/DABA yang dirangkai silang berjaya menyingkirkan 94.8 % air yang dihasilkan dalam tindak balas esterifikasi. Peratus penyingkiran air yang tinggi oleh membran poliimeda ini telah mencetuskan peningkatan sebanyak 17.9 % dalam hasilan biodiesel yang dicapai oleh reaktor membran berbanding dengan reaktor kelompok di bawah keadaan tindak balas yang sama. Membran poliimeda 6FDA-NDA/DABA yang dirangkai silang merupakan membran bersifat hidrofilik yang menunjukkan darjah pengampulan yang boleh diabaikan pada larutan tindak balas, dan kestabilan haba yang tinggi pada suhu serta tekanan tindak balas yang tinggi.

STUDIES ON THE SULFONATED CARBON NANOTUBES CATALYST AND MEMBRANE REACTOR FOR BIODIESEL PRODUCTION

ABSTRACT

This study focused on the synthesis of biodiesel using sulfonated multi-walled carbon nanotubes (s-MWCNTs) as catalyst and pervaporation membrane reactor as the conversion technology. First, s-MWCNTs were synthesized and utilized as catalysts to transform palm fatty acid distillate (PFAD) into biodiesel. The biodiesel yields achieved by the s-MWCNTs prepared via thermal treatment with concentrated sulfuric acid, the in situ polymerization of acetic anhydride and sulfuric acid, the thermal decomposition of ammonium sulfate ($(NH_4)_2SO_4$) and the in situ polymerization of poly(sodium4-styrenesulfonate) were 78.1 %, 85.8 %, 88.0 % and 93.4 %, respectively. Sulfonation via the thermal decomposition of $(NH_4)_2SO_4$ was the most suitable method to prepare s-MWCNTs because it is a facile and acid-free method. Next, the effects of the concentration of $(NH_4)_2SO_4$ solution and the ultrasonication period of MWCNTs in the $(NH_4)_2SO_4$ solution were studied and optimized. The results showed that the best performance of the s-MWCNTs was obtained by ultrasonicating the purified MWCNTs in a 10 wt% $(NH_4)_2SO_4$ solution for 10 min and heating at 235 °C for 30 min. s-MWCNTs prepared by this method demonstrated good thermal stability, good dispersibility in methanol and high Brunauer-Emmett-Teller (BET) surface area coupled with a large pore width. Then, the optimized s-MWCNTs were subjected to process parameters study, kinetic study, catalyst reusability and regeneration study to reveal the

potential of s-MWCNTs as a catalyst for biodiesel production. The process parameters studied included the methanol-to-PFAD ratio (8 – 30), catalyst loading (1 – 3 wt %), reaction temperature (80 – 200 ºC) and reaction time (1 – 5 h). A high FAME yield of 93.5 % was obtained at a methanol-to-PFAD ratio of 20, catalyst loading of 3 wt %, reaction temperature of 170 ºC and reaction time of 2 h. The s-MWCNTs exhibited good catalytic activity, with a FAME yield higher than 75 % even after 5 repeated runs. The regeneration of the spent s-MWCNTs (after 5 runs) with sulfuric acid was able to restore the catalytic activity to its original level. A pseudo-homogeneous kinetic model for the esterification of PFAD with methanol using s-MWCNTs as a catalyst was then developed based on the experimental results. The pre-exponential factor, molar heat and activation energy for the esterification were found to be 1.9×10^2 L $mol^{-1}min^{-1}$, 84.1 kJ mol^{-1} and 45.8 kJ mol^{-1}, respectively. Then, the polyimide, copoly(1,5-naphthalene/3,5-benzoicacid-2,2'-bis(3,4-dicarboxyphenyl) hexafluoropropanedimide (6FDA-NDA/DABA) was synthesized and modified via thermal cross-linking to serve as a membrane in membrane reactor. At 10 h of reaction time, the thermally cross-linked 6FDA-NDA/DABA polyimide membrane was able to remove 94.8 % of the generated water from the reaction mixture. The high removal percentage of water by the polyimide membrane has triggered a 17.9 % increment of FAME yield achieved by pervaporation membrane reactor as compared to the FAME yield achieved by the batch reactor under the same reaction conditions. The thermally cross-linked polyimide membrane was a hydrophilic membrane which demonstrated negligible swelling degree in the reaction mixture and high thermal stability under high reaction temperature and pressure.

CHAPTER ONE

INTRODUCTION

This chapter provides detail information of the research project. Brief definition, current demand and market supply of biodiesel are included at the beginning of this chapter. In addition, information about esterification process is also included. This chapter concludes with problem statement, objectives and thesis organization of this research project.

1.1 Current status of energy requirement and the potential of biodiesel

Human civilisation has always relied on the utilisation of energy. As illustrated in Figure 1.1, the industrial sector, consisting of diverse industrial groups that include manufacturing, agriculture, mining and construction, accounted for 52 % of global energy used in 2010; the transportation sector, providing services, such as moving people and goods by road, rail, air, water and pipeline, uses 26 %; the residential sector for household activities comprise 14 % of the total and the commercial sector, which consists of businesses, institutions, and organisations that provide services, comprises 8 %. The International Energy outlook 2013 (IEO 2013) predicted the global energy consumption will grow by 56 % between 2010 and 2040 (EIA, 2013). This prediction increases the demand of resources for energy production. According to the statistical review conducted by the International Energy Agency (IEA, 2013), global energy production depends heavily on oil (32%), coal (29%) and natural gas (21%) to satisfy the global energy demand, as shown in Figure 1.2.

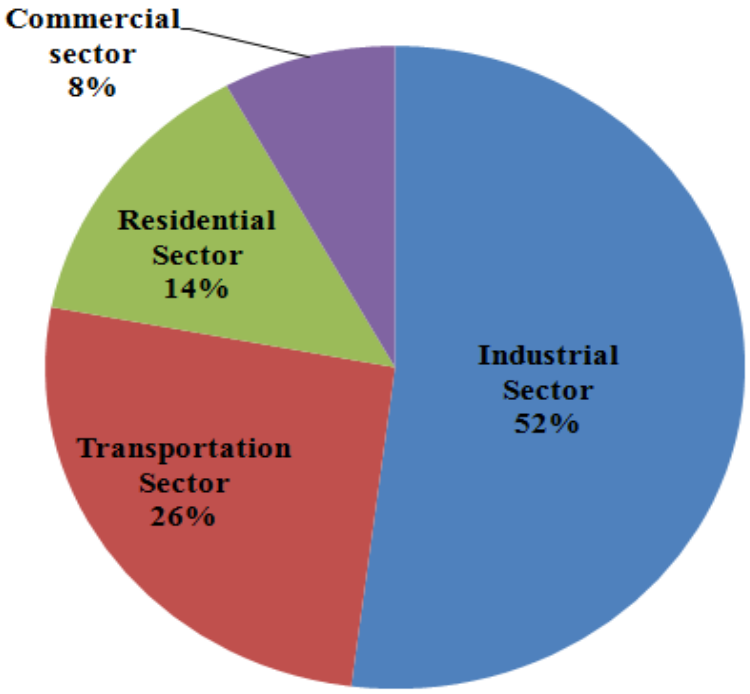

Figure 1.1. Global energy consumption in 2010 (EIA, 2013).

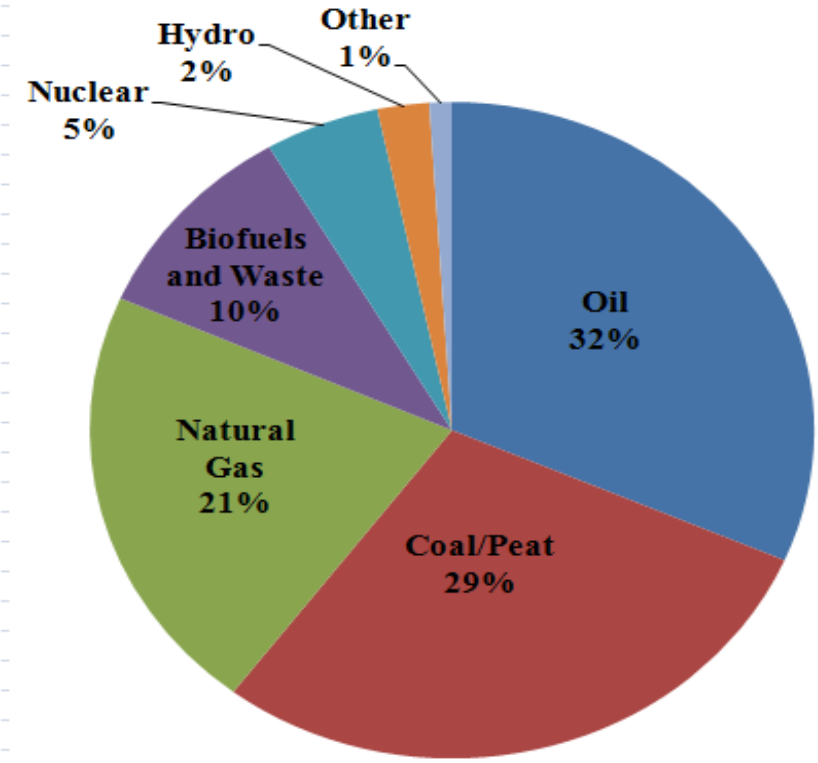

Figure 1.2. World energy production in 2011 (IEA, 2013).

Fossil fuels such as petroleum, coal and natural gas have been hailed as major energy resources in the world since its discovery. However, fossil fuels are the world's slowest-growing source of energy, and their supplies are decreasing daily. In addition, the growing emission of carbon dioxide, sulfur dioxide, hydrocarbons and volatile organic compounds (VOCs) from the combustion of fossil fuels could result in air pollution, global warming and climate change. These negative impacts on the environment are the target of current energy policies that emphasize cleaner, more efficient and environmentally friendly technologies to increase the supply and usage of energy (Hammond et al., 2008, Hoekman, 2008, Monni and Raes, 2008, Sawyer, 2009). Thus, developments in alternative renewable energy sources have become indispensable for sustainable environmental and economic growth. Among the explored alternative energy sources, considerable attention has been focused on biodiesel because it is widely available from inexhaustible feedstock that can effectively reduce its production cost.

1.2 Biodiesel

Biodiesel is a mixture of monoalkyl esters of long-chain fatty acids derived from renewable lipid feedstocks, such as vegetable oil and animal fats. The chemical name for biodiesel depends on the alcohol source used in the production process. The alcohols used to produce biodiesel are usually primary or secondary monohydric aliphatic alcohols such as methanol, ethanol, propanol, butanol and amyl alcohol. Therefore, biodiesel is known as fatty acid methyl ester (FAME) when the alcohol source is methanol. If ethanol is used as the alcohol source, the mixture will be named as fatty acid ethyl esters. Methanol is the most common and widely used

alcohol in the production of biodiesel because of its low cost, high availability and most importantly its physical and chemical advantages as compared to other alcohol sources. The reaction rate between methanol and triglycerides is the highest among all alcohols because methanol is a polar alcohol with the shortest carbon chain. The composition of FAME depends on the feedstock used during the synthesis process. Because biodiesel has similar physical properties to diesel fuels, it has established its commercial value in the automobile markets of Europe, the United State of America, Japan, Brazil and India (Janaun and Ellis, 2010). Moreover, the implementation of the "directive on the promotion of the use of biofuels" for transport in the EU (Directives 2003/30/EC) mandated the increased use of biofuels to power transportation from 2% to 5.75% between 2005 and 2010, triggering a huge demand for biodiesel (Mabee, 2007). Unlike conventional diesel fuel, biodiesel offers several advantages, including renewability, higher combustion efficiency (Fazal et al., 2011), cleaner emission (Janaun and Ellis, 2010), higher cetane number, higher flash point, better lubrication (Lin et al., 2011) and biodegradability (Wardle, 2003).

Currently, virgin vegetable oil is the most common feedstock for biodiesel production which accounts more than 95% of the world total biodiesel production owing to its easy availability. The practice of using edible oil as feedstock for biodiesel production has raised objections from various organizations especially non-governmental organization (NGO), claiming that biodiesel is competing with the food industry causing the depletion of vegetable oil supply and subsequently increase in vegetable oil prices. It is believed that large scale production of biodiesel from edible oil may eventually bring global imbalance in the food demand and supply market (Monbiot, 2004). Therefore, a possible solution to overcome the food versus

fuel issue is to produce biodiesel from non-edible oil. Various types of non-edible oil sources such as *Jatropha* oil (Om Tapanes et al., 2008), beef tallow (Nelson and Schrock, 2006), waste cooking oil (Lam et al., 2010), *Cerbera odollam* (sea mango) (Kansedo et al., 2009), microalgae (Ahmad et al., 2011) and palm fatty acid distillate (PFAD) (Cho et al., 2012a, Cho et al., 2012b) have been introduced as potential feedstock for biodiesel production in order to ensure that biodiesel is being produced in a more sustainable manner.

1.3 Transesterification/Esterification Reaction

Direct use of vegetable oils, animal fats or fatty acids is not suitable owing to their high kinematic viscosity and low volatility. Moreover, such practice will cause serious problems for example deposition, ring sticking and injector chocking in engine (Muniyappa et al., 1996). Therefore, several modification techniques, such as dilution, microemulsion, pyrolysis, transesterification and esterification have been used to reduce the viscosity of vegetable oil (Andrade et al., 2011). Of these processes, transesterification or esterification are the most widely used; these methods involve the alcoholysis of vegetable oil or fatty acid to produce alkyl ester as main product and glycerol (for transesterification) or water (for esterification) as by-product. Transesterification and esterification are reversible reactions in which excess alcohol is used to shift the equilibrium towards the product side (Helwani et al., 2009). The mechanism of transesterification consists of three consecutive reversible reaction steps. The first step involves the conversion of triglycerides (TG) to diglycerides (DG) and later to monoglycerides (MG). Subsequently, the monoglycerides are converted to glycerol. Each reaction step produces an alkyl ester. Thus, a total of three alkyl esters are produced in the transesterification process

(Sharma and Singh, 2008). The overall reaction that occurs in transesterification and esterification are simplified in Figure 1.3 and Figure 1.4, respectively.

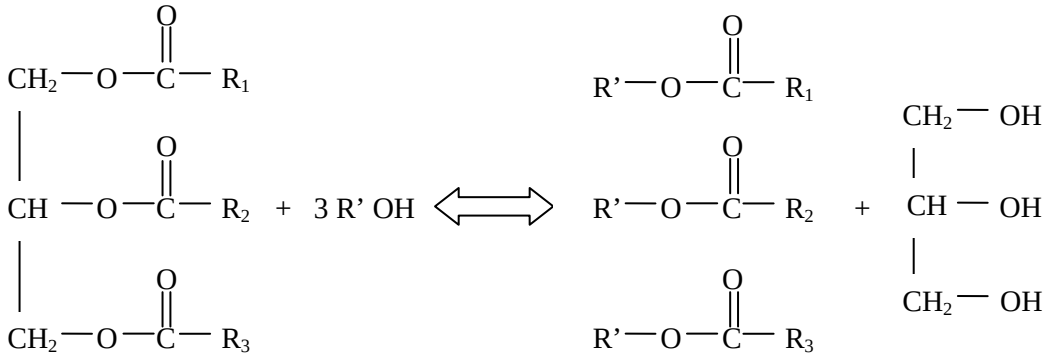

Figure 1.3: Transesterification of triglycerides with alcohol.

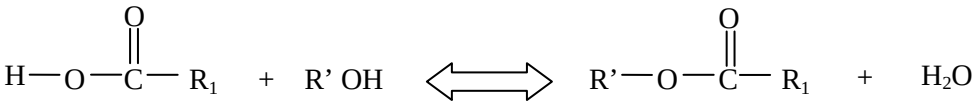

Figure 1.4: Eesterification of fatty acid with alcohol.

Transesterification reaction is a relatively slow if it is carried out in normal room temperature due to the two-phase nature of alcohol-oil mixture that has contrast polarity. Therefore, catalyst is needed to overcome this limitation and thus improve the reaction rate and products yield. There are generally 3 groups of catalysts that have been commonly used in catalytic transesterification/esterification reaction either homogeneously or heterogeneously (Marchetti et al., 2007). The 3 groups of catalyst are shown as below:

i. Alkali catalyst

Sodium hydroxide (NaOH) and potassium hydroxide (KOH) are the most common homogeneous alkali catalysts used in the commercial production of biodiesel (Marchetti et al., 2007). Heterogeneous alkali catalysts include metal oxides (Semwal et al., 2011), mixed metal oxides (Yu et al., 2011) and metal complex (Abreu et al., 2003). However, alkali-catalyzed transesterification especially homogeneous alkali catalysts require reactant with high purity. High content of free fatty acid (FFA) and water in the reactant will cause soap formation (saponification) (Marchetti et al., 2007).

ii. Acid catalyst

Sulfuric acid (H_2SO_4) and sulfonic acid are the two most common used homogeneous acid catalysts. Meanwhile, sulfated oxides (Semwal et al., 2011) and ion exchange resin (Chouhan and Sarma, 2011) are the example of heterogeneous acid catalysts. This type of catalyst gives very high ester yield but the reaction is very slow (Marchetti *et al*., 2007). However, acid catalyst is suitable to be used for oils with higher FFA content.

iii. Enzyme

Enzyme used in the transesterification reaction is also known as biocatalyst. Lipase is normally used in transesterification. However, enzyme is more expensive than chemical catalyst (alkali or acid catalyst) and it can be poisoned by short-chained alcohol and glycerol (Marchetti et al., 2007, Su et al., 2007).

The convention methods used to produce biodiesel include:

i. Homogeneous transesterification/esterification

This method involves the use of homogeneous enzyme, alkali or acid catalysts to produce biodiesel. After reaction, the catalysts are removed by water washing (Xie and Li, 2006).

ii. Heterogeneous transesterification/esterification

Heterogeneous catalysts are considered as the second generation of catalysts in transesterification/esterification. This approach involves the use of immobilized enzyme, heterogeneous base or acid catalysts. Although heterogeneous catalysis has the advantage of easy catalyst separation as compared to homogeneous catalysis, this method still having its own limitation of requiring higher reaction temperature and reaction time.

Esterification via pervaporation membrane reactor or reactive separation is another possible technology for biodiesel production. Pervaporation membrane reactor involves the use of membrane as a selective barrier to simultaneously remove water from the product stream. Pervaporation membrane reactor requires catalyst to speed up the reaction to produce high yield of biodiesel. The common catalysts involved in membrane reactor are homogeneous alkali and acid catalysts (Dubé et al., 2007). However, biodiesel produced by this type of membrane reactor required further purification process to remove the homogeneous catalysts. Therefore, pervaporation membrane reactor using heterogeneous catalysts offers an alternative to produce biodiesel with less processing steps. Since non-edible oils that contain high level of FFA become more common in biodesel production, heterogeneous acid catalysts are more appropriate to serve as catalyst in the pervaporation membrane reactor. Recently, research on the catalysts used in biodiesel production has been focused on carbon-based acid catalysts especially sulfonated multi-walled carbon nanotubes (s-MWCNTs) because of their intrinsic properties, such as high surface area; high purity compared to activated carbon, which can avoid self-poisoning; and well-developed surface morphology and porosity (Shu et al., 2009). Therefore, the novel integrated pervaporation membrane reactor using s-MWCNTs as catalyst is proposed for biodiesel production. In addition, the incorporation of ultrasonication treatment in the preparation of the s-MWCNTs was another highlight in this study.

1.4 Problem Statement

Even though heterogeneous catalysts can overcome some of the disadvantages encountered by homogeneous catalysts, there are still a lot of limitations in the production of biodiesel using conventional heterogeneous catalysts and conversion technologies. Therefore, the problem statement in biodiesel production can be divided into two categories: the limitations of conventional heterogeneous catalysts and the limitations of conventional biodiesel conversion technologies.

The limitations of conventional heterogeneous catalysts in biodiesel production include:

i. Mass transfer resistance

   Mass transfer resistance exists because of the presence of a three-phase system (alcohol, oil and heterogeneous catalyst) and in the reaction mixture. This three-phase system reduces the diffusion of reactants into the pores of the catalysts that contain active sites. Thus, the reaction rate will be affected.

ii. Low reusability and stability of the conventional heterogeneous catalysts.

   Leaching of active sites and adsorption of organic substances onto the catalysts' surface are the main factors that cause low reusability and stability of the heterogeneous catalysts. High operating costs are required because catalysts with low reusability and stability have to be regenerated more frequent to restore their catalytic activity.

iii. High cost of catalysts.

Most of the heterogeneous catalysts in biodiesel production are metal catalysts that are expensive and non-renewable compared to carbon-based catalysts. Moreover, the cost of biocatalysts such as enzymes is even higher than some of the metal catalysts. The high cost of catalysts prohibits the production of biodiesel to be economically feasible.

The limitations of conventional biodiesel conversion technologies include:

i. Limitation caused by thermodynamic equilibrium.

Owing to the reversible nature, esterification/transesterification reaction can never reach complete conversion. Large quantity of alcohol is required to drive the reaction towards higher biodiesel production.

ii. Wastewater issue.

Biodiesel produced by homogeneous esterification/transesterification requires further purification step to remove the homogeneous catalysts. The washing step generates wastewater.

iii. High energy requirement.

High usage of energy is needed in the preparation of most of the heterogeneous catalysts because of the calcination process occurs at high temperature.

iv. Multiple downstream processing steps.

Biodiesel produced by conventional conversion technologies required to undergo various separation processes. The downstream processing steps increase the overall biodiesel production cost.

Each of the mentioned limitation will be discussed in detail in Chapter 2. Based on the above limitations, membrane reactor using s-MWCNTs as catalysts is believed to possess the potential to overcome the limitations encountered by the conventional production methods.

1.5 Objectives

i. To synthesis sulphated supported MWCNTs catalyst for esterification of PFAD.

ii. To optimize the transformation conditions and characterize the s-MWCNTs.

iii. To study the effect of process parameters and to develop a kinetic model for the esterification of PFAD using s-MWCNTs as catalyst.

iv. To study the reusability and regeneration of the s-MWCNTs.

v. To develop an integrated membrane reactor system for the esterification of PFAD using s-MWCNTs as catalyst.

1.6 Scope of study

The first step in this study was to examine the possible sulfonation methods to change the MWCNTs into promoted catalyst for the esterification of PFAD to produce fatty acid methyl esters. This is a crucial step to determine the suitable sulfonation method used for the study.

Secondly, the effect of the sulfonation parameters such as concentration of ammonium sulfate ($(NH_4)_2SO_4$) solution and the duration of ultrasonication treatment of MWCNTS and $(NH_4)_2SO_4$ solution mixture were studied and optimized. The s-MWCNTs will be characterized using various physicochemical techniques such as Raman spectra, pulse chemisorptions, thermogravimetric analysis (TGA), nitrogen sorption analysis and ultraviolet-visible spectroscopy (UV-Vis).

Then, the research work will be followed by the esterification process study of FAME production using the s-MWCNTs. The effect of the process parameters on the yield of FAME was also studied and optimized. Besides, reusability and regeneration of the s-MWCNTs will be examined. Furthermore, a kinetic model for the esterification catalyzed by s-MWCNTs will be developed based on the results generated in the process study to determine the equilibrium constants and activation energy of the esterification.

Lastly, a membrane reactor with s-MWCNTs as catalyst will be developed to produce FAME via reactive separation. Owing to the ability to withstand high reaction pressure and temperature, copoly(1,5-naphthalene/3,5-benzoicacid-2,2'-bis(3,4-dicarboxyphenyl) hexafluoropropanedimide (6FDA-NDA/DABA) was selected as the membrane for the membrane reactor. The synthesized membrane will be characterized using various physicochemical techniques such as contact angle analysis, Fourier transform infrared (FTIR), thermal gravimetric analysis (TGA), X-ray diffraction analysis (XRD) and scanning electron microscopy analysis (SEM).

1.7 Organization of thesis

This thesis consists of five chapters. Chapter one provides an outline of the overall research project which includes the introduction on biodiesel and oil sources for biodiesel production. Problem statement was written after reviewing the current scenario for biodiesel market. The objectives of this research project were then carefully formulated with the intention to address the problems encountered by the biodiesel industry. Lastly, organization of the thesis highlights the content of each chapter.

Chapter two gave an overall review of various research works reported in the literature in this area of study which includes production of biodiesel using functionalized MWCNTs and membrane technology. The methods to functionalize MWCNTs and the concepts of membrane separation in biodiesel production were reported. In addition, feasibility and advantages of using functionalized MWCNTs and membrane technology for biodiesel production were also being discussed.

Experimental materials and methodology were discussed in chapter three. This chapter describes detail information on the overall flow of this research work and some experimental methods in conducting this research project. In addition, material, chemicals and equipments used in this study were also reported. This chapter also includes the information that is required for the calculation of yield and data analysis.

Chapter four is the heart of the thesis since it includes detail discussion on the results obtained in the present research work. The research works begins with the characterization of PFAD and feasibility study of various sulfonation methods for transforming carbon nanotubes into catalysts for the esterification of PFAD. This is followed by the optimization of the sulfonation parameters and the characterization of s-MWCNTs using various physicochemical techniques. In addition, process study, catalyst reusability/deactivation and regeneration of the s-MWCNTs and kinetic study of the esterification of PFAD using s-MWCNTs are being reported in this chapter. Finally, the production of biodiesel via membrane reactor and the characterization of membrane are reported at the end of chapter four.

Chapter five, the last chapter of this thesis, provides a summary on the results obtained in this research project. This chapter concludes the overall research project and gives some recommendations for future studies related to this research work.

CHAPTER TWO

LITERATURE REVIEW

This chapter reviews on the studies reported in the literature related to this research project. Initially, the classification of heterogeneous catalyst and its limitations were reviewed and reported in this chapter. In addition, the advantages of functionalized MWCNTs as biodiesel catalyst, the possible methods to transform MWCNTs into catalyst for biodiesel production and the process parameters for biodiesel production using functionalized MWCNTs were also discussed in detail. Besides, the catalyst life time and regeneration were reported. This was followed by discussing on the limitations in conventional biodiesel conversion technology. Furthermore, review on the concept of membrane reaction in biodiesel production and possible combination of membrane and catalyst were reported at the end of this chapter.

2.1 Classification of Heterogeneous Catalyst for Biodiesel Production

Heterogeneous catalytic transesterification is considered to be a green technology because the catalysts are reusable (Suppes et al., 2004), minimal wastewater is produced during the process (Chouhan and Sarma, 2011), biodiesel is more easily separated from glycerol (Lee and Saka, 2010, Chouhan and Sarma, 2011), and the solid acid catalysts can esterify and transesterify the reactants simultaneously (Furuta et al., 2004). Common base heterogeneous catalysts used in transesterification include metal complexes (Abreu et al., 2003), mixed metal oxides

(Chouhan and Sarma, 2011), transition metal oxides (Chouhan and Sarma, 2011), boron group based catalysts (Chouhan and Sarma, 2011) and alkali metal oxides (Xie et al., 2007, Chouhan and Sarma, 2011). Alternatively, ion-exchange resins (Liang et al., 2009) and sulfated oxides (Li and Huang, 2009, Lam and Lee, 2011, Yee et al., 2011) have been reported as heterogeneous acid catalysts used in transesterification. Different types of heterogeneous catalyst were shown in Figure 2.1.

2.2 Limitations of Conventional Heterogeneous Catalysts for Biodiesel Production

2.2.1 Mass transfer limitation

The heterogeneous catalytic reaction usually faces a mass transfer resistance problem because of the presence of a three-phase system (triglycerides, alcohol and solid catalyst) in the reaction mixture that limits the pore diffusion process and reduces the active sites available for the catalytic reaction, thereby decreasing the reaction rate (Mbaraka and Shanks, 2006). The mass transfer limitation can be overcome by using a co-solvent that could increase oil/alcohol miscibility, enhancing the contact between the reactants and solid catalysts, thus accelerating the reaction (Lee and Saka, 2010). Common co-solvents used in tranesterification include tetrahydrofuran (THF) (Li and Xie, 2006, Sawangkeaw et al., 2007), n-hexane (Peña et al., 2008) and dimethyl sulfoxide (Li and Xie, 2006).

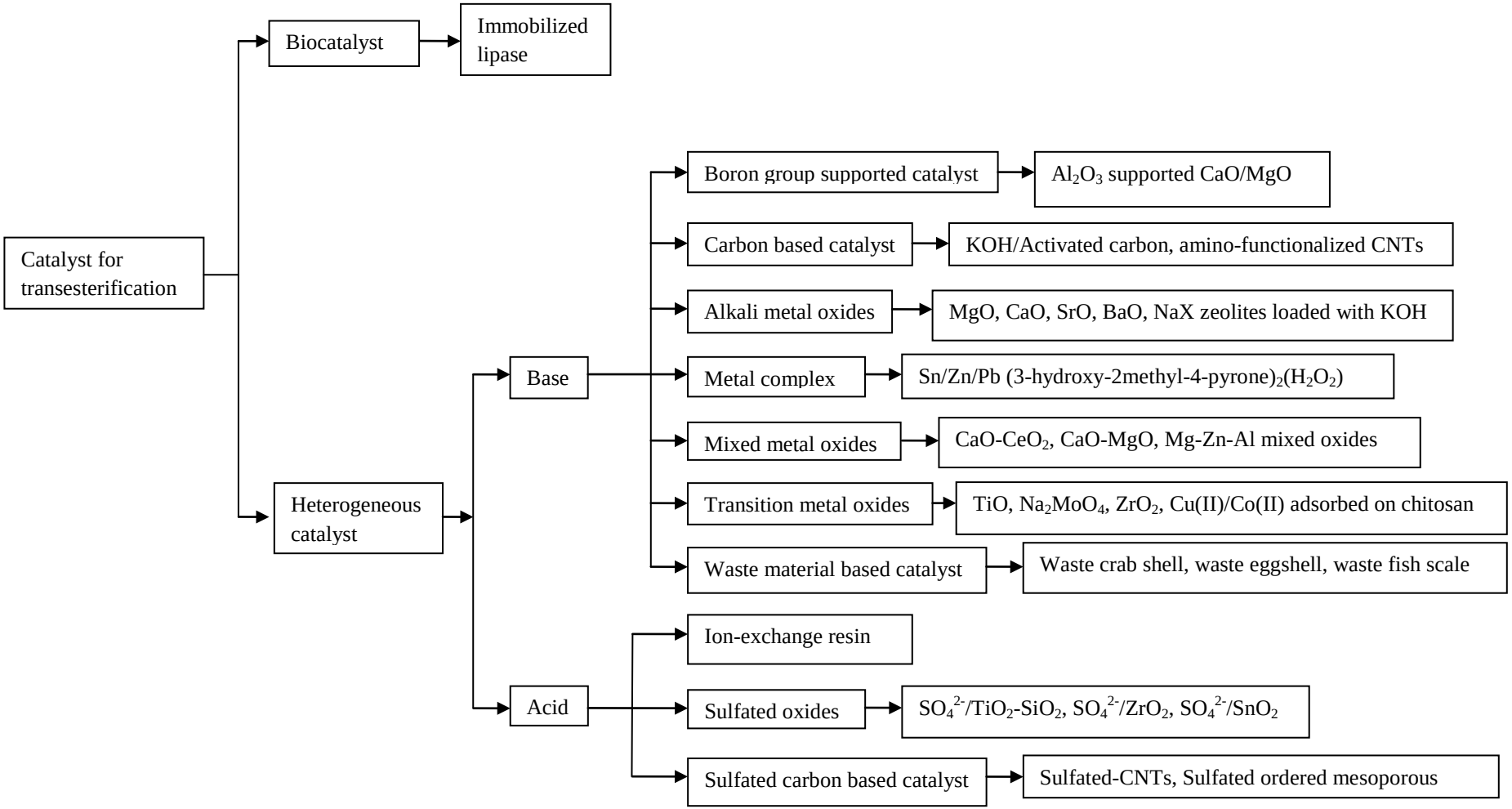

Figure 2.1 Classification of heterogeneous catalysts used in transesterification/esterification.

However, adding a co-solvent may also cause the deactivation of the catalysts. Due to glycerol's solubility in methanol and insolubility in the co-solvent, glycerol drops form when the methanol content decreases as the reaction proceeds. The formed glycerol drops adhere to the catalyst particles, causing them to agglomerate and eventually deactivate the catalyst (Guan et al., 2009, Lee and Saka, 2010). This indicates that the co-solvent may not always be useful in transesterification with heterogeneous catalysts. The use of a co-solvent also increases the overall processing steps and energy consumption owing to the need to separate the co-solvent after reaction (Šalić and Zelić, 2011). Another alternative to address the mass transfer problem is the use of catalyst supports that provide high specific surface areas and pores for active species to anchor and eventually increase the active sites for reaction. Therefore, the contact between the catalysts and large TG or fatty acid molecules is enhanced (Zabeti et al., 2009). Generally, all types of materials that are thermally stable and chemically inert can be used as catalyst supports (Chorkendorff and Niemantsverdriet, 2003). Alumina (Ebiura et al., 2005, Xie and Li, 2006, Lee et al., 2009, Verziu et al., 2009, Sankaranarayanan et al., 2011, Yee et al., 2011a, Umdu and Seker, 2012), silica (Liu et al., 2007, Albuquerque et al., 2008, Faria et al., 2008, Kim et al., 2011, Pal et al., 2011, Xie and Yang, 2011) and carbon (Shu et al., 2009a, Shu et al., 2009b, Villa et al., 2009, Baroutian et al., 2010, Shu et al., 2010, Villa et al., 2010, Wan and Hameed, 2011) are the most common catalyst supports for transesterification or esterification.

2.2.2 Low Reusability and Stability of the Catalysts

Low catalyst reusability and stability are the major hurdles encountered when using heterogeneous catalysts for transesterification (Lee and Saka, 2010). Leaching of the active species and fouling of the catalyst surface by organic substances in the reaction media have been identified as the main factors in catalysts deactivation (Alonso et al., 2007, Lee et al., 2009, Lee and Saka, 2010). Although calcium oxide (CaO) is very active in the chemical reaction that produces biodiesel, significant leaching of CaO was observed during transesterification (Granados et al., 2009, Kouzu et al., 2009). Kouzu et al. (2009) reported that 10.5 wt % of CaO was found to have leached away from the solid base catalyst in the first cycle of transesterification, causing the yield of biodiesel to drop when the catalyst was recycled and reused. Additionally, it was reported that the leaching of CaO was more significant in the presence of glycerol due to the formation of calcium diglyceroxide (Granados et al., 2009). Mootabadi et al. (2010) reported that when BaO (an alkaline earth metal oxide) was used to produce biodiesel from palm oil, 14 wt % of the catalyst was found to have leached into the biodiesel layer after reaction. In addition, the experiment conducted by López et al. (2005) showed that ETS-10 (Na, K) exhibited a significant drop in triacetin conversion from 90 % in the first cycle to 56 % in the second cycle, eventually dropping to 28 % in the fifth cycle. The reaction liquid was analysed to contain 14 wt % of the Na originally presents in ETS-10 (Na, K). The leaching of the active species into the reaction media usually occurred when the catalysts were prepared via the wet impregnation method (Alonso et al., 2007, Ramos et al., 2008, Verziu et al., 2009). The leaching of metal oxide catalysts is more severe in the presence of polar substances, such as water, FFA, methanol and glycerol (Granados et al., 2009, Lee and Saka, 2010), limiting the use of only refined

oil in transesterification. In addition to leaching, the adsorption of organic substances onto the catalysts' surface is another cause of catalyst deactivation. Ngamcharussrivichai et al. (2008) reported that more than 12 wt % of organic substances (methyl esters, glycerol and MG/DG) deposited onto a CaO-ZnO catalyst used in the transesterification of palm kernel oil.

2.2.3 High Cost of Catalyst

The high cost of conventional heterogeneous catalysts is another drawback that limits their use in biodiesel production (Mo et al., 2008). Most of the metal catalysts are expensive compared to conventional homogeneous catalysts (Lee and Saka, 2010). Due to their superacidity, SO_4^{2-}/SnO_2, SO_4^{2-}/ZrO_2 and SO_4^{2-}/TiO_2 have been used to produce biodiesel from oil sources with high contents of free fatty acids (FFA) (Lam et al., 2009, Lam et al., 2010, Yee et al., 2011b). These catalysts have shown good catalytic activities and stability when esterifying and transesterifying oils with high contents of FFA simultaneously. However, these catalysts, especially Zr, have not been widely applied in commercial biodiesel production mainly because they are rare and expensive metals (Zong et al., 2007, Refaat, 2011). Although enzymes (lipases) are potentially more flexible than homogeneous alkali and acid catalysts in managing a wide range of feedstock conditions and are able to drastically reduce the amount of wastewater generated (Fjerbaek et al., 2009, Yan et al., 2012), their high market price is the major barrier that prevents their industrial application (Fjerbaek et al., 2009, Bajaj et al., 2010, Tan et al., 2010, Taher et al., 2011).

2.1 Advantages of Carbon Nanotubes (CNTs) Over Conventional Catalysts in Biodiesel Production

The limitations of the conventional transesterification catalysts described above could be improved by using CNTs as catalyst supports. CNTs are cylinder-shaped macromolecules, a few nanometers in radius, that can grow up to 20 cm in length (Zhu et al., 2002). The CNT walls are composed of a hexagonal lattice of carbon atoms. CNTs can be categorised as single-walled carbon nanotubes (SWCNTs) with diameters ranging between 0.4 and 3 nm or multi-walled carbon nanotubes (MWCNTs) with diameters reaching up to 100 nm (Balasubramanian and Burghard, 2005). The intrinsic properties of CNTs, such as high surface area, well-defined morphology and chemical composition, inherent size, hollow geometry, and their ability to graft specific functional groups onto their surfaces, make them suitable to be catalyst supports (Balasubramanian and Burghard, 2005, Wildgoose et al., 2006, Peng and Wong, 2009, Tessonnier et al., 2009). The advantages of CNTs over other conventional catalysts in biodiesel production will be discussed in the following section.

2.3.1 High Surface Area and Well Developed Porosity

Table 2.1 shows the surface area, average pore diameter and porosity type of the various catalysts used in transesterification. The data shows that the specific surface area of MWCNTs is higher than that of most conventional heterogeneous catalysts.

Table 2.1: Specific surface area, average pore diameter and type of porosity for the various transesterification/esterification catalysts.

Catalyst	Specific surface area (m^2/g)	Average pore diameter (Å)	Porosity (Köhn and Fröba, 2003)	References
Single-walled carbon nanotubes (SWCNTs)	400-900	-	Microporous	(Serp et al., 2003)
MWCNTs	200-400	-	Mesoporous	(Serp et al., 2003)
Activated carbon (AC)	700-1200	-	Microporous	(Serp et al., 2003)
CaO	8.1-21.0	44.00-85.91	Mesoporous[a]	(Meher et al., 2006, Arzamendi et al., 2008, Mootabadi et al., 2010)
SrO	1.05-11.0	135.60	Mesoporous[a]	(Liu et al., 2007a, Mootabadi et al., 2010)
BaO	4.0	123.80	Mesoporous[a]	(Mootabadi et al., 2010)
VOP	2-4	-	-	(Di Serio et al., 2007)
MgO	96 ± 4	-	-	(Arzamendi et al., 2008)
Mg_9Al_1 thoroughly washed	96.0	-	-	(Fraile et al., 2010)
K/BaO	6.1	50.20	Mesoporous[a]	(D'Cruz et al., 2007)
Li/BaO	4.0	66.40	Mesoporous[a]	(D'Cruz et al., 2007)
Na/BaO	3.8	66.40	Mesoporous[a]	(D'Cruz et al., 2007)
Na/CaO (with 1.25 wt % of Na)	12.5	167.17	Mesoporous[a]	(Meher et al., 2006)
K/CaO (with 1.25 wt % of K)	18.7	203.79	Mesoporous[a]	(Meher et al., 2006)
CaO/ZrO_2 (Ca to Zr ratio of 0.25)	18.9	79.00	Mesoporous[a]	(Molaei Dehkordi and Ghasemi, 2012)
WO_3/ZrO_2 (powder)	57.0	130.00	Mesoporous[a]	(Park et al., 2008)
WO_3/ZrO_2 (pellet)	40.0	110.00	Mesoporous[a]	(Park et al., 2008)
$CaTiO_3$	4.9	-	-	(Kawashima et al., 2008)
$Ca_2Fe_2O_5$	0.71	-	-	(Kawashima et al., 2008)
$CaZrO_3$	1.8	-	-	(Kawashima et al., 2008)
$CaCO_3$	0.6 ± 0.1	-	-	(Arzamendi et al., 2008)

Ca_3La_1	62.6	-	-	(Yan et al., 2009)
γ- Al_2O_3	143.1	134.30	Mesoporous[a]	(Kim et al., 2004)
NaOH/ γ- Al_2O_3	120.7	137.80	Mesoporous[a]	(Kim et al., 2004)
Na/ γ- Al_2O_3	97.7	148.20	Mesoporous[a]	(Kim et al., 2004)
Na/NaOH/ γ- Al_2O_3	83.2	155.00	Mesoporous[a]	(Kim et al., 2004)
K_2CO_3/Al_2O_3	118.0	130.20	Mesoporous[a]	(D'Cruz et al., 2007)
SBA-15	413	4.20	Microporous[a]	(Albuquerque et al., 2008)
SBA-CaO (with 14 wt % of CaO)	7.4	5.40	Microporous[a]	(Albuquerque et al., 2008)
SBA-15/MgO	252.0	37.60	Mesoporous[a]	(Li and Rudolph, 2007)
MCM-41/MgO	391.0	27.00	Mesoporous[a]	(Li and Rudolph, 2007)
KIT-6/MgO	112.0	46.80	Mesoporous[a]	(Li and Rudolph, 2007)
$Mg(OH)_2.4\ MgCO_3$	20 ± 0.5	-	-	(Arzamendi et al., 2008)
SO_4^{2-}/SnO_2	6.77	164.00	Mesoporous[a]	(Lam et al., 2009)
SO_4^{2-}/SnO_2-SiO_2	13.90	137.00	Mesoporous[a]	(Lam et al., 2009)
SO_4^{2-}/SnO_2-Al_2O_3	14.04	132.00	Mesoporous[a]	(Lam et al., 2009)
Tungstated zirconia (WZ)	68.0-89.2	-	-	(López et al., 2007)
Sulfated zirconia (SZ)	134.4 ± 5.3	-	-	(López et al., 2005)
Amberlyst-15	37.8 ± 2.6	-	-	(López et al., 2005)
Nafion NR50	0.02	-	-	(López et al., 2005)
Supported phosphoric acid (SPA)	2.6 ± 0.1	-	-	(López et al., 2005)
Titanosilicate (ETS-10)	440.8 ± 11.8	-	Microporous	(López et al., 2005)
Zeolite Hβ	620.0	-	-	(López et al., 2005)
Eggshell	1.1	-	-	(Viriya-empikul et al., 2010)
Golden apple snail shell	0.9	-	-	(Viriya-empikul et al., 2010)
Meretrix venus shell	0.5	-	-	(Viriya-empikul et al., 2010)
Waste mud crab shell	13.0	-	-	(Boey et al., 2009)
Calcined waste fish scale	39.0	-	-	(Chakraborty et al., 2011)
Cesium-exchanged NaCsX zeolites	450	-	-	(Leclercq et al., 2001)

[a] The porosity of the catalysts is defined based on the definition stated by Köhn and Fröba, 2003.

Moreover, due to their mesoporous nature and the absence of microporosity, MWCNTs allow high accessibility of the active sites to reactants and products, thus reducing mass transfer limitations (Serp and Castillejos, 2010, Soares et al., 2010). The surface area of porous supports is highly correlated with their pore sizes, which means that supports with large amounts of ultrafine micropores possess high surface areas (Ryoo et al., 2003). Although the mass transfer limitation encountered in the liquid phase reaction can be significantly reduced by using a catalyst support with a high external surface area (Pham-Huu et al., 2001), that limitation will still exist if the catalyst support possesses only micropores, especially when large molecules are involved (Rodríguez-reinoso, 1998, Ryoo et al., 2003), because the active phase particles that are located in the micropores limit the accessibility to the reactants and products, thus reducing the effectiveness of the microporosity (Rodríguez-reinoso, 1998). Activated carbon is supposed to be an ideal choice as a catalyst support because it has a larger surface area compared with MWCNTs (Serp et al., 2003). However, the large surface area of activated carbon is mainly concentrated in its microporosity (Rodríguez-reinoso, 1998, Serp et al., 2003), which may affect the catalytic activity in transesterification involving large molecules such as triglycerides and long chain fatty acids. Therefore, a catalyst support with a large and easily accessible surface area, coupled with the right pore size distribution, is needed (Rodríguez-reinoso, 1998). Therefore, mesoporous materials such as MWCNTs, mesoporous activated carbon (Qiu et al., 2015) and mesoporous sugar catalyst prepared by incompletely carbonised D-glucose (Mar and Somsook, 2012) are potential catalyst supports for transesterification.

2.3.2 Excellent Catalyst Stability

Unlike other conventional transesterification catalysts, which are prepared by precipitation or impregnation methods, CNTs can be tuned to be catalytically active via functionalization with specific functional groups onto their surfaces (Balasubramanian and Burghard, 2005, Peng and Wong, 2009). It has been reported that the leaching problem under liquid-phase reaction conditions occurs because the active species are not covalently bonded to the solid support (Li et al., 2011). CNTs appear to be the perfect candidate to serve as a catalyst support for transesterification or esterification because the functional groups or active species can be chemically modified to covalently bond to the CNTs (Balasubramanian and Burghard, 2005). Because covalent bonding provides the best stability, accessibility and selectivity for the catalysts (Jiang et al., 2004), CNTs are an ideal alternative catalyst support to overcome the low stability and leaching problems encountered by the conventional catalysts used in transesterification.

2.3.3 Low Catalysts Cost

As mentioned in section 2.2.3, the high cost of metal catalysts prevents them from being used in the production of biodiesel. Replacing precious metal catalysts with functionalized CNTs as catalyst supports in transesterification can be more economically feasible. Various technologies, such as electric arc discharge (Iijima et al., 1992, Balasubramanian and Burghard, 2005, Paradise and Goswami, 2007), laser ablation pyrolysis (Guo et al., 1995, Thess et al., 1996, Balasubramanian and Burghard, 2005, Paradise and Goswami, 2007), chemical vapour deposition (CVD) (Allouche et al., 2003, Balasubramanian and Burghard, 2005, Paradise and Goswami,

2007), plasma and laser assisted CVD (Jung et al., 2004, Bondi et al., 2006) and mechanothermal methods (Manafi et al., 2009) have been developed to produce both SWCNTs and MWCNTs. Among these techniques, CVD was determined to be the best method that could produce CNTs in large quantities with low production cost (Paradise and Goswami, 2007). Due to the great efforts of the CNT industries in the past 10 years, the price of MWCNTs has decreased significantly from 45000 to 100 USD per kg (Zhang et al., 2013, Quintero et al., 2014). Even though the price of MWCNTs is already lower than ZrO_2 (183 USD per kg) and WO_3 (249 USD per kg) (Inframat Corporation., 2015), intensive researches are still carried out to reduce the mass production cost of MWCNT. The price of MWCNTs is forecasted to drop until 10 USD per kg in the future (Zhang et al., 2013). The price of MWCNTs is much lower than the price of enzymes (lipases) for industrial-scale use, which cost approximately 1000 USD per kg (Chen et al., 2011).

2.3.4 Other Excellent Properties of CNTs

Even though CNTs are considered to be inert compared to other catalyst support materials such as alumina and silica, the presence of five-membered rings at the caps, unsaturated valences at the edges and defects in the graphitic hexagonal crystallites lead to relatively higher reactive sites (Rodríguez-reinoso, 1998, Balasubramanian and Burghard, 2005) that enable CNTs to be functionalized through chemical methods. Furthermore, compared to activated carbon, the high purity of CNTs can avoid self-poisoning (Zeng et al., 2006, Serp and Castillejos, 2010, Soares et al., 2010) and eventually increase the catalyst's life-time.

The ability to introduce a variety of functional groups onto the CNTs' surface with the purpose of designing specific physicochemical properties (Peng and Wong, 2009, Hussain et al., 2011) allows CNTs to serve as catalyst supports in various catalytic reactions, especially transesterification. In general, the oil sources can be classified as oil with high contents of water and FFA or refined oil. To avoid soap formation when reacting an oil with high FFA and water contents, such as jatropha oil or waste cooking oil (Lam et al., 2010), CNTs can be functionalized with an acid group. On the other hand, for reactions with refined oil, CNTs can be functionalized with a base group. Moreover, the impressive mechanical properties and thermal stability (Zeng et al., 2006, Paradise and Goswami, 2007, Serp and Castillejos, 2010) exhibited by CNTs have encouraged the development of mixed matrix membrane (MMM) used for transesterification. The role of functionalized CNTs can be extended beyond catalyst support to include membrane filling to enhance the mechanical strength, as well as the chemical and thermal stability, of the membrane (Ismail et al., 2009).

2.1 Functionalization Methods to Transform CNTs into Catalysts for Transesterification/Esterification

CNTs can become catalytically active via chemical functionalization. The CNTs involved in biodiesel production are usually MWCNTs (Shu et al., 2009, Villa et al., 2009) because of their lower price compared to SWCNTs. MWCNTs must be functionalized with acidic groups to convert the non-edible oils that contain high level of FFA to biodiesel. Prior to functionalization, CNTs need to be purified to remove the metal catalysts used in the synthesized of the CNTs, as well as other

carbon-based impurities. The purification and functionalization of MWCNTs to transform catalysts for transesterification/esterification will be discussed in detail in the following sections.

2.4.1 Purification of CNTs

The purification of CNTs is needed to remove impurities, such as amorphous carbon, graphite compound, fullerenes and metal particles, that form during the CNTs' synthesis process (Paradise and Goswami, 2007). Among the available purification techniques, liquid phase oxidation by refluxing in an acid solution (Peng et al., 2005, Yu et al., 2008) has been adopted to purify MWCNTs prior to functionalization to generate catalyst supports for transesterification. This acid treatment is usually associated with the ultrasonication treatment because it can help to disentangle and open the tube caps, forming defects in the sidewalls, followed by oxidation along the walls. Aside from purification, the acid treatment plays another vital role by incorporating the ends and sidewalls of the MWCNTs with a high density of oxygen-containing groups (mainly the carboxyl groups) (Balasubramanian and Burghard, 2005). The presence of carboxyl groups on the sidewalls of the MWCNTs is crucial because these groups can undergo a variety of reactions that enable the MWCNTs to be functionalized with specific functional groups (Jiang et al., 2004). The MWCNTs used in the production of biodiesel are usually treated in concentrated nitric acid (HNO_3), a mixture of HNO_3 and hydrochloric acid (HCl) (in a ratio of 1:1) or a mixture of concentrated H_2SO_4 and HNO_3 (in a ratio of 3:1) in the temperature range of 50-80 °C for 3 to 24 h (Peng et al., 2005, Yu et al., 2008, Yun et al., 2011). The purified and treated MWCNTs are

denoted as MWCNTs-COOH (Yun et al., 2011). The MWCNTs-COOH are then ready to be functionalized with specific functional groups (base, acid or enzyme), depending on the feedstock used in transesterification.

2.4.2 Functionalization with acid catalyst groups

The process of functionalizing CNTs with a sulfonic group (SO_3H) is known as sulfonation (Yu et al., 2008). SO_3H has been identified as a promising catalyst group for use in transesterification because high yields of biodiesel can be obtained (Han et al., 2009, Liang and Yang, 2010, Melero et al., 2010, Karimi et al., 2012). Thus, SO_3H seems to be the perfect candidate to be grafted onto the surface of MWCNTs for the catalysis of transesterification/esterification. There are 7 types of sulfonation methods that have been reported to functionalize MWCNTs with SO_3H groups.

2.4.2.1 Thermal Treatment with Concentrated H_2SO_4

Functionalization of MWCNTs via a thermal treatment with concentrated H_2SO_4 is the only reported sulfonation method that has been used to transform MWCNTs into catalysts for biodiesel production (Shu et al., 2009). S-MWCNTs with a high density of SO_3H groups can be prepared by treating MWCNTs with concentrated H_2SO_4 at high temperature (Peng et al., 2005). The synthesis route of s-MWCNTs is shown in Figure 2.2. MWCNTs-COOH obtained from acid oxidation were first mixed with concentrated H_2SO_4 (96-98 %) (Peng et al., 2005, Yu et al., 2008, Shu et al., 2009) and then sonicated for 30 min (Yu et al., 2008, Zhou et al.,

2010). The temperature reported for this sulfonation method ranged between 120-300 °C. The functionalization process was carried out for 10-28 h under a blanket of nitrogen (80 ml/min) (Peng et al., 2005, Yu et al., 2008, Shu et al., 2009, Zhou et al., 2010) to purge or remove moisture in the reaction chamber (Erickson et al., 1997). After the treatment, the product was washed repeatedly with distilled water to remove excess acid and then was dried at 120 °C for 12 h (Peng et al., 2005, Yu et al., 2008). The s-MWCNTs are denoted as s-MWCNTs (Yu et al., 2008). It was reported that a higher sulfonation temperature could produce MWCNTs with a higher density of SO_3H groups (Shu et al., 2009) because high temperatures favour the surface functionality of MWCNTs with SO_3H groups. The s-MWCNTs were found to disperse well in alcohol (ethanol) (Yu et al., 2008, Zhou et al., 2010). This property is believed to provide good contact between the oil, alcohol and catalyst, thus enhancing the reaction rate of transesterification/esterification.

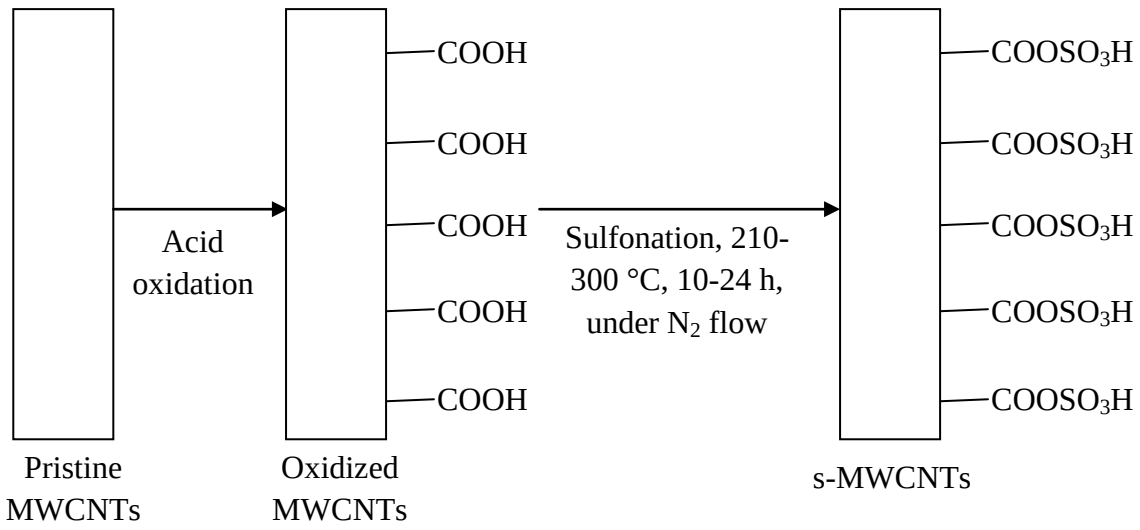

Figure 2.2: Sulfonation of MWCNTs via thermal treatment with concentrated H_2SO_4.

2.4.2.2 In Situ Polymerization of Acetic Anhydride and H_2SO_4

This sulfonation method is usually used to adopt metal nanoparticles (Pd, Ni and Sn) to serve as catalysts for oxidation processes such as ethylene glycol electro-oxidation and ethanol oxidation (Sun et al., 2009, Ramulifho et al., 2012). MWCNTs-COOH from acid oxidation were added to a mixture of 20 ml of H_2SO_4 (95-97 % purity) and 300 ml of acetic anhydride ($(CH_3\text{-}CO)_2O$). The mixture was continuously stirred for 2 h at 70 °C and allowed to cool to room temperature. The resulting product was repeatedly washed with ultrapure water and dried overnight in an oven at 70 °C. The synthesis route is shown in Figure 2.3.

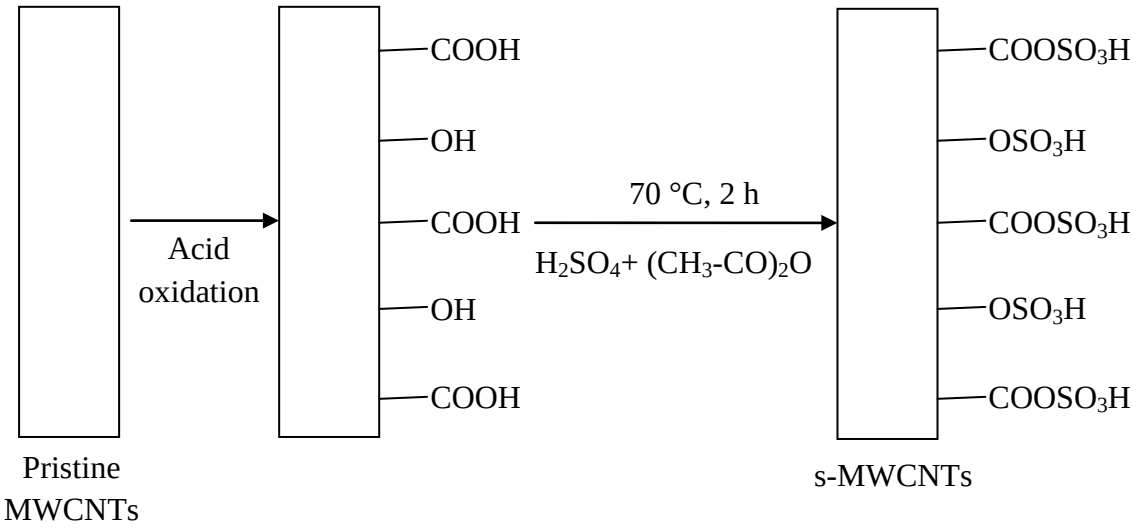

Figure 2.3: Sulfonation of MWCNTs via in situ polymerization of $(CH_3\text{-}CO)_2O$ and H_2SO_4 (Sun et al., 2009, Ramulifho et al., 2012).

2.4.2.3 In Situ Polymerization of 4-Styrenesulfonate

In situ polymerization of 4-styrenesulfonate is another sulfonation approach that can be used to anchor SO_3H groups on the MWCNTs' surface. Two types of 4-styrenesulfonate mixtures have been reported to functionalize MWCNTs: sodium 4-styrenesulfonate (NaSS) mixed with ammonium persulfate ($(NH_4)_2S_2O_8$) and 4-styrenesulfonate mixed with isoamyl nitrite (Du et al., 2008, Sun et al., 2008). In the first combination, a predetermined amount of NaSS and purified MWCNTs were mixed with some deionised (DI) water and stirred vigorously for 10 h at room temperature. Then, $(NH_4)_2S_2O_8$ was added, and the mixture was heated to 65 °C with continuous stirring for 48 h to start the polymerization. The mixture was then washed several times with DI water and filtered. Then, a large amount of 4 M H_2SO_4 was added to the filtered product and stirred for 24 h at room temperature to transform the s-MWCNTs from the Na^+ form to the H^+ form. In the second combination, a proper amount of isoamyl nitrite, purified MWCNTs and 4-styrenesulfonate were stirred for 1 h at room temperature. Then, the temperature was gradually increased to 70 °C with continued stirring for 2 h. The resulting product was washed with dimethylformamide and hot chloroform 3 times and then dried at 70 °C overnight in a vacuum oven to form the s-MWCNTs (Sun et al., 2008). The synthesis routes for both combinations of 4-styrenesulfonate are shown in Figure 2.4. The s-MWCNTs produced by this sulfonation method were used to increase platinum utilisation in fuel cells (Du et al., 2008, Sun et al., 2008).

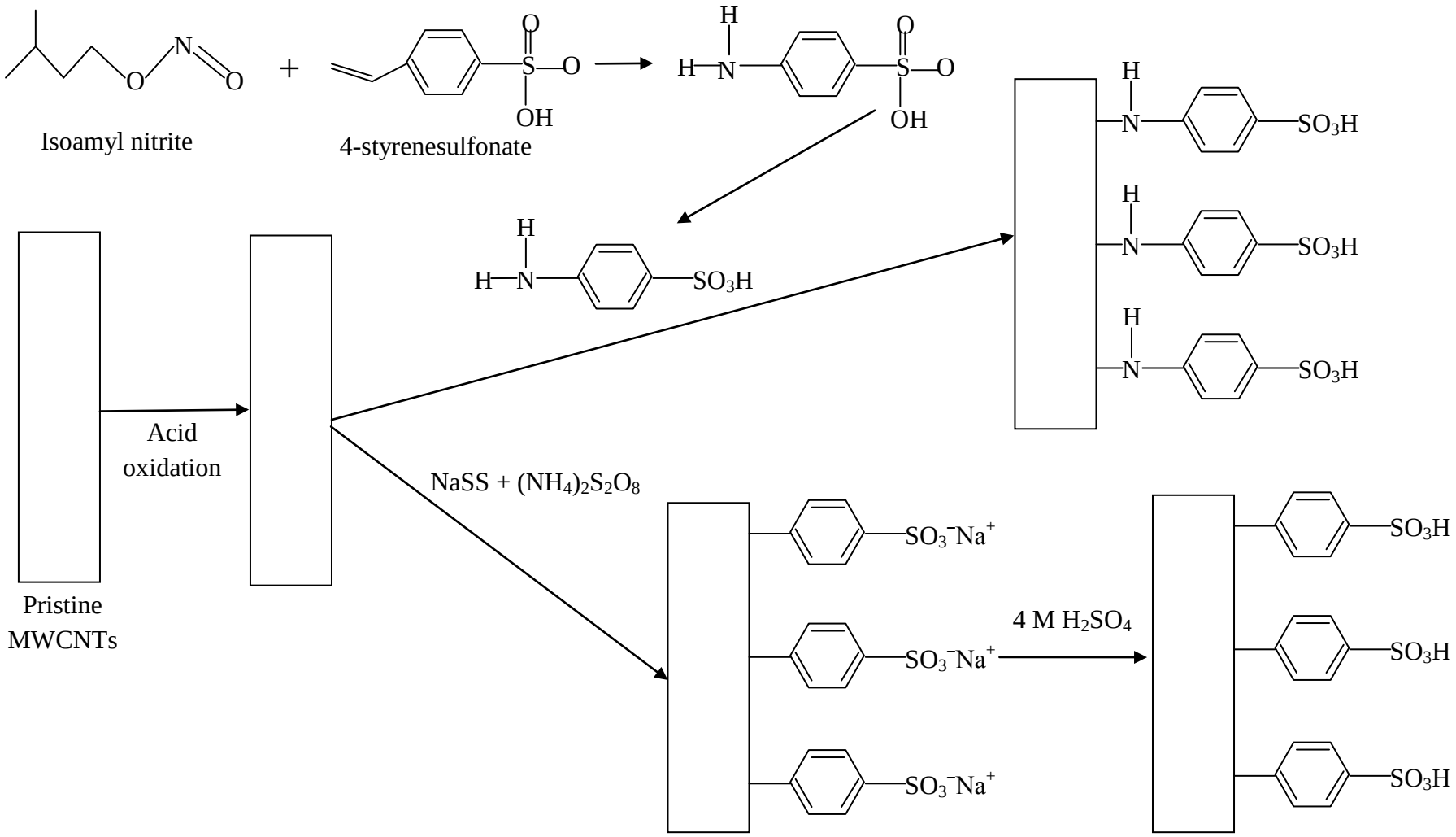

Figure 2.4: Sulfonation of MWCNTs via in situ polymerization of 4-styrenesulfonate (Du et al., 2008, Sun et al., 2008).

2.4.2.4 Thermal Decomposition of Ammonium Sulfate ($(NH_4)_2SO_4$)

First, the MWCNTs were mixed with a predetermined weight percentage of the $(NH_4)_2SO_4$ solution. After the mixture was well agitated, it was heated at 235 °C for 30 min to produce s-MWCNTs (Xu et al., 2005, Du et al., 2008). The synthesis route for this sulfonation method is illustrated in Figure 2.5. Hydrogen atoms are always found on the surface of the MWCNTs because they are usually produced from hydrocarbon materials (Xu et al., 2005, Ho et al., 2008). Therefore, it is believed that the SO_3 groups produced from the decomposition of $(NH_4)_2SO_4$ at 235 °C react with carbon via the surface hydrogen atoms on the MWCNTs to form the SO_3H groups. This method is normally used to sulfonate the MWCNT-supported platinum catalysts for proton exchange membrane fuel cells and polymer electrolyte fuel cells (Xu et al., 2005, Du et al., 2008).

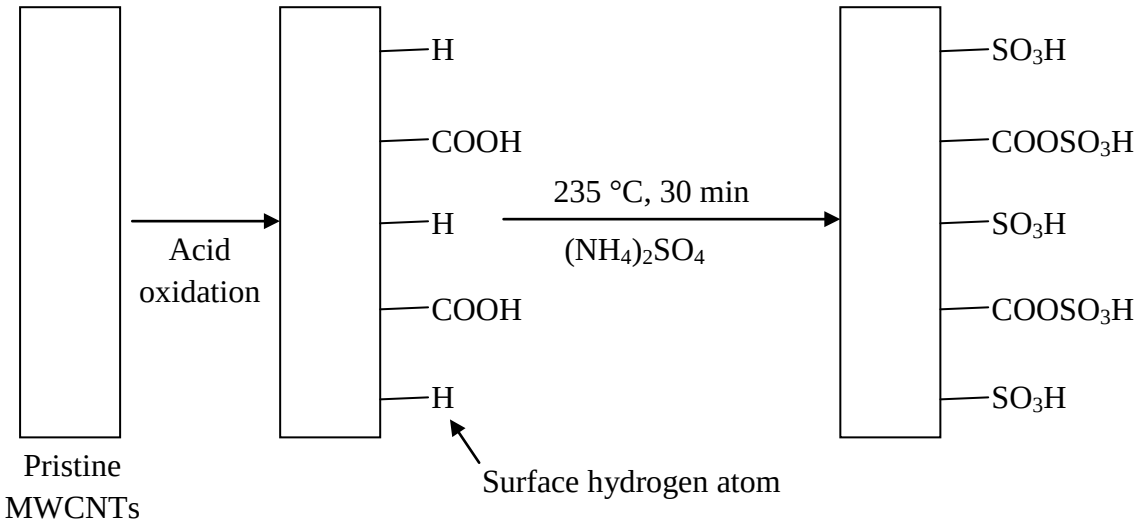

Figure 2.5: Sulfonation of MWCNTs via thermal decomposition of $(NH_4)_2SO_4$ (Xu et al., 2005, Du et al., 2008).

2.4.2.5 Thermal Treatment of *p*-Toluenesulfonic Acid (TsOH) with D-glucose

MWCNTs can also be sulfonated via the thermal treatment of TsOH with D-glucose. The s-MWCNTs prepared by this method are also known as carbohydrate-derived solid acid catalysts (Zhang et al., 2010). The aqueous mixture of purified MWCNTs, TsOH and D-glucose was suspended by ultrasonication for 2 h. Then, the suspension was thermally treated in a Teflon-sealed autoclave at 180 °C for 24 h. The products were filtered and washed repeatedly with deionised water and ethanol and then dried in a vacuum oven at 50 °C for 24 h (Zhang et al., 2010, Fu et al., 2011). MWCNTs sulfonated by this method are denoted as MWCNTs/C-SO_3H (Fu et al., 2011). The possible mechanism in the synthesis of MWCNTs/C-SO_3H is illustrated in Figure 2.6. Glucose was dehydrated to form 5-(hydroxymethyl)-2-furaldehyde (HMF), which would then absorb on to the MWCNTs' surface via π-π^* interactions. Next, the HMF was hydrothermally carbonised and reacted with TsOH to produce C-SO_3H on the surface of the MWCNTs (Zhang et al., 2010, Fu et al., 2011). Finally, the MWCNTs/C-SO_3H was further reacted with pyrrole to obtain the MWCNTs/C-SO_3H/Ppy composite. This carbon base solid catalyst was used as the electrode material for electrochemical capacitors (Fu et al., 2011) and in catalysing the esterification reaction of succinic acid and ethanol (Zhang et al., 2010).

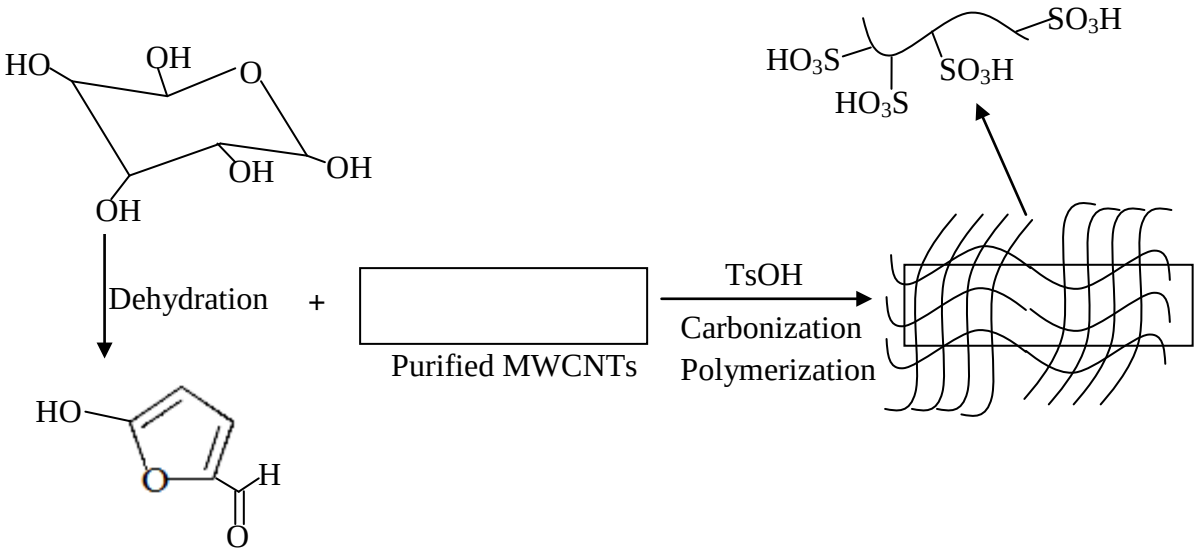

Figure 2.6: Proposed mechanism for the synthesis of MWCNTs/C-SO_3H via thermal treatment of TsOH with D-glucose (Zhang et al., 2010, Fu et al., 2011).

2.4.2.6 Reaction with Aminomethane sulfonic/Aminobenzene sulfonic Acid

The reaction of MWCNTs with aminomethane sulfonic or aminobenzene sulfonic acid is another sulfonation approach that has been used to graft SO_3H groups onto MWCNTs. Before the reaction with aminomethane sulfonic or aminobenzene sulfonic acid, MWCNTs-COOH was dispersed in a thionyl chloride ($SOCl_2$) solution with the aid of sonication for 2 h and then was refluxed with stirring at temperatures in the range of 60-65 °C for 12-24 h (Tripathi et al., 2011, Yun et al., 2011). The residual $SOCl_2$ was removed by either distillation (Tripathi et al., 2011) or filtration of the homogeneous suspension and then washed with excess distilled water (Yun et al., 2011) to obtain MWCNTs-COCl. The aminomethane sulfonic acid solution was prepared by dissolving 2 g of aminomethane sulfonic acid in 250 ml of deionised water. Then, the MWCNTs-COCl powder was added to the solution and stirred for 24 h at 80 °C. The resulting product was recovered by filtration through a nylon membrane, followed by drying at 100 °C (Yun et al., 2011). In contrast, for the

reaction with aminobenzene sulfonic acid, the MWCNTs-COCl was first dispersed in THF and then reacted with a 4-aminobenzene sulfonic acid solution in a slightly basic medium under reflux (60 °C). The mixture was filtered and washed several times with deionised water followed by drying in a vacuum oven for 24 h at 60 °C (Tripathi et al., 2011).

Yang et al. (2008) reported a different approach to sulfonate MWCNTs with 4-aminobenzenesulfonic acid. A mixture containing 150 ml H_2SO_4 (96 %), 200 mg purified MWCNTs and 100 g $(NH_4)_2S_2O_8$ was stirred for 6 h. Then, 5.54 g of 4-aminobenzenesulfonic acid was added to the mixture and stirring was continued for 2 h to effectively disperse the aniline (aminobenzene) throughout the mixture. This was followed by the addition of 2.208 g $NaNO_2$ and the slow addition of 2,2-azobisisobutyronitrile (AlBN) (1.2 g). The mixture was then homogenised for 6 h at 80 °C in an oil bath. The resulting product was filtered and washed with deionised water, acetone and fresh N,N-dimethylformamide (DMF) and then dried in a vacuum oven for 24 h at 50 °C. This type of s-MWCNTs was used in fuel cell applications (Yang et al., 2008, Tripathi et al., 2011, Yun et al., 2011). Figure 2.7 summarized the sulfonation routes of MWCNTs with aminomethane sulfonic or aminobenzene sulfonic acid.

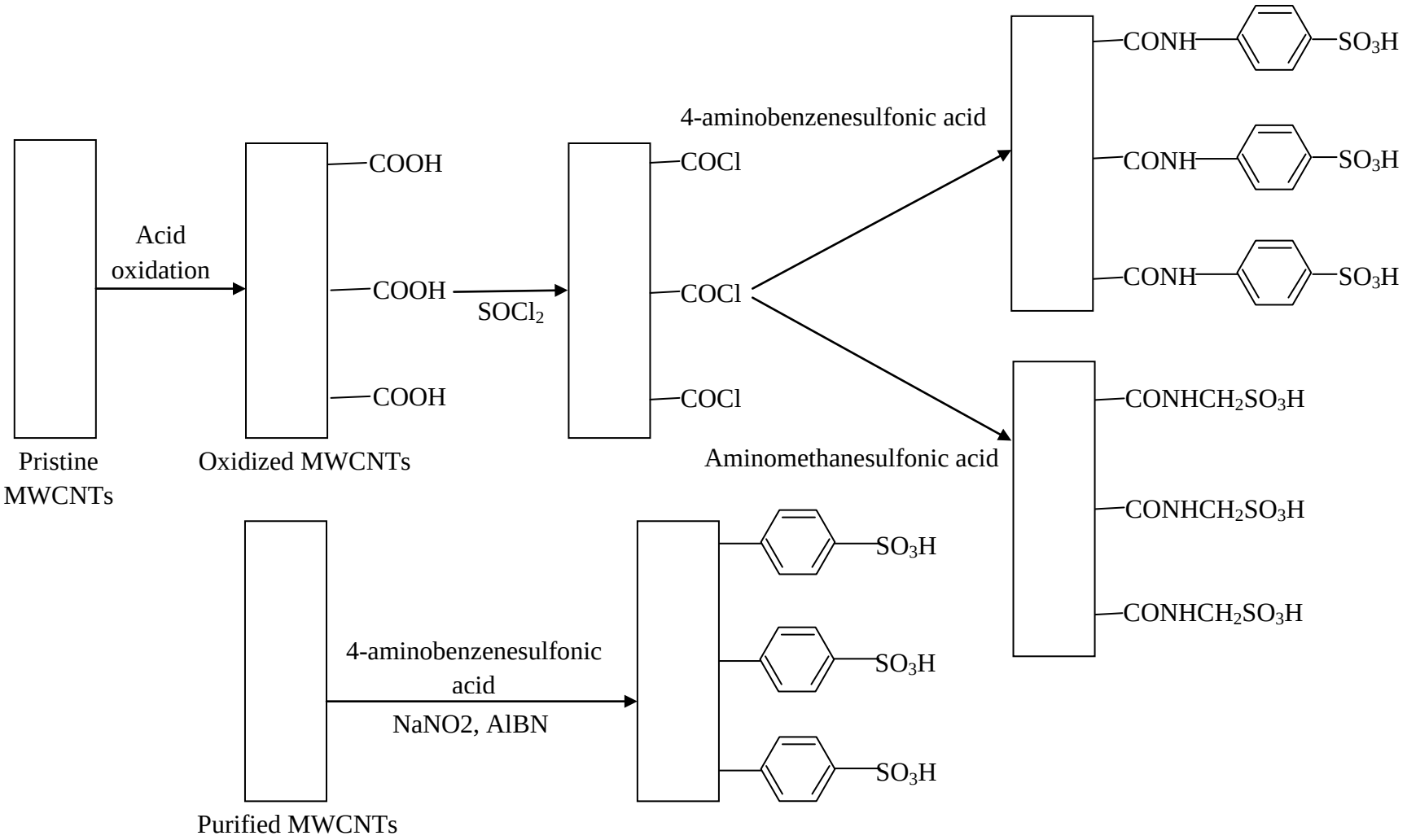

Figure 2.7: Sulfonation of MWCNTs via reaction with aminomethanesulfonic/aminobenzenesulfonic acid (Yang et al., 2008, Tripathi et al., 2011, Yun et al., 2011).

2.4.2.7 Oxidation of Thiol Groups by H_2O_2

In this type of sulfonation method, fluorinated single-walled carbon nanotubes (CNT-F) were used instead of MWCNTs-COOH. First, 70 mg of phosphorus pentasulfide (P_4S_{10}) was stirred into a solution that contained 60 mg of sodium and 7 ml of ethanol for 15 min to generate hydrogen sulfide (H_2S), which further reacted with sodium ethoxide to produce soluble NaSH in the suspension. Then, 22 mg of CNT-F was added to the suspension and heated at 70 °C for 3 h. The black product was filtered, washed with ethanol (3 portions in 10 ml) and dried under vacuum to obtain sidewall thiolated carbon nanotubes (CNT-SH). Then, CNT-SH was oxidised in 5 ml of 30 % H_2O_2 at 60 °C for 1 h. The product was filtered, washed with ethanol and re-suspended in 10 % H_2SO_4 (10 ml) with constant stirring for 1 h to complete the protonation. The final product was filtered, washed until a neutral pH was obtained, and then dried at 80 °C for 12 h (Adams et al., 2009). Figure 2.8 illustrates the sulfonation route of CNT-F via the oxidation of thiol groups by H_2O_2.

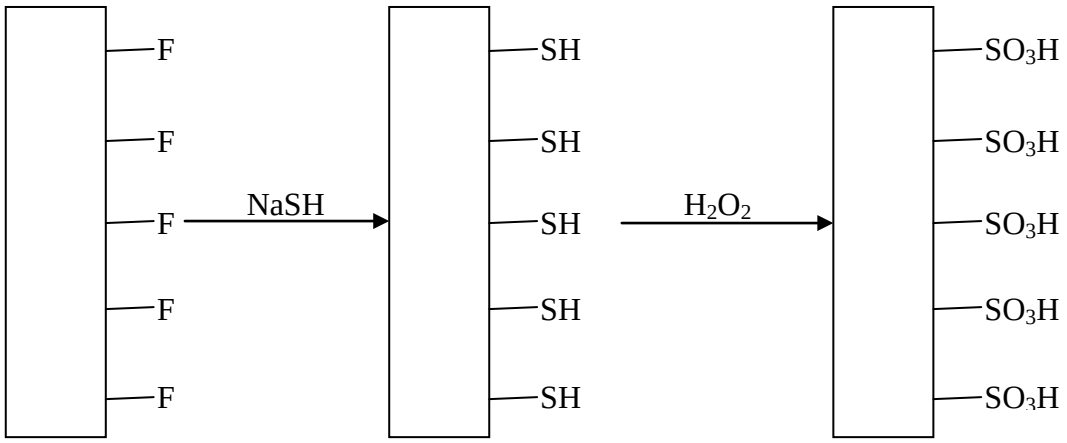

Figure 2.8: Sulfonation route of CNT-F via the oxidation of thiol groups by H_2O_2 (Adams et al., 2009).

2.1 Process Parameters for Biodiesel Production Using Functionalized CNTs as Catalyst

To produce biodiesel in a more sustainable and cost effective manner, the most important process parameters that should be taken into consideration will be discussed in the following sections.

2.5.1 Reaction Temperature

Villa et al. (2010) investigated the effects of the reaction temperature on the catalytic activity of amino-functionalized MWCNTs (Et_3N-CNT) in the transesterification of glyceryl tributyrate with methanol. At 90 °C, a complete conversion of glyceryl tributyrate could be achieved in 2 h. If the reaction temperature was lower than 75 °C, 6 h were needed to achieve 90 % conversion. A higher energy consumption and higher pressure were needed to maintain methanol in the liquid phase at the higher reaction temperature; thus, a lower reaction temperature is more suitable. However, the lower reaction temperature needed a longer reaction time. At a reaction temperature of 60 °C and a reaction time of 8 h, a conversion of 77 % was reported.

The CNTs-based solid acid catalyst s-MWCNTs produced via thermal treatment with concentrated H_2SO_4 were used to catalyse the esterification of oleic acid with methanol to produce methyl oleate. An increase in the reaction temperature from 120 to 135 °C caused a significant increase in the conversion of oleic acid, from 93.2 to 95.5 %, in a reaction time of 1.5 h. The conversion slightly decreased to

95.4 % when the temperature was further increased to 145 °C. The decrease in oleic acid conversion implied that the reaction equilibrium was achieved (Shu et al., 2009b).

Due to the slower reaction rate of acid catalysed transesterification/esterification, the reaction temperature required for acid catalysts is higher than that for basic catalysts. However, acid catalysts are more flexible than basic catalysts because they are less sensitive to FFA and can perform transesterification and esterification reactions simultaneously (Lotero et al., 2005, Miao et al., 2009). Therefore, s-MWCNTs can potentially produce biodiesel from cheaper feedstocks, such as non-edible oils, waste cooking oils and even unrefined crude oils with high FFA content, to reduce the overall biodiesel production cost. Irrespective of the type of catalysts used to produce biodiesel, the conversion of oil to FAME was found to be positively affected by increasing the reaction temperature. This increase can be easily justified because transesterification/esterification is an endothermic process (Shanmugam et al., 2004, Samart et al., 2009). According to the Le Chatelier's principle, by increasing the temperature, the equilibrium of the reaction can shift to the forward direction, favouring the conversion of oil or FFA into FAME.

2.5.2 Methanol to Oil Ratio

The molar ratio of the oil/FFA to methanol is another crucial factor in transesterification or esterification. Based on the stoichiometric equation, three moles of methanol per mole of TG are required for transesterification. Meanwhile, one mole of methanol per mole of fatty acid is needed for esterification (Marchetti et al., 2007a). Due to the reversible nature of both the transesterification and esterification reactions, a large excess of methanol is required to drive the reaction forward towards the formation of FAME (Marchetti et al., 2007b). Different molar ratios of methanol to glyceryl tributyrate (6:1, 12:1, 24:1 and 60:1) were studied in the transesterification reaction catalysed by Et_3N-CNT. It was reported that the system became more active with a higher amount of methanol. Complete conversion was achieved for molar ratios of 24:1 and 60:1 in 4 h and 2 h, respectively. When using a molar ratio of 12:1, 77 % conversion was obtained after 8 h. In contrast, for a molar ratio of 6:1, a fast deactivation of the catalysts was observed, which may have been due to the strong adsorption of oil (glyceryl tributyrate) to the active sites. Considering the overall production cost of biodiesel, the optimum methanol to glyceryl tributyrate ratio was determined to be 12:1 (Villa et al., 2010).

In the esterification reaction with s-MWCNTs as the catalyst, the effect of different molar ratios of methanol to oleic acid (5.2:1, 5.8:1, 6.4:1, 7:1 and 7.6:1) was studied. The oleic acid conversions for methanol to oleic acid ratios of 5.2 and 6.4 were 94.4 and 95.9 %, respectively. Further increasing the molar ratio to 7.6 only caused a slight 0.2 % increase in the oleic acid conversion, to 96.1 %. Therefore, the optimum methanol to oleic acid ratio for the esterification catalysed by s-MWCNTs

was reported to be 6.4:1 (Shu et al., 2009b). It is believed that both the transesterification and esterification reactions begin with the chemisorptions of the triglycerides and fatty acids on the active sites of the catalysts. These chemisorbed molecules are then protonated at the carbonyl group to form carbocations, which are then attacked by methanol to produce esters. In an environment with excess methanol, the attack of the methanol molecules on the carbocations is enhanced, thus increasing the conversion. However, if the molar ratio of methanol to oil/fatty acid is too extreme, the catalyst active sites will be flooded by an excess of methanol instead of triglycerides or fatty acid. Therefore, a concentration of methanol that is too high in the transesterification/esterification system will prevent the TG or fatty acid molecules from being protonated at the active sites of the catalysts (Shu et al., 2009a, Shu et al., 2009b). In addition, the higher the methanol to oil/fatty acid ratios, the more difficult the separation of the non-polar phase from the polar phase (de Boer and Bahri, 2011).

2.5.3 Catalyst Concentration

Shu et al. (2009) studied the effect of various s-MWCNTs loadings on the conversion of oleic acid with methanol. The amount of s-MWCNTs used in the reaction varied from 0.14 to 0.24 wt % based on the weight per cent of oleic acid. The reaction temperature and methanol ratio were fixed at 135 ºC and 6.4, respectively. The conversion of oleic acid was found to be positively affected by the catalyst concentration because the total number of available active sites for reaction increased when the catalyst concentration increased. An increase in the catalyst concentration from 0.14 to 0.20 wt. % caused an increase in the conversion of oleic

acid from 93.6 to 95.4 %. However, a further increase in the catalyst loading, from 0.2 to 0.24 wt %, caused only a minor conversion increase of 0.6 %. Therefore, the reported optimum catalyst concentration for the esterification of oleic acid using s-MWCNTs was determined to be 0.2 wt %.

Regardless of the MWCNTs' functionality (either base or acid catalyst groups), the catalyst concentration used in the reaction was strongly dependent on the amount of functional groups grafted on the MWCNTs (Villa et al., 2009, Villa et al., 2010).

2.5.4 Reaction Time

The reaction time for the transesterification catalysed by Et_3N-CNTs was greatly influenced by the reaction temperature and methanol to oil ratio used during the reaction. At a fixed catalyst concentration and methanol to oil ratio, complete conversion was achieved in only 2 h if the reaction temperature was increased to 90 ^{o}C. As the reaction temperature decreased to 75 ^{o}C, the reaction time required to achieve 90 % conversion was increased to 6 h, whereas at 60 ^{o}C, it took 8 h to achieve only 77 % conversion. However, when using the highest methanol to oil ratio, 60:1, complete conversion was achieved in 2 h. Meanwhile, for a methanol to oil ratio of 24:1, 50 % more time (4 h) was required to achieve complete conversion (Villa et al., 2010). It is believed that the same situation arises wherein an increase in catalyst concentration can reduce the reaction time because the active sites available for reaction are increased.

Regardless of the catalyst types (homogeneous or heterogeneous) (Vicente et al., 1998, Lam et al., 2009, Yee et al., 2011) and the technologies (reactive extraction and supercritical technology) (Zeng et al., 2008, Gui et al., 2009) used to produce biodiesel, the conversion or yield of biodiesel is found to increase with longer reaction times until equilibrium is achieved.

2.2 Catalyst Life-time and Regeneration

Similar to other transesterification catalysts, the Et_3N-CNTs also suffered from a significant deactivation after the first reaction cycle in which the conversion of glyceryl tributyrate dropped to almost 60 % in the second run of the reaction and continued to drop for subsequent cycles. This decrease was due to the strong adsorption of triglycerides on the active sites. However, these adsorbed triglycerides can be easily removed by washing the spent catalyst in methanol several times and drying at 80 °C after each transesterification cycle. The washed and regenerated catalyst was deactivated slightly but still showed an extremely stable catalytic activity in which the conversion was maintained above 90 %, even after 6 reaction cycles (Villa et al., 2009). Thus, it was recommended that the amino-functionalized MWCNTs be pre-contacted with methanol for 10 min before adding the oil to avoid the adsorption of triglycerides to the inner and outer catalyst surfaces (Villa et al., 2010). Villa et al. (2009) studied the leaching of grafted amine by performing acid-base titrations on the spent catalyst. The titration result showed that the generated pH of the spent Et_3N-CNT catalyst was 10.26 and that the content of the corresponding basic groups in the catalyst was 0.96 mmol/g. In comparison to the freshly

synthesized Et_3N-CNT catalyst, with a basic site density of 1.00 mmol/g, the leaching of the basic groups was only 4 % after the 6 cycles.

Thus far, no studies have been performed to investigate the reusability and regeneration of s-MWCNTs used in biodiesel production. The regeneration has only been applied to other sulfonated carbon-based catalyst. The regeneration of the spent sulfonated carbon-based catalyst after treatment with 5 % diluted H_2SO_4 could achieve a FAME yield of 60 %. On the other hand, the washing of the spent catalyst in methanol and cyclohexane did not affect the regeneration of the catalyst activity, producing a FAME yield of below 10 %. This low value might due to the leaching of SO_3H groups from polycyclic aromatic hydrocarbons during the extensive methanol washing (Chen and Fang, 2011).

2.3 Limitations of Conventional Biodiesel Conversion Technologies

Similar to conventional heterogeneous catalysts, conventional biodiesel technologies also encountered a lot of limitations which eventually prohibit the feasibility of the entire biodiesel process. The limitations will be discussed in detail in the following section.

2.7.1 Limitation Caused by Thermodynamic Equilibrium

In the conversion of vegetable oil and fatty acid by transesterification and esterification process respectively, the reversible reaction between the reactant and product indicates that the formation of biodiesel is highly dependent on the proportion of the reactant and the conditions of the transesterification or esterification process. In addition, owing to the reversible nature of both transesterification and esterification reactions, complete conversion of oil or fatty acid into biodiesel can never be achieved. According to Le Chatelier's principle, simultaneously separation of product (biodiesel) or by-product (glycerol or water) from the reaction mixture can improve the conversion of oil or fatty acid into biodiesel. Besides, large quantities of alcohol can also be used to shift the equilibrium of the reaction to the product side and increase the yield of biodiesel (Othman et al., 2010). Unfortunately, high consumption of alcohol is associated with higher production cost.

2.7.2 Wastewater Issue Caused by the Washing of Homogeneous Catalysts

The consumption of alcohol could be reduced by using acid or alkaline catalysts, which could improve the reaction rate and biodiesel yield. However, homogeneous acid solutions that catalyze transesterification/esterification processes, such as H_2SO_4 (Sahoo et al., 2007), HCl (Boucher et al., 2008), or sulfonic acids (Guerreiro et al., 2006) have been largely ignored because they increase the time consumption of the process, require a higher reaction temperature and are corrosive by nature. Although the use of homogeneous alkaline catalysts, such as sodium (Rashid et al., 2008) and potassium hydroxide (Rashid and Anwar, 2008) could

overcome these limitations, it has been reported that the alkaline catalyzed reaction is sensitive to the purity of the reactant. The presence of water and FFA in the raw feedstock could induce a saponification process in which the free fatty acid produced by the hydrolysis of triglycerides reacts with the alkaline catalyst to form soap. The dissolved soap in the glycerol phase would increase the solubility of methyl ester in the glycerol and complicate the subsequent separation process (Vicente et al., 2004). Also, the removal of either the homogeneous acidic or alkaline catalyst using hot distilled water would eventually result in the need to dispose of wastewater (Xie and Li, 2006).

2.7.3 High Energy Requirement

Supercritical alcohol transesterification provides a new path for the production of biodiesel without the aid of a catalyst. The supercritical condition could overcome the mass transfer limitation by enabling the mixture of triglyceride and alcohol to become a homogeneous phase (Pinnarat and Savage, 2008). However, the major drawbacks of this non-catalytic process are its large energy requirement and its infeasibility for large-scale industrial application because of the increased production cost imposed by the high reaction temperature and pressure (Yin et al., 2008).

2.7.4 Multiple Downstream Processing Step

Both the catalytic and non-catalytic transesterification downstream processes will receive a mixture of biodiesel, glycerol, unreacted reactant and catalyst. Ineffective biodiesel separation and purification may cause severe diesel engine problems, such as plugging of filters, coking on injectors, carbon deposits, excessive engine wear, oil ring sticking, engine knocking, and thickening and gelling of lubricant oil (Demirbas, 2007). In order to obtain high-purity biodiesel, the downstream of the transesterification process will undergo various complementary separation stages, such as glycerol separation, catalyst neutralization and biodiesel purification. The multiple downstream processes are time-consuming and require additional cost. A recent report revealed that the current downstream processing alone constituted over 60-80% of the total cost of a transesterification process plant (Tai-Shung, 2007). In addition, the multiple separation and purification stages could cause loss of the biodiesel, resulting in a decrease in the pure biodiesel yield.

2.4 Concept of Membrane Reactor

A membrane reactor is also known as a membrane-based reactive separator (Sanchez Marcano and Tsotsis, 2002). According to IUPAC, a membrane reactor is defined as a device that combines reaction and separation in a single unit (Caro, 2008). Generally, the classification of a membrane reactor is based on four concepts (Ertl et al., 2008): the reactor design (extractor, distributor or contactor), the membrane used in the reaction (organic, inorganic, porous or dense membrane), whether it is an inert or catalytic membrane reactor and the reaction that occurs in membrane reactor (such as dehydrogenation (Caro, 2008), esterification (Caro, 2008,

Buonomenna et al., 2010), water dissociation (Caro, 2008) or wastewater treatment (Drioli et al., 2008)). As illustrated in Figure 2.9, there are two basic configurations of membrane reactor (Lipnizki et al., 1999a). Figure 2.9A shows the layout of a membrane reactor system in which the membrane reactor appears as an external process unit. On the other hand, the membrane reactor shown in Figure 2.9B combines the reactor and membrane separator into a single unit. In comparison to the conventional biodiesel production process, the main advantage offered by the membrane reactor, especially the integrated membrane system, is the reduction of the capital and operating costs because of the elimination of the intermediate processing steps (Sanchez Marcano and Tsotsis, 2002). Recently, the membrane reactor has been applied as a promising technology in biodiesel production (Dubé et al., 2007, Cao et al., 2008b, Baroutian et al., 2010). The esterification/transesterification via membrane reactor is commonly carried out in the pervaporation membrane reactor with conventional configuration shown in Figure 2.9A (Sarkar et al., 2010, Guo et al., 2014). Thus far, no studies have been performed to investigate the feasibility of biodiesel production via membrane reactor with integrated unit.

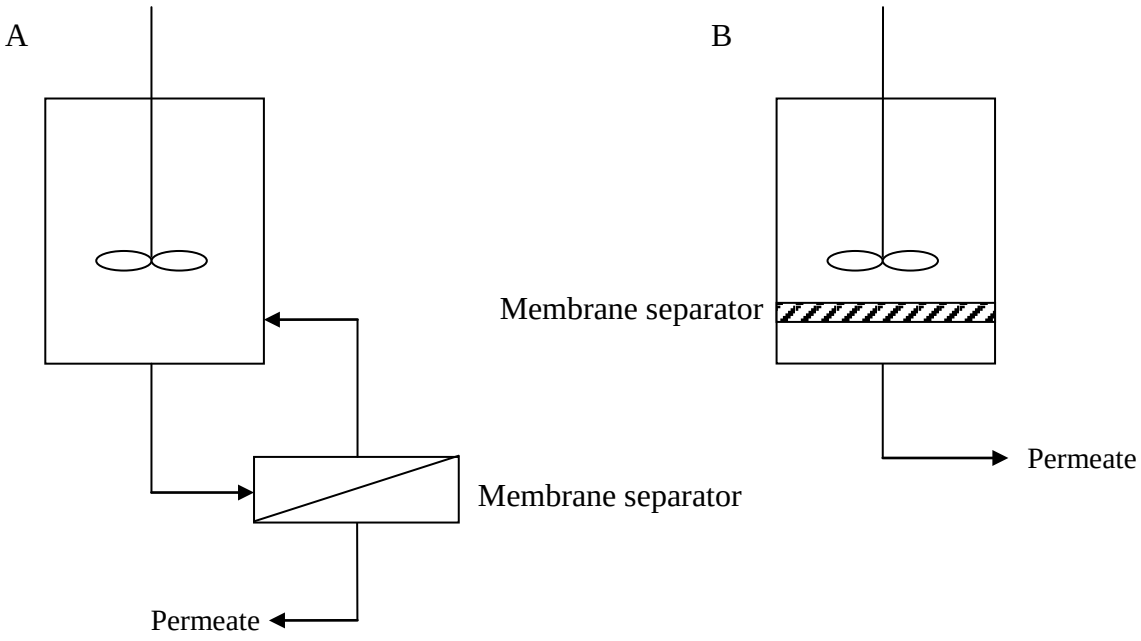

Figure 2.9: Basic layout of membrane reactor: A a conventional membrane reactor system B an integrated membrane reactor system (Lipnizki et al., 1999a).

2.5 Membrane Technology in Biodiesel Production: Concepts and Principles

Membrane separation involves the use of a selective barrier (membrane) to regulate the transport of substances, such as gases, vapours and liquids, at different mass transfer rates (Sirkar and Ho, 1992, Böddeker, 2008). The mass transfer rates of different substances are controlled by the permeability of the barrier toward the feed components (Böddeker, 2008). In the production of biodiesel, the membrane plays an important role by removing glycerol from the product (biodiesel) stream (Guerreiro et al., 2006, Saleh et al., 2010) or retaining the un-reacted triglycerides within the membrane (Dubé et al., 2007, Cao et al., 2008b, Baroutian et al., 2011) as shown in Figure 2.10 and 2.11 respectively. There are two basic principles of operation in

biodiesel production via membrane technology; separation based on oil droplet size (Cao et al., 2008b, Cao et al., 2008a) or catalytic of the target component toward the membrane (Guerreiro et al., 2006, Shao and Huang, 2007, Guerreiro et al., 2010).

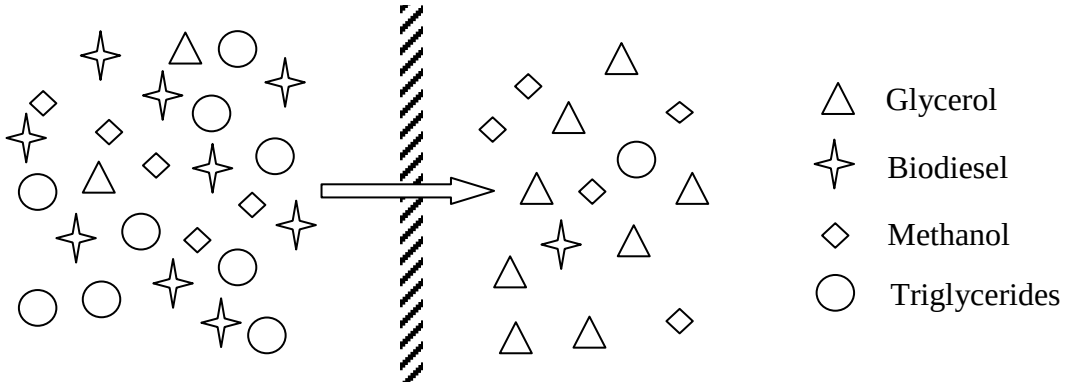

Figure 2.10: Schematic diagram of membrane to remove glycerol from the product stream.

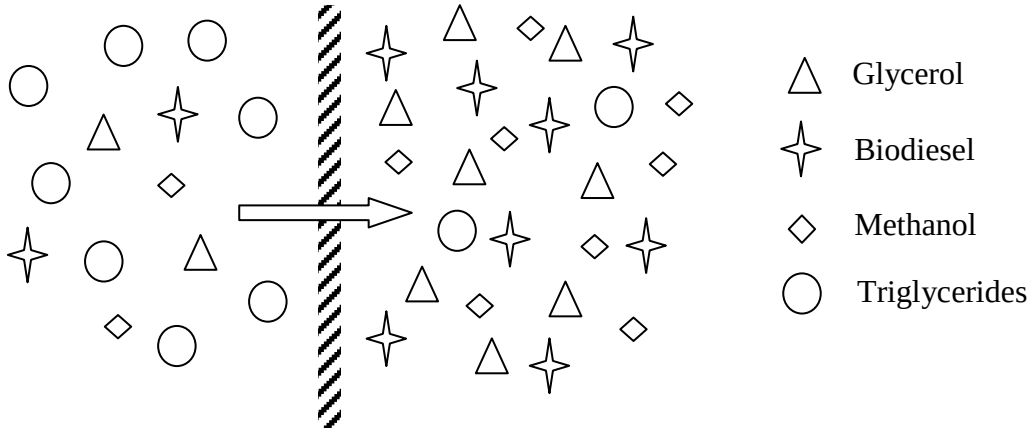

Figure 2.11: Schematic diagram of membrane to retain un-reacted triglycerides within the membrane.

2.9.1 Membrane Separation Based on Oil Droplet Size

Membrane separation based on oil droplet size requires a micro-porous membrane, which is typically a ceramic membrane (Cao et al., 2008a, Baroutian et al., 2010, Baroutian et al., 2011) or a carbon membrane (Dubé et al., 2007). The operation principle of the membrane used in a membrane reactor for biodiesel production is illustrated in Figure 2.12 (Dubé et al., 2007). Because of the difference in polarity, methanol is immiscible with oils and lipids (Cao et al., 2008a). Therefore, a mixture of methanol and lipid will exist in a two-phase system or as an emulsion of lipid droplets suspended in a methanol rich phase (Dubé et al., 2007, Cao et al., 2008a). The immiscibility of the lipid and the methanol is the main cause of the mass transfer limitation in the transesterification reaction, but this emulsified system is favoured in the operation of a membrane reactor (Dubé et al., 2007). In the emulsified system, transesterification is believed to occur at the interface between lipid droplets and the continuous methanol phase in which they are dispersed (Ataya et al., 2006). It has been reported that biodiesel and glycerol, as well as the catalysts (both acid and alkaline catalysts), are soluble in methanol (Zhou et al., 2006, Cao et al., 2008a). Thus, the unreacted lipids will be suspended and dispersed in a mixture of methanol, biodiesel, glycerol and catalyst on the membrane retentate side (Cao et al., 2008a). Because of its smaller molecular size, methanol and other soluble components, such as biodiesel, glycerol and catalysts, are able to pass through the microporous membrane into the permeate stream when the transmembrane pressure (TMP) is increased (Baroutian et al., 2010). Meanwhile, the emulsified lipid droplets with larger molecular size are trapped within the membrane to be continuously converted into biodiesel (Dubé et al., 2007, Cao et al., 2008a, Baroutian et al., 2010).

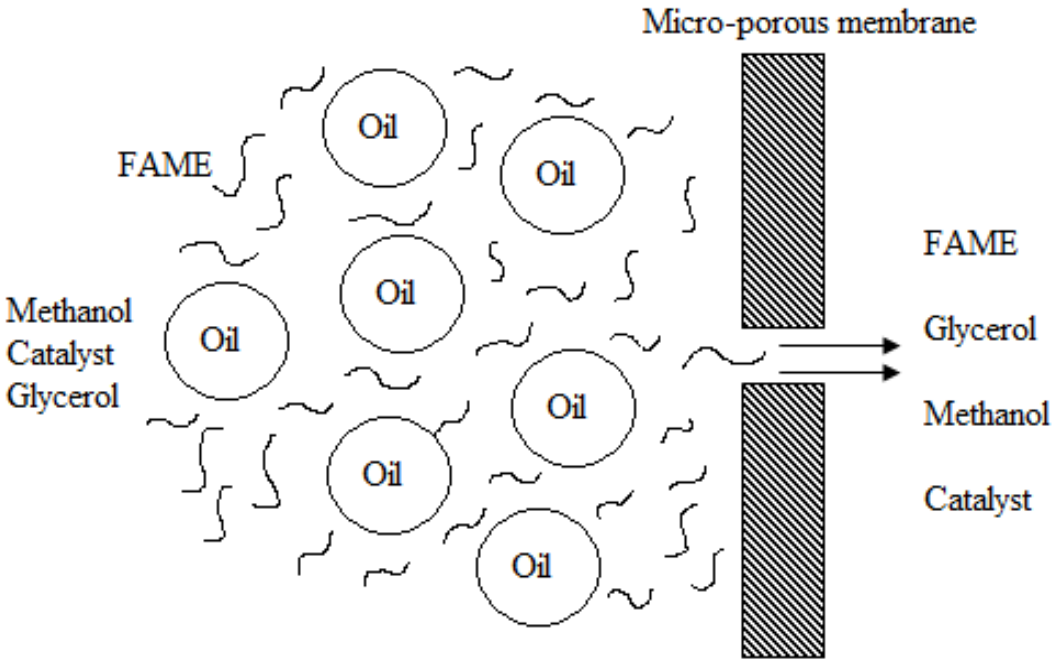

Figure 2.12: Separation of oil and FAME by micro-porous membrane (Dubé et al., 2007).

2.9.2 Membrane Separation Based on Catalytic of Target Component to Membrane

Membrane separation based on the catalytic of the target component to the membrane involves a non-porous dense polymer membrane, such as poly(vinyl alcohol) (PVA) (Guerreiro et al., 2006, Guerreiro et al., 2010, Shi et al., 2010). The operation of this type of membrane is based on the interaction between the target component and the polymer functional groups of the membrane (Guerreiro et al., 2006). In biodiesel production via this type of catalytic charged membrane, glycerol and methanol are able to form hydrogen bonds with the OH groups in the polymer membrane (Guerreiro et al., 2006). Therefore, the glycerol and methanol are continuously removed from the mixture during the reaction (Guerreiro et al., 2006,

Saleh et al., 2010). Meanwhile, the unreacted lipids and the produced biodiesel are retained within the membrane because of their difference in chemical properties with the polymer group of the membrane. In this case, the separation is carried out under atmospheric pressure (Guerreiro et al., 2006).

2.9.3 Membrane Separation Based on Pervaporation

Separation by pervaporation does not rely on the relative volatilities of the components but on the relative rates of permeation through a membrane. Pervaporation is also performed with a non-porous dense membrane that is usually made from a polymer or zeolite (Sharma et al., 2004, Shao and Huang, 2007). Therefore, pervaporation has always been hailed as “clean technology” to replace conventional energy-intensive separation processes, such as evaporation and distillation (Sae-Khow and Mitra, 2010). Pervaporation is most often applied to the dehydration of organic solvents, the removal of organic compounds from aqueous solutions and the separation of organic-organic mixtures (Khayet et al., 2004). However, based on the concept of the affinity membrane, pervaporation is believed to be a possible operation principle in biodiesel production. The concept and applications of pervaporation have been reviewed in detail in several articles (Lipnizki et al., 1999a, Lipnizki et al., 1999b, Shao and Huang, 2007, Pangarkar and Pal, 2008, Sae-Khow and Mitra, 2010).

The pervaporation process is distinct from other membrane process because it combines permeation and evaporation in a single module. A phase change occurs for molecules that permeate through the membrane toward the downstream site (Pangarkar and Pal, 2008). By applying a lower pressure at the permeate side of the membrane, a driving force is created to remove target solutes from the solution mixture (Sae-Khow and Mitra, 2010). Solution-diffusion is the well-recognized mechanism to describe mass transport through non-porous membranes (Lipnizki et al., 1999b, Shao and Huang, 2007, Sae-Khow and Mitra, 2010). The permeation of solute molecules through the membrane occurs in five main steps, which are shown in Figure 2.13 (Sae-Khow and Mitra, 2010). First, the solutes in the reaction mixture diffuse through the liquid boundary layer of the membrane feed (P_{L1} to P_{L2}). At the membrane-liquid interface, specific solutes are selectively partitioned into the membrane (P_{L2} to P_{M1}). Under a pressure difference, the solute molecules diffuse across the membrane (P_{M1} to P_{M2}) (Sae-Khow and Mitra, 2010). Next, the desorption of solute molecules into the vapour phase occurs at the downstream surface of the film (P_{M2} to P_{V1}) (Pangarkar and Pal, 2008, Sae-Khow and Mitra, 2010). Lastly, the gas molecules of the solute diffuse away from the membrane through the boundary layer on the permeate side (P_{V1} to P_{V2}) (Sae-Khow and Mitra, 2010). The sorption of solutes into the membrane depends on the interaction between the solutes and the polymer functional groups in the membrane (Pangarkar and Pal, 2008). Therefore, glycerol molecules have a high probability of being selectively partitioned by the membrane because hydrogen bonds are formed between the glycerol molecules and the OH groups of the polymer membrane (Guerreiro et al., 2006).

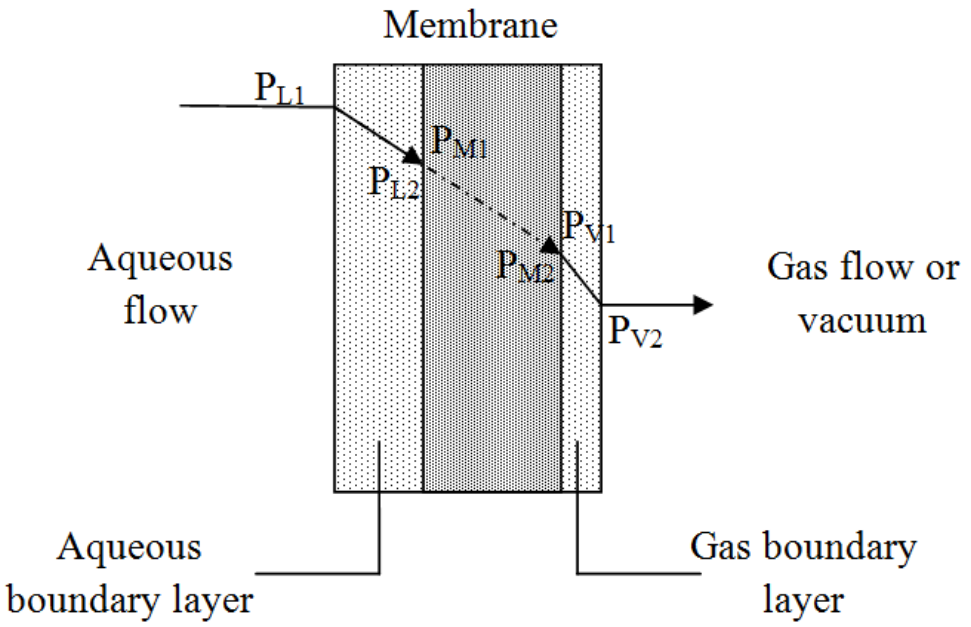

Figure 2.13: Permeation of solute molecules through non-porous dense membrane (Sae-Khow and Mitra, 2010).

Flux and selectivity are the two most important parameters in pervaporation. Flux is defined as the amount of permeate collected per unit area of membrane surface per unit time. The selectivity of solutes is governed by sorption and diffusion, depending on the solute. Sorption depends on the solubility parameter of the solutes and the membrane material. Apart from the physical properties of the solutes, such as the size, shape and molecular weight, the availability of inter/intramolecular free space in the polymer also affects the diffusion coefficient (Pangarkar and Pal, 2008). The last two steps in pervaporation, the desorption step (P_{M2} to P_{V1}) and the diffusion of gas phase from the membrane through the boundary layer (P_{V1} to P_{V2}), are rapid and nonselective, offering the least resistance in the overall transport process (Pangarkar and Pal, 2008).

2.6 Possible Combinations of Membrane and Catalyst in Biodiesel Production

Catalytic membranes in biodiesel production can be classified into two categories: membranes that do not incorporate catalyst and membranes that do incorporate catalyst. In addition, the potential application of MMM with embedded functionalized CNTs in biodiesel production will be discussed. The role of the membrane in this particular configuration is as a medium to provide intimate contact between the oil and the alcohol (Buonomenna et al., 2010).

2.10.1 Membrane without Incorporated Catalyst

This type of noncontact configuration between the membrane and the catalyst is also known as the catalytically inert membrane (Buonomenna et al., 2010) in which the catalysts are added to the reactants but not embedded inside the membrane. The most common catalytically inert membranes in biodiesel production are the TiO_2/Al_2O_3 in ceramic membrane (Baroutian et al., 2010, Baroutian et al., 2011), filtanium ceramic membrane (Cao et al., 2008a, Cao et al., 2008b) and carbon membrane (Dubé et al., 2007) with the separation concept based on oil droplet sizes. The pore sizes of these membranes range from 0.02-0.05 μm (Dubé et al., 2007, Cao et al., 2008b, Baroutian et al., 2010). The catalysts used for catalytically inert membranes include H_2SO_4 (Dubé et al., 2007) or KOH/NaOH (Cao et al., 2008a, Cao et al., 2008b, Baroutian et al., 2010). The schematic diagram for the transesterification reaction via catalytically inert membrane is shown in Figure 2.14 (Cao et al., 2008b, Cao et al., 2008a, Baroutian et al., 2010).

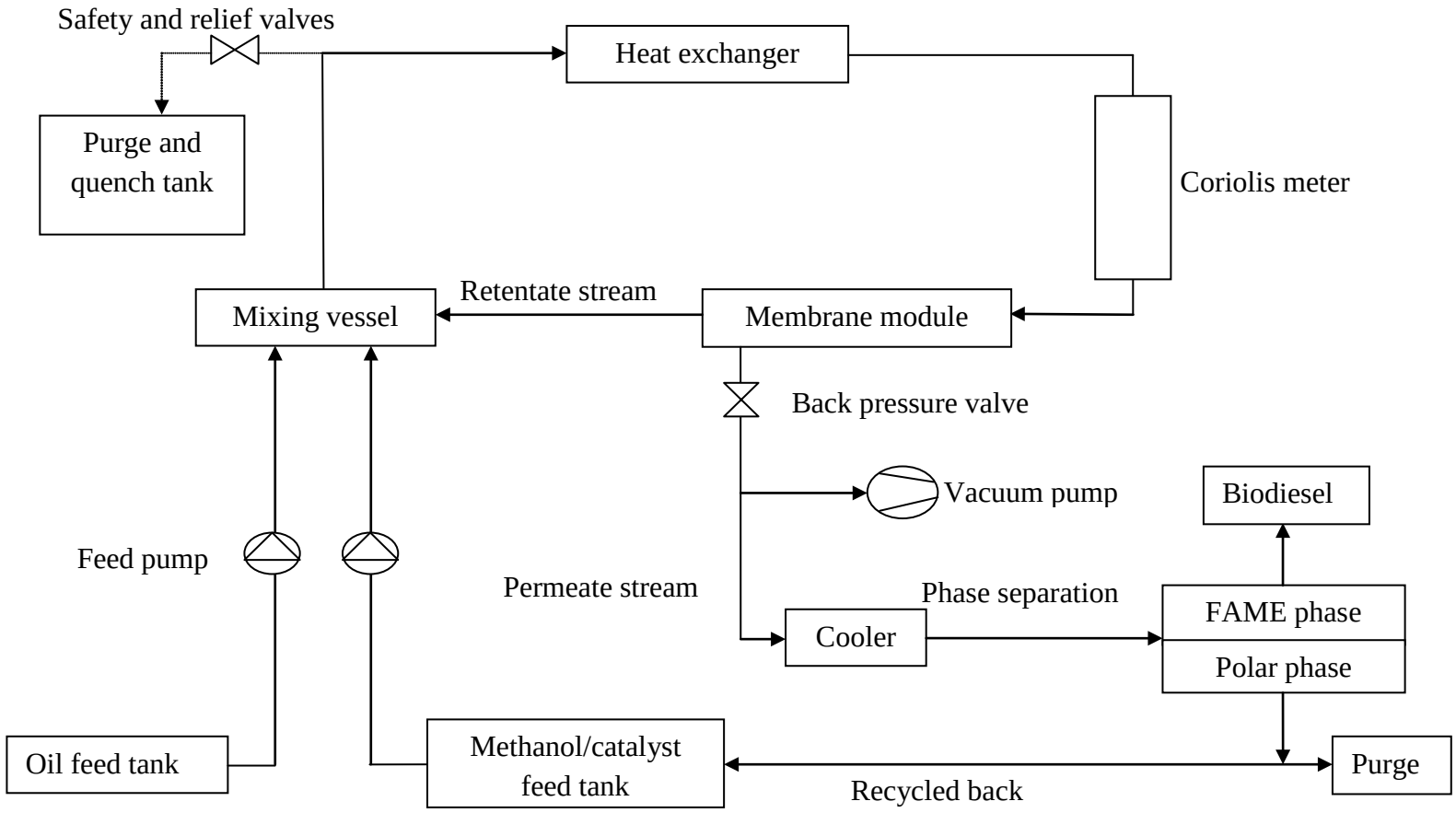

Figure 2.14: Schematic diagram of transesterification reaction via catalytically inert membrane (Cao et al., 2008a, Cao et al., 2008b, Baroutian et al., 2010a).

Initially, a pre-determined amount of oil and a homogeneous mixture of methanol/KOH are charged into a mixing vessel for pre-mixing. Next, the reaction mixture is heated to the desired reaction temperature before charging into the membrane reactor. The permeate stream consists of FAME (biodiesel), glycerol, methanol and catalysts (Dubé et al., 2007, Cao et al., 2008a, Baroutian et al., 2010). Oil droplets with molecular size of 12 µm (larger than the pore size of membrane) (DeRoussel et al., 2001, Cao et al., 2008b) are trapped on the retentate side and recycled back into the mixing vessel (Cao et al., 2008b). The backpressure valve and cooler bring the permeate stream to atmospheric conditions (Cao et al., 2008b). The permeate stream can subsequently be separated into non-polar and polar phases (Cao et al., 2008a). The non-polar phase (collectively known as the FAME-rich phase) consists of more than 85% FAME, and the remainder consists of methanol, trace amount of DG and catalysts (Cao et al., 2008b). Meanwhile, the polar phase, which is also known as the glycerine-rich phase, contains a mixture of glycerol, methanol, catalysts and FAME (Cao et al., 2008b). The results have shown that this catalytic membrane reactor was capable of achieving a high oil-to-FAME conversion of more than 90% for both H_2SO_4 and KOH catalysts (Dubé et al., 2007). Methanol that permeates through the membrane is recycled back to the membrane reactor in order to reduce the overall methanol to oil molar ratio (Cao et al., 2006).

A packed bed membrane reactor consisting of a catalyst supported by activated carbon (Baroutian et al., 2011) was used to avoid the permeation of catalysts through the membrane. The catalysts were prepared by adding activated carbon ranging from 550-810 µm in size into a potassium hydroxide solution. The mixture was subsequently agitated at a temperature of 25 ºC for 24 hours. Next, the

catalysts were packed inside the tubular TiO_2/Al_2O_3 ceramic membrane reactor (Baroutian et al., 2011). The highest oil to FAME conversion for this packed bed membrane reactor was 93.5% (Baroutian et al., 2011), which was comparable to the conversion achieved by the membrane reactor with the addition of H_2SO_4 or KOH catalysts. Moreover, it has been reported that high-quality biodiesel was produced from such a reactor without washing or purification steps (Baroutian et al., 2011).

2.10.2 Membrane with Incorporated Catalyst

A membrane that incorporates catalyst in which the catalyst is immobilised in the polymeric matrix is commonly known as a catalytically active membrane (Buonomenna et al., 2010). Polymeric membranes (Guerreiro et al., 2006, Guerreiro et al., 2010, Zhu et al., 2010) are usually used as catalytically active membranes (Sarkar et al., 2010). A membrane can be made catalytically active by heterogenisation of homogeneous catalysts or incorporation of heterogeneous catalysts inside the polymer matrix (Buonomenna et al., 2010). The catalytically active membrane combines reaction and separation in a single step, realising the concept of reactive separation (Buonomenna et al., 2010); for this reason, the membrane is known as a separative reactor (Stankiewicz, 2003). Presently, PVA membranes are the only reported polymer membranes that have been tested in biodiesel production (Guerreiro et al., 2006, Guerreiro et al., 2010, Sarkar et al., 2010, Zhu et al., 2010) because of their high hydrophilicity, good thermal properties and good chemical resistance (Guan et al., 2006).

A PVA membrane must be modified before it can be transformed into a catalytically active membrane. There are two important steps in preparing a catalytic PVA membrane: crosslinking of PVA followed by esterification of the free PVA-OH groups (Guerreiro et al., 2006, Guerreiro et al., 2010). Sulfosuccinic acid (Guerreiro et al., 2006), succinic acid (Castanheiro et al., 2006), fumaric acid (Guan et al., 2006), maleic acid (Figueiredo et al., 2008) and glutaraldehyde (GA) (Wang and Hsieh, 2010) can be used as the membrane crosslinking agents. Higher degrees of crosslinking can enhance the thermal stability of the membrane (Guan et al., 2006), but they can also cause the membrane to be less hydrophilic and more brittle (Kim et al., 1994). In biodiesel production, increased crosslinking can reduce the degree of membrane swelling in oil and method, thereby reducing the biodiesel yield because oil and methanol are prohibited from diffusion into the membrane in the catalytic reaction (Guerreiro et al., 2006). It has been reported that 92% conversion of oil into FAME can be achieved in 8 hours of reaction time by a membrane made of PVA and poly(styrene sulfonic acid) (PSSA) which is also known as PSSA/PVA membrane. In addition to functionalization with SO_3H groups, the annealing temperature is also of critical importance during the synthesis of the membrane because it controls the degree of crosslinking and the number of SO_3H groups available in the membrane. Such a blended membrane also showed a stable conversion of 80% after 5 repeated runs (Zhu et al., 2010). Heterogeneous catalysts can also be embedded into the polymer matrix in place of homogeneous catalysts. Hydrotalcite, $Mg_6Al_2(OH)_{16}(CO_3^{2-}).4H_2O$ is a suitable solid base catalyst for biodiesel production because of its large specific surface area (Bastiani et al., 2004) and strong Lewis basicity (Roelofs et al., 2000). This catalytic membrane is prepared by dispersing 1 g

of hydrotalcite into a 10% PVA solution. The membrane showed a promising yield of biodiesel (more than 95%) (Guerreiro et al., 2010).

Polymer materials with high thermal stability are preferable in heterogeneous transesterification/esterification because the reaction is usually carried out at temperature higher than 130 ºC (Di Serio et al., 2006, Jitputti et al., 2006, Shu et al., 2009). Therefore, the 4,4'-(hexafluroisopropylidene) diphthalic anhydride (6FDA) base polyimide membrane is a potential candidate for the development of membrane reactor for biodiesel production due to the excellent thermal stability, good chemical resistance to most organic solvents and the attractive mechanical properties. This polyimide membrane can be synthesis via chemical imidization method. This 6FDA based polyimide membrane is extensively being applied in gas separation and pervaporation process. The major advantage of using the 6FDA based polyimide membrane is the hydrophilicity and hydrophobicity of the membrane can be adjusted by using different types of diamine during the synthesis (Le et al., 2012). A schematic diagram of the transesterification/esterification reaction via catalytically active membrane is shown in Figure 2.15. A pre-determined amount of oil/fatty acid and methanol were mixed, heated and pumped into a membrane reactor. Glycerol/water was continuously removed from the reaction mixture once it was produced. The permeate stream contained a binary mixture of glycerol or water/methanol, which was recovered in cold trap immersed in liquid nitrogen. Meanwhile, the retentate that contained unreacted oil was returned to the mixing vessel to be circulated back into the membrane reactor for further reaction (Guerreiro et al., 2006, Figueiredo et al., 2008).

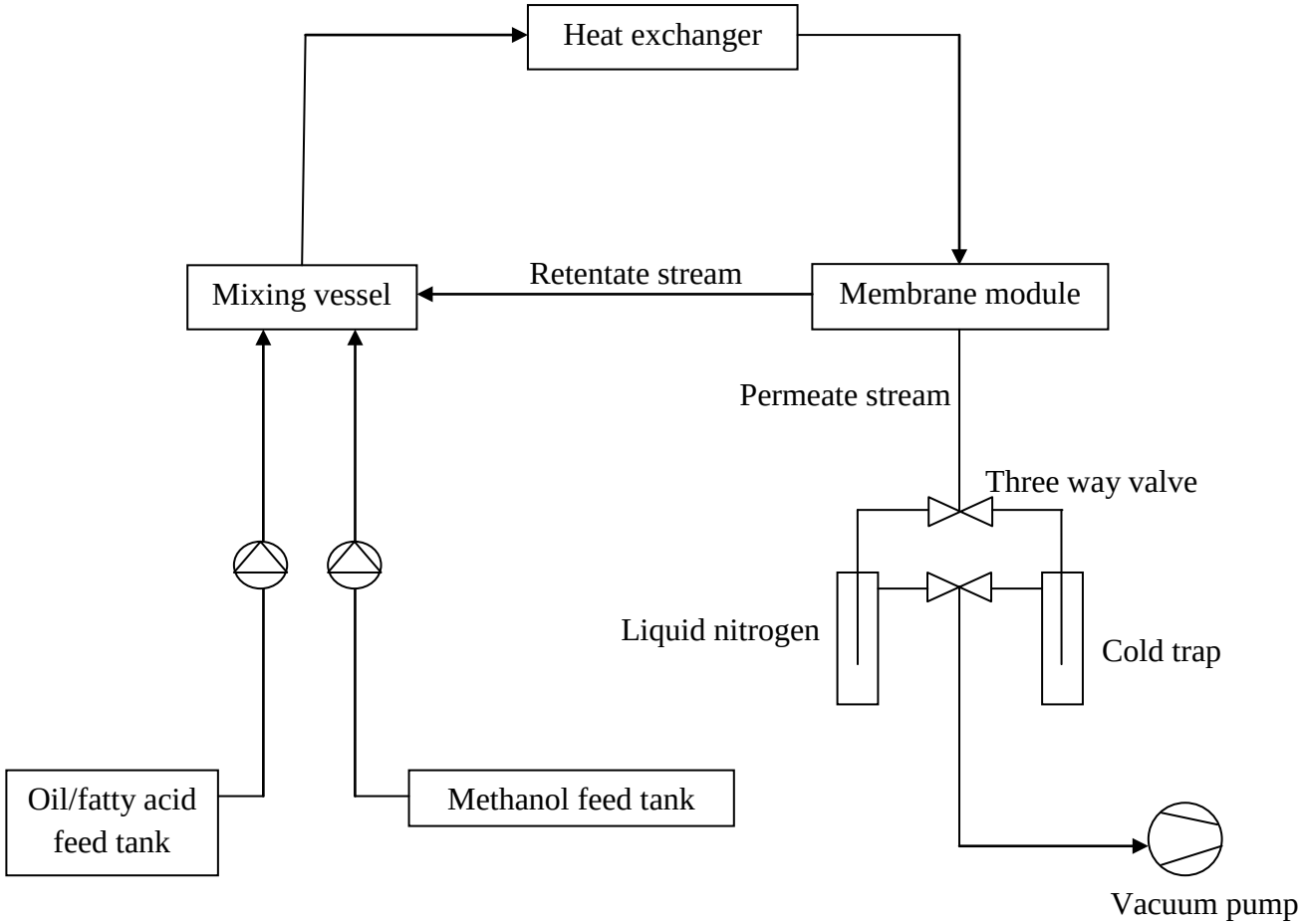

Figure 2.15: Schematic diagram of transesterification/esterification reaction via catalytically active membrane (Guerreiro et al., 2006, Figueiredo et al., 2008).

Glycerol/water and methanol are able to permeate through the PVA membrane because of the hydrogen bonds formed between the glycerol/water and methanol molecules and the OH groups in the polymer. It has been reported that no oil or FAME were detected in the permeate stream, indicating that product loss can be avoided (Guerreiro et al., 2006). As compared to the catalytically inert membrane, the advantage of this catalytically active membrane is the elimination of the purification process for the post-reaction permeate stream.

2.1 Advantages of Membrane Reactor

The catalytic membrane reactor is a new technology for biodiesel production. This technology offers an alternative approach to overcome the common limitations arising from conventional biodiesel production processes. The advantages of the catalytic membrane reactor for biodiesel production will be discussed in the following section.

2.11.1 Environmentally Friendly Process

The production of biodiesel via catalytic membrane reactor is undeniably an environmentally friendly process because of its low energy consumption. Transesterification in a catalytic membrane reactor is carried out under mild operating conditions. The highest reported reaction temperature in a membrane reactor was 70 ºC (Dubé et al., 2007), which is quite similar to the conventional homogeneous transesterification (65 ºC) (Berchmans and Hirata, 2008) but much lower than either heterogeneous or supercritical transesterification. The reaction

temperature for transesterification using a solid basic catalyst, such as magnesium oxide (MgO), calcined hydrotalcite (CHT), zinc oxide (ZnO), KNO_3/KL zeolite and KNO_3/ZrO_2, falls in the range of 180-200 ºC (Di Serio et al., 2006, Jitputti et al., 2006). It has been reported that at approximately, 100 ºC, and alkaline catalysts exhibited very low catalytic activity that only produced a FAME yield of 20% (Di Serio et al., 2006). Additionally, transesterification by solid acid catalysts like tungstated zirconia (WZ), sulfated tin oxide (SO_4/SnO_2), sulfated zirconia–alumina (SZA) and sulfated zirconia (SO_4^{2-}/ZrO_2) were carried out in the range of 200-300 ºC (Furuta et al., 2004, Jitputti et al., 2006, Chen et al., 2007). In addition, there is more hidden energy required in the synthesis of heterogeneous catalysts because most heterogeneous catalysts must be calcined at high temperatures, ranging from 200-500°C (Albuquerque et al., 2008, Lu et al., 2009). Unlike solid catalysts, catalytically active membranes (for example, functionalized poly(vinyl alcohol) (PVA) membranes with SO_3H groups) are fabricated in a low temperature environment (Guerreiro et al., 2006). Of all of the reported biodiesel production methods, supercritical transesterification requires extremely high reaction temperature (240-340°C) and reaction pressure (5.7-8.6 MPa) (Hawash et al., 2009). As compared to biodiesel produced in a catalytic membrane reactor (70 °C and 173.4 kPa), the reaction temperature and pressure required for the supercritical process are 5 and 50 times higher, respectively.

From the perspective of chemical requirements, the catalytic membrane reactor could reduce the usage of solvents and chemicals that are harmful to the environment. For the conventional production method, the reported concentration for

the alkaline catalyst is in the range of 0.5-1% (NaOH) (Marchetti et al., 2007). The concentration of the acid catalyst varied from 1-4%, depending on the FFA content in the oil (Wang et al., 2006, Narasimharao et al., 2007). Compared to the catalyst concentration in the conventional methods, the use of catalysts in the catalytic membrane reactor is lower: 0.05% for the basic catalyst (Tremblay et al., 2008) and 2% for the acid catalyst (Dubé et al., 2007). The catalytically inert membrane reactor and some catalytically active membranes also consume much less methanol than supercritical technology in which the methanol to oil ratio is normally higher than 40 (Barnwal and Sharma, 2005, Sharma and Singh, 2009).

The problem of waste water generation can be greatly reduced if biodiesel is produced through membrane technology. In homogeneous transesterification, the crude biodiesel produced after separation from the glycerol phase still contain catalysts, unreacted alcohol, soaps and free glycerol (Leung et al., 2010). The common approaches to the purification of the biodiesel include washing with distilled water, ether or the use of a solid adsorbent. Adsorbent such as Magnesol can selectively adsorb those hydrophilic materials such as glycerol, MG and DG. Other solid absorbents like activated clay, activated carbon and activated fibre can also be used to purify biodiesel (Atadashi et al., 2011). However, washing with hot distilled or deionised water is the best way to purify biodiesel because both glycerol and methanol are highly soluble in water (Karaosmanoğlu et al., 1996, Leung et al., 2010). In both acid and base-catalysed transesterification, the washing process consists of two steps: neutralisation and water washing. Hot distilled/deionised water at 60-80 °C showed promising performance for washing the FAME phase because of

the higher diffusivity of glycerol from FAME to the water phase at higher washing temperature (Atadashi et al., 2011). Although in the production of biodiesel via catalytically inert membrane, washing would still be needed to remove the catalyst in the permeate stream, but fewer washing steps would be required because of a lower catalyst concentration (0.05%) consumption (Tremblay et al., 2008). In the conventional separation method, 10 litres of water are consumed to wash 1 litre of biodiesel. In contrast, only 0.002 litres of water per litre biodiesel would be needed to purify biodiesel produced via the membrane method (Saleh et al., 2010). Assuming a biodiesel production of 20 million tonnes per year (Licht, 2007) and a biodiesel density of 900 kg/m^3 (Knothe et al., 2005), approximately 59 billion gallons of wastewater are produced by the conventional separation method, and this amount of wastewater could be significantly reduced to only 12 billion gallons by applying membrane separation to biodiesel production and purification. The catalytically active membrane has the potential to eliminate the wastewater problem because the washing step is not required. When the catalyst is embedded in the polymer matrix, thus, the neutralisation and washing steps are not required. Additionally, glycerol is separated from the membrane as it is formed, eliminating the need for the washing step to remove free glycerol content from the FAME phase.

2.11.2 Lower Investment Cost

In the catalytic membrane reactor, both the separation and catalysis processes are combined in single unit operation (Vankelecom, 2002). The integration of these processes into a catalytic reactor is able to reduce the number of operating units, as well as the number of processing steps, thereby is the leading to a reduction

in the size and complexity of the plant and a consequent reduction of the investment cost (Dittmeyer et al., 2004). The catalytically active membrane reactor has the potential to simplify FAME and glycerol separation, catalyst neutralisation.

Even though the phase separation between FAME and water can be easily carried out, the equilibrium solubility of water in FAME after washing is higher than the water content stated in the international standard (Gomes et al., 2010) (500 ppm for both ASTM and EN standard (Knothe et al., 2005)). Therefore, vacuum drying is usually required to remove water from the FAME before storage (Gomes et al., 2010). The neutralisation unit in a conventional production plant (Sdrula, 2010) could also be eliminated because the catalyst is embedded inside the polymer matrix and would not mix with the reactant.

A combination of centrifugation and water washing is used to enhance the separation of glycerol and impurities from the FAME phase. For this method, sufficient residence time is required for the less dense oil to float to the surface of the water, thereby resulting in the preferential separation of the heavy phase. Because glycerol is fully miscible with water and insoluble in the FAME phase, almost all of the glycerol is easily removed by this separation method. However, there are several disadvantages to this method, such as its high initial investment cost, high power consumption and the requirement for considerable maintenance (Saleh et al., 2010). This separation step is unnecessary if biodiesel is produced via catalytically active membrane because glycerol can be simultaneously removed from the reaction mixture, and the need for phase separation between FAME and glycerol is eliminated.

2.11.3 Overcoming the Limitation Caused by Chemical Equilibrium

Another attractive benefit offered by catalytic membrane reactors for biodiesel production is the ability of the process to overcome the limitation imposed by chemical equilibrium and achieve complete conversion. As noted, the transesterification reaction is a reversible reaction that can never reach 100% completion (Cao et al., 2008b). The typical conversion for transesterification is 98% or lower (Knothe et al., 2005).

According to Le Chatelier's principle, the equilibrium of the esterification or transesterification reaction can be shifted toward higher conversion by having one reactant in excess or by selectively removing of one of the products generated in the reaction (Castanheiro et al., 2006). Therefore, a higher methanol to oil ratio is needed to increase oil conversion (Shi et al., 2010). Unlike other conventional methods, the catalytic membrane reactor is capable of driving the transesterification reaction further toward completion by simultaneously removing the products from the reaction mixture. The separation depends on the type of membrane used in the catalytic membrane reactor. With a micro-porous membrane, FAME and glycerol (Dubé et al., 2007, Cao et al., 2008a, Cao et al., 2008b, Baroutian et al., 2010, Baroutian et al., 2011) are separated from the reaction mixture, while for a dense polymeric pervaporation membrane, glycerol and methanol are separated into the permeate stream (Guerreiro et al., 2006). The catalytic membrane reactor can enhance and increase the overall reaction rate when an enzyme (lipase) is used as the catalyst. In the conventional lipase-catalysed transesterification, glycerol is easily adsorbed onto the surface of the lipase, reducing the activity and operational stability

of the lipase (Su et al., 2007). Therefore, the continuous removal of glycerol by membrane technology can decrease the inhibition of lipase, thereby increasing the overall reaction rate (Vankelecom, 2002).

2.11.4 High Process Flexibility of Feedstock Conditions

Water and FFA found in oil sources can create significant problems in transesterification (Atadashi et al., 2011). The presence of water or moisture in the feedstock can cause hydrolysis of the formed methyl esters back to FFA (Van Gerpen and Knothe, 2005), resulting in reduced product. At the same time, water will also hydrolyse triglyceride to diglyceride and FFA, especially at higher temperatures (Atadashi et al., 2011). It has been reported that 0.1% water in an oil source is sufficient to reduce the conversion of oil to FAME during the transesterification reaction (Demirbas, 2007). In short, the presence of water will result in the production of more FFA and reduce the FAME yield. FFA in the reaction mixture will react with water and an alkaline catalyst, such as KOH or NaOH, to form a saponified product (soap).

The homogeneous two-step acid-base catalysed transesterification reaction has been proposed as one of the biodiesel production methods for oil with high FFA content. First, the high FFA oil is subjected to acid esterification to remove the FFA from the oil. The acid esterification is carried out at a temperature of 50 °C for one hour to convert FFA to esters using an acid catalyst (H_2SO_4, 1% w/w), thereby reducing the FFA concentration to below 2%. The second step is alkaline based

catalysed transesterification, which is carried out at 65 °C for two hours using a NaOH catalyst. The reported FAME yield for this two-step transesterification is approximately 90%, which is much higher than the one-step alkaline based transesterification (Berchmans and Hirata, 2008). Although this process can achieve high FAME yield, it involves a greater number of processing steps and reagents. After acid esterification, the reaction mixture must be allowed to settle for two hours; next, the methanol-water fraction in the top layer is removed before alkaline based transesterification. More NaOH is needed in two-step process because it not only serves as a catalyst but also neutralises H_2SO_4 in the acid esterification.

The catalytic membrane reactor, especially with a catalytically active membrane, appears to be a suitable alternative to produce biodiesel from oil with high FFA content because it can be easily modified into an 'acidic membrane' by introducing SO_3H as a functional acid group into the polymer matrix. Furthermore, the water or moisture content found in oil sources can be separated by polymer membranes, such as PVA and polyacrylonitrile (PAN), during the pervaporation process (Chapman et al., 2008), thereby preventing the water from hydrolysing the produced FAME back to FFA. Therefore, cheaper feedstocks such as non-edible oils, waste cooking oils and even unrefined crude oils with high FFA content can be used in biodiesel production (Hasheminejad et al., 2011).

2.11.5 Complying with International Standards

High free glycerol content in biodiesel can cause gum formation around injector tips and valve heads, causing problems in the fuel system. In addition, the burning of glycerine produces the toxic compound acrolein (Hasheminejad et al., 2011). Therefore, the produced biodiesel should be separated from these impurities. Experimental results indicate that membrane separation technology is able to reduce the free glycerol content in biodiesel to a level below 0.02 mass percent, which fulfils the international standards (Saleh et al., 2010, Gomes et al., 2011). In membrane separation, only 0.225% of water by mass was added to FAME to improve separation efficiency (Saleh et al., 2010). Furthermore, compared to conventional biodiesel purification methods, membrane separation can produce biodiesel with higher purity and reduce the loss of ester during the refining process. Moreover, the water content, density at 20 ºC and kinematic viscosity of the biodiesel purified by the membrane technology were also found to comply with the international standards (He et al., 2006).

2.12 Summary

Based on the potentials of s-MWCNTs and membrane technology which can overcome the limitations encountered by the conventional heterogeneous catalysts and conventional biodiesel conversion technologies, the novel integrated pervaporation membrane reactor using s-MWCNTs as catalyst is proposed as for biodiesel production. The MWCNTs will be functionalized with SO_3H group to behave as the catalyst for the esterification of PFAD and the membrane will be synthesized from 6FDA-based polyimide.

CHAPTER THREE

MATERIALS AND METHODOLOGY

This chapter describes in detail about all the experimental works done in this study. This chapter is divided into seven sections. The first section provides information on the raw materials and chemicals used in this study. Then, the detail procedures of the preparation of s-MWCNTs are presented in section two. This is followed by section three, the fabrication of the 6FDA-based polyimide membrane. Then, section four reports the procedures of the esterification of PFAD using s-MWCNTs as catalyst in batch reaction and reactive separation. Next, the reactor system configurations used to conduct the esterification of PFAD in batch reaction and reactive separation are presented in section five. The subsequent section provides detail calculation or measurement of FAME yield. Lastly, at the end of this chapter, information on the characterization of the PFAD, s-MWCNTs and the 6FDA-based polyimide membrane is presented.

3.1 Raw Materials and Chemicals

This section reports the raw materials and chemicals used in the experiment work.

3.1.1 Raw Materials

PFAD used in this study was supplied by a local edible oil manufacturing company. MWCNTs with diameters and lengths ranging from 40 to 60 nm and 1 to 2μm, respectively were purchased from Shenzhen Nanotechnologies Port Co.

3.1.2 Chemicals

All the chemicals used in this study are listed in Table 3.1 with complete details of purity, name of suppliers and purpose of use.

Table 3.1: Lists of chemical reagents used in this study.

Chemicals	Purity (%)	Supplier	Purpose of use
Acetic anhydride ($(CH_3CO)_2O$)	99	Acros Organics, Malaysia	Sulfonation of MWCNTs and as drying agent during the preparation of polymer
Ammonium persulfate ($(NH_4)_2S_2O_8$)	98	Acros Organics, Malaysia	Sulfonation of MWCNTs
Ammonium sulfate ($(NH_4)_2SO_4$)	-	Fisher Scientific Malaysia	Sulfonation of MWCNTs
3,5-diaminobenzoic acid (DABA)	99	Merck, Malaysia	Preparation of polymer
4,4'-(hexafluroisopropylidene) diphthalic anhydride (6FDA)	99	Sigma-Aldrich, Malaysia	Preparation of polymer
n-Hexane	99	Fisher Scientific Malaysia	Solvent for gas chromatography analysis
Methanol	99	Fisher Scientific Malaysia	Esterification reaction and preparation of polymer
3-methylpyridine	99	Merck, Malaysia	Catalyst for polymer synthesis
N-methyl-pyrrolidone (NMP)	99	Merck, Malaysia	Solvent for polymer synthesis
Methyl Heptadecanoate	99	Sigma-Aldrich, Malaysia	Internal standard for gas chromatography analysis
Methyl Linoleate	99	Fluka Chemie, Germany	Standard for gas chromatography analysis

Methyl Oleate	99	Fluka Chemie, Germany	Standard for gas chromatography analysis
Methyl Palmitate	99	Fluka Chemie, Germany	Standard for gas chromatography analysis
Methyl Stearate	99	Fluka Chemie, Germany	Standard for gas chromatography analysis
1,5-naphthalene diamine (NDA)	99	Merck, Malaysia	Preparation of polymer
Nitric acid (HNO_3)	69-70	J.T. Baker, Germany	Purification of MWCNTs
Poly(sodium 4-styrenesulfonate)	-	Sigma-Aldrich, Malaysia	Sulfonation of MWCNTs
Sodium chloride (NaCl)	99	Fisher Scientific Malaysia	Zeta potential measurement
Sulfuric Acid (H_2SO_4)	96	Fisher Scientific Malaysia	Sulfonation of MWCNTs
Tetrahydrofuran (THF)	99	Merck, Malaysia	Solvent for membrane fabrication

3.2 Preparation of s-MWCNTs

3.2.1 Purification of MWCNTs

1 g of pristine MWCNTs was added into 100 ml of HNO_3. The mixture was subjected to 1 h of ultrasonication treatment before being heated to 80 °C for 8 h. The treated MWCNTs were then filtered, washed with distilled water until the pH of the filtrate was the same as the pH of the distilled water and then dried at 120 °C for 12 h to obtain MWCNTs-COOH, which were then subjected to sulfonation (Peng et al., 2005, Yu et al., 2008).

3.2.2 Sulfonation by In Situ Polymerization of Poly(sodium 4-styrenesulfonate)

In this process, 0.4 g of MWCNTs-COOH was vigorously stirred in a mixture of 0.8 g poly(sodium 4-styrenesulfonate) and 100 ml deionised water (DI) at room temperature for 10 h. Subsequently, 1.6 g $(NH_4)_2S_2O_8$ was added, and the mixture was stirred and heated to 65 °C for 48 h to initiate polymerization. After cooling to room temperature, the mixture was diluted with 100 ml of DI water, followed by sonication for 1 h, and then washed repeatedly with DI water. The mixture was filtered, mixed with 500 ml of 4 M H_2SO_4 and then stirred at room temperature for 24 h. Finally, the mixture was filtered, washed with DI water until the pH of the filtrate was the same as that of the pH of distilled water and then dried at 120 °C for 12 h (Du et al., 2008).

3.2.3 Sulfonation by In Situ Polymerization of Acetic Anhydride and H_2SO_4

In this process, 0.2 g MWCNTs-COOH was loaded into a mixture containing 300 ml acetic anhydride and 20 ml concentrated H_2SO_4. The mixture was stirred and heated to 70 °C for 2 h. The mixture was then continuously stirred until reaching room temperature. The resultant product was filtered, washed with distilled water until the pH of the filtrate was the same as the pH of distilled water and then dried at 120 °C for 12 h (Sun et al., 2009, Ramulifho et al., 2012).

3.2.4 Sulfonation by Thermal Decomposition of $(NH_4)_2SO_4$

In this process, 0.4 g of MWCNTs-COOH was mixed with 30 ml 10 % $(NH_4)_2SO_4$ solution and sonicated for 10 min. The mixture was then heated to 235 °C for 30 min. The mixture was then washed with distilled water to remove excess $(NH_4)_2SO_4$ and dried at 120 °C for 12 h (Xu et al., 2005, Du et al., 2008).

3.2.5 Sulfonation by Thermal Treatment with Concentrated H_2SO_4

In this process, 1 g of MWCNTs-COOH was mixed with 50 ml concentrated H_2SO_4 and sonicated for 30 min. The mixture was then stirred for 12 h at 250 °C under nitrogen flow (100 ml min^{-1}). After cooling to room temperature, the product was filtered, washed with distilled water until the pH of the filtrate was the same as the pH of distilled water and then dried at 120 °C for 12 h (Peng et al., 2005).

3.3 Fabrication of 6FDA-Based Polyimide Membrane

3.3.1 Preparation of Polymer

In this study, copoly(1,5-naphthalene/3,5-benzoicacid-2,2'-bis(3,4-dicarboxyphenyl)hexafluoropropanedimide (6FDA-NDA/DABA) with NDA to DABA ratio of 7:3 was prepared. First, 0.014 mol of NDA and 0.06 mol of DABA were mixed with 20 g of N-methyl-pyrrolidone (NMP). The mixture was stirred under nitrogen atmosphere at room temperature to obtain a clear solution. Prior to the addition of 40 g of NMP, 0.02 mol of 6FDA was added into the mixture. The mixture was stirred for 8 h at room temperature (25 – 30 °C) under nitrogen environment. Next, 0.08 mol of acetic anhydride and 0.02 mol of 3-methylpyridine were slowly added into the mixture. The mixture was continued stirring for another 12 h. The resulting polymer was precipitated with methanol and isolated by filtration. The polymer was repeatedly washed with methanol and dried at 100 °C for overnight (Le et al., 2012, Ong et al., 2012).

3.3.2 Fabrication of Dense Polymeric Membranes

A 10 wt% of polymer solution was prepared by dissolving the synthesis 6FDA-NDA/DABA into tetrahydofuran (THF). The solution was filtered using 0.22 µm polytetrafluoroethylene (PTFE) syringe filter. Then the filtered solution was casted on a glass petri dish and left in room temperature for solvent evaporation for 3 to 5 days. After that, the flat-sheet membranes were dried in a vacuum oven at 180 °C for 24 h and cooled down naturally. The vacuum oven dried membranes were then subjected to thermal treatment in a nitrogen environment furnace. The

membranes were heated to 425 °C with a ramping rate of 5 °C per min for 30 min (Le et al., 2012, Ong et al., 2012).

3.4 Esterification of PFAD

3.4.1 Batch Reaction

The esterification to convert PFAD to biodiesel was performed in a pressurised batch reactor equipped with a thermocouple and a magnetic stirrer. First, a pre-determined amount of s-MWCNTs (1 – 3 wt %) was stirred in methanol (ratio 8 – 30) for 10 min to avoid the adsorption of PFAD to the active sites. Then, 10 g of PFAD was charged into the reactor. The reaction was started when the desired temperature was reached and stable. Upon completion, the mixture was cooled to room temperature and filtered. The excess methanol was removed using a rotary evaporator. The volume of the crude fatty acid methyl esters was measured and recorded.

3.4.2 Reactive Separation

Esterification of PFAD with methanol via reactive separation was conducted in pervaporation membrane reactor. The 6FDA-NDA/DABA membrane was sealed at the bottom part of the membrane reactor. In order to reduce the effect of reaction pressure generated by the evaporation of methanol, the esterification of PFAD via membrane reactor was carried out at lower reaction temperature of 135 °C. First, 3 wt % of s-MWCNTs was stirred in methanol (ratio 20) for 10 min. Then, 5 g of PFAD was charged into the reactor. Next, the reaction mixture was heated to desired

temperature. After the desired temperature was reached, vacuum pump was turned on to maintain the permeate downstream pressure at 5 mmHg. The permeate was collected in a cold trap immersed in liquid nitrogen. Upon completion of the reaction, the mixture was cooled to room temperature and filtered. The excess methanol was removed using a rotary evaporator. The volume of the crude fatty acid methyl esters was measured and recorded. The total flux was calculated using the following equation:

$$J = \frac{Q\,(g)}{A\,(m^2) \times t\,(h)} \tag{3.1}$$

where J is the flux (g m^{-2} h^{-1}), Q is the total weight of the permeate collected at time (t) and A is the effective surface area of the membrane.

3.5 Reactor System for The Esterification of PFAD

3.5.1 Batch-Type Reactor

Esterification of PFAD using sulfonated MWCNTs was first performed in a batch-type reactor system as shown in Figure 3.1. The stainless steel batch reactor was equipped with thermocouple, pressure indicator, heater, magnetic stirrer and pressure inlet and release valve. The heater used in this study was equipped with a programmable proportional-integral-derivative (PID) temperature controller. The stirring speed of the reactants was controlled by a hotplate and maintained at 230 rpm.

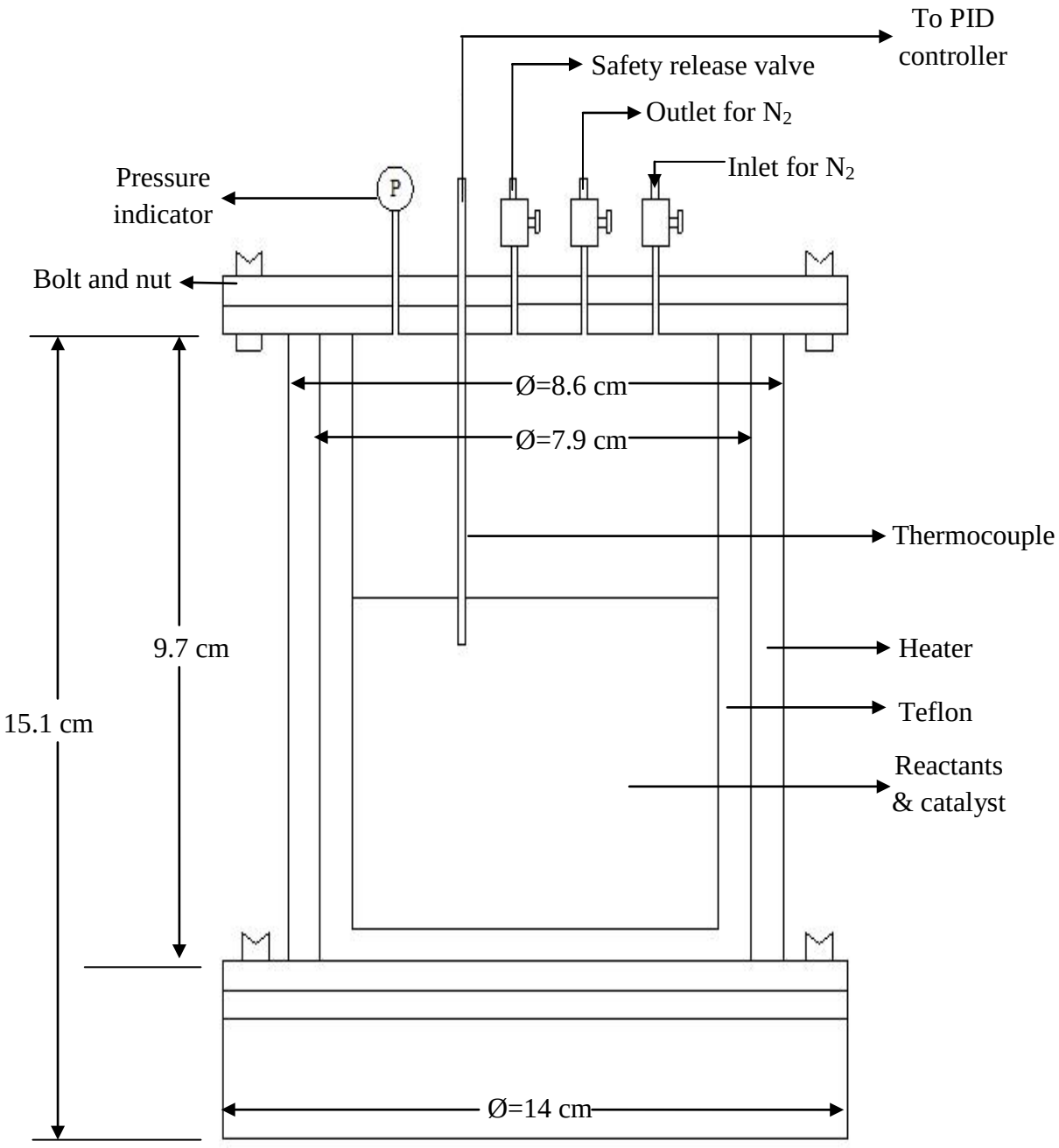

Figure 3.1: Schematic diagram for the batch-type reactor system (not to actual scale).

3.5.2 Pervaporation Membrane Reactor

Esterification of PFAD via reactive separation was performed using membrane reactor as shown in Figure 3.2. The differences between the batch reactor and pervaporation membrane reactor included the modification on the base of the

pervaporation membrane reactor to accommodate the membrane and the elimination of Teflon vessel during esterification via reactive separation. The membrane was placed on top of the porous membrane support which was also known as filter holder. The vapour that diffuses through the membrane will be channelled to a condenser that immersed in liquid nitrogen.

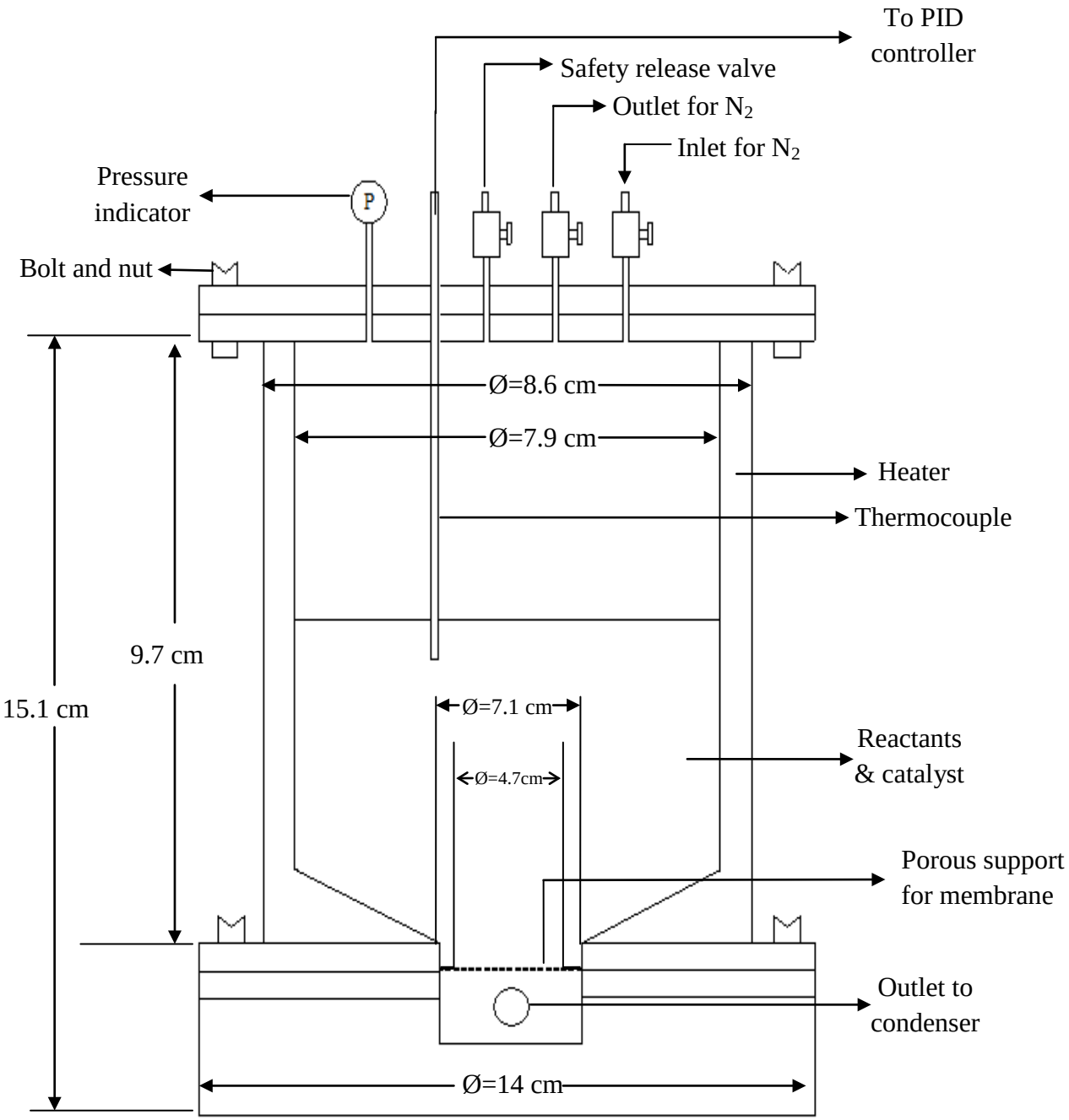

Figure 3.2: Schematic diagram for the membrane reactor system (not to actual scale).

3.6 Measurement of FAME Yield

3.6.1 FAME Yield Analysis Using Gas Chromatography (GC)

To analyze the product composition, only the upper layer of the samples was used. The yield of FAME was calculated based on the analysis result from GC. The sample was diluted before being analyzed using GC. The dilution factor used in this study was 38 (Kansedo, 2009) in which 500 µL of product sample was diluted with 9000 µL of hexane and 500 µL of methyl heptadecanoate that serves as internal standard (IS). The composition and yield of FAME were analyzed using gas chromatography (PerkinElmer, claurus 500) equipped with flamed ionized detector (FID) and Nukol^{TM} capillary column (15m × 0.53mm; 0.5µm film). N-hexane was used as the solvent while helium was used as the carrier gas. The oven temperature was set at 110 °C and then increased to 220 °C at a rate of 10 °C/min. The temperature of the detector and injector were set at 220 and 250 °C respectively. The peaks of different methyl esters were identified by comparing the retention time of each component in the reaction samples with the peak of pure methyl ester standard compounds. The yields of FAME were then calculated using the ratio of the peak area of the sample to the internal standard.

3.6.2 Calculation of FAME Yield

The amount of FAME contained in the sample was calculated based on the peak areas obtained from the analysis of the sample using GC. Figure 3.3 shows a samples GC spectrum for the product of the FAME produced via the esterification of PFAD. Identification of each peaks in the spectrum based on the retention time is listed in Table 3.2.

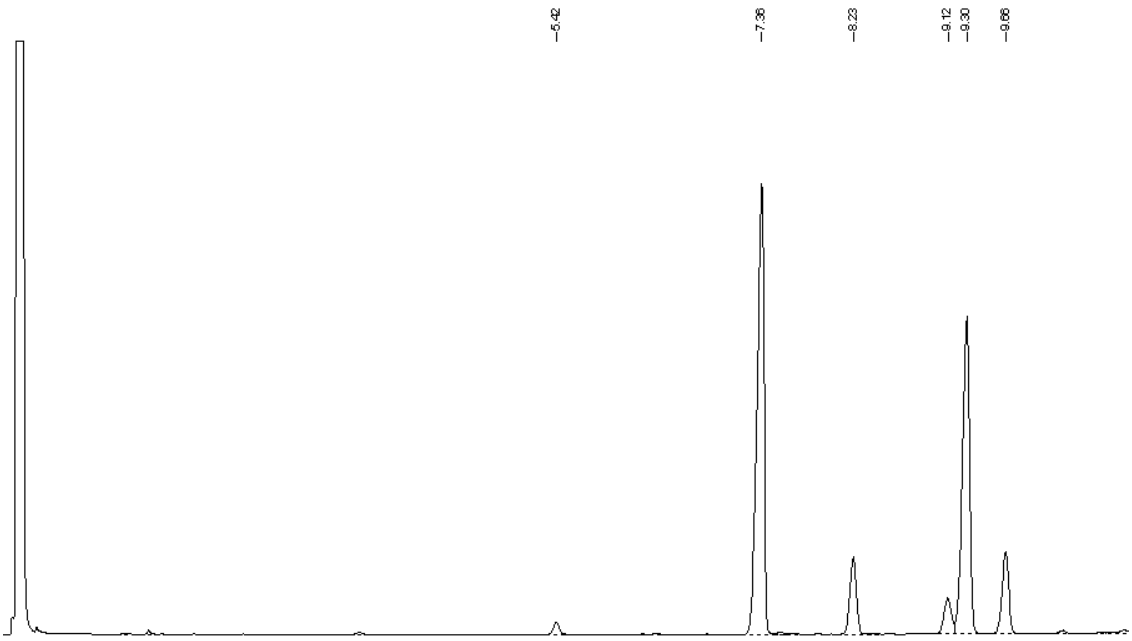

Retention time (min)

Figure 3.3: GC spectrum of PFAD FAME.

Table 3.2: Identification of each peak in GC spectrum of PFAD FAME.

Retention time (min)	Type of FAME
5.42	Methyl myristate
7.36	Methyl Palmitate
8.23	Methyl heptadecanoate (IS)
9.12	Methyl stearate
9.30	Methyl oleate
9.66	Methyl linoleate

The amount of FAME in the samples was calculated using the basis of ratio of peak area to each standard according to Equation 3.2.

$$\text{Weight of FAME (g)} = \frac{R_S}{R_f} \times C_{IS} \times V \times DF \qquad (3.2)$$

where;

R_s = Ratio of peak area of individual methyl ester to peak area of IS in the sample.

$$R_s = \frac{\text{Peak area (FAME) in sample}}{\text{Peak area (IS) in sample}}$$

R_f = Ratio of peak area of individual methyl ester to peak area of IS in standard reference.

$$R_f = \frac{\text{Peak area (FAME) in standard reference}}{\text{Peak area (IS) in standard reference}}$$

C_{IS} = Concentration of IS used; which is 1.00 g/L.

V = Volume of oil, formed after evaporation of the reaction filtrate, ml.

DF = Dilution factor

According to Jiputti *et al*. (2006), the yield of FAME can be calculated using Equation 3.3 as shown below:

$$\text{FAME Yield (wt \%)} = \frac{\text{Weight of FAME (g)}}{\text{Weight of PFAD used (g)}} \times 100\% \quad (3.3)$$

3.7 Characterization of Raw Material, Catalyst and Membrane

3.7.1 Characterization of PFAD

The PFAD provided by a local edible oil company was sent to MY CO2 Sdn. Bhd. in Perai, Penang for characterization. The purpose of the characterization was to obtain the fatty acid composition of PFAD.

3.7.2 Zeta Potential

The zeta potentials of MWCNTs were measured with a Zetasizer Nano-ZS (Malvern Instruments). Prior to the measurement, 1mM of sodium chloride (NaCl) solution was prepared. The concentration of pristine MWCNTs, MWCNTs-COOH and s-MWCNTs in the 1mM NaCl solution was 10 ppm. Subsequently, the mixture was sonicated for 15 min to form a homogeneous solution. Finally, the zeta potential of each sample was measured for three times and the average value was obtained.

3.7.3 Fourier Transform Infrared (FTIR)

The presence of the SO_3H groups was confirmed by FTIR analysis using a SHIMADZU IRPrestige-21 spectrometer over the frequency range of 4000 – 400 cm^{-1}. A mixture of s-MWCNTs sample and potassium bromide was pelleted into a thin pellet, and the IR spectrum was collected after 32 scans. On the other hand, the structure of the 6FDA-NDA/DABA polyimide membrane was confirmed by using the attenuated total reflectance (ATR) mode over the frequency range of 4000 – 400 cm^{-1}. Similarly, the IR spectrum was collected after 32 scans.

3.7.4 Ammonia-Temperature Programmed Desorption (NH_3-TPD)

NH_3-TPD is used to determine the acid strength of the catalyst. Experiments were carried by using using a Micromeritics: Auto Chem II 2920 instrument. Prior to the adsorption of NH_3, 50 mg of MWCNTs sample was placed in a U-shape quartz tube in a temperature-controlled oven and connected to a thermal conductivity detector (TCD). The sample was first dried at 120 ºC with heating rate of 10 ºC in helium (30 cm^3/min) for 1 h. Then, the sample was cooled to 40 ºC under the same helium flow. Subsequently, the sample was exposed to a flow of ammonia gas in mixture (15 % NH_3 in helium) and wait until saturation (a stable baseline was obtained). All the NH_3-TPD profiles were performed from 50 ºC to 600 ºC.

3.7.5 Pulse Chemisorptions

The density of the acid sites of the catalyst was determined by pulse chemisorption using a Micromeritics: Auto Chem II 2920 instrument. The gas used to quantify the total acid sites of the catalyst was 15 % NH_3 in helium. Firstly, 50 mg of sample was placed in a U-shape quartz tube in a temperature-controlled oven and connected to a TCD. The sample was then dried at 120 ºC with heating rate of 10 ºC in helium (30 cm^3/min) for 1 h. The temperature was then cooled to 40 ºC under the same helium flow. Next, 15 % NH_3 in helium was introduced using a pulse method and wait until saturation (a stable baseline was obtained).

3.7.6 Nitrogen Adsorption-Desorption

The specific surface area, average pore width and pore volume were investigated by nitrogen sorption analysis using a Micromeritics ASAP2020 surface area and porosity analyser. The specific surface area was calculated using a Brunauer-Emmer-Teller (BET) plot in a relative pressure range (P/P_o). The total pore volume was determined from the amount of N_2 adsorbed at a P/P_o of 0.99. In addition, the Barrett-Joyner-Halenda (BJH) average pore diameter was determined from the desorption branch of the isotherm.

3.7.7 Raman Spectroscopy Analysis

Raman spectroscopy is a non-destructive method used to analyse the morphology of MWCNTs. The intensity ratio of the D- to G-band (I_D/I_G) in the Raman spectrum is a measure of the average defectiveness of MWCNTs. In this

study, a RenishawInVia (Wotto-under-edge, UK) Raman microscope with a laser excitation of 633 nm was used to investigate the degree of defects in the MWCNTs caused by different ultrasonication periods.

3.7.8 Ultraviolet-Visible Spectroscopy (UV-Vis)

The dispersion of s-MWCNTs in methanol was examined using the Agilent Technologies Cary 60 UV-Vis at a wavelength of 500 nm. Prior to transfer into the cuvette, s-MWCNTs in a methanol solution at a concentration of 5 mg/L were sonicated using a tip sonicator (Hielscher UP200S).

3.7.9 Thermal Gravimetric Analysis (TGA)

The thermal degradation and stability of pristine MWCNTs, MWCNTs-COOH, s-MWCNTs and 6FDA-NDA/DABA polyimide membrane were investigated using a TA Instruments SDT Q600. MWCNTs samples in powder form were placed in an alumina crucible and heated under an air atmosphere at a heating rate of 10 °C/min from room temperature to 900 °C. On the other hand, the membrane samples were cut and crushed into very small pieces before placing in an alumina crucible and heated under nitrogen environment (100 ml/min) at a ramping rate of 10 °C/min from room temperature to 800 °C.

3.7.10 Transmission Electron Microscopy (TEM)

Transmission electron microscopy (TEM) is used to examine the surface morphology of the catalyst sample. The test is performed by using TEM; Philips, model CM12. Initially, the MWCNTs sample was dispersed in ethanol before transferring onto a 400 mesh copper grid supported with carbon film and left at room temperature for few minutes to evaporate the ethanol.

3.7.11 Scanning Electron Microscopy (SEM)

The structure and surface morphology of the 6FDA-NDA/DABA polyimide membrane before and after thermal treatment were examined using a TM3000 tabletop microscope, HITACHI, Japan. Prior to the scanning, the membranes were fractured under liquid nitrogen to avoid polymer deformation.

3.7.12 X-Ray Diffraction (XRD)

Wide angle X-ray diffraction (XRD) measurements of the 6FDA-NDA/DABA polyimide membrane were carried out by a Siemens D5000 X-ray diffractometer at room temperature with Cu Kα radiation operated at 40 kV and 30 mA. The diffraction range was set from 20 to 90º with a sweep rate of 0.04º/s. The average intersegmental distance of polymer chains (d-space) were reflected by the broad peak centering on each X-ray pattern. The average d-spacing for the membrane was determined based on Bragg's law as shown in the following equation:

$$n\lambda = 2d\sin\theta \quad (3.4)$$

where n is an integral number (1, 2, 3…), λ is the X-ray wavelength, d is the d-spacing and θ represents the diffraction angle.

3.7.13 Contact Angle Analysis

Contact angle measurement of the 6FDA-NDA/DABA polyimide membrane was carried out at room temperature by sessile drop technique using a Ramé-Hart standard goniometer Model 250. The membranes were cut into small piece and placed on a glass slide with double side adhesive tape. Then, the glass slide with membrane sample was placed on the equipment. After making sure the reservoir was fully filled with deionized water, a controlled volume (6 µl) of deionized water was dropped onto the membrane. The images were capture and the contact angles were measured by the DROPimage Advanced V2.4 software program. The contact angle of the membrane was the mean average of 10 single measurements.

3.7.14 Tensile Strength Analysis

Prior to the test, the 6FDA-NDA/DABA polyimide membrane was cut into dumbbell-shaped specimens with a length of 3.8 cm. A table-mounted Instron universal testing machine was used to perform the tensile strength test at room temperature. A gauge length of 10 mm with a stretching speed of 0.5 mm/min was used. The tensile strength and elongation at break were determined.

3.7.15 Membrane Swelling Analysis

The 6FDA-NDA/DABA polyimide membrane was cut into a small piece with the dimension of 1cm × 1cm. Then, the membranes were weighted prior to the swelling tests. The dry membranes were then immersed in four different solutions in sealed vessels. The solutions involved in this test included pure methanol, PFAD, distilled water and the FAME mixture that contained FAME and unreacted PFAD. The swelling tests of membrane in PFAD and FAME were performed at a temperature of 60 ºC. Meanwhile, the swelling tests of membrane in pure methanol and distilled water were carried out at temperature of 30 ºC. The excess solvent was wiped out from the membrane surface before taking the measurement. The membranes were weighted every 24 h until their weight reached equilibrium. The swelling degree of membrane, Q was calculated as the following:

$$Q = \frac{W - W_0}{W_0} \tag{3.5}$$

where W is the weight of swollen membrane and W_0 is the initial weight of the membrane.

3.8. Experiment Flow Diagram

The overall experiment flow diagram for this study is illustrated in Figure 3.4.

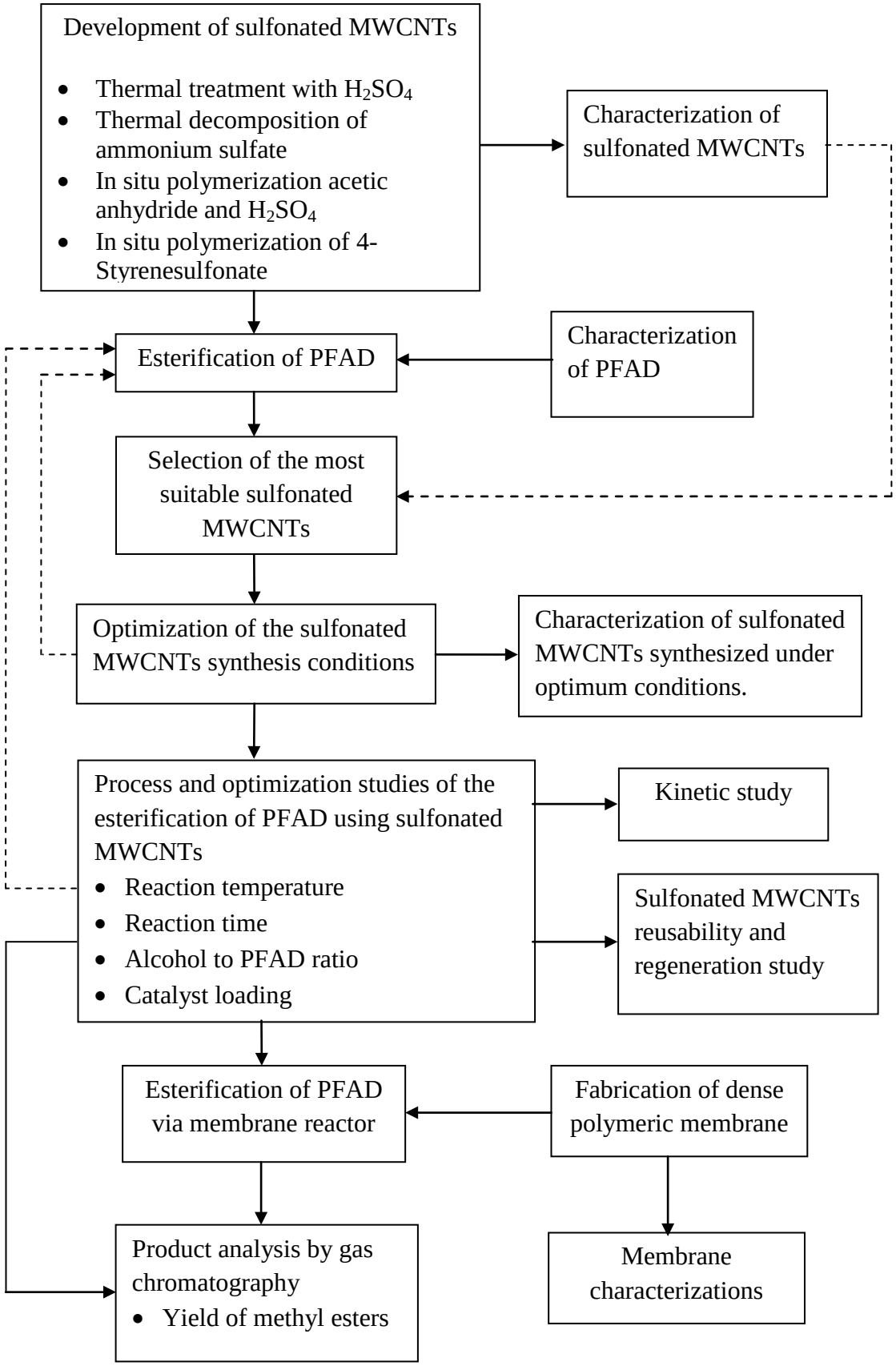

Figure 3.4: Schematic diagram for overall research methodology.

CHAPTER FOUR

RESULTS AND DISCUSSION

Chapter four reports the results and discussion of the study. This chapter is divided into nine sections covering all the experiment works that have been carried out. Section 4.1 presents the results on characterization of PFAD obtained from local edible oil company. This is then followed by the proposed mechanism of FAME formation using s-MWCNTs as a catalyst. Section 4.3 reports the screening study of various sulfonation methods for transforming MWCNTs into catalysts for the esterification of PFAD. Sections 4.4 and 4.5 present the results on the synthesized of s-MWCNTs via thermal decomposition of $(NH_4)_2SO_4$ as well as the process study of the esterification of PFAD using s-MWCNTs, respectively. Next, the catalyst reusability and leaching study, regeneration of the s-MWCNTs and kinetic parameters study are discussed in detail in Sections 4.6, 4.7 and 4.8, respectively. The final section reveals the feasibility of biodiesel production using membrane reactor.

4.1 Characterization of PFAD

The PFAD obtained from local edible oil company is ensured to be obtained from the same batch to avoid variations in fatty acid composition. The fatty acid composition of the obtained PFAD is summarized in Table 4.1.

Table 4.1: Fatty acid composition of PFAD.

Properties	Analysis Result
Fatty Acid Composition (wt %):	
- Myristic acid (C14:0)	1.19
- Palmitic acid (C16:0)	47.96
- Stearic acid (C18:0)	4.32
- Oleic acid (C18:1)	36.26
- Linoleic acid (C18:2)	8.73
- Others	1.54
FFA content (% wt/wt)	98.46

As shown in the table, PFAD contains almost equal amount of saturated (myristic acid, palmitic acid and stearic acid) and unsaturated fatty acids (oleic acid and linoleic acid). The fatty acid composition of PFAD is very similar to palm oil (Joelianingsih et al., 2008) because it is a by-product from the distillation of palm oil. From the characterization above, the average molecular weight of PFAD was calculated to be 264.89 g/mol.

4.2 Proposed Mechanism of FAME Formation Using s-MWCNTs as a Catalyst

The type of acid sites in the s-MWCNTs needs to be determined before predicting the mechanism of FAME formation using s-MWCNTs as a catalyst. Lewis or Brönsted acidity of the catalyst sample can be identified through pyridine-FTIR spectroscopy. Figure 4.1 shows the pyridine-FTIR spectra of s-MWCNTs before and after pyridine adsorption. The peaks at 1646, 1626, 1549 and 1476 cm^{-1} appear only in the spectra of the s-MWCNTs after pyridine adsorption (Fig. 1b). The peaks at 1646, 1626, 1549 cm^{-1} were assigned to the vibration of pyridinium (PyH^+) species (Ng et al., 2006, Ng et al., 2013, Upare et al., 2013), indicating the presence of Brönsted acid site in the s-MWCNTs. The peak at 1476 cm^{-1} could also be due to the coordination of pyridine to Brönsted acid site since no IR bands corresponding to Lewis acid site was observed at 1455 cm^{-1} (Venezia et al., 2011).

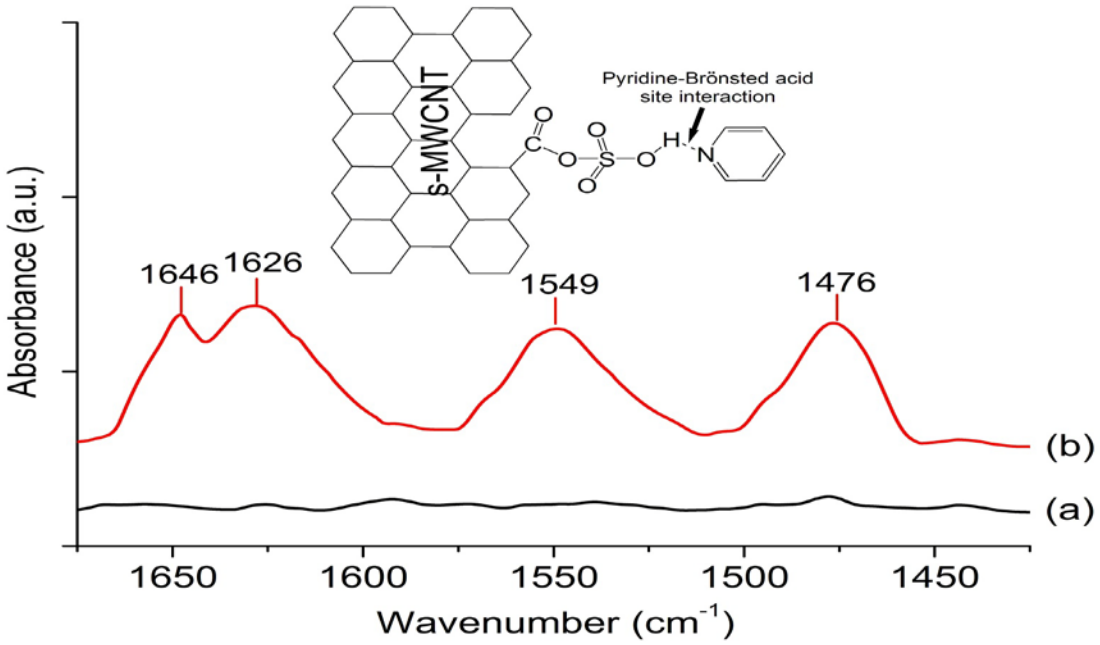

Figure 4.1: Pyridine-FTIR spectra of: A s-MWCNTs before pyridine adsorption, B s-MWCNTs after pyridine adsorption at room temperature (10^{-6} mbar at equilibrium for 2 min).

The mechanism of FAME formation using s-MWCNTs as a catalyst is shown in Figure 4.2. The three electronegative oxygen atoms in the SO_3H group are strong electron withdrawing atoms favouring the dissociation of hydrogen atom into hydrogen ion. As a result, the hydrogen ion tends to be attached by the carbonyl oxygen atom of the fatty acid forming a carbocation (step 1). This is followed by the interaction between the methanol molecule with the carbocation via a nucleophilic attack to form a tetrahedral intermediate (step 2). The proton is then transferred from one oxygen atom to another (step 3) and a water molecule is eliminated by the tetrahedral intermediate (step 4). Finally, the loss of the acidic proton and elimination of water molecule regenerates the SO_3H group on the surface of MWCNTs and an atom of fatty acid methyl ester is produced (step 5).

4.3 Screening Study of Various Sulfonation Methods for Transforming MWCNTs into Catalysts for the Esterification of PFAD

The performance of the s-MWCNTs synthesized via various sulfonation methods were evaluated through the esterification of PFAD and the characterization of catalyst properties.

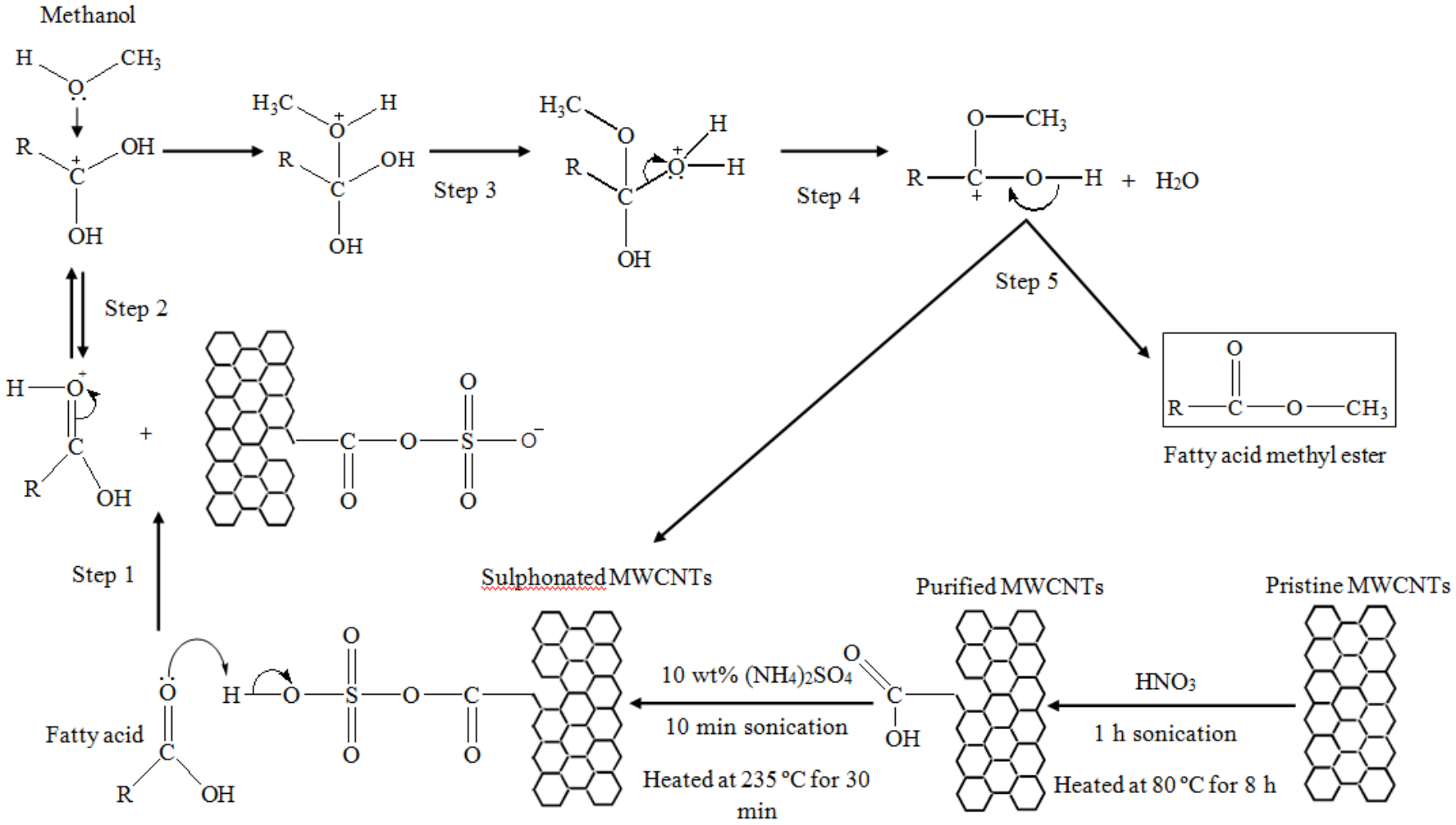

Figure 4.2: Proposed reaction mechanism of FAME formation using s-MWCNTs as a catalyst.

4.3.1 FAME Yield Achieved by Various s-MWCNTs

The purposes of refluxing MWCNTs in HNO_3 before sulfonation were to remove impurities, such as amorphous carbon, graphite compounds, fullerenes, metal particles and most importantly to decorate the ends and sidewalls of MWCNTs with a high density of carboxyl groups for the sulfonation process. The acid treatment was combined with ultrasonication for 1 h to open the tube caps and create defects in the sidewalls to increase the oxidation and sulfonation rate of the MWCNTs (Balasubramanian and Burghard, 2005). As shown in Table 4.2, MWCNTs sulfonated via the in situ polymerization of 4-styrenesulfonate produced the highest FAME yield of 93.4 %. MWCNTs sulfonated via the thermal decomposition of $(NH_4)_2SO_4$ and in situ polymerization of acetic anhydride and H_2SO_4 produced similar FAME yields of 88.0 % and 85.8 %, respectively. Moreover, the lowest FAME yield of 78.1 % was obtained for MWCNTs sulfonated via thermal treatment with concentrated H_2SO_4. The performance of various s-MWCNTs in esterification was highly dependent on the acid density.

Table 4.2: FAME yield and acid density achieved by various s-MWCNTs.

Method of sulfonation	FAME yield (%)	Acid density (mmol/g)
MWCNTs sulfonated by thermal treatment with concentrated H_2SO_4	78.1	0.016
MWCNTs sulfonated by in situ polymerization of acetic anhydride and H_2SO_4	85.8	0.030
MWCNTs sulfonated by thermal decomposition of $(NH_4)_2SO_4$	88.0	0.029
MWCNTs sulfonated by in situ polymerization of poly(sodium4-styrenesulfonate)	93.4	0.061

4.3.2 Characterization of the s-MWCNTs Synthesized via Various Sulfonation Methods

Properties of the s-MWCNTs prepared by various sulfonation methods were examined using various testing instrument such as pulse chemisorptions, zeta potential analysis, Fourier transform infrared spectroscopy (FTIR) and ammonia temperature programmed desorption (NH_3-TPD).

4.3.2.1 Acid Density of the s-MWCNTs

Because SO_3H groups are active sites for the esterification of PFAD and methanol, the conversion or yield of FAME is directly proportional to the density of SO_3H groups on the surface of MWCNTs. The densities of SO_3H groups grafted on the MWCNT surfaces are listed in Table 4.2. Among the sulfonation methods, the in situ polymerization of poly(sodium4-styrenesulfonate) yielded the highest acid site density of 0.061 mmol/g. Thus, the MWCNTs sulfonated via the in situ polymerization of poly(sodium4-styrenesulfonate) produced the highest FAME yield of 93.4 %. The acid densities of MWCNTs sulfonated via the in situ polymerization of acetic anhydride and H_2SO_4 and thermal decomposition of $(NH_4)_2SO_4$ were 0.03 mmol/g and 0.029 mmol/g, respectively. Therefore, similar FAME yields were achieved by these two types of s-MWCNTs. Sulfonation via thermal treatment with concentrated H_2SO_4 produced the lowest acid group density and FAME yield of 0.016 mmol/g and 78.1%, respectively.

In addition to having the highest density of SO_3H groups, the MWCNTs sulfonated via the in situ polymerization of poly(sodium4-styrenesulfonate) may have shown the highest FAME yield due to the resonance structures generated by the benzenesulfonic acid group contained in poly(sodium4-styrenesulfonate). The presence of the three electronegative oxygen atoms not only makes SO_3H a strong acidic group but also an electron-withdrawing group (EWG). As shown in Figure 4.3, when the SO_3H group is attached to a benzene molecule, it will remove the electron density from the conjugated π system of the benzene ring via resonance or inductive electron withdrawal, which deactivates the π system by making it more electrophilic.

However, the presence of positive charges in the ortho positions via the deactivation of the benzene ring by SO_3H favours an esterification reaction because the charges at these positions can play a role similar to that of the sulfur atom in the SO_3H group to serve as active sites for the esterification of PFAD with methanol. Among the four sulfonation methods, only the in situ polymerization of poly(sodium4-styrenesulfonate) can produce s-MWCNTs with benzenesulfonic acid groups, which possess more active sites for the esterification of PFAD with methanol and thereby enhance the reaction rate and FAME yield.

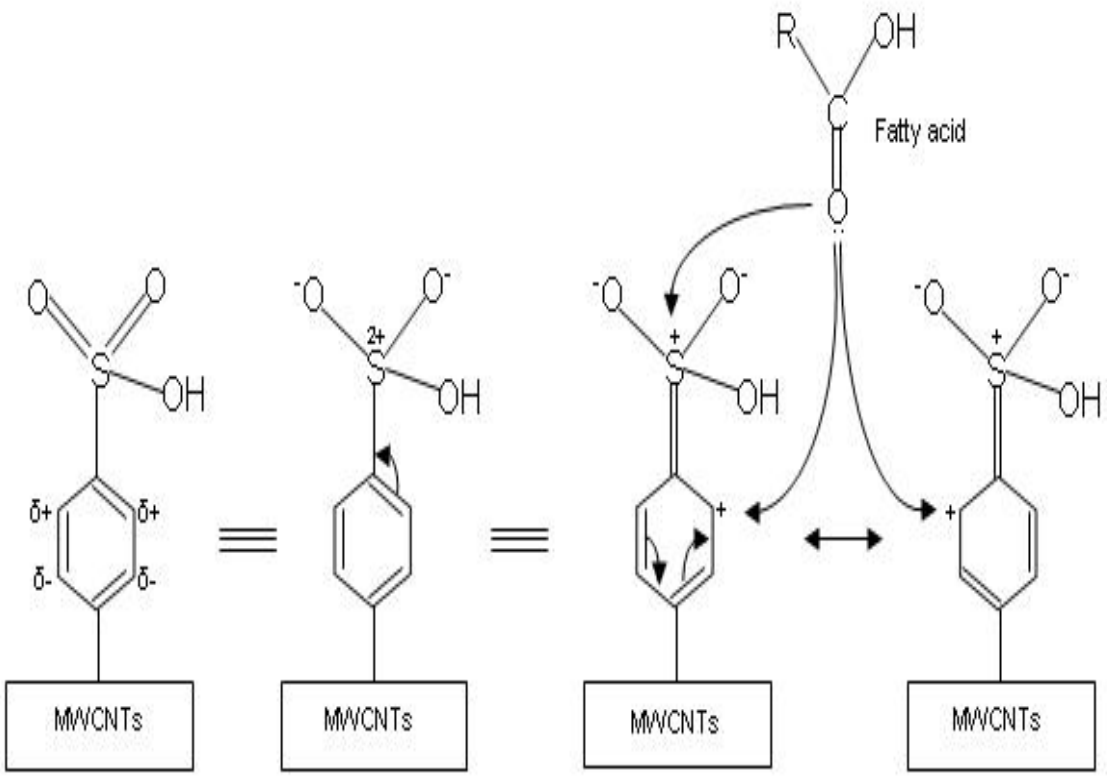

Figure 4.3: Possible active sites for the esterification of PFAD generated by the resonance structures of benzenesulfonic acid group attached to the surface of MWCNTs sulfonated via in situ polymerization of poly(sodium4-styrenesulfonate).

4.3.2.2 Zeta Potential Analysis of the s-MWCNTs

The zeta potential is an electrical potential at the boundary of the hydrodynamic shear plane on the surface of a charged particle in suspension (Lin et al., 2003, Kuo, 2009, Simate et al., 2012). The magnitude of the zeta potential shows the degree of repulsion or attraction between the suspended particles and thus indicates the potential stability of the colloidal system (Simate et al., 2012). In other words, the zeta potential can also be used as an indicator to investigate and compare the surface modification of MWCNTs before and after the acid purification and sulfonation processes. Zeta potential data for the pristine, purified and s-MWCNTs are shown in Table 4.3. The zeta potential value for pristine MWCNTs in this study was -24.5 mV. Moreover, the zeta potential values for the purified and the four types of s-MWCNTs ranged between -54 and -61 mV. Similarly, the zeta potentials of acid-purified and oxidant modified MWCNTs are reportedly more negative than the pristine MWCNTs (Li et al., 2003, Li et al., 2006, Lu and Chiu, 2006, Kuo, 2009, Pu et al., 2013). The high negative surface charge of the acid-purified and s-MWCNTs was due to the presence of acidic groups, such as COOH acid and SO_3H groups. In general, particles with zeta potentials more negative than -30 mV are considered stable in the suspension (Mukherjee et al., 2008). Therefore, the zeta potential analysis proved that the acid purification and sulfonation processes could modify the surface of MWCNTs.

Table 4.3: Zeta potential of pristine, modified and s-MWCNTs.

MWCNTs	Zeta potential, mV
Pristine MWCNTs	-24.5
MWCNTs-COOH	-54.2
MWCNTs sulfonated by thermal treatment with concentrated H_2SO_4	-57.8
MWCNTs sulfonated by thermal decomposition of $(NH_4)_2SO_4$	-57.9
MWCNTs sulfonated by in situ polymerization of acetic anhydride and H_2SO_4	-58.2
MWCNTs sulfonated by in situ polymerization of poly(sodium4-styrenesulfonate)	-60.7

4.3.2.3 FTIR Analysis of the s-MWCNTs

The FTIR spectra of the purified MWCNTs and the four types of s-MWCNTs are shown in Figure 4.4. The spectra show significant differences between the purified MWCNTs and s-MWCNTs; the peaks at 1409, 1254, 1062 and 675 cm^{-1} appear only in the spectra of the s-MWCNTs. The peak at 3691 cm^{-1} was assigned to the -OH groups (Lam et al., 2009). The formation of -OH groups on the s-MWCNTs is very useful because it enhances the catalytic activities of the solid acid catalysts (Park et al., 2008). The band at 3000 cm^{-1} was attributed to the stretching mode of C-H. The band at 1409 cm^{-1} was attributed to the stretching mode of sulfate groups (Peng et al., 2005). The peak at 1254 cm^{-1} also indicated the presence of sulfonate groups (Tripathi et al., 2011). Moreover, the absorption peak at 1062 cm^{-1} was

attributed to asymmetric and symmetric O=S=O stretching vibrations, and the peak at 675 cm^{-1} indicated the presence of S-O groups on the surface of the functionalised MWCNTs (Lin and Wu, 2009). In short, the FTIR spectra indicated the feasibility of grafting SO_3H groups on the surfaces of MWCNTs using the four different sulfonation methods.

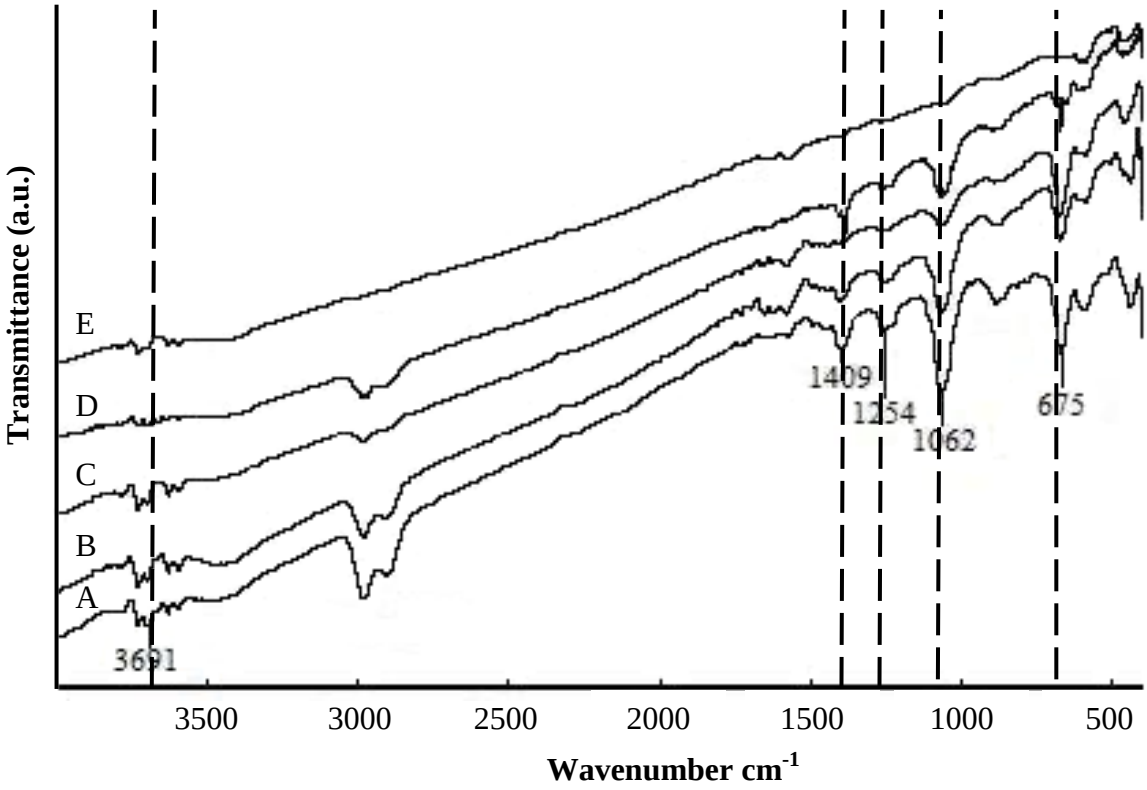

Figure 4.4: FT-IR spectra of various s-MWCNTs: A purified MWCNTs, B MWCNTs sulfonated by thermal treatment with concentrated H_2SO_4, C MWCNTs sulfonated by thermal decomposition of $(NH_4)_2SO_4$, D MWCNTs sulfonated by in situ polymerization of acetic anhydride and H_2SO_4, E MWCNTs sulfonated by in situ polymerization of poly(sodium4-styrenesulfonate).

4.3.2.4 TPD Analysis of the s-MWCNTs

The TPD profiles of desorbed ammonia (NH_3) on different s-MWCNTs are shown in Figure 4.5. The desorption peaks observed at temperatures above 200 °C were attributed to strong acid sites (Lam et al., 2009). The NH_3-TPD results show

that the desorption peaks of all of the s-MWCNTs were observed at temperatures above 200 °C, which further demonstrates the ability of all tested sulfonation methods to graft strong acid groups on the surface of MWCNTs, although the resulting acid densities are different. The NH_3-TPD results also indicate that the s-MWCNTs are stable at the reaction temperature (170 °C) because of the high stability of the active sites on the catalysts. Thus, the problem of leaching of the sulfate groups from s-MWCNTs into the reaction medium can be reduced and thereby enhance the reusability of the catalysts.

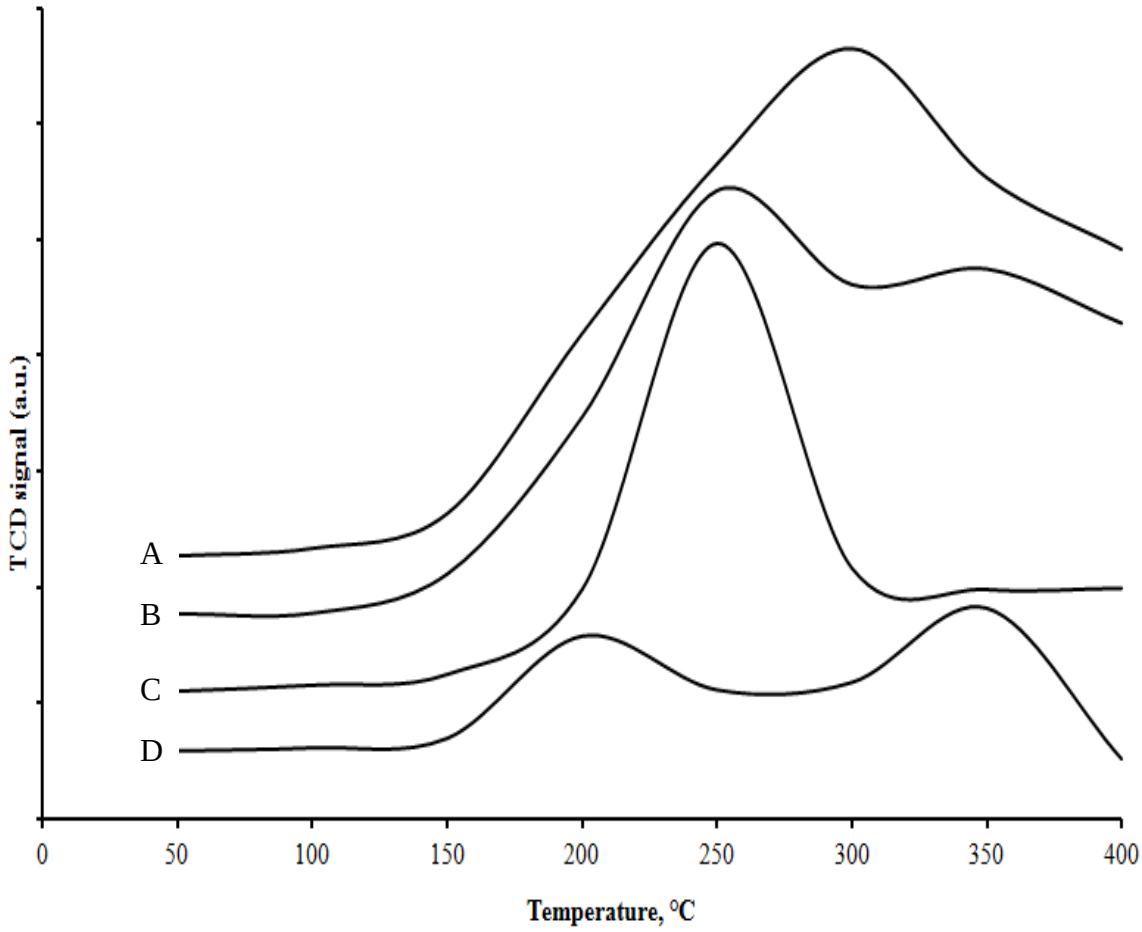

Figure 4.5: NH_3-TPD profiles for different s-MWCNTs: A MWCNTs sulfonated by thermal treatment with concentrated H_2SO_4, B MWCNTs sulfonated by thermal decomposition of $(NH_4)_2SO_4$, C MWCNTs sulfonated by in situ polymerization of acetic anhydride and H_2SO_4, D MWCNTs sulfonated by in situ polymerization of poly(sodium4-styrenesulfonate).

4.3.3 The importance of Catalyst Washing after Sulfonation Process

Interestingly, the washing of the catalyst after sulfonation is extremely important because it significantly affects the yield of FAME. Prior to the esterification, the s-MWCNTs prepared by thermal treatment with concentrated H_2SO_4 were subjected to three different washing conditions: unwashed, semi-washed and washed. The unwashed s-MWCNTs were obtained when the mixture of MWCNTs and H_2SO_4 was filtered and directly dried in an oven without washing with distilled water. Meanwhile, when the mixture of MWCNTs and H_2SO_4 was diluted with distilled water, filtered and dried in oven, the s-MWCNTs obtained were considered as the semi-washed s-MWCNTs. Lastly, the washed s-MWCNTs were obtained when the mixture of MWCNTs and H_2SO_4 was filtered and washed repeatedly with distilled water until the pH of the filtrate was the same as the pH of distilled water before drying in oven. As shown in Table 4.4, the unwashed s-MWCNTs produced the highest FAME yield of 95.1 %, which was similar to the FAME yield achieved by using homogeneous H_2SO_4 as catalysts (Wang et al., 2006, Narasimharao et al., 2007). This result further indicates that most of the catalytic effect of the unwashed s-MWCNTs during the esterification of PFAD was attributed to the excess H_2SO_4 attached to the MWCNTs but not the SO_3H groups covalently bonded to the MWCNTs. A similar explanation can be applied to s-MWCNTs that have not been thoroughly washed, for which the FAME yield was higher than that of the thoroughly washed s-MWCNTs. Therefore, the reproducibility of the unwashed and not thoroughly washed s-MWCNTs in the ensuing esterification reaction was expected to be significantly reduced because the attached H_2SO_4 had been leached into the reaction medium.

Table 4.4: Effect of catalyst washing after sulfonation via thermal treatment with concentrated H_2SO_4 on the yield of FAME.

Catalysts washing condition	FAME yield (%)
Unwashed s-MWCNTs	95.1
Semi-washed s-MWCNTs	85.8
Washed s-MWCNTs	78.1

4.3.4 Catalyst Reusability of s-MWCNTs Synthesized via Various Sulfonation Methods

The reusability of the s-MWCNTs was evaluated through five consecutive cycles. After esterification, the s-MWCNTs were separated from the reaction mixture by filtration and then sonicated in methanol for 20 min. Next, the catalyst was filtered and repeatedly rinsed with methanol. The washed catalysts were then dried at 120 °C for 12 h. The recovered catalyst was then subjected to esterification under the same reaction conditions. The FAME yields achieved by the s-MWCNTs in five consecutive cycles are shown in Figure 4.6. As shown by the figure, there was a significant drop of s-MWCNTs prepared by in situ polymerization of poly(sodium4-styrenesulfonate) in the third run of repeated use might be due to the leaching of active sites into the reaction medium. However, the results show that the four types of s-MWCNTs could maintain the FAME yield above 70 % after five cycles. The high reusability of the s-MWCNTs in the esterification was attributed by the ability of MWCNTs to form strong covalent bonds with SO_3H groups.

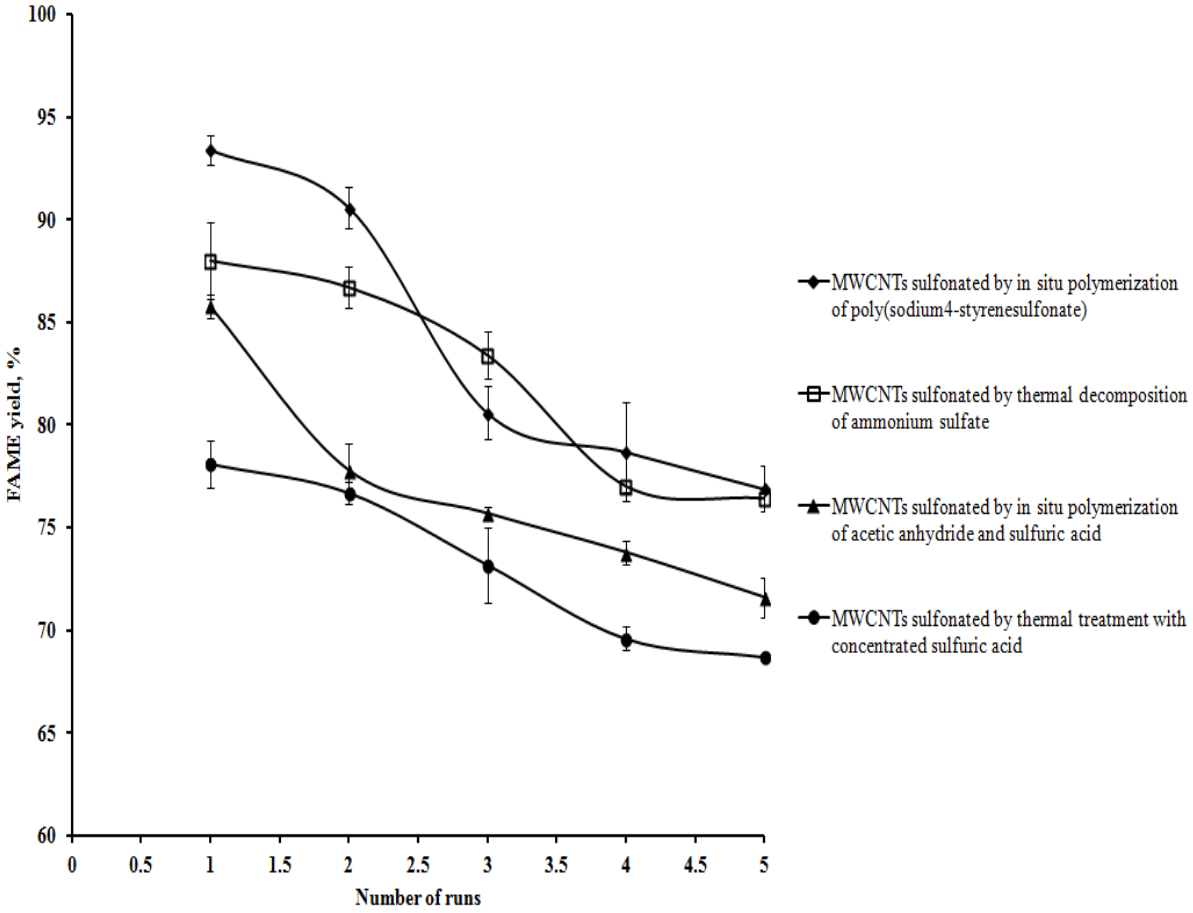

Figure 4.6: Reusability of the s-MWCNTs in the esterification of PFAD (reaction temperature of 170 °C, methanol to palm fatty acid distillate ratio of 20, catalyst loading of 2 wt% and reaction period of 3 h).

Even though the s-MWCNTs prepared via the in situ polymerization of poly(sodium4-styrenesulfonate) showed the highest FAME yield, this particular method required a longer synthesis duration (approximately 4 days) and involved more chemicals and processing steps as shown in Table 4.5. Conversely, the in situ polymerization of acetic anhydride and H_2SO_4 and thermal treatment using H_2SO_4 required the use of concentrated H_2SO_4 as sulfonating agent. The use of concentrated H_2SO_4 will generate wastewater from the repeating washing process. Sulfonation via the thermal decomposition of $(NH_4)_2SO_4$ seems to be the best method to prepare s-MWCNTs because this sulfonation method is facile and acid-free. Therefore,

sulfonation via the thermal decomposition of $(NH_4)_2SO_4$ was selected to be the main sulfonation method. More detail studies were carried out regarding to this particular sulfonation method.

Table 4.5: Sulfonation conditions of s-MWCNTs prepared by various sulfonation method.

Sulfonation method	Sulfonating agent	Sulfonation period, (h)	Requirement of inert environment	Amount of chemical/ processing steps involved
MWCNTs sulfonated by thermal decomposition of $(NH_4)_2SO_4$	$(NH_4)_2SO_4$	0.5	No	Less
MWCNTs sulfonated by thermal treatment with concentrated H_2SO_4	Concentrated H_2SO_4	12	Nitrogen environment	Less
MWCNTs sulfonated by in situ polymerization of acetic anhydride and H_2SO_4	Concentrated H_2SO_4	2	No	Moderate
MWCNTs sulfonated by in situ polymerization of poly(sodium4-styrenesulfonate)	4 M of H_2SO_4	83	No	High

4.4 s-MWCNTs Synthesized via the Thermal Decomposition of $(NH_4)_2SO_4$

The sulfonation procedures of the thermal decomposition of $(NH_4)_2SO_4$ carried out in this study were modified according to previously reported literature (Xu et al., 2005, Du et al., 2008). The major modification was the incorporation of the ultrasonication treatment to the mixture of MWCNTs-COOH and $(NH_4)_2SO_4$ solution. Ultrasonication treatment is usually used to break the agglomerates and to disperse MWCNTs in the sulfonating agent prior to the sulfonation process. However, the role and effects of the ultrasonication treatment in the sulfonation process have not been thoroughly studied. Thus, this study focuses on the effects of different ultrasonication periods to the MWCNTs/$(NH_4)_2SO_4$ solution mixture to obtain s-MWCNTs with the best catalytic performance. The effects of the concentration of the $(NH_4)_2SO_4$ solution (ranging from 1 to 20 wt %) and the ultrasonication period of MWCNTs in $(NH_4)_2SO_4$ solution (ranging from 1 to 20 min) were studied and optimized.

4.4.1 Effect of the Ultrasonication Treatment Period

The FAME yield achieved by s-MWCNTs synthesized using different ultrasonication periods and concentrations of $(NH_4)_2SO_4$ solution is shown in Figure 4.7. The MWCNTs-COOH sulfonated with 1, 5 and 10 wt% $(NH_4)_2SO_4$ exhibited similar result trends in which the FAME yield significantly increased when the ultrasonication period of the mixture increased from 1 to 10 min. Next, the FAME yield increased gradually and eventually became constant with further increases of the ultrasonication period to 15 min and 20 min, respectively. Due to weak van der Waals interactions, MWCNTs often aggregate into bundles or ropes, in which each

bundle can consist of up to several hundred MWCNTs arranged in a hexagonal lattice (Kis et al., 2004, Donaldson et al., 2006). In this work, ultrasonication treatment served to disperse and mix homogeneously the MWCNTs-COOH with the $(NH_4)_2SO_4$ solution, enabling easy interactions of the MWCNTs-COOH with $(NH_4)_2SO_4$ solution. As a result, the FAME yield increased with a longer ultrasonication period because the mixing intensity of the MWCNTs in the $(NH_4)_2SO_4$ solution was higher, thus improving the contact between MWCNTs-COOH and the $(NH_4)_2SO_4$ solution.

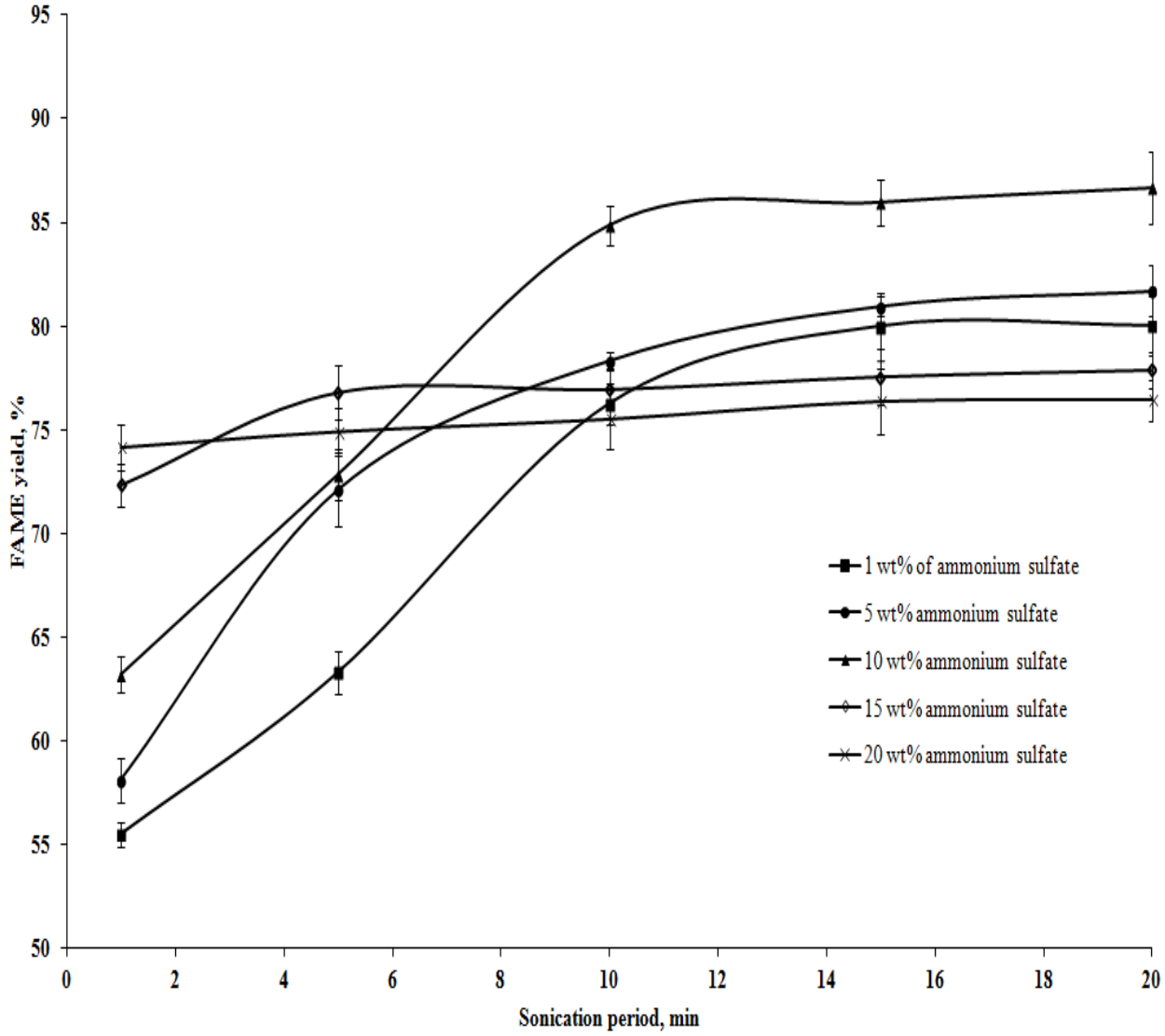

Figure 4.7: FAME yield achieved by s-MWCNTs prepared using different ultrasonication periods and concentrations of $(NH_4)_2SO_4$ solution.

The surface of MWCNTs will be attacked by the generated localized sonochemistry and cause defects in it (Wang et al., 2013). These defects can be verified using Raman spectroscopy analysis. The D-band in a Raman spectrum indicates the presence of structural defects, and the G-band is referred to as graphite in nanotubes. Changes in the D- and G-bands in Raman spectra are useful information for monitoring the structural modifications of the nanotube sidewalls caused by defects or the attachment of different chemical species (Dresselhaus et al., 2005). The I_D/I_G ratio for the pristine MWCNTs was 0.90 (< 1), indicating that the pristine MWCNTs contained more graphite than defect sites. When the pristine MWCNTs were subjected to acid purification coupled with 1 h of ultrasonication treatment to produce MWCNTs-COOH, the I_D/I_G ratio increased to 1.01, indicating that acid purification and ultrasonication treatment caused defects on the surface of the MWCNTs. This claim was strengthened by the results of the Raman spectra shown in Table 4.6, in which the I_D/I_G ratio of the s-MWCNTs increased when the ultrasonication period of the sulfonation mixture increased.

Table 4.6: Effects of different sonication periods on the I_D/I_G ratio and acid density of MWCNTs sulfonated with a 10 wt% $(NH_4)_2SO_4$ solution.

Sonication period, min	[a] I_D/I_G ratio	[b] Acid density, mmol/g
1	1.02	0.0148
5	1.08	0.0210
10	1.17	0.0300
15	1.22	0.0329
20	1.35	0.0340

[a] Results of the I_D/I_G ratio were obtained from Raman spectroscopy analysis.
[b] Results of acid density were obtained using pulse chemisorption.

The carbon atoms located at the opened tube caps are sp^2 hybridized, in which a double bond exists between two carbon atoms. These sp^2-hybridized carbons are relatively more reactive than the sp^3-hybridized carbons located in the regular graphene framework. The generated SO_3H groups will attack the partial carbon-carbon double bonds to transform the sp^2-hybridized carbon atoms into more chemically stable sp^3-hybridized carbon atoms (Balasubramanian and Burghard, 2005). Thus, the role of ultrasonication treatment in this sulfonation process is not only to mix or disperse MWCNTs-COOH in $(NH_4)_2SO_4$ solution but also to open the tube caps and create defects along the sidewall for sulfonation. This finding was supported by the relationship between the I_D/I_G ratio of the Raman spectrum and the acid density of the s-MWCNTs shown in Table 4.6, where the acid density of the s-MWCNTs increased with longer ultrasonication treatment resulting from more defects (higher I_D/I_G ratio) on the surface of the MWCNTs.

Interestingly, the increase in sonication period was found to have insignificant effect to the FAME yield when the s-MWCNTs were prepared at high $(NH_4)_2SO_4$ concentration (15 and 20 wt%). The FAME yield of MWCNTs-COOH sulfonated with 15 wt% $(NH_4)_2SO_4$ only showed an increase of 5% when the sonication period was extended from 1 to 5 min. Next, the FAME yield was constant although the sonication period was increased. In addition, the increase in sonication period did not cause any significant effect to the FAME yield produced by the MWCNTs-COOH sulfonated with 20 wt% $(NH_4)_2SO_4$. The FAME yield was almost constant (increment not more than 4%) throughout the period of ultrasonicating the mixture from 1 to 20 min. This observation was believed to be caused by the

interaction effect between sonication period and the concentration of $(NH_4)_2SO_4$ solution which will be discussed in the following section. The optimum duration of the ultrasonication treatment to produce the s-MWCNTs in this study was 10 min.

4.4.2 Effect of $(NH_4)_2SO_4$ Solution Concentration

As shown in Figure 4.7, two different result trends were obtained in the sulfonation of MWCNTs-COOH using different $(NH_4)_2SO_4$ solution concentrations. The first result trend was exhibited by s-MWCNTs prepared using low concentrations of $(NH_4)_2SO_4$ solution (1, 5 and 10 wt %), in which the yield of FAME increased gradually when the concentration of the $(NH_4)_2SO_4$ solution increased. In addition, the other result trend was exhibited by MWCNTs-COOH sulfonated using high concentrations of $(NH_4)_2SO_4$ solution (15 and 20 wt %), in which the catalysts underperformed compared to the catalysts prepared using low concentrations of the $(NH_4)_2SO_4$ solution.

Both result trends can be explained through Figure 4.8, which shows the acid site density of s-MWCNTs prepared using different concentrations of the $(NH_4)_2SO_4$ solution. These results indicated that the acid site density of the catalysts increased when the concentration of the $(NH_4)_2SO_4$ solution increased. In sulfonation via the thermal decomposition of $(NH_4)_2SO_4$, the generated SO_3H groups will react with the surface hydrogen atoms that naturally contain MWCNTs-COOH and with the carboxyl groups created during acid purification to form the SO_3H groups (Du et al., 2008). Thus, when the concentration of the $(NH_4)_2SO_4$ solution increased, more

SO_3 groups were produced to form a higher density of SO_3H groups, which served as the active sites for the esterification of PFAD with methanol.

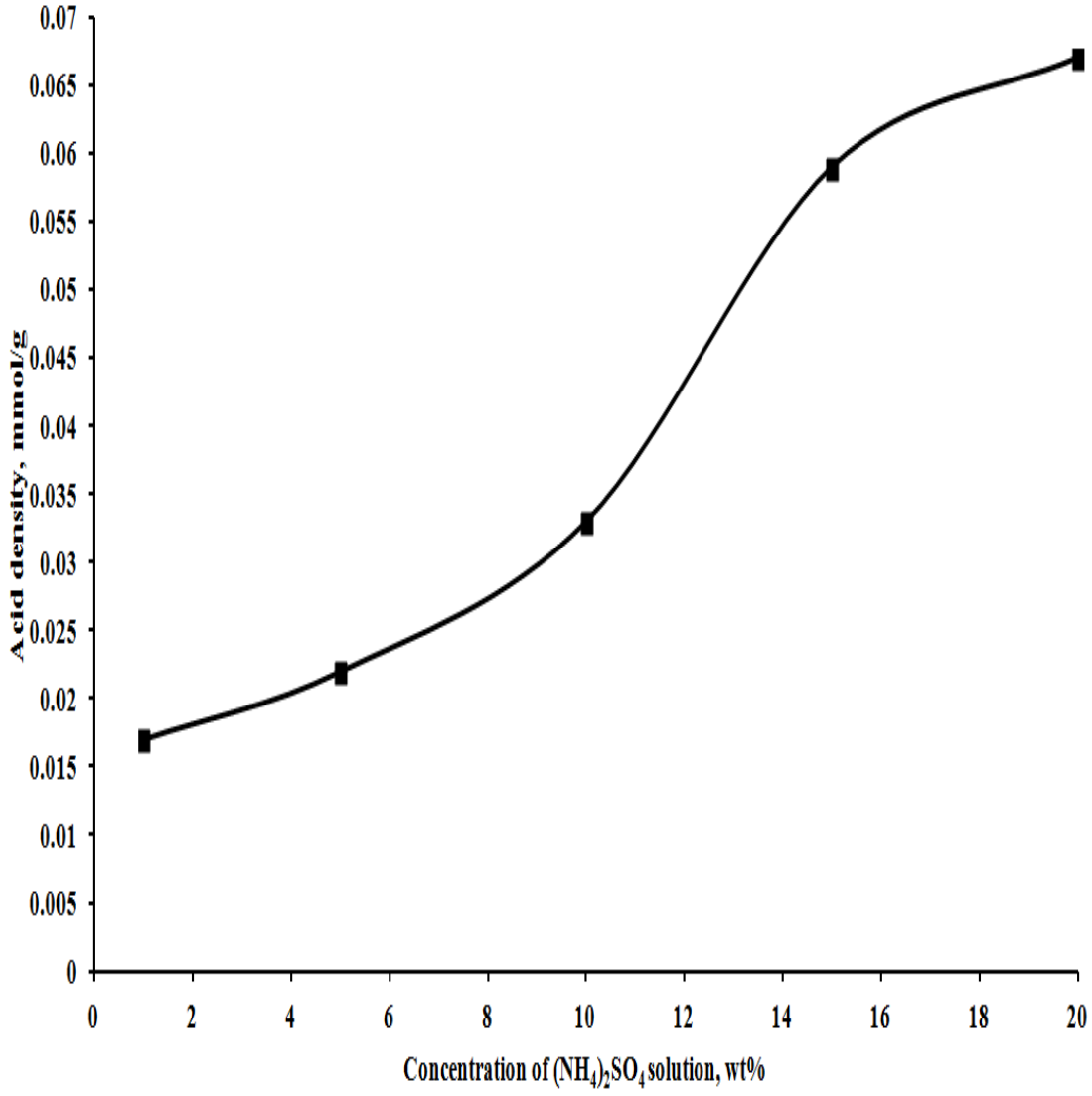

Figure 4.8: Effect of the concentration of $(NH_4)_2SO_4$ solution on acid density of s-MWCNTs subjected to 20 min of ultrasonication treatment.

However, extremely high concentrations of $(NH_4)_2SO_4$ solution may cause an adverse effect on the catalysts. Although there was a significant increase in acid site density (more than two-fold) when the concentration of the $(NH_4)_2SO_4$ solution was increased from 10 to 20 wt % as shown in Figure 4.8, the FAME yield achieved by the s-MWCNTs prepared using high concentrations of $(NH_4)_2SO_4$ solution and a long ultrasonication treatment period was the lowest among all s-MWCNTs. This was due to the interaction effect between long sonication period and high concentration of $(NH_4)_2SO_4$ solution. The viscosity of the solution mixture (MWCNTs in $(NH_4)_2SO_4$ solution) may increase in high concentration of $(NH_4)_2SO_4$ which could affect the dispersibility of MWCNTs-COOH in the resultant solution. As a result, the MWNCTs tend to remain as bundle. Therefore, only the MWCNTs that located at the outer perimeter of the bundle will be exposed to the $(NH_4)_2SO_4$ solution. The degree of defect created on the surface of MWCNTs was believed to decrease. Moreover, under high concentration of $(NH_4)_2SO_4$, the defect-surface will be oversaturated by SO_3H groups (Xu et al., 2005). In addition, when the surface of s-MWCNTs were saturated with SO_3H groups, the surface became highly negatively charged and thus causing difficultly for the lone-pair electron of the carbonyl group of the fatty acids to reach the OH groups of the SO_3H. From the above results, the optimum concentration of $(NH_4)_2SO_4$ solution for this sulfonation process is 10 wt%.

The s-MWCNTs with the best performance could be obtained by ultrasonicating purified MWCNTs in a 10 wt% $(NH_4)_2SO_4$ solution for 10 min and heating at 235 °C (decomposition temperature of $(NH_4)_2SO_4$) for 30 min (Du et al., 2008).

4.4.3 Characterization of the s-MWCNTs Synthesized via Thermal Decomposition of $(NH_4)_2SO_4$

The properties of s-MWCNTs synthesized via thermal decomposition of $(NH_4)_2SO_4$ under the optimum conditions were characterized using various characterization instrument such as UV-Vis, TGA and nitrogen adsorption-desorption.

4.4.3.1 Dispersibility of s-MWCNTs in Methanol

The UV-Vis spectra of the pristine MWCNTs, MWCNTs-COOH and s-MWCNTs were shown in Figure 4.9. As indicated by the unstable absorbance spectrum which decreased since the beginning of the analysis, the pristine MWCNTs were proven to have poor solubility in methanol. This was due to the hydrophobic property of the carbon framework and the intrinsic van der Waals interactions that caused the agglomeration of pristine MWCNTs into bundle (Zhou et al., 2010). On the other hand, the UV-Vis spectra showed that the MWCNT-COOH and s-MWCNTs remained colloidally stable and well dispersed in methanol after 720 min (12 h). The absorbance of the s-MWCNTs and methanol mixture decreased gradually at the beginning of the analysis, which was most likely due to the aggregation of the MWCNTs to a micron-sized cluster that then settled to the bottom of the cuvette. The s-MWCNTs were stable and remained dispersed after 100 min until 720 min.

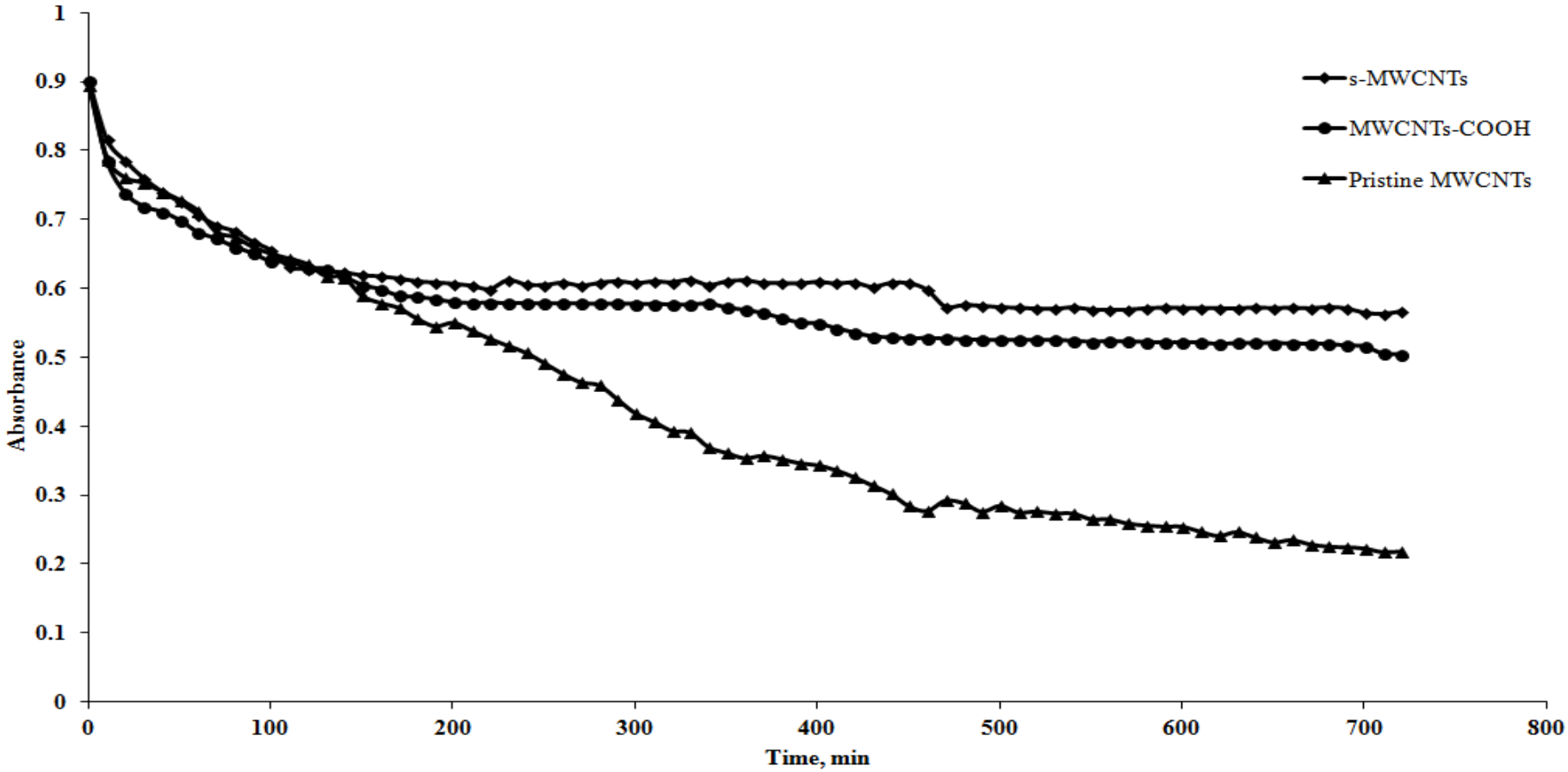

Figure 4.9: Sedimentation curve of s-MWCNTs, MWCNTs-COOH and pristine MWCNTs in methanol at a concentration of 0.005 mg/mL.

The dispersibility of the s-MWCNTs in methanol was caused by the surface modification of the introduced SO_3H and COOH groups onto the surface of MWCNTs via the acid purification and sulfonation process. The SO_3H and COOH groups on the surface of the MWCNTs were believed to form hydrogen bonds with methanol and thus enabled the s-MWCNTs to remain dispersed in methanol. Thus, the interactions between the SO_3H and COOH groups of the s-MWCNTs and alcohol were considered a weak interaction (Zhou et al., 2010), resulting in a slight decrease in absorbance after 460 min. The absorbance spectrum of MWCNTs-COOH in methanol mixture was similar to that of s-MWCNTs, indicating that surface modification (acid purification and sulfonation) could improve the dispersibility of the hydrophobic MWCNTs in hydrophilic solvent.

The above dispersibility result implied that s-MWCNTs were able to form a homogeneous solution with methanol during the esterification of PFAD. The dispersibility behaviour of s-MWCNTs is required for the application of s-MWCNTs as a heterogeneous catalyst. The major drawback in heterogeneous-catalysed transesterification/esterification is the presence of the three-phase-system (triglycerides/fatty acids, alcohol and solid catalyst) in the reaction mixture, which prohibits the diffusion of fatty acids and reduces the availability of active sites for the reaction, thus decreasing the reaction rate (Mbaraka and Shanks, 2006). Thus, the dispersibility of the s-MWCNTs and the high miscibility of PFAD in methanol can minimise the mass transfer resistance due to the reduction of reaction phases.

4.4.3.2 Thermal Degradation and Stability of Pristine MWCNTs, MWCNTs-COOH and s-MWCNTs

The weight loss and derivative weight loss curves for pristine MWCNTs, MWCNTs-COOH and s-MWCNTs are shown in Figure 4.10 A and B. The results in Figure 4.10 A indicated that all of the samples were stable up to 500 ºC, with negligible weight loss. Thus, the s-MWCNTs should possess good thermal stability at the reaction temperature of 170 °C. Among the three MWCNT samples, the pristine MWCNTs underwent thermal decomposition at the lowest temperature, in which a sharp weight loss was observed at 500 °C, and then completely decomposed at 650 °C. In addition, the starting and complete decomposition temperatures of MWCNTs-COOH were extended to 550 °C and 680 °C, respectively. This observation indicated that the thermal stability of MWCNTs was increased after acid purification by HNO_3 because of the removal of metal catalysts and amorphous carbon. The thermal stability of MWCNTs was further increased by the sulfonation process, in which the s-MWCNTs started to decompose at 600 °C and completely decomposed at 700 °C. The s-MWCNTs decomposed at a higher temperature because more energy was required to decompose the grafted SO_3H groups to release oxygen (Adams et al., 2009) prior to the decomposition of carbon.

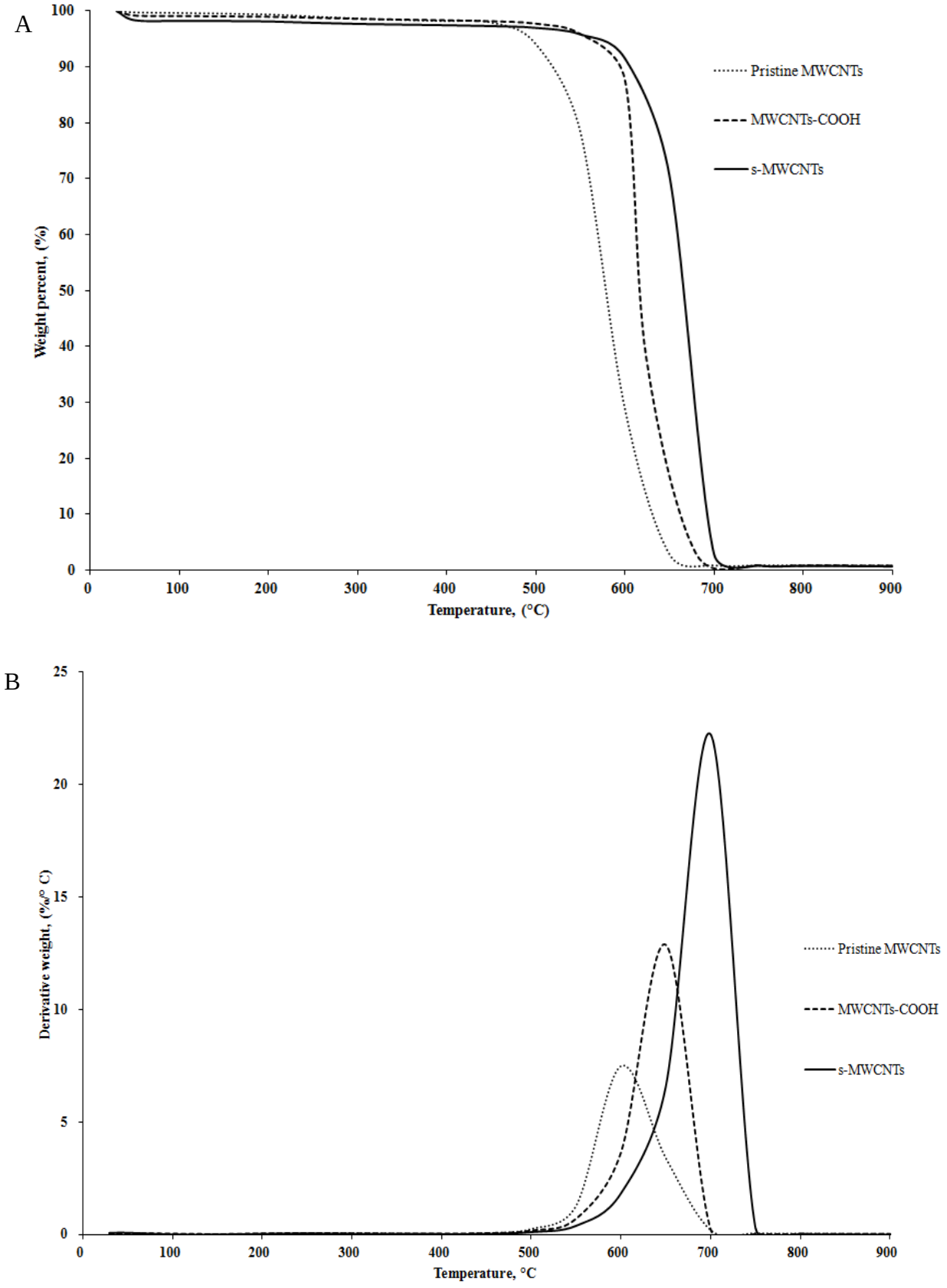

Figure 4.10: TGA analysis of A weight (wt %) B derivative weight (wt %/°C) of pristine MWCNTs, MWCNTs-COOH and s-MWCNTs.

4.4.3.3 BET Surface Area Analysis

The BET surface area, average pore width, pore volume and sulfonation parameters of the s-MWCNTs (synthesized from a 10 wt% $(NH_4)_2SO_4$ solution coupled with 10 min of ultrasonication treatment) are compared to the other reported carbon-based catalysts in Table 4.7. These results indicated that the BET surface area, average pore width and pore volume of the s-MWCNTs produced in this study increased significantly compared to those of pristine MWCNTs. The increase in the BET surface area of s-MWCNTs was due to the repulsion force induced by COOH and SO_3H groups on the surface of MWCNTs, which reduced the problem of agglomeration of the MWCNTs. In addition, the s-MWCNTs possessed a larger average pore width than the pristine MWCNTs because the acid purification and ultrasonication treatment enhanced the defects on the surface of the MWCNTs. Moreover, the BET surface area and pore diameter of s-MWCNTs obtained in this study were larger than those of the majority of reported carbon-based catalysts (except biochar) used for biodiesel production. The mass transfer limitation encountered by heterogeneous-catalysed transesterification/esterification can be greatly reduced using a catalyst support with a high BET surface area. However, this limitation will still exist if the catalyst support contains only micropores, particularly if large molecules (fatty acids) are involved, because the active sites located in the micropores prohibit accessibility to reactants. These results showed that although the BET surface area and acid density of s-MWCNTs (obtained in this study) were lower than those of other carbon-based catalysts, such as sulfonated biochar, sulfonated ordered mesoporous carbon, H_2SO_4 sulfonated peanut hull char and H_2SO_4 sulfonated MeadWestvaco activated carbon, the FAME yield produced by the s-MWCNTs was actually higher than those obtained using carbon-based catalysts.

Table 4.7: BET surface area, average pore width, pore volume and sulfonation parameters of s-MWCNTs and other sulfonated carbon-based catalysts.

Carbon-base acid catalysts	Sulfonating agent	Sulfonation period, (h)	Sulfonation temperature, (° C)	Requirement of inert environment	Requirement of sonication, (min)	Pore diameter, (nm)	BET surface area, (m^2/g)	Pore volume, (cm^3/g)	Acid density, (mmol/g)	References
Un-purified MWCNTs	-	-	-	-	-	7.85	27.26	0.05	-	In this study
s-MWCNTs	$(NH_4)_2SO_4$	0.5	235	No	10	12.3	92.37	0.25	0.03	In this study
s-MWCNTs	Concentrated H_2SO_4	10	120 – 210	Nitrogen environment (Zhou et al., 2010)	30 (Zhou et al., 2010)	7.48	41.27	-	3.09	(Shu et al., 2009a)
Sulfonated biochar	Fuming H_2SO_4	15	150	Nitrogen environment	-	3.17	949.00	0.85	1.70	(Dehkhoda and Ellis, 2013)
Sulfonation of incompletely carbonised D-glucose	Concentrated H_2SO_4	15	150	Nitrogen environment	-	-	2.00	-	0.7	(Takagaki et al., 2006)
Sulfonation of incompletely carbonised D-glucose	Fuming H_2SO_4	15	150	Nitrogen environment	-	-	1.00	-	1.2	(Takagaki et al., 2006)

Sulfonation of incompletely carbonised D-glucose	Concentrated H_2SO_4	15	150	Nitrogen environment	-	-	4.13	-	1.5	(Zong et al., 2007)
C400-SO_3H	Concentrated H_2SO_4	13	150 – 160	Dry nitrogen environment	-	-	< 1	-	0.64	(Mo et al., 2008)
Sulfonated incomplete carbonised mung bean vermicelli	Concentrated H_2SO_4	10	100	Nitrogen environment	-	-	18.1	-	1.53	(Mar and Somsook, 2012)
Sulfonated ordered mesoporous carbon	4-benzene-diazoniumsulfonate in ethanol/water solution in the presence of H_3PO_2	1	5	No	-	4.2	741.00	0.85	1.700[a]	(Liu et al., 2008)
Vegetable oil asphalt-base carbon catalyst	Concentrated H_2SO_4	10	210	No	-	43.9	7.48	-	2.21	(Shu et al., 2009a)
H_2SO_4 sulfonated peanut hull char	Concentrated H_2SO_4	12 – 18	100	No	No	1.05	242	0.13	5.65	(Kastner et al., 2012)
H_2SO_4 sulfonated MeadWestvaco activated carbon	Concentrated H_2SO_4	12 – 18	100	No	No	1.1	1391	0.76	2.59	(Kastner et al., 2012)

[a]The acid density was determined using potentiometric titration.

This was due to the larger pore width of s-MWCNTs, which enabled easy access of methanol and fatty acids to active sites for reaction. The spatial widths of stearic acid, oleic acid and linoleic acid are 0.25, 0.72 and 1.13 nm, respectively (Cook and McMaster, 2002). Thus, the pore width of 12.3 nm exhibited by the s-MWCNTs in this study was sufficiently large to enable fatty acid molecules to diffuse and reach the active sites.

4.4.4 Comparison of the Catalyst Properties and Sulfonation Parameters of s-MWCNTs and Other Sulfonated Carbon-Based Catalysts

As shown in Table 4.7, the sulfonating agent, $(NH_4)_2SO_4$ solution, used in this study was environmentally benign compared to concentrated H_2SO_4. Although the sulfonation temperature of MWCNTs via the thermal decomposition of $(NH_4)_2SO_4$ was higher, it required only 30 min of sulfonation time compared to other sulfonated carbon-based catalysts prepared via thermal treatment with concentrated H_2SO_4, which required a minimum sulfonation period of 10 h. In addition, sulfonation via the thermal decomposition of $(NH_4)_2SO_4$ did not require an inert environment, thus helping to reduce the number of operating steps and cost in preparing the catalyst for biodiesel production. Moreover, the sulfonation method used in this study required less sonication time compared to the sulfonation process via thermal treatment with concentrated H_2SO_4 (Zhou et al., 2010). Thus, the information presented in Table 2 indicates that s-MWCNTs not only can be synthesized using a simpler and faster method but also possess a high BET surface area and a well-developed pore size.

4.5 Process Study of the Esterification of PFAD Using s-MWCNTs as a Catalyst

The esterification of PFAD with methanol using s-MWCNTs as a catalyst has been minimally studied. Therefore, in this work, the process parameters, such as reaction temperature, methanol-to-PFAD ratio, catalyst loading and reaction period, for the esterification of PFAD using s-MWCNTs were studied.

4.5.1 Effect of the Methanol-to-PFAD Ratio

Figure 4.11 shows the effect of different methanol-to-PFAD ratios on the FAME yield at a reaction temperature of 170 °C and a catalyst loading of 2 wt %. The FAME yield increased gradually as the methanol-to-PFAD ratio increased from 8 to 20. However, the high methanol-to-PFAD ratio of 30 caused an adverse effect on the FAME yield, in which the FAME yield not only decreased significantly but also underperformed compared to the lowest methanol-to-PFAD ratio of 8. According to Le Chatelier's principle, an excess amount of methanol is required to drive the reversible reaction forward toward the formation of FAME (Othman et al., 2010). In addition, as proposed in the reaction mechanism of esterification using sulfonated catalysts begins with the attachment of fatty acids to the active sites of the catalysts through chemisorption. This step is followed by the protonation of the chemisorbed molecules at the carbonyl group to form carbocations. FAME is produced when the carbocations are attacked by methanol molecules. Therefore, in the condition of excess methanol, the collisions between the carbocations and methanol molecules are increased, thus enhancing the conversion. However, if the methanol-to-PFAD ratio is too extreme, fatty acids are prohibited from forming

carbocations because the catalyst active sites are flooded with methanol instead of fatty acids (Shu et al., 2009a, Shu et al., 2009b), thereby causing deactivation of the catalyst. Moreover, the FAME yield decreases in an environment of excess methanol due to the slower reaction caused by dilution of the reaction system (Lam et al., 2009). Therefore, the most suitable methanol-to-PFAD ratio in this study was 20 because high FAME yield was obtained in this ratio.

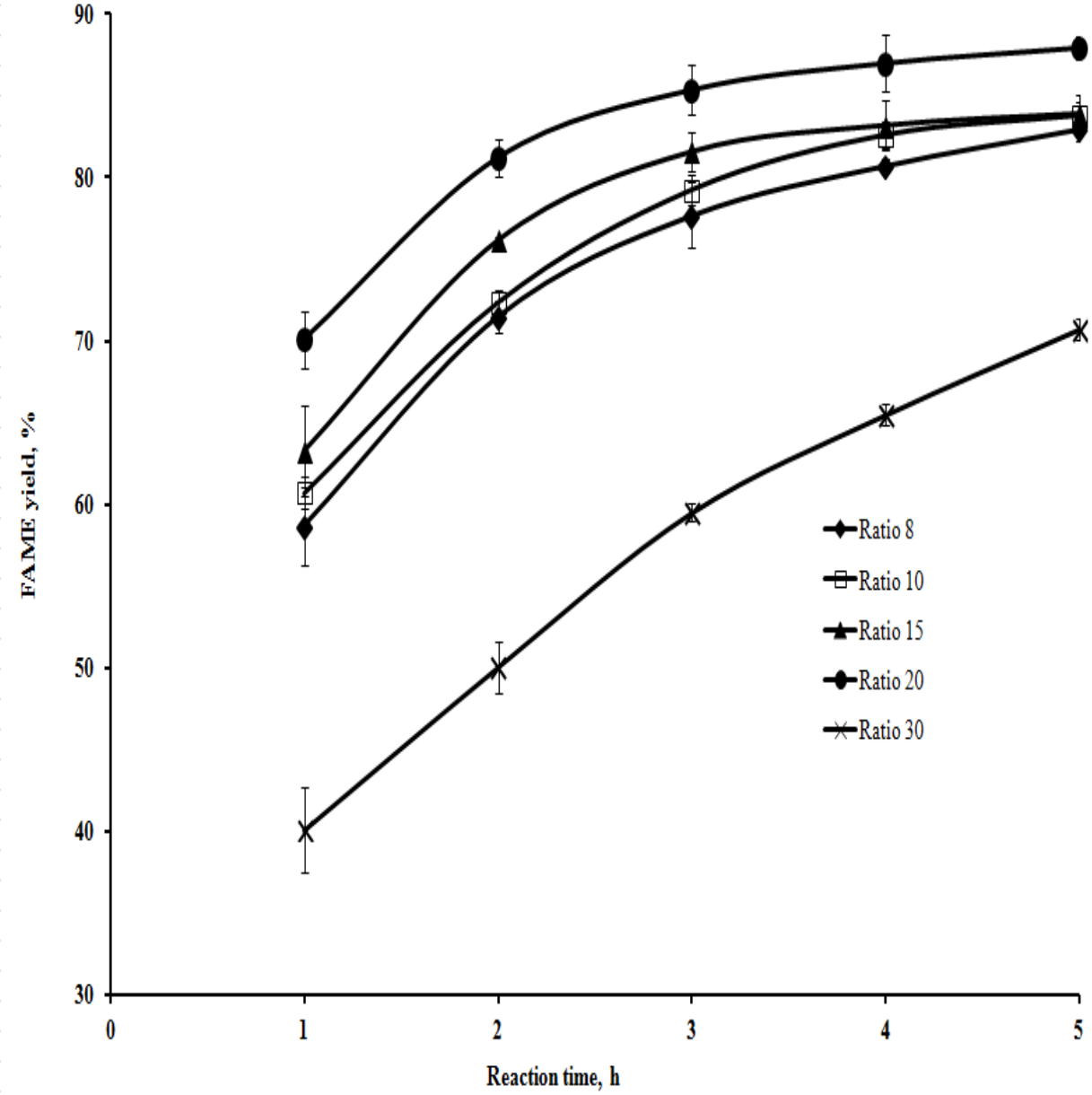

Figure 4.11: Effect of the methanol-to-PFAD ratio on the FAME yield at a reaction temperature of 170 °C and a catalyst loading of 2 wt %.

4.5.2 Effect of Catalyst Loading

The effect of s-MWCNTs loading on the FAME yield is illustrated in Figure 4.12. The reaction was carried out at a reaction temperature of 170 °C and a methanol-to-oil ratio of 20. The FAME yield was found to be positively affected by the catalyst loading, in which the yield increased when the amount of catalysts used for the reaction increased. This relationship was related to the increase in the total number of active sites available for esterification with an increase in the catalyst concentration (Shah et al., 2014). If the catalyst loading was below 2 wt %, the equilibrium of the reaction was achieved after 3 h of reaction time. However, as the catalyst loading increased to 3 wt %, only 2 h of reaction time was required to bring the reaction to the equilibrium state. Furthermore, an increase of only 0.5 wt % (2.5 to 3 wt %) in the catalyst loading caused a substantial increase in the FAME yield, increasing from 83.0 to 93.5 % in only 2 h of reaction time. Therefore, this result further strengthens the fact that the rate of esterification reaction was enhanced by the use of the catalyst. Since the FAME yield achieved by 3 wt% of catalyst loading was close to 100 %, the further increase of catalyst loading did not have much potential to increase the FAME yield significantly. Note that the FAME yield produced using 3 wt % s-MWCNTs in 2 h of reaction time was close to the ester content (96.5 %) stated in the European Standard (EN 14214) for biodiesel. Therefore, the selected catalyst loading for this study was 3 wt %.

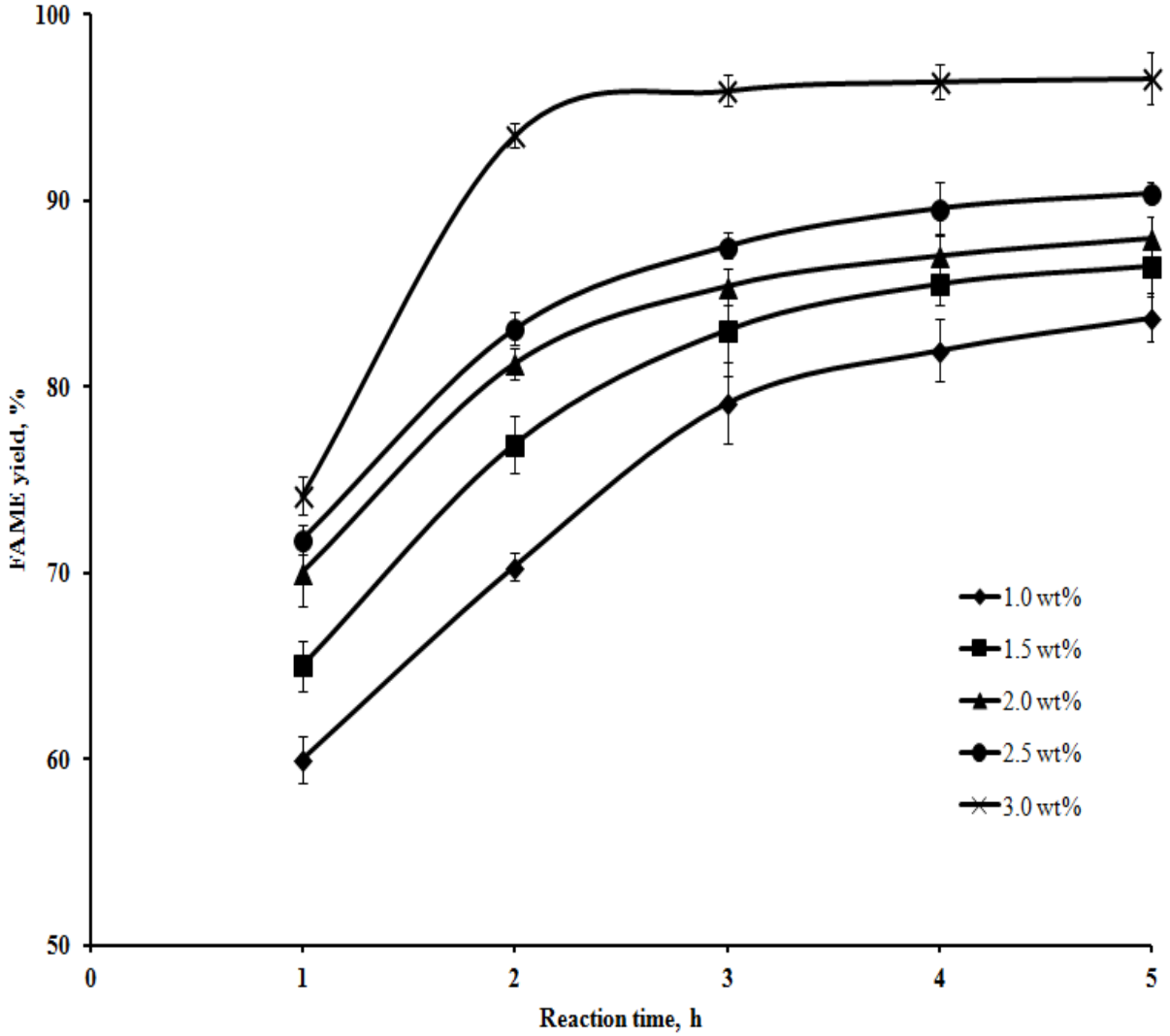

Figure 4.12: Effect of the catalyst loading on the FAME yield at a reaction temperature of 170 °C and a methanol-to-oil ratio of 20.

4.5.3 Effect of Reaction Temperature

Figure 4.13 illustrates the effect of the reaction temperature on the FAME yield at a catalyst loading of 3 wt % and a methanol-to-oil ratio of 20. At low reaction temperatures (80 ºC and 100 ºC), the maximum FAME yield was merely 25.0 %, even at 5 h of reaction time. However, when the reaction temperature increased from 100 to 150 ºC, a three-fold increase in the FAME yield was observed. Subsequently, an average increment of 8 % was observed when the reaction

temperature was further increased to 170 ºC. With the further increase of the reaction temperature to 200 ºC, the FAME yield was barely changed (less than 4 % on average). Similar to transesterification, esterification is also an endothermic process, in which the enthalpy of the process is positive. Therefore, by increasing the temperature, the equilibrium of the reaction was shifted to the forward direction, which favoured the conversion of PFAD into FAME. In addition, as the reaction temperature increased, the methanol and PFAD molecules gained more kinetic energy, causing the collision frequency between the reactant molecules to increase, thereby eventually enhancing the mass transfer rate of the reaction system. Reaction temperature of 170 ºC was selected in this study because no significant increase in FAME yield was observed when the reaction temperature was increased to 200 ºC. The FAME yield between temperature 200 to 240 ºC was expected to be similar unless the temperature exceeded 240 ºC in which supercritical esterification occurred.

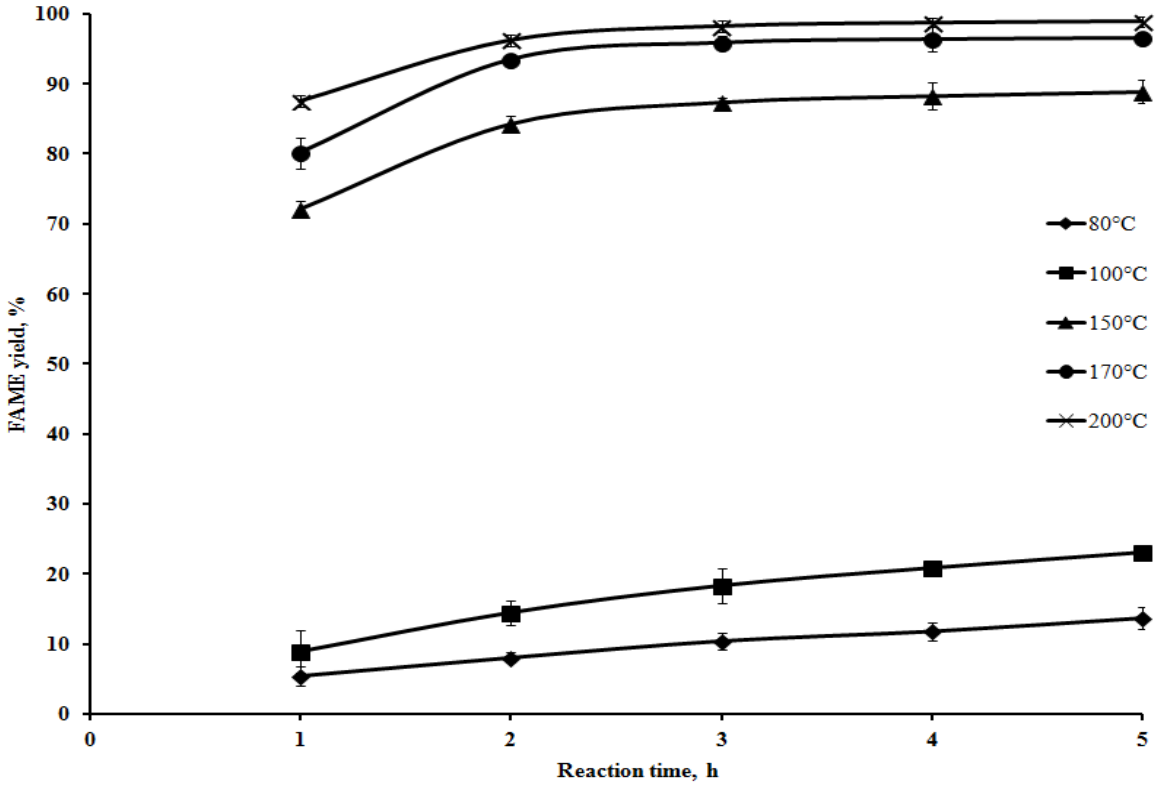

Figure 4.13: Effect of the reaction temperature on the FAME yield at a catalyst loading of 3 wt % and a methanol-to-oil ratio of 20.

4.5.4 Effect of Reaction Time

As shown in Figure 4.11, 4.12 and 4.13, the FAME yield was found to increase with longer reaction times until equilibrium was achieved. Note that the reaction time always reflects the rate of a reaction. Therefore, it is believed that the time required for a reaction to achieve complete conversion or equilibrium state was correlated to other reaction parameters, such as alcohol ratio, catalyst loading and reaction temperature. In this study, the reaction time was influenced by the catalyst loading and reaction temperature. The reaction time to reach the equilibrium state was reduced to 2 h at higher catalyst loadings, as shown in Figure 4.12. In addition, the reaction time was also reduced at a higher reaction temperature. From Figure 4.13, at low reaction temperatures (80 ºC and 100 ºC), equilibrium was hardly observed, even with a high concentration of catalyst used to catalyse the reaction. However, at temperatures of 150 ºC and above, the equilibrium of the reaction was reached at 2 h of reaction time.

Through process study, a high FAME yield of 93.5 % can be obtained under the following conditions: reaction temperature of 170 ºC, catalyst loading of 3 wt %, methanol-to-PFAD ratio of 20 and reaction time of 2 h.

4.5.5 Comparison of Process Parameters of s-MWCNTs and Various Carbon-Based Catalysts

The process parameters of s-MWCNTs and various carbon-based catalysts are shown in Table 4.8. The oil source used for the production of FAME using sulfonated carbon-based catalysts has only been limited to a pure and single component, such as oleic acid and triacetin. Thus far, there have only been two studies reported on the application of sulfonated carbon-based catalysts in the production of biodiesel using cottonseed and soybean oil as feedstock (Shu et al., 2009a, Kastner et al., 2012). Thus, unlike previous studies, the current study showed the ability of s-MWCNTs to produce a high FAME yield using the low-value industrial by-product (PFAD) as an oil source. The esterification/transesterification was performed at a low temperature (60 to 80 ºC) when pure components (oleic acid and triacetin) were used as a feedstock and methanol was used as the alcohol source. However, when PFAD and cottonseed oil were used, a higher reaction temperature was required (between 170 and 260 ºC), which might be due to the higher viscosity of triglycerides and mixture of fatty acids in PFAD. The methanol-to-oil ratio required for s-MWCNTs was almost similar to that in studies using cottonseed or soybean as an oil source. Interestingly, the s-MWCNTs obtain in this study required a lower catalyst concentration than most of the reported carbon-based catalysts to achieve a similar FAME yield. In addition, a high FAME yield can be achieved within 2 h using the s-MWCNTs as catalysts compared to some reported sulfonated carbon-based catalysts, which required 5 to 10 h to obtain a similar FAME yield. The reduction in catalyst concentration and reaction time can further reduce the overall production costs of biodiesel.

Table 4.8: The process parameters of s-MWCNTs and various carbon-based catalysts.

Carbon-based acid catalysts	Oil source	Alcohol source	Reaction temperature, (°C)	Alcohol to oil ratio	Catalyst concentration, (wt%)	Reaction time, (h)	FAME yield, (%)	References
s-MWCNTs in this study	PFAD	Methanol	170	20	3	2	93.5	-
s-MWCNTs (by thermal treatment of H_2SO_4)	Cottonseed oil	Methanol	240	18.2	0.2	2	83.2	(Shu et al., 2009a)
s-MWCNTs (by thermal treatment of H_2SO_4)	Oleic acid	Methanol	135	5.8	0.2	1.5	95.5	(Shu et al., 2009b)
Sulfonation of incompletely carbonised D-glucose (treated with concentrated H_2SO_4)	Oleic acid	Ethanol	100 – 180	10	7.1	-	29.0[a]	(Takagaki et al., 2006)
Sulfonation of incompletely carbonised D-glucose (treated with fuming H_2SO_4)	Oleic acid	Ethanol	100 – 180	10	7.1	-	56.7[*]	(Takagaki et al., 2006)

Sulfonation of incompletely carbonised D-glucose	Oleic acid	Methanol	80	10	5	5	95.0	(Zong et al., 2007)
C400-SO_3H	Triacetin	Methanol	60	6	0.12 g/ml	1	91.2 (conversion)	(Mo et al., 2008)
Sulfonated incomplete carbonised mung bean vermicelli	Oleic acid	Methanol	80	10	2	6	80	(Mar and Somsook, 2012)
Sulfonated ordered mesoporous carbon	Oleic acid	Ethanol	80	10	3.5	10	73.6	(Liu et al., 2008)
Vegetable oil asphalt-base carbon catalyst	Cottonseed oil	Methanol	260	18.2	0.2	3	89.9	(Shu et al., 2009a)
H_2SO_4 sulfonated peanut hull char	5 wt% palmitic and stearic acid spiked in soybean oil	Methanol	57 – 59	20	4 – 7.5	6	70.0	(Kastner et al., 2012)
H_2SO_4 sulfonated MeadWestvaco activated carbon	5 wt% palmitic and stearic acid spiked in soybean oil	Methanol	57 – 59	20	4 – 7.5	6	97.0	(Kastner et al., 2012)

[a] FAME yield was calculated based on the given formation rate of ethyl oleate in 1 h of reaction time.

4.6 Catalyst Reusability and Leaching Analysis

The most significant advantage for using heterogeneous catalysts over homogeneous catalysts is the ability of the heterogeneous catalysts to be recovered, reused and regenerated. Therefore, the s-MWCNTs were subjected to five consecutive runs to evaluate the reusability of the catalysts under the optimum conditions: reaction temperature of 170 °C, methanol-to-PFAD ratio of 20, catalyst loading of 3 wt % and reaction time of 2 h. After each run, the reaction mixtures were carefully separated and then the s-MWCNTs were recovered and washed with methanol before being subjected to a new reaction run with fresh reactants. The FAME yield achieved by the s-MWCNTs in five consecutive runs is shown in Figure 4.14. Although the catalytic activity of s-MWCNTs declined with repeated use, they were still able to maintain the FAME yield at 75 % after 5 catalytic runs. As reported in the literature, for alkaline earth metal oxide catalysts, such as CaO, BrO and SrO, the FAME yields dropped significantly to the level below 30 % at the third use; even under an ultrasonic-assisted reaction, the FAME yields achieved at the third use was still below 70 % (Mootabadi et al., 2010). In addition, for sulfated zirconia, tungstated zirconia, or even some popular commercial biodiesel catalysts, such as Amberlyst-15, Nafion NR50 and ETS 10, the triacetin conversion was reported to be lower than 30 % at the fifth use of the catalysts (López et al., 2005). This was due to the ability of MWCNTs to form covalent bond with SO_3H group as compared to other catalysts in which the active species were not covalently bonded to the solid support (Balasubramanian and Burghard, 2005). Therefore, the s-MWCNTs exhibited better catalytic performance and higher reusability than the conventional biodiesel catalysts. The decrease in the catalytic activity of the s-MWCNTs may be due to two reasons: the blockage of acid sites by the deposition of organic matter on

the catalyst surface and the leaching of the sulfonic groups into the reaction medium (Alonso et al., 2007, Lee et al., 2009, Lee and Saka, 2010).

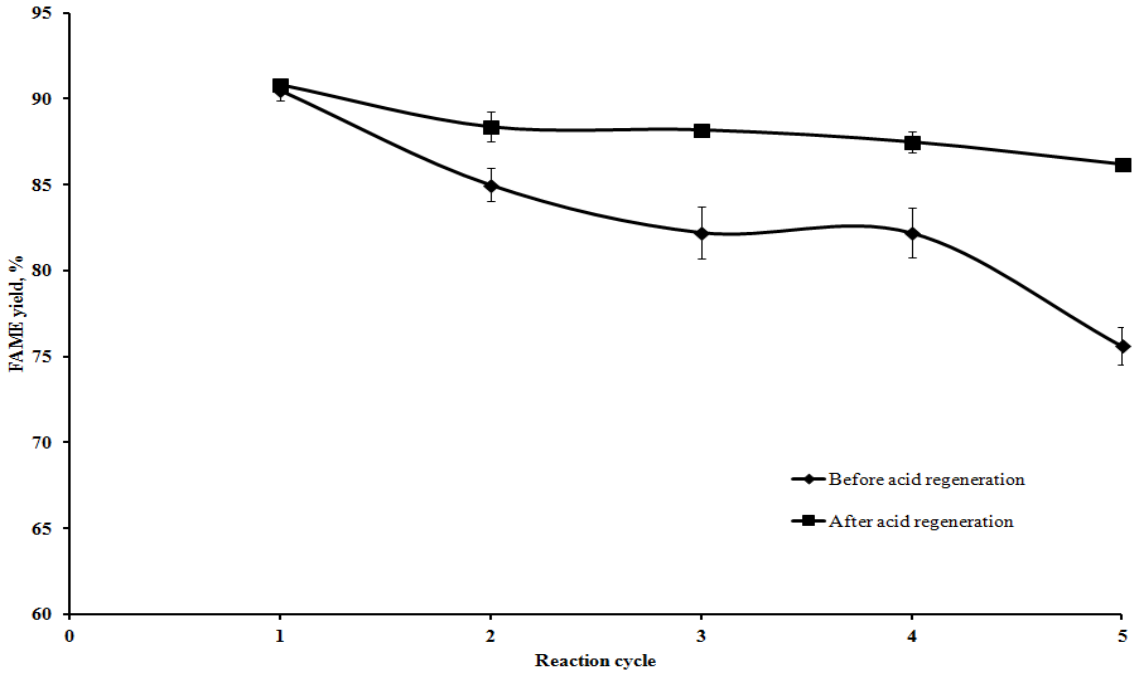

Figure 4.14: Reusability of the s-MWCNTs and the regenerated s-MWCNTs in the esterification of PFAD under reaction conditions: methanol-to-PFAD ratio of 20, catalyst loading of 3 wt %, reaction temperature of 170 °C and reaction time of 2 h.

The hypothesis of the deactivation of s-MWCNTs due to acid site blockage by hydrocarbon species was rejected based on the FT-IR analysis. Figure 4.15 shows the FTIR spectra in the range of 400 – 4000 cm^{-1} for the reused s-MWCNTs from the first to the fifth run. The peak at 3691 cm^{-1} was assigned to the -OH groups (Lam et al., 2009). The absence of strong signals at 1600 – 1800 cm^{-1} indicated that carbonaceous materials, such as fatty acids and FAME, were not present on the surface of the s-MWCNTs. This lack of blockage by hydrocarbon species further indicated that the simple methanol washing used in this study can effectively remove the fatty acids or FAME that adsorbed onto the catalyst surface.

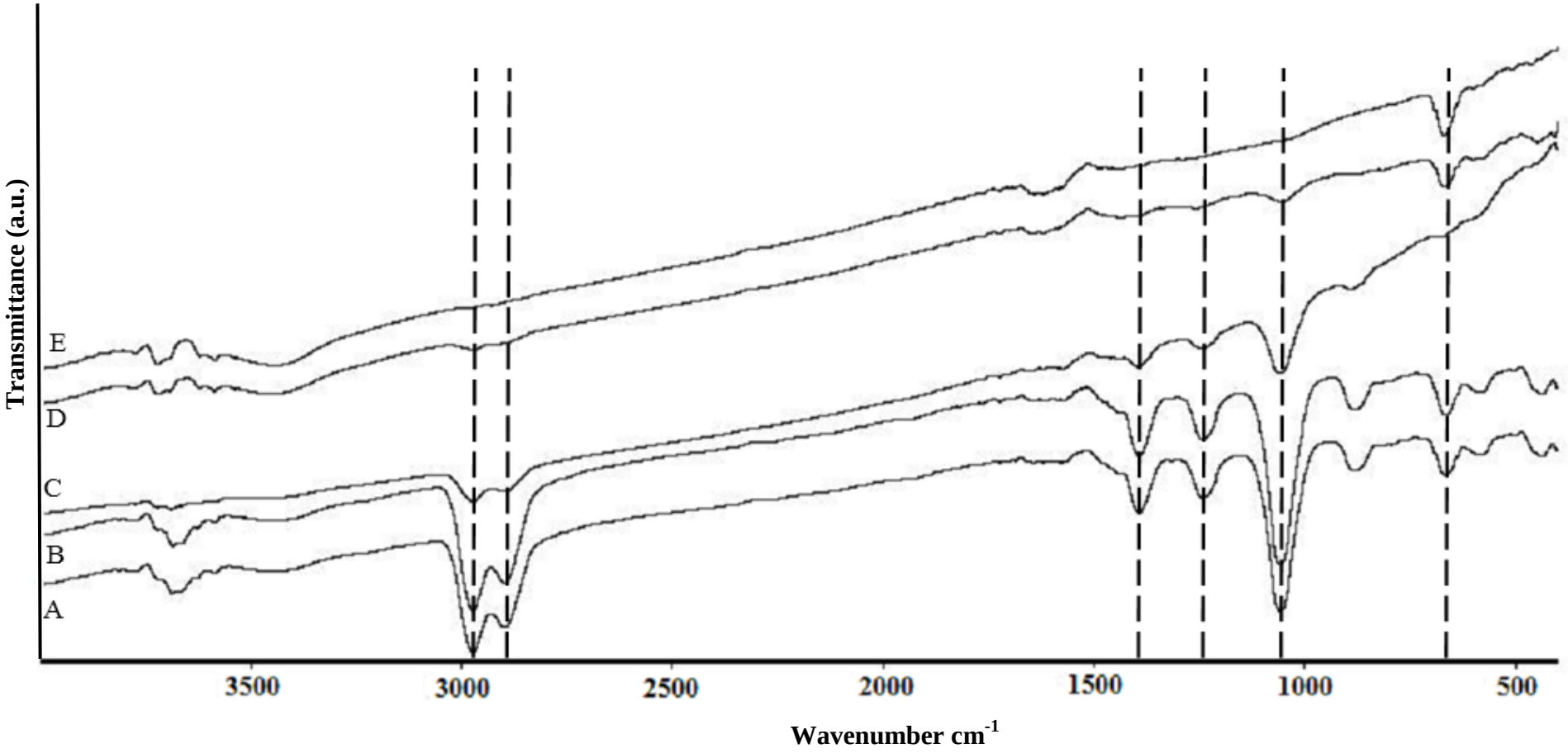

Figure 4.15: FT-IR spectra of spent s-MWCNTs for different repeated reaction runs: A first use, B second use, C third use, D fourth use, and E fifth use.

The leaching of sulfonic groups into the reaction medium was determined according to the ASTM D5453 testing method. Prior to testing, the reaction product mixture was not subjected to any washing or purification treatment. The test result indicated that the sulfur content in FAME was 0.01 % by mass. Therefore, the declining catalytic activity of the s-MWCNTs was due to the leaching of sulfonic groups into the reaction medium. Although the NH_3-TPD analysis shown in Figure 4.16 demonstrated that the acid strength of the as-synthesized s-MWCNTs occurred at 250 °C, leaching of the active sites into reaction medium at a reaction temperature of 170 °C was still possible. However, the leaching of the sulfonic groups suffered by the s-MWCNTs was not at a severe level because the sulfur content in the reaction product complied with the ASTM D6751 standard, in which the maximum limit of sulfur content is 0.05 % by mass.

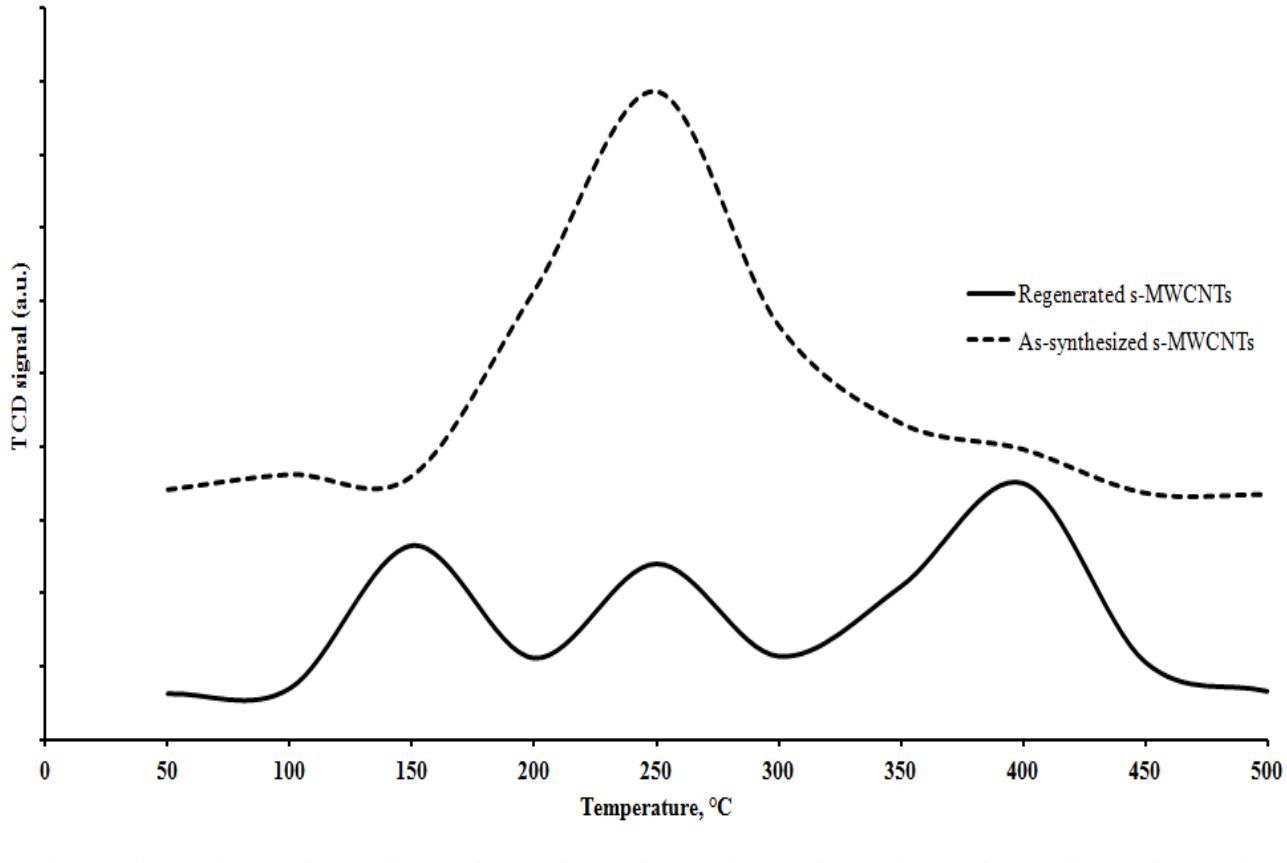

Figure 4.16: NH_3-TPD profiles for as-synthesized and regenerated s-MWCNTs.

4.7 Regeneration of s-MWCNTs

Regeneration of the spent catalyst was required because the catalytic activity of the s-MWCNTs declined after repeated use. At first, re-sulfonation in 10 wt% of $(NH_4)_2SO_4$ solution was the approach to restore the catalytic activity of the spent s-MWCNTs. However, after five consecutive runs under optimum reaction conditions, the spent s-MWCNTs became hydrophobic and did not disperse in $(NH_4)_2SO_4$ solution. This was due to the reduction of COOH group in the s-MWCNTs. As shown in Figure 4.15, the peak of COOH group (in the wave length of 3000 – 2500 cm^{-1}) was hardly to be detected in the s-MWCNTs after five repeated used. Therefore, reflux in concentrated acid (H_2SO_4) was used to regenerate the spent s-MWCNTs. After acid regeneration, the regenerated s-MWCNTs were subjected to another five consecutive esterification runs under the same reaction conditions, and the FAME yields achieved are shown in Figure 4.14. The results indicated that the activity of the regenerated s-MWCNTs was restored to its original level. Moreover, the regenerated s-MWCNTs exhibited better and higher catalytic performance than the un-regenerated s-MWCNTs because the high FAME yields of 86.2 % can be obtained after five repeated uses. The improved catalytic performance of the regenerated s-MWCNTs was due to the increase in the acid site density after acid regeneration. In comparison to the as-synthesized s-MWCNTs with an acid side density of 0.03 $mmolg^{-1}$ (determined by pulse chemisorption), the acid density of the regenerated s-MWCNTs increased significantly to 0.28 $mmolg^{-1}$. In addition, the strength and thermal stability of the acid sites of the regenerated s-MWCNTs was improved after acid regeneration. As shown in Figure 4.16, the ammonia desorption peak of the regenerated s-MWCNTs was extended to a much higher temperature of

400 °C compared to the as-synthesized s-MWCNTs, in which the ammonia desorption peak was observed at 250 °C.

Figure 4.17 shows the TEM images of the as-synthesized s-MWCNTs and the regenerated s-MWCNTs. The TEM observations revealed that the as-synthesized s-MWCNTs possessed a longer open-ended tube length (Figure 4.17 A) compared to that of the regenerated s-MWCNTs (Figure 4.17 B). After acid regeneration, the s-MWCNTs were cut into shorter tubes, as highlighted in Figure 4.17 B. Therefore, the surface area available for the esterification reaction was enhanced.

A

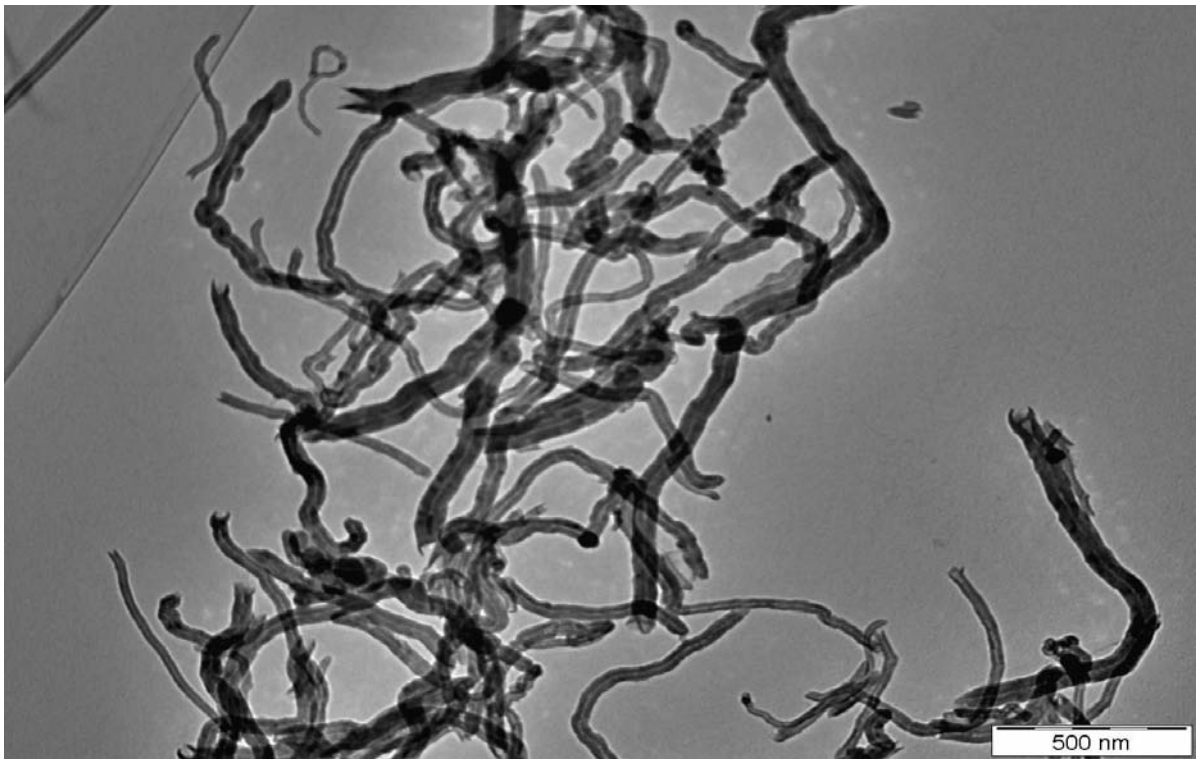

Figure 4.17: TEM images of A as-synthesized s-MWCNTs and B regenerated s-MWCNTs.

B

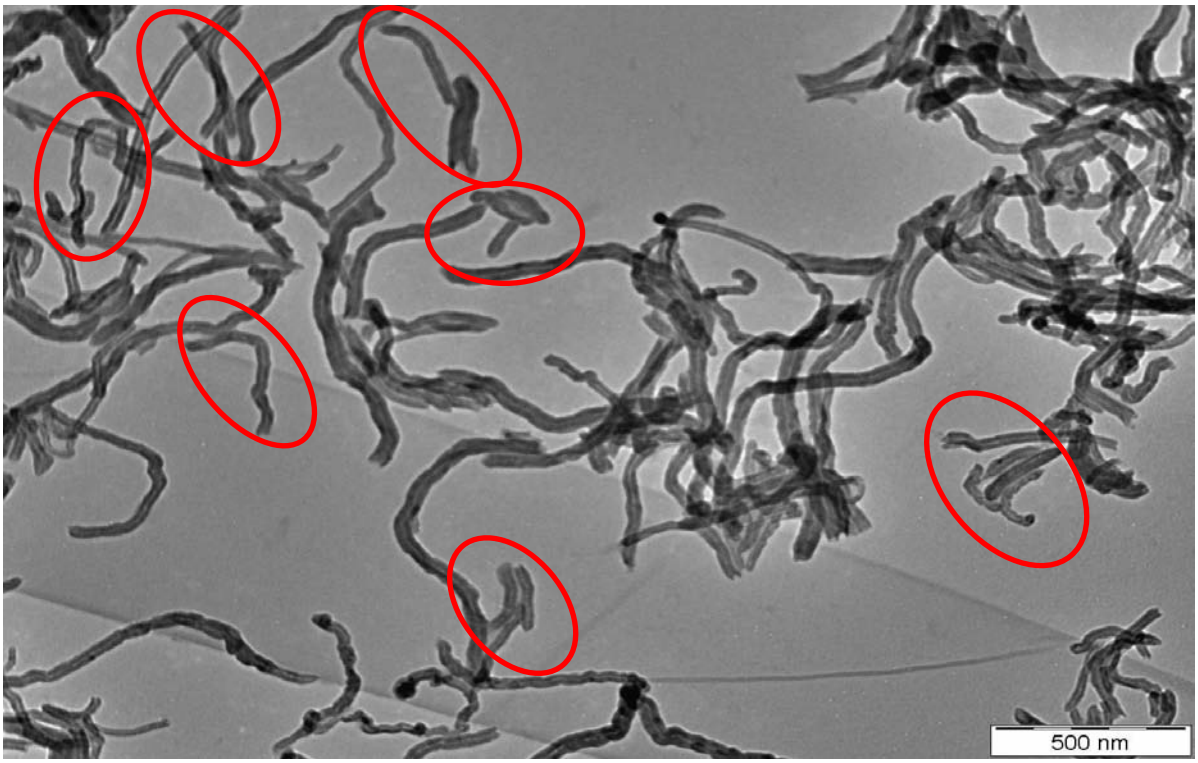

Figure 4.17: Continued.

4.8 Kinetic Model

In general, the kinetic model for heterogeneously catalysed esterification can be well represented by a pseudo-homogeneous model. Therefore, in this study, a pseudo-homogeneous model was developed to illustrate the kinetics of the esterification of PFAD with methanol using s-MWCNTs as catalyst based on the following assumptions (Tesser et al., 2005, Berrios et al., 2007, Su et al., 2008, Su, 2013):

(1) The rate of the esterification reaction under the operating conditions is kinetically controlled.

(2) The entire reaction system is considered to be an ideal solution in which internal and external mass transfer resistance does not exist.

(3) The rate of non-catalysed and self-catalysed esterification is negligible relative to the reaction rate catalysed by the s-MWCNTs.

Based on these assumptions, the reaction is assumed to be an elementary second order reversible reaction and pseudo-homogeneous. The reaction rate of the esterification of PFAD with methanol is expressed as:

$$-\frac{d[RCOOH]}{dt} = k_1[RCOOH][CH_3OH] - k_2[RCOOCH_3][H_2O] \quad (4.1)$$

where [RCOOH] is the molar concentration of PFAD, [CH_3OH] is the molar concentration of methanol, [$RCOOCH_3$] is the molar concentration of FAME, [H_2O] is the molar concentration of water, and k_1 and k_2 are the forward and backward reaction rate constants, respectively.

The relationships between the reactants or products concentration to the yield of FAME are defined as below:

$$[RCOOH] = [RCOOH]^0 - x[RCOOH]^0 = [RCOOH]^0(1-x) \quad (4.2)$$

$$[CH_3OH] = [CH_3OH]^0 - x[RCOOH]^0 \quad (4.3)$$

$$\left[RCOOCH_3\right] = x\left[RCOOH\right]^0 \tag{4.4}$$

$$\left[H_2O\right] = x\left[RCOOH\right]^0 \tag{4.5}$$

where $\left[RCOOH\right]^0$ is the initial concentration of PFAD and x is the conversion of PFAD.

Substitute Equation 4.2 to 4.5 into Equation 4.1,

$$-\frac{d\left\{\left[RCOOH\right]^0(1-x)\right\}}{dt} = k_1\left[RCOOH\right]^0(1-x)\left\{\left[CH_3OH\right]^0 - x\left[RCOOH\right]^0\right\} - k_2\left(x\left[RCOOH\right]^0\right)^2$$

$$\Rightarrow -\left[RCOOH\right]^0\frac{d(1-x)}{dt} = k_1\left[RCOOH\right]^0(1-x)\left\{\left[CH_3OH\right]^0 - x\left[RCOOH\right]^0\right\} - k_2\left(x\left[RCOOH\right]^0\right)^2$$

$$\Rightarrow -\left[RCOOH\right]^0\left(\frac{d(1)}{dt} - \frac{d(x)}{dt}\right) = k_1\left[RCOOH\right]^0(1-x)\left\{\left[CH_3OH\right]^0 - x\left[RCOOH\right]^0\right\} - k_2\left(x\left[RCOOH\right]^0\right)^2$$

$$\Rightarrow \left[RCOOH\right]^0\left[\frac{dx}{dt}\right] = k_1\left[RCOOH\right]^0(1-x)\left\{\left[CH_3OH\right]^0 - x\left[RCOOH\right]^0\right\} - k_2x^2\left\{\left[RCOOH\right]^0\right\}^2$$

$$\Rightarrow \frac{dx}{dt} = k_1(1-x)\left\{\left[CH_3OH\right]^0 - x\left[RCOOH\right]^0\right\} - k_2x^2\left[RCOOH\right]^0$$

$$\Rightarrow \frac{dx}{dt} = k_1\left\{\left[CH_3OH\right]^0 - x\left[RCOOH\right]^0 - x\left[CH_3OH\right]^0 + x^2\left[RCOOH\right]^0\right\} - k_2x^2\left[RCOOH\right]^0$$

$$\Rightarrow \frac{dx}{dt} = k_1\left\{x^2\left[RCOOH\right]^0 - x\left(\left[RCOOH\right]^0 + \left[CH_3OH\right]^0\right) + \left[CH_3OH\right]^0\right\} - k_2x^2\left[RCOOH\right]^0$$

$$\Rightarrow \frac{dx}{dt} = k_1\left[RCOOH\right]^0\left\{\left[x^2 - x(1 + \frac{\left[CH_3OH\right]^0}{\left[RCOOH\right]^0}) + \frac{\left[CH_3OH\right]^0}{\left[RCOOH\right]^0}\right] - x^2\frac{k_2}{k_1}\right\}$$

Let $\frac{[CH_3OH]^0}{[RCOOH]^0} = \theta$ and $k_e = \frac{k_1}{k_2}$

$$\frac{dx}{dt} = k_1[RCOOH]^0\left\{\left[x^2 - x(1+\theta) + \theta\right] - \frac{x^2}{k_e}\right\}$$

$$\frac{dx}{dt} = k_1[RCOOH]^0\left[\left(1 - \frac{1}{k_e}\right)x^2 - (1-\theta)x + \theta\right] \quad (4.6)$$

where θ is the molar ratio of methanol to PFAD and k_e is the equilibrium rate constant.

At the equilibrium state, $\frac{dx}{dt} = 0$ and $x = x_e$ (x_e is the PFAD conversion at equilibrium), Equation 4.6 can be rearranged into Equation 4.7. Thus, k_e can be determined experimentally on the basis of the PFAD conversion at equilibrium.

$$k_1[RCOOH]^0\left[\left(1 - \frac{1}{k_e}\right)x_e^2 - (1-\theta)x_e + \theta\right] = 0$$

$$\Rightarrow (\theta - x_e)(1 - x_e) - \frac{x_e}{k_e} = 0$$

$$\Rightarrow k_e = \frac{x_e^2}{(\theta - x_e)(1 - x_e)} \quad (4.7)$$

Once k_e is determined, Equation 4.6 is integrated to obtain a linear equation to determine k_1 numerically.

$$\int_0^x \frac{1}{\left(1-\frac{1}{k_e}\right)x^2-(1+\theta)x+\theta}dx=\int_0^t k_1[RCOOH]^0 dt \tag{4.8}$$

From the integral formula table, three solutions can be obtained for Equation 4.8,

$$\int_0^x \frac{1}{ax^2-bx+c}dx=\frac{2}{\sqrt{4ac-b^2}}\tan^{-1}\frac{2ax+b}{\sqrt{4ac-b^2}} \qquad \text{when } 4ac-b^2>0$$

$$\int \frac{1}{ax^2+bx+c}dx=\frac{1}{\sqrt{b^2-4ac}}\ln\left[\frac{2ax+b-\sqrt{b^2-4ac}}{2ax+b+\sqrt{b^2-4ac}}\right] \qquad \text{when } 4ac-b^2<0$$

$$\int_0^x \frac{1}{ax^2-bx+c}dx=-\frac{2}{2ax+b} \qquad \text{when } 4ac-b^2=0$$

For this study, $4ac-b^2$ is always < 0, Equation 4.8 can be transformed into:

$$\frac{1}{\sqrt{\left[-(1+\theta)\right]^2-4\theta\left(1-\frac{1}{k_e}\right)}}ln\left[\frac{2\left(1-\frac{1}{k_e}\right)x-(1+\theta)-\sqrt{\left[-(1+\theta)^2-4\theta\left(1-\frac{1}{k_e}\right)\right]}}{2\left(1-\frac{1}{k_e}\right)x-(1+\theta)+\sqrt{\left[-(1+\theta)^2-4\theta\left(1-\frac{1}{k_e}\right)\right]}}\right]_0^x=k_1[RCOOH]^0 t$$

Let $\left(1-\frac{1}{k_e}\right)=\alpha$ and $\sqrt{(1+\theta)^2-4\alpha\theta}=\beta$,

$$\frac{1}{\beta}ln\left[\frac{2\alpha x-(1+\theta)-\beta}{2\alpha x-(1+\theta)+\beta}\right]_0^x=k_1[RCOOH]^0t$$

$$\Rightarrow ln\left[\frac{2\alpha x-(1+\theta)-\beta}{2\alpha x-(1+\theta)+\beta}\right]_0^x=\beta k_1[RCOOH]^0t$$

$$\Rightarrow ln\left[\frac{2\alpha x-(1+\theta)-\beta}{2\alpha x-(1+\theta)+\beta}\right]-ln\left[\frac{-(1+\theta)-\beta}{-(1+\theta)+\beta}\right]=\beta k_1[RCOOH]^0t$$

By using the rule of thumb in natural logarithms where $\ln a-\ln b=\ln\frac{a}{b}$,

$$\Rightarrow ln\left[\frac{2\alpha x-(1+\theta)-\beta}{2\alpha x-(1+\theta)+\beta}\times\frac{-(1+\theta)-\beta}{-(1+\theta)+\beta}\right]=\beta k_1[RCOOH]^0t$$

$$\Rightarrow ln\left[\frac{-2\alpha x(1+\theta)+2\alpha\beta x+(1+\theta)^2-\beta(1+\theta)+\beta(1+\theta)-\beta^2}{-2\alpha x(1+\theta)-2\alpha\beta x+(1+\theta)^2+\beta(1+\theta)-\beta(1+\theta)-\beta^2}\right]=\beta k_1[RCOOH]^0t$$

$$\Rightarrow ln\left[\frac{2\alpha x(-1-\theta+\beta)+(1+\theta)^2-\beta^2}{2\alpha x(-1-\theta-\beta)+(1+\theta)^2-\beta^2}\right]=\beta k_1[RCOOH]^0t$$

It has been defined earlier that $\beta=\sqrt{(1+\theta)^2-4\alpha\theta}$. Therefore, $\beta^2=(1+\theta)^2-4\alpha\theta$.

$$\Rightarrow ln\left[\frac{2\alpha x(-1-\theta+\beta)+(1+\theta)^2-(1+\theta)^2+4\alpha\theta}{2\alpha x(-1-\theta-\beta)+(1+\theta)^2-(1+\theta)^2+4\alpha\theta}\right]=\beta k_1[RCOOH]^0t$$

$$\Rightarrow ln\left[\frac{2\alpha x(-1-\theta+\beta)+4\alpha\theta}{2\alpha x(-1-\theta-\beta)+4\alpha\theta}\right]=\beta k_1[RCOOH]^0 t$$

$$\Rightarrow ln\left[\frac{2\alpha[(-1-\theta+\beta)x+2\theta]}{2\alpha[(-1-\theta-\beta)x+2\theta]}\right]=\beta k_1[RCOOH]^0 t$$

$$\Rightarrow ln\left[\frac{(-1-\theta+\beta)x+2\theta}{(-1-\theta-\beta)x+2\theta}\right]=\beta k_1[RCOOH]^0 t \qquad (4.9)$$

Rearrangement of Equation 4.9 can provide an explicit expression for x (Equation 4.10) to determine the variation in the conversion of PFAD with time.

$$x=\frac{2\theta[e^{\beta k_1[RCOOH]^0 t}-1]}{(-1-\theta+\beta)+(1+\theta+\beta)e^{\beta k_1[RCOOH]^0 t}} \qquad (4.10)$$

The influence of temperature on the reaction rate was examined using the Arrhenius equation,

$$k_1=A_1 e^{-E_1/RT} \qquad (4.11)$$

$$k_e=A_e e^{-E_e/RT} \qquad (4.12)$$

where A_1 and A_e are the pre-exponential or frequency factors for the forward reaction rate constant and the equilibrium constant, respectively. Furthermore, E_1 and E_e represent the activation energy of the forward and equilibrium reactions, respectively. R is the ideal constant, and T is the reaction temperature in units of Kelvin.

4.8.1 Reaction Rate Constants

The equilibrium rate constant k_e can be determined from the final FAME yield using Equation 4.7. Then, by using the calculated k_e, the values of α and β can be obtained. As defined in Equation 4.9, the reaction rate constant k_1 must be determined by the experimental FAME yield obtained for different reaction times. Figure 4.18, 4.19 and 4.20 show the correlation between $\ln\left[\frac{(-1-\theta+\beta)x+2\theta}{(-1-\theta-\beta)x+2\theta}\right]$ and $\beta \cdot [RCOOH]^{\circ} \cdot t$, under all the experimental conditions presented in Figure 4.11, 4.12 and 4.13. The straight lines with high R^2 (more than 0.93) observed in Figure 4.18, 4.19 and 4.20 demonstrated the validity of the proposed kinetic model. Hence, the values of k_1 were obtained as the slope of each straight line in the figures.

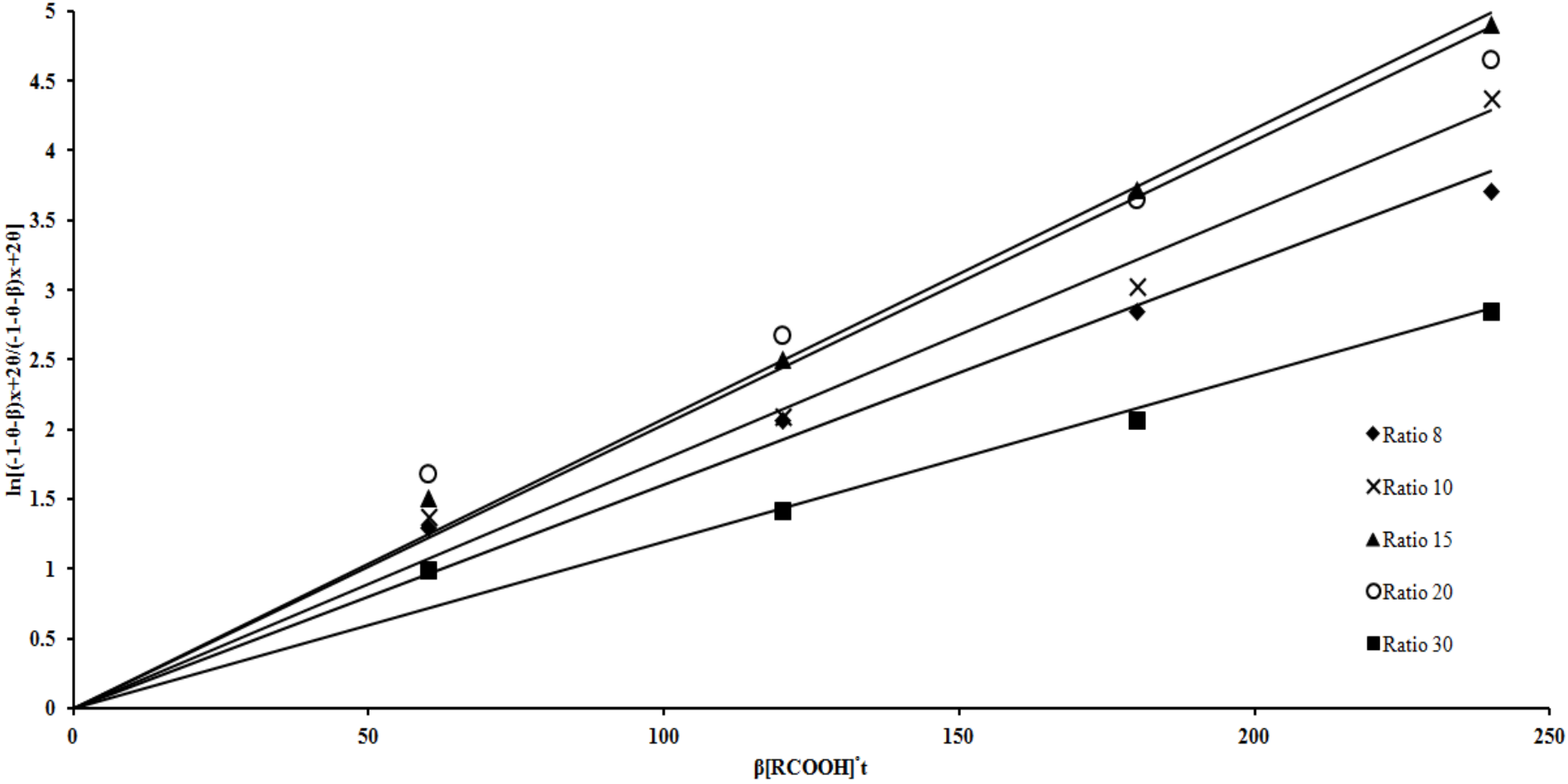

Figure 4.18: Correlation between $\ln\left[\frac{(-1-\theta+\beta)x+2\theta}{(-1-\theta-\beta)x+2\theta}\right]$ and $\beta.\ [RCOOH]^{\circ}.\ t$ at different levels of the methanol-to-PFAD ratio.

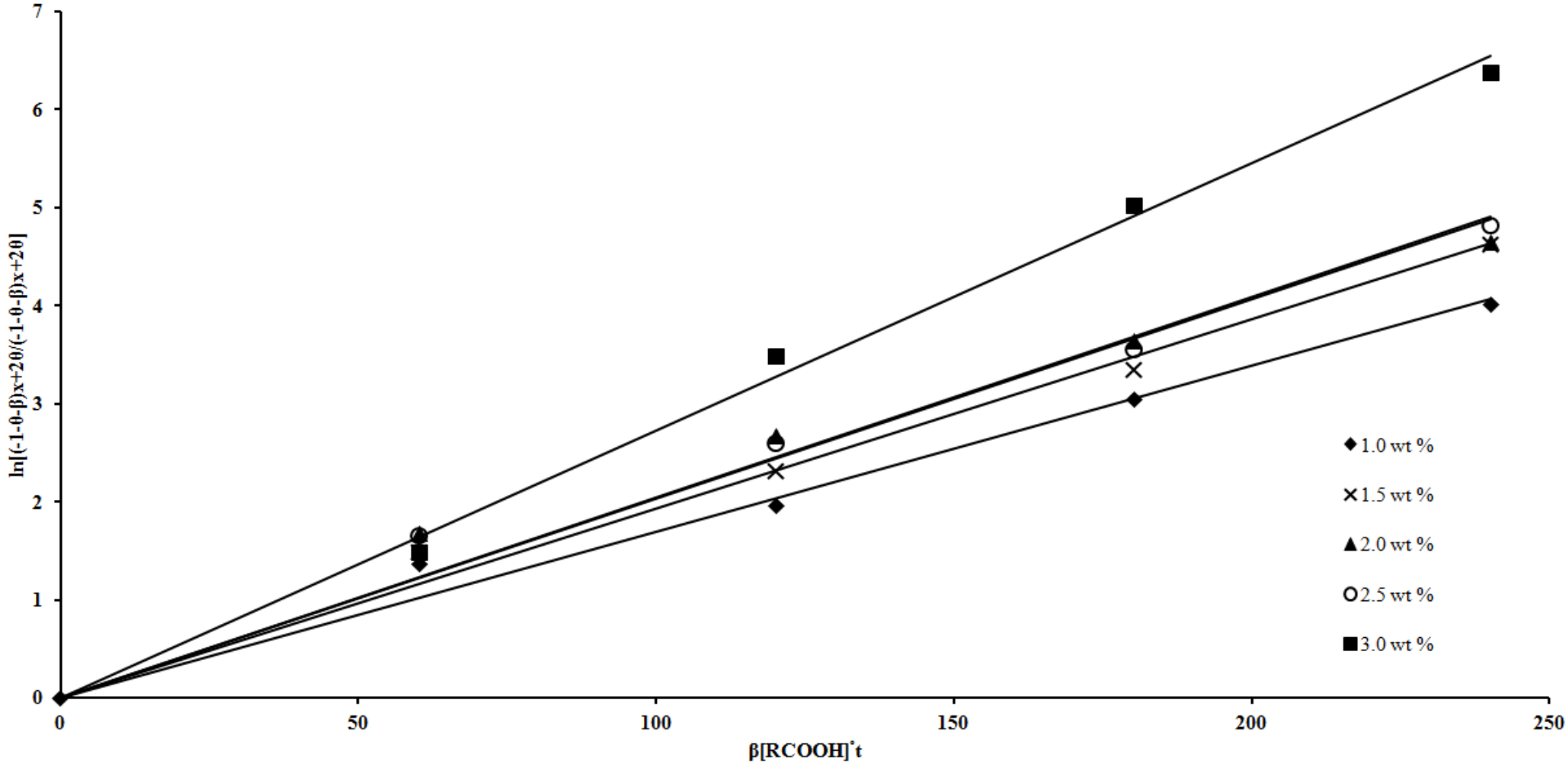

Figure 4.19: Correlation between $\ln\left[\frac{(-1-\theta+\beta)x+2\theta}{(-1-\theta-\beta)x+2\theta}\right]$ and $\beta.\ [RCOOH]^{\circ}.\ t$ at different levels of the catalyst loading.

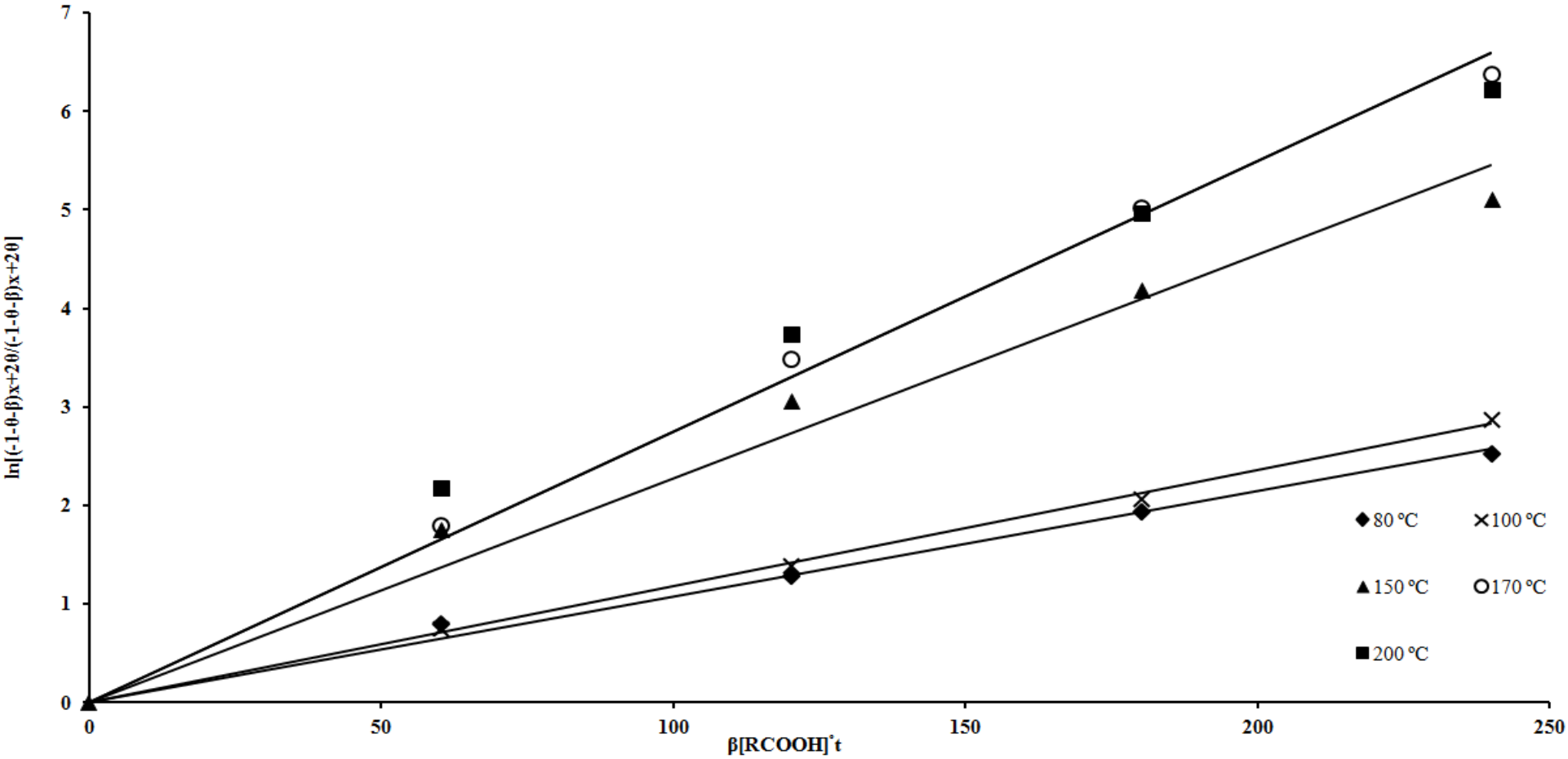

Figure 4.20: Correlation between $\ln\left[\frac{(-1-\theta+\beta)x+2\theta}{(-1-\theta-\beta)x+2\theta}\right]$ and $\beta.\ [RCOOH]^{\circ}.\ t$ at different levels of the reaction temperature.

The calculated values of k_e and k_1 for different methanol-to-PFAD ratios, catalyst loadings and reaction temperatures are summarised in Table 4.9. The values of k_e and k_1 were observed to increase as the catalyst loading and reaction temperature increased. A different trend was obtained for the k_e of the methanol-to-PFAD ratio, in which the k_e decreased slightly when the ratio increased. This difference might be due to the similar equilibrium FAME yield that was obtained even though the increase of methanol-to-PFAD ratio was significant. It was expected that the FAME yield would increase significantly through the increase of methanol-to-PFAD ratio. However, as shown in Figure 4.11, the equilibrium FAME yield obtained for methanol-to-PFAD ratio 8, 10, 15 and 20 were very close to each other. Thus, according to Equation 4.7, k_e decreased when methanol-to-PFAD ratio increased because of similar x_e. However, the k_1 of the methanol-to-PFAD ratio increased when the ratio increased from 8 to 20. This indicated that the rate of the esterification can be increased by using a higher methanol ratio. In addition, both k_e and k_1 for a methanol-to-PFAD ratio of 30 were much lower than those of the other ratios because deactivation of catalyst occurred at the extremely high methanol content.

The current study further verified the fact that esterification is an endothermic reaction because, compared to other parameters, such as methanol-to-PFAD ratio and catalyst loading, the k_e increased significantly with an increase in the reaction temperature. This result was in agreement with those reported in the literature (Goto et al., 1991, Bart et al., 1994, Aafaqi et al., 2004, Su et al., 2008, Su, 2013).

Table 4.9: The kinetic parameters for the esterification of PFAD with methanol using s-MWCNTs as a catalyst for different levels of methanol-to-PFAD ratio, catalyst loading and reaction temperature.

Reaction Parameters	Equilibrium constant, k_e	Forward reaction rate, k_1 (L mol^{-1} min^{-1})	R^2
Methanol:PFAD ratio			
8	0.39	4.97×10^{-4}	0.9502
10	0.33	5.08×10^{-4}	0.9722
15	0.21	5.77×10^{-4}	0.9882
20	0.21	6.17×10^{-4}	0.9329
30	0.05	2.45×10^{-4}	0.9565
Catalyst loading (wt %)			
1.0	0.16	4.72×10^{-4}	0.9675
1.5	0.19	5.66×10^{-4}	0.9765
2.0	0.21	6.17×10^{-4}	0.9329
2.5	0.26	6.51×10^{-4}	0.9574
3.0	0.50	9.81×10^{-4}	0.9920
Reaction temperature (°C)			
80	9.71×10^{-4}	3.05×10^{-5}	0.9851
100	3.07×10^{-3}	6.00×10^{-5}	0.9965
150	0.23	7.00×10^{-4}	0.9363
170	0.50	9.80×10^{-4}	0.9905
200	0.70	1.03×10^{-3}	0.9317

4.8.2 Activation energy, Pre-Exponential Factor and Enthalpy of Reaction

As shown in the previous section, both k_e and k_1 were significantly affected by the reaction temperature. Therefore, the dependence of k_e and k_1 on the reaction temperature can be illustrated by the Arrhenius equations. Equation 4.11 and 4.12 were linearized, and the Arrhenius-van't Hoff plot was used by plotting ln *k* as a function of the reciprocal temperature (in units of Kelvin) to determine the pre-exponential factor, activation energy and enthalpy of the esterification. The Arrhenius-Van't Hoff plot is shown in Figure 4.21; the pre-exponential factor was obtained from the intercept of the straight line, while the activation energy (for forward and backward) and the enthalpy of esterification were obtained from the slope of the straight line. The pre-exponential factors of the forward and equilibrium reactions were 1.9×10^2 and 2.7×10^9 L mol^{-1} min^{-1}, respectively. The activation energy for forward reaction was 45.80 kJ mol^{-1}. The high value of the activation energy implied that the esterification reaction was a temperature-dependent reaction. This high value of activation energy also indicated that the esterification was kinetically controlled instead of diffusion controlled (Su et al., 2008, Su, 2013), which further verified the assumption of the absence of external and internal mass transfer resistance in the pseudo-homogeneous kinetic model. The endothermic nature of the esterification of PFAD with methanol was confirmed due to the positive value of the reaction enthalpy (84. 10 kJ mol^{-1}).

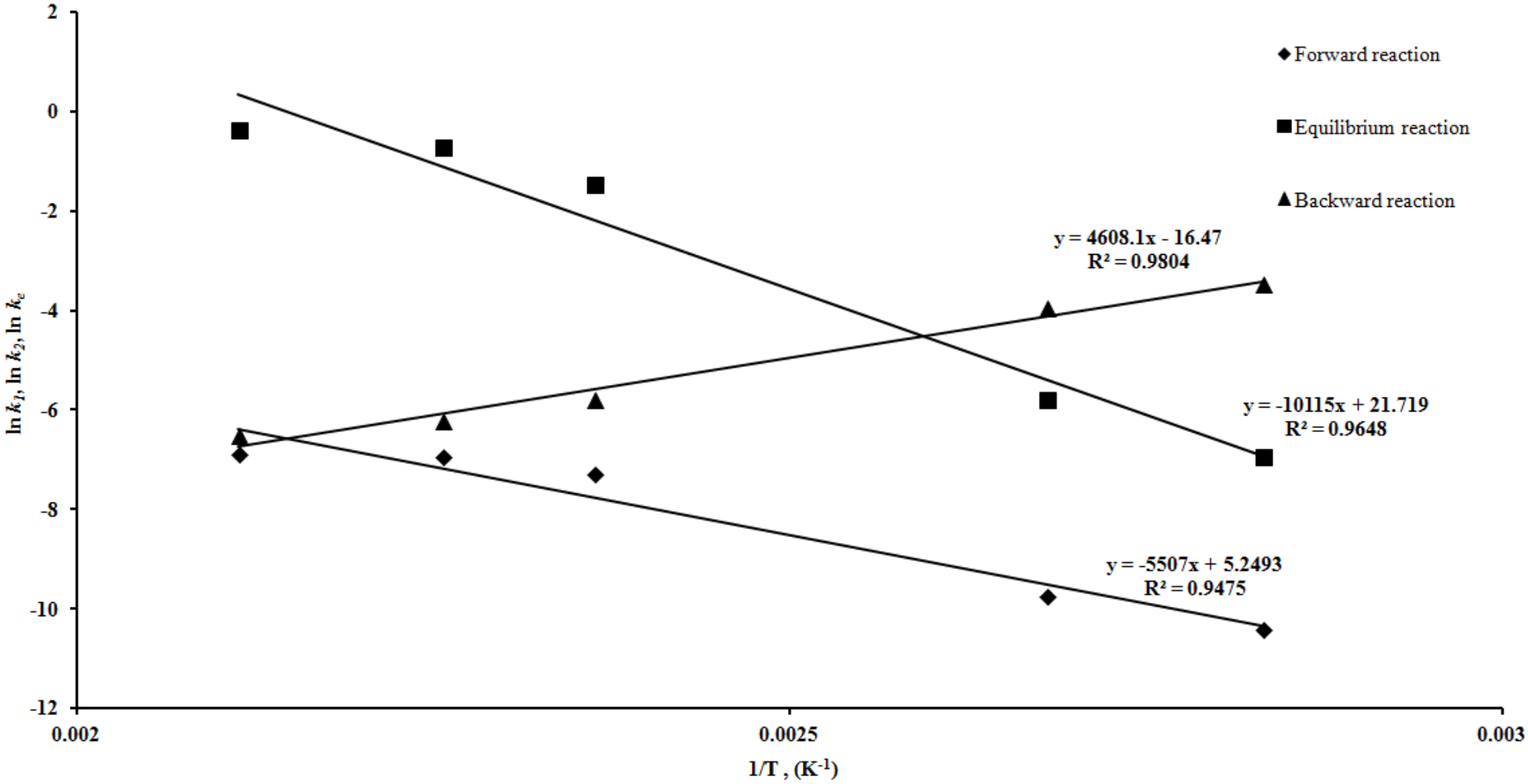

Figure 4.21: Arrhenius-Van't Hoff plot for the forward, backward and equilibrium reactions in the temperature range of 353 – 473 K.

However, the activation energy for the backward reaction was found to have a negative value (-38.30 kJ mol^{-1}) that was much smaller than the activation energy of the forward reaction. The negative or low activation energy indicated that the reaction rate decreased when the reaction temperature increased, which also meant that the reaction was mass-transfer controlled (Nijhuis et al., 2003, Su et al., 2008, Melero et al., 2009). Therefore, for the reversible endothermic reaction, such as esterification, the increase in the reaction temperature not only increased the reaction rate of the forward reaction but also suppressed the backward reaction.

4.8.3 Goodness-of-Fit of the Experimental Data to the Developed Kinetic Model

After all the kinetic parameters were determined, the model was used to simulate the predicted PFAD conversion at the reaction conditions used in the actual experiments. Equation 4.10 was used to compute the simulated PFAD conversion. Figure 4.22 shows the correlation between the simulated and experimental PFAD conversions. A line of unit slope with almost perfect fit with many points corresponding to zero error between the experimental and predicted values was observed. The simulated values matched the experimental values very well, with an R^2 value very close to unity of 0.9866. This agreement indicated that the developed kinetic model was reliable in representing this particular esterification reaction system and can thus be used to predict the PFAD conversion of the reaction under other operating parameters as well.

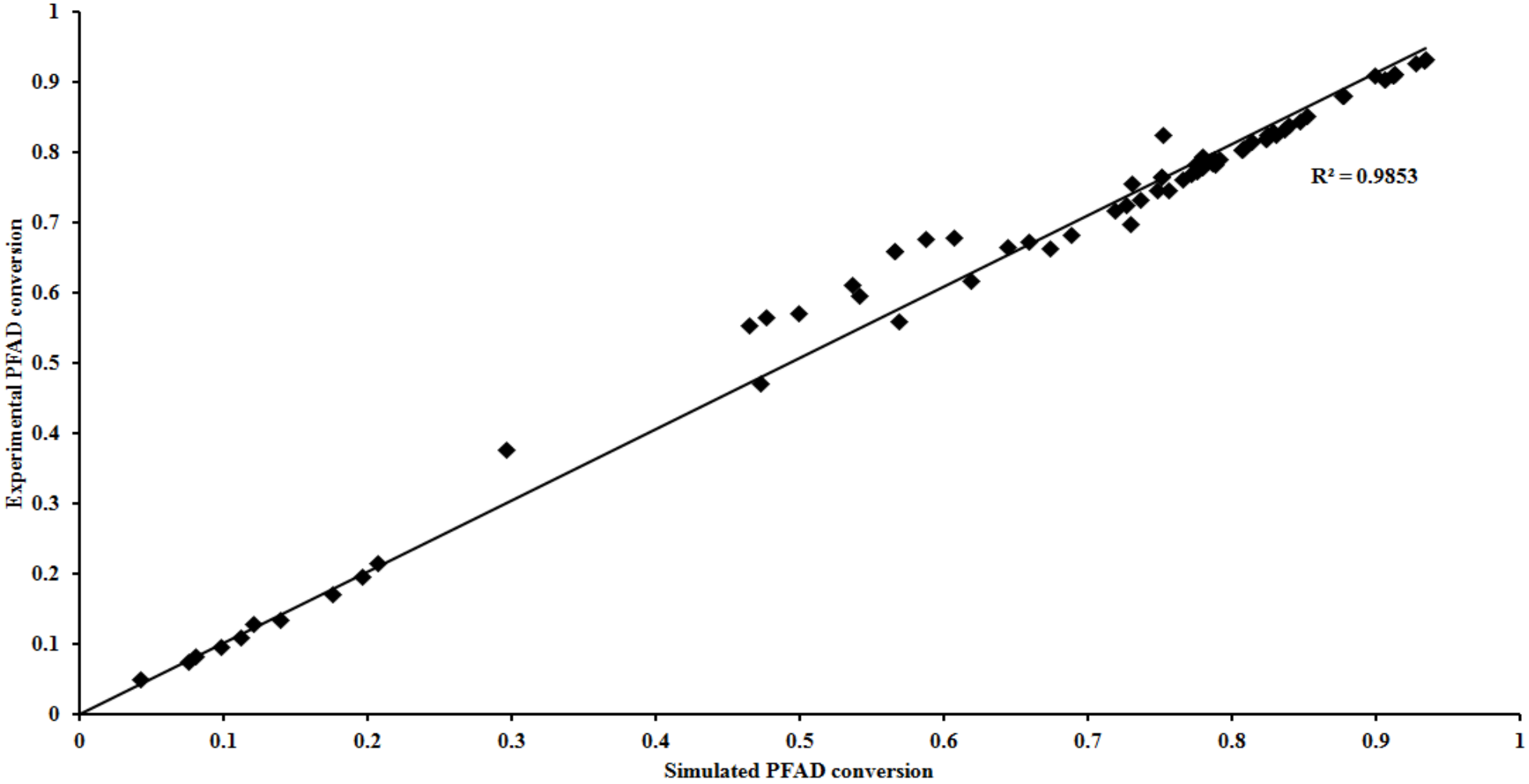

Figure 4.22: Correlation between the simulated and the experimental FAME yield.

4.8.4 Comparison of the Activation Energy Exhibited by s-MWCNTs and Various Biodiesel Production Catalysts

Table 4.10 presents the comparison of the activation energy exhibited by s-MWCNTs and various catalysts for biodiesel production (Darnoko and Cheryan, 2000, Tesser et al., 2005, Pasias et al., 2006, Vicente et al., 2006, Berrios et al., 2007, Aranda et al., 2008, Su et al., 2008, Vyas et al., 2009, Liu et al., 2010, Gan et al., 2012, Sivakumar et al., 2013, Su, 2013). Note that the activation energy obtained in this study was actually lower than the activation energy exhibited by most of the catalysts, especially the popular KOH. This lower activation energy indicated that a heterogeneous process is not necessarily more energy intensive than the homogeneous process in biodiesel production. As defined in Equation 4.11, the esterification reaction rate is inversely proportional to the activation energy, in which the lower the activation energy is, the higher is the reaction rate. The reaction can be effectively enhanced by the reduction of the activation energy. Therefore, the s-MWCNTs appear to be an attractive and promising alternative for the catalyst in biodiesel production because of the lower activation energy required for the reaction.

Table 4.10: Comparison of the activation energy of biodiesel production using various catalysts.

Oil source	Reaction temperature (°C)	Catalysts	Catalyst loading (wt % of oil)	Alcohol source	Alcohol-to-oil molar ratio	Activation energy (kJ mol^{-1})	Reference
PFAD	170	s-MWCNTs	3.0	Methanol	20.0	45.80	This study
Palm oil	50 - 65	KOH	1.0- 1.2	Methanol	6.0	147.70	(Darnoko and Cheryan, 2000)
Oleic acid	50 - 100	Acid sulfonic resin, Relite CFS	3.5 – 8.8	Methanol	8.3 – 10.7	58.58	(Tesser et al., 2005)
Free fatty acids in vegetable oils	90 - 120	Purolite CT275	2.0	Methanol	6.6 (methanol: free fatty acid)	70.34	(Pasias et al., 2006)
Brassica carinata oil	25 - 65	KOH	1.5	Methanol	6.0	209.21	(Vicente et al., 2006)
Sunflower oil	60	H_2SO_4	5.0 (based on oleic acid)	Methanol	60.0 (methanol: oleic acid ratio)	50.75	(Berrios et al., 2007)
Fatty acid by enzymatic hydrolysis of soybean oil	60 - 80	Cation-exchange resin, Dowex Monosphere 88	26.8	Methanol	1.0 – 20.0	59.44	(Su et al., 2008)
Palm oil	130 - 160	Methanesulfonic acid	0.05	Methanol	10.0	15.84	(Aranda et al., 2008)
	130 - 160	H_2SO_4	0.05	Methanol	10.0	27.31	
Jatropha oil	50 - 70	KNO_3/Al_2O_3	6.0	Methanol	12.0	112.79	(Vyas et al., 2009)
Soybean oil	65	SrO	2.0	Methanol	12.0	40.17	(Liu et al., 2010)
	65	$Ca(OCH_2CH_3)_2$	2.0	Methanol	12.0	54.39	
	65	CaO	2.0	Methanol	12.0	81.17	
	65	$Ca(OCH_3)_2$	2.0	Methanol	12.0	73.64	
Waste cooking oil	65	Amberlyst-15	4.0	Methanol	15:1	77.17	(Gan et al., 2012)
Fatty acid by enzymatic hydrolysis of soybean oil	30 - 70	HCl	0.1 – 1.0 M	Methanol	1.0 – 20.0	44.86	(Su, 2013)
Ceiba Pentandra oil	65	KOH	1.0	Methanol	6.0	105.42	(Sivakumar et al., 2013)

4.9 Esterification of PFAD via Pervaporation Membrane Reactor

Although the use of s-MWCNTs can overcome the limitations caused by the homogeneous and conventional heterogeneous catalysts, the esterification of PFAD is still being limited by the thermodynamic equilibrium. Therefore, the feasibility of pervaporation membrane reactor in enhancing the FAME yield of the esterification of PFAD with methanol was investigated in this study.

4.9.1 Synthesis Route of 6FDA-NDA/DABA Polyimide

6FDA-NDA/DABA is synthesized from 4,4'-(hexafluroisopropylidene) diphthalic anhydride (6FDA) and two types of diamine, 1,5-naphthalene diamine (NDA) and 3,5-diaminobenzoic acid (DABA). The chemical structures of the monomers and the synthesis route of 6FDA-NDA/DABA polyimide are shown in Figure 4.23. First, the amine groups (NH_2) of NDA and/or DABA moieties will react with the carbonyl carbon of the 6FDA moieties via nucleophilic attack, leading to opening of the anhydride ring of 6FDA to form poly(amic acid). The reaction is usually carried out in room temperature because the formation of poly(amic acid) is an exothermic process (Anthamatten et al., 2004). Subsequently, chemical imidization occurs under the catalyzation of 3-methylpyridine to convert the poly(amic acid) into polyimide. Water is generated as by-product. The presence of water in the polymer mixture was unfavoured because water will hydrolyze the anhydride groups to form carboxyl acid, resulting the formation of low molecular weight poly(amic acid) (Padavan and Wan, 2010). Therefore, acetic anhydride which serves as dehydration agent was added to remove the generated water.

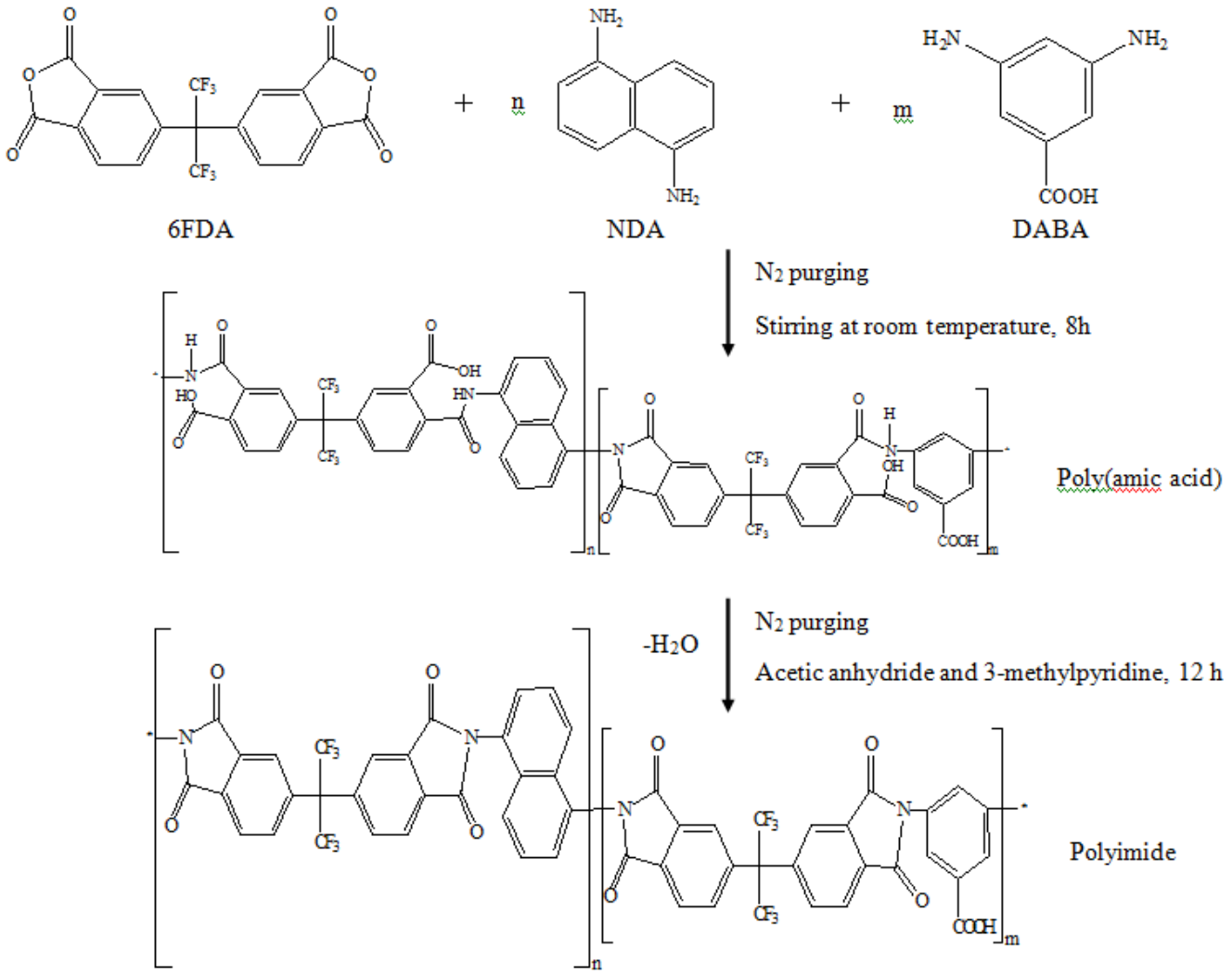

Figure 4.23: Synthesis route of 6FDA-NDA/DABA polyimide (Le et al., 2012, Ong et al., 2012).

4.9.2 Thermal Cross-linking of 6FDA-NDA/DABA Polyimide Membrane

Even though it was reported that polyimide membrane possessed low degree of swelling in aqueous solution compared to other conventional membrane materials such as PVA and chitosan. However, its swelling might still affect significantly the performance of pervaporation (Le et al., 2012). Therefore, cross-linking is a simple but efficient method to reduce the swelling of the membrane, thus enhancing the membrane performance (Castanheiro et al., 2006, Le et al., 2012). Since 6FDA-NDA/DABA polyimide membrane contained COOH groups in DABA moiety, high temperature thermal cross-linking is a simple and facile method to cross-link the membrane. Thermal cross-linking is a kind of decarboxylation-induced cross-linking reaction that occurred at high temperature (Le et al., 2012). Therefore, thermal cross-linking can only be performed for COOH-group containing polyimide. The mechanisms of thermal cross-linking of the polyimide membrane are presented in Figure 4.24. The thermal cross-linking of the polyimide membrane begins with the formation of an anhydride between the COOH groups of two adjacent DABA moieties under high temperature. Then, decarboxylation of the anhydride occurs to form two phenyl free radicals by releasing a molecule of CO and a molecule of CO_2. Subsequently, these highly reactive intermediates interact with each other to form a linkage between two polymer chains (Qiu et al., 2011, Le et al., 2012).

A

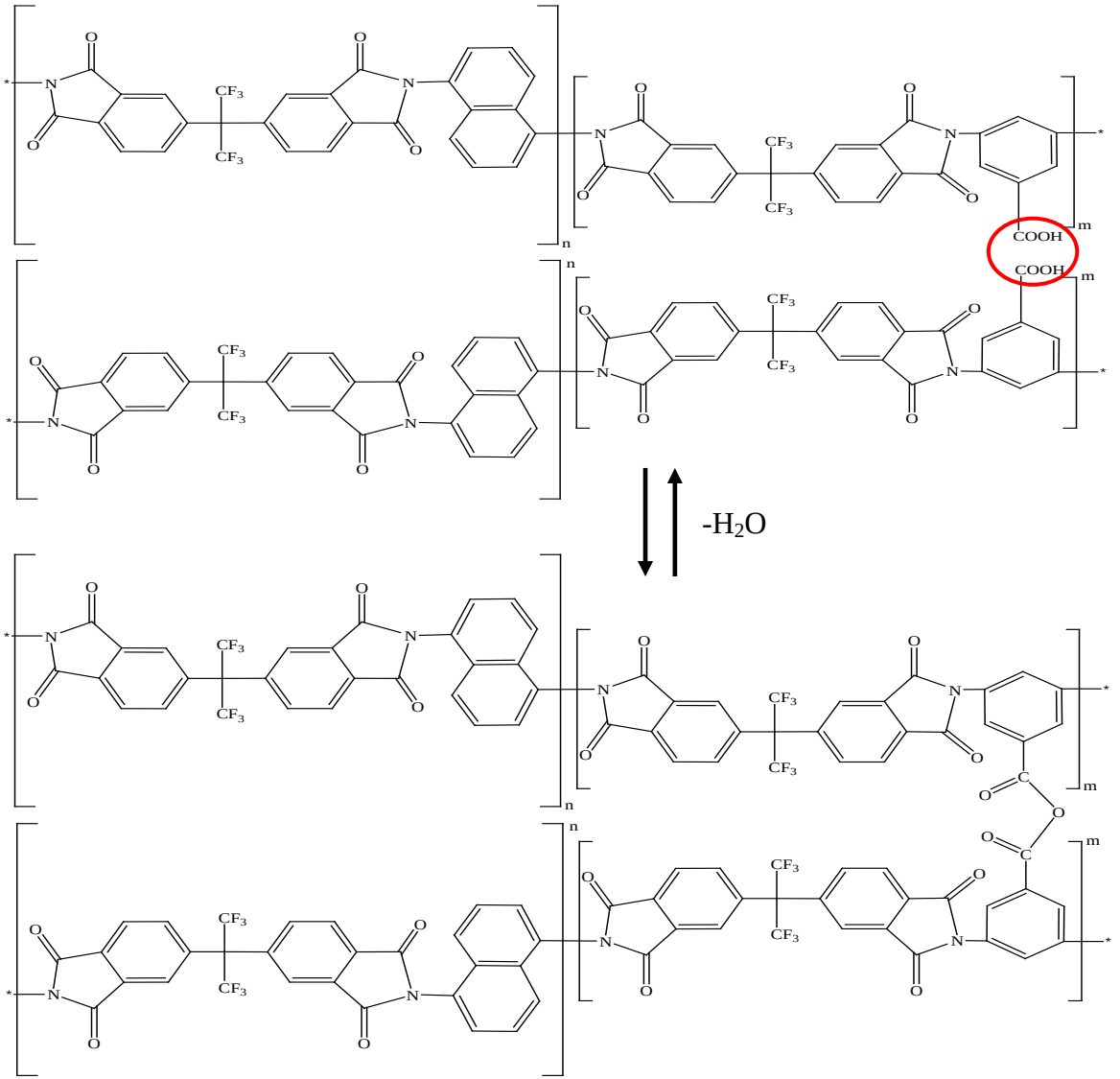

Figure 4.24: Cross-linking mechanisms of polyimide membrane: A anhydride formation B decarboxylation C cross-linking.

B

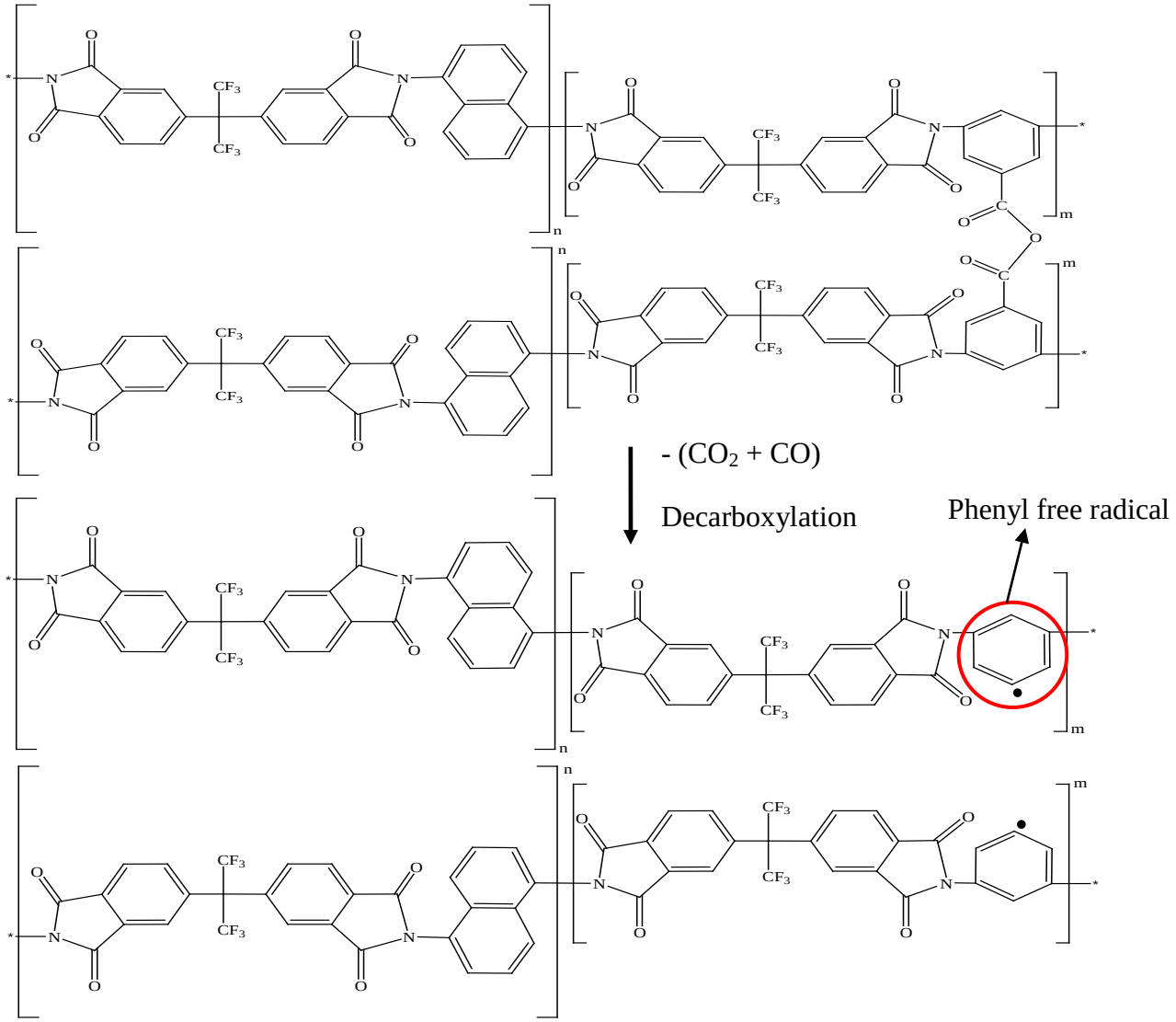

Figure 4.24: Continued.

C

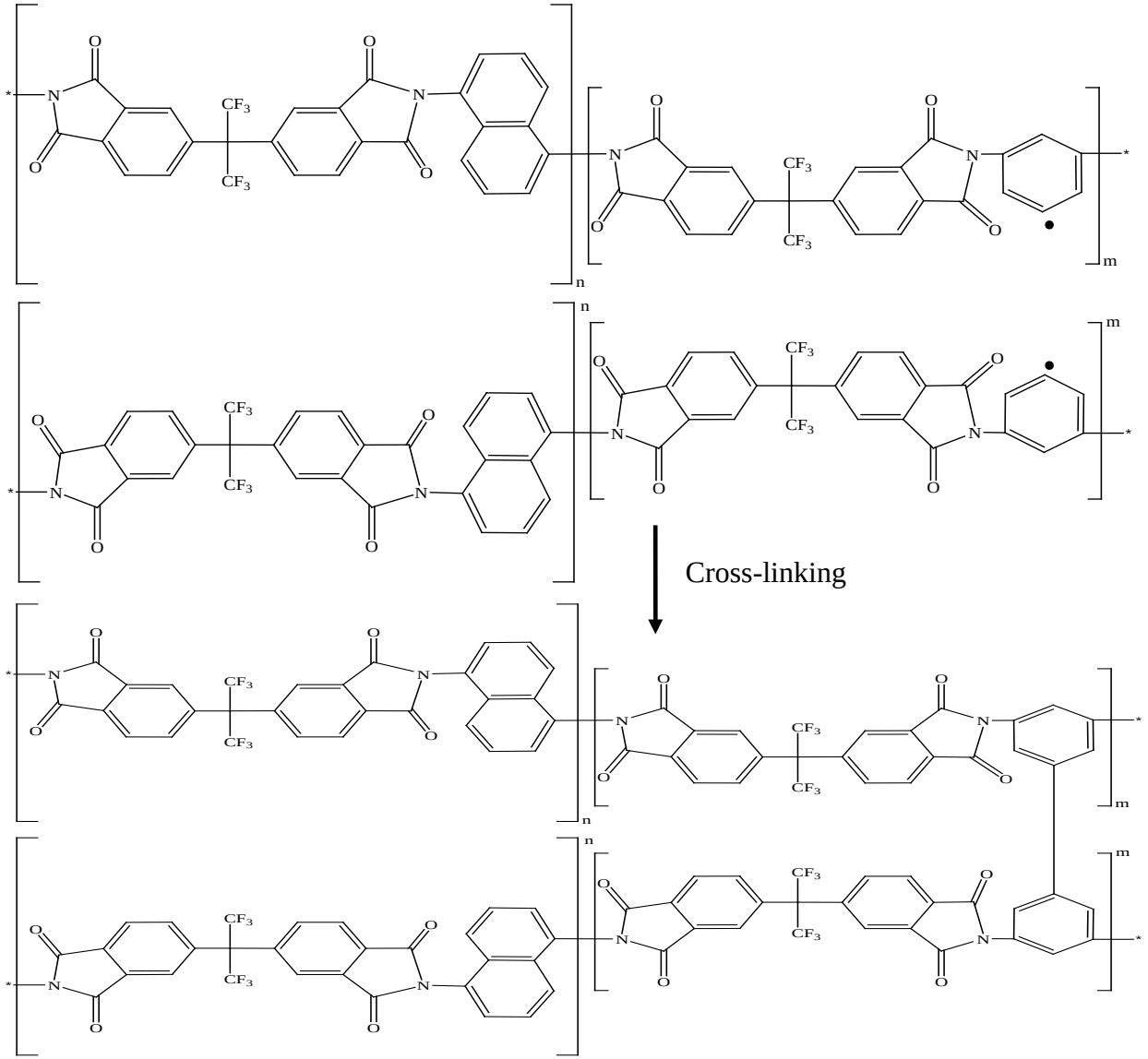

Figure 4.24: Continued.

4.9.3 Feasibility Study of the Esterification of PFAD via Pervaporation Membrane Reactor

The feasibility study of the integration of reactor and separator through pervaporation membrane reactor system was investigated in this study. This enables to combine the reactor and membrane separator into a single unit. The process of biodiesel production via membrane reactor is also known as reactive separation in which reaction and separation occur in one single step.

The esterification of PFAD via pervaporation membrane reactor was first carried out by using the as-synthesized 6FDA-NDA/DABA polyimide membrane (without cross-linking). However, leakage of reactants (methanol and PFAD) and catalyst (s-MWCNTs) into the permeate side was found within 2 h of reaction time due to the swelling under high temperature and pressure that spoiled the membrane. Therefore, the reaction was carried out using the thermally cross-linked 6FDA-NDA/DABA polyimide membrane. In order to reduce the effect of reaction pressure resulted from the evaporation of methanol, the esterification of PFAD via membrane reactor was carried out at lower reaction temperature. The reaction was performed at a reaction temperature of 135ºC, a methanol to PFAD ratio of 20 and a catalyst loading of 3 wt% for 3, 5 and 10 h of reaction period. Figure 4.25 displays the FAME yield achieved by batch reactor and pervaporation membrane reactor in the esterification of PFAD. At reaction time of 3, 5 and 10 h, the FAME yields achieved by batch reactor were 45.9 %, 55.5 % and 58.4 %, respectively. However, by performing the esterification of PFAD in a pervaporation membrane reactor, higher FAME yields of 49.1 %, 61.4 % and 68.8 % were achieved for reaction time of 3, 5 and 10 h, respectively. Thus, esterification of PFAD via pervaporation membrane

reactor produced higher FAME yield than the batch reactor regardless to the reaction duration. This was due to the simultaneously removal of water from the reaction mixture by the dense 6FDA-NDA/DABA polyimide membrane. According the Le Chatelier's principle, by removing one of the generated products during the reaction, the equilibrium of the esterification reaction can be shifted toward higher FAME yield (Castanheiro et al., 2006).

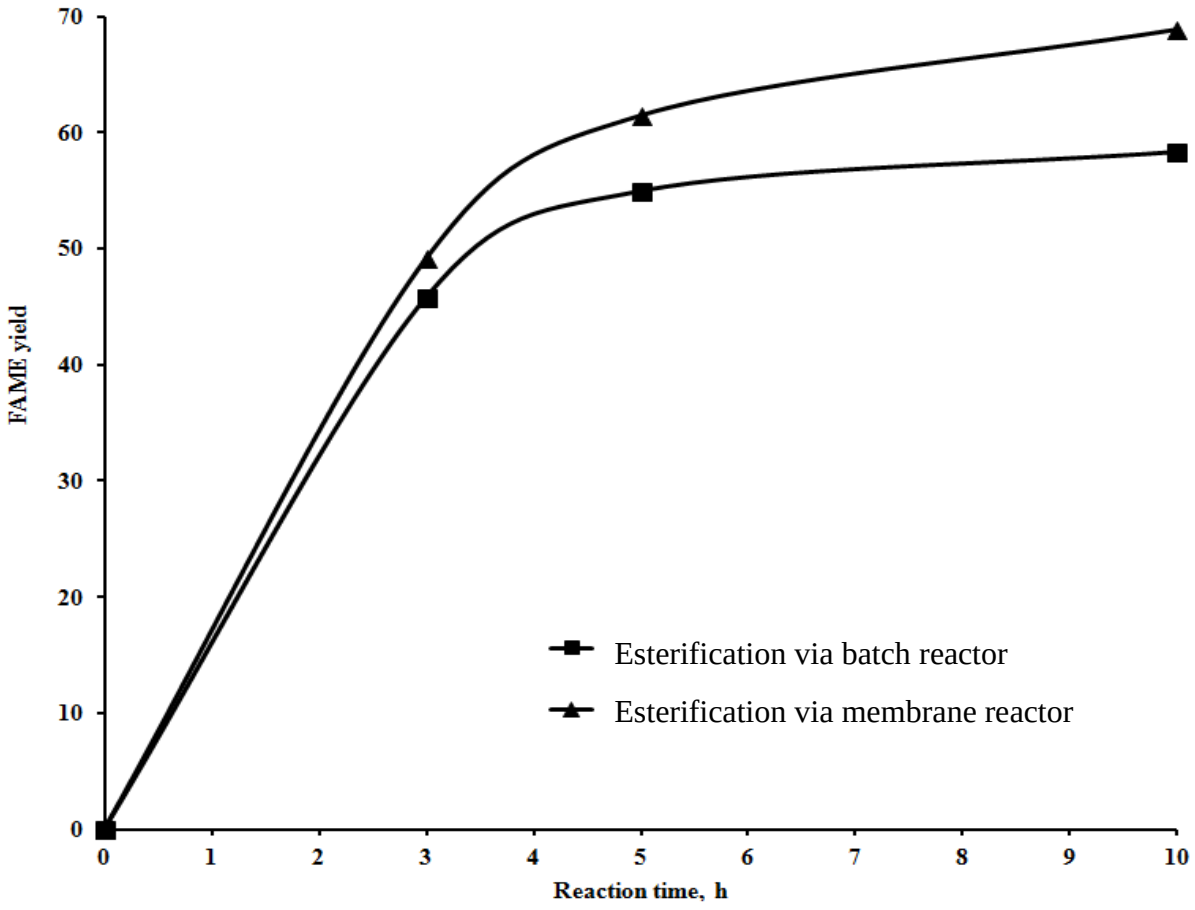

Figure 4.25: FAME yield of the esterification of PFAD in batch reactor and pervaporation membrane reactor at a reaction temperature of 135 ^{o}C, a catalyst loading of 3 wt % and a methanol-to-oil ratio of 20.

Even though the FAME yields produced by pervaporation membrane reactor were higher than batch reactor, the difference of FAME yields between batch reactor and pervaporation membrane reactor was observed to be more significant with longer reaction period. As shown in Figure 4.25**,** at shorter reaction time of 3 h, the FAME yields produced by batch reactor and pervaporation membrane reactor were quite similar (45.5 % and 49.1 %, respectively), showing only an 7.2 % of increment. This was due to the concentration of water produced during the esterification was not significant in the reaction system. Therefore, limited water was available to be removed by the membrane to shift the esterification reaction towards higher conversion. On the other hand, the FAME yield produced by pervaporation membrane reactor at 5 and 10 h of reaction time exhibited an increment of 11.7 % and 17.9 %, respectively, as compared to batch reactor. This was due to the amount of water produced in the esterification was higher at longer reaction time. This increased the pervaporation rate of water through the membrane and subsequently increased the production rate of FAME.

Furthermore, the changes of permeation flux, water concentration in permeate and water removal percentage from the reaction mixture were displayed in Table 4.11. Both the permeation flux and water concentration in permeate were found to be increased as the esterification was carried out at longer reaction time. This was expected because when the esterification reaction was continuously carried out for longer reaction time, methanol and water produced during esterification were continuously removed from the reaction mixture by the membrane reactor. Interestingly, at the initial stage of the reactive separation, the water produced during the reaction was not significantly removed from the reaction mixture.

Table 4.11: Permeation flux, water concentration in permeate and water removal percentage from the reaction mixture for the esterification of PFAD in pervaporation membrane reactor at a reaction temperature of 135 °C, a methanol-to-oil ratio of 20 and a catalyst loading of 3 wt %.

Reaction time, (h)	Flux, (g m^{-2} h^{-1})	Concentration of water in permeate, (wt %)	Water removal percentage from the reaction mixture, (%)[a]
3	26.9	19.8	9.8
5	53.0	29.0	37.5
10	67.6	32.2	94.8

[a] The detail calculations were shown in the appendix.

As shown in Table 4.11, at 3 h of reaction time, only 9.8 % of the generated water was permeated through the membrane into the permeate side. The remaining 90.2 % of the generated water was retained at the product site. In esterification, the amount of water generated is fully dependent on the conversion of PFAD. At shorter esterification reaction time where the conversion of PFAD was low, thus less amount of water was produced. In addition, the low amount of water in the reaction system became more insignificant because of the dilution under high methanol ratio. In pervaporation, concentration of the target component in the feed site is one of the main factors that affect the trans-membrane flux. Therefore, a low concentration of water at the feed site caused a reduction in driving force for the transportation of water across the membrane (Ong et al., 2012). The percentage of water being removed simultaneously from the product stream increased when the reaction was performed at longer reaction duration. By increasing the reaction time from 3 to 5 h,

the percentage of the generated water permeated through the membrane increased significantly from 9.8 % to 37.5 %. At 10 h of reaction time where more PFAD was converted into FAME causing the amount of water in the reaction mixture became more significant, thus increased the driving force of the pervaporation process. The percentage of water being removed through the membrane achieved 94.8 %. The high removal percentage of water from the reactant mixture increased the rate to shift the esterification towards higher FAME production. This was further supported by the highest increment of 17.9 % in FAME yield between batch reactor and pervaporation reactor at 10 h of reaction time.

4.10 Membrane Characterizations

The properties of the 6FDA/NDA-DABA polyimide membrane were characterized using various characterization instruments such as FT-IR analysis, contact angle analysis, TGA, XRD analysis, membrane swelling analysis and tensile strength analysis. Those characterizations are very important to prove that the 6FDA/NDA-DABA polyimide has the potential to be used in the esterification of PFAD via reactive separation.

4.10.1 FTIR Analysis of the 6FDA-NDA/DABA Polyimide Membrane

The successful formation of 6FDA-NDA/DABA polyimide was confirmed by the FTIR analysis. The FTIR spectrum of 6FDA-NDA/DABA polyimide is shown in Figure 4.26. In general, polyimide exhibits several characteristic vibration bands such as the symmetric/asymmetric C=O stretching vibration, C-N stretching vibration and the imide-five-ring deformation vibration (Le et al., 2012, Mrsevic et al., 2012). The absorption peaks at 1720 and 1784 cm^{-1} were attributed to the asymmetric stretch and symmetric stretch of C=O group, respectively (Albrecht et al., 2003, Qiao and Chung, 2006, Le et al., 2012). Meanwhile, the peak at 1358 cm^{-1} indicated the presence of C-N stretching (Albrecht et al., 2003, Mrsevic et al., 2012). Besides, the bands at 1102 and 719 cm^{-1} were assigned to the transverse stretching of C-N-C groups (Le et al., 2012) and the imide-five-ring deformation vibration of the amide groups (Mrsevic et al., 2012), respectively.

The presence of NDA in the 6FDA-NDA/DABA polyimide can be verified by the characteristic peaks of the naphthalene structure. The strong bands of 1417 and 786 cm^{-1} indicated the out-of-plane vibrations of H atoms and the distributed naphthalene structure (Le et al., 2012). The weak bands in the range of 1458-1665 cm^{-1} were assigned to the C=C stretching in the naphthalene structure (Qiao and Chung, 2006). Furthermore, various peaks in the region of 1000 – 1400 cm^{-1}, including a strong peak at 1161 cm^{-1} also indicated the presence of NDA moiety (Le et al., 2012).

However, due to the low amount of DABA in the polyimides and the wide range vibration of OH groups at 3100 – 3600 cm^{-1}, the DABA moiety is indistinguishable in FTIR spectra (Le et al., 2012). In addition, it is also very difficult to identify the presence of phenyl free radical cross-linking in the thermally cross-linked polyimide membrane since both spectra were similar. Therefore, other characterization technique such as TGA was required to prove the existence of the cross-linking in the membrane.

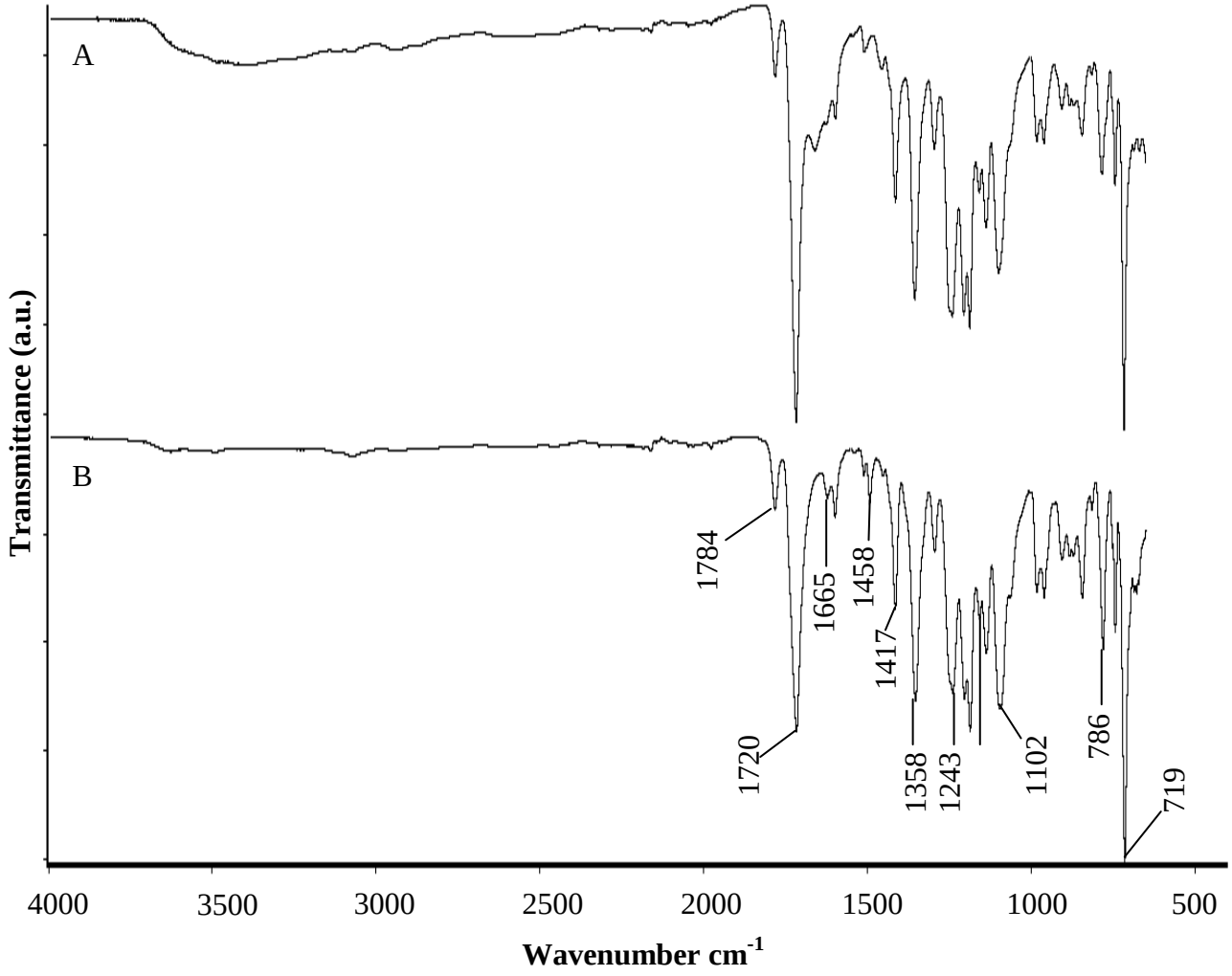

Figure 4.26: FT-IR spectra of A as-synthesized 6FDA-NDA/DABA polyimide membrane and B thermally cross-linked 6FDA-NDA/DABA polyimide membrane.

4.10.2 TGA

Besides investigating the thermal stability of the membrane, TGA can also be used to confirm the decarboxylation-induced thermal cross-linking in this study. The weight loss and derivative weight loss curves for the as-synthesized 6FDA-NDA/DABA polyimide membrane and the thermally cross-linked 6FDA-NDA/DABA polyimide membrane are shown in Figure 4.27 A and B. Two stages of weight loss were observed in the temperature profile of the as-synthesized polyimide membrane: in the temperature range of 30 - 100 ºC and 300 - 455 ºC. The weight loss of the as-synthesized polyimide membrane between 30 and 100 ºC was attributed to the removal of the moisture. Then, the weight loss in the temperature range of 300 - 455 ºC of the as-synthesized polyimide membrane was due to the removal of COOH groups in DABA moiety through decarboxylation, producing CO_2 and CO (Le et al., 2012). As shown in Figure 4.24 A, B and C, decarboxylation-induced thermal cross-linking involved 2 COOH groups from nearby DABA moiety which indicated that 2 moles of DABA will produce 1 mole of CO_2 and 1 mole of CO. Since, 0.006 mole of DABA was used during the synthesis of 6FDA/NDA-DABA membrane, 0.003 mol of CO_2 and 0.003 mole of CO were produced during the decarboxylation-induced thermal cross-linking. Therefore, a total theoretical weight of 0.22 g of CO_2 and CO was generated. As shown in Figure 4.27 A, the weight loss for the as-synthesized polyimide membrane in the second stage was about 0.28 g which was in agreement with the theoretical weight of CO_2 and CO generated from the decarboxylation-induced thermal cross-linking.

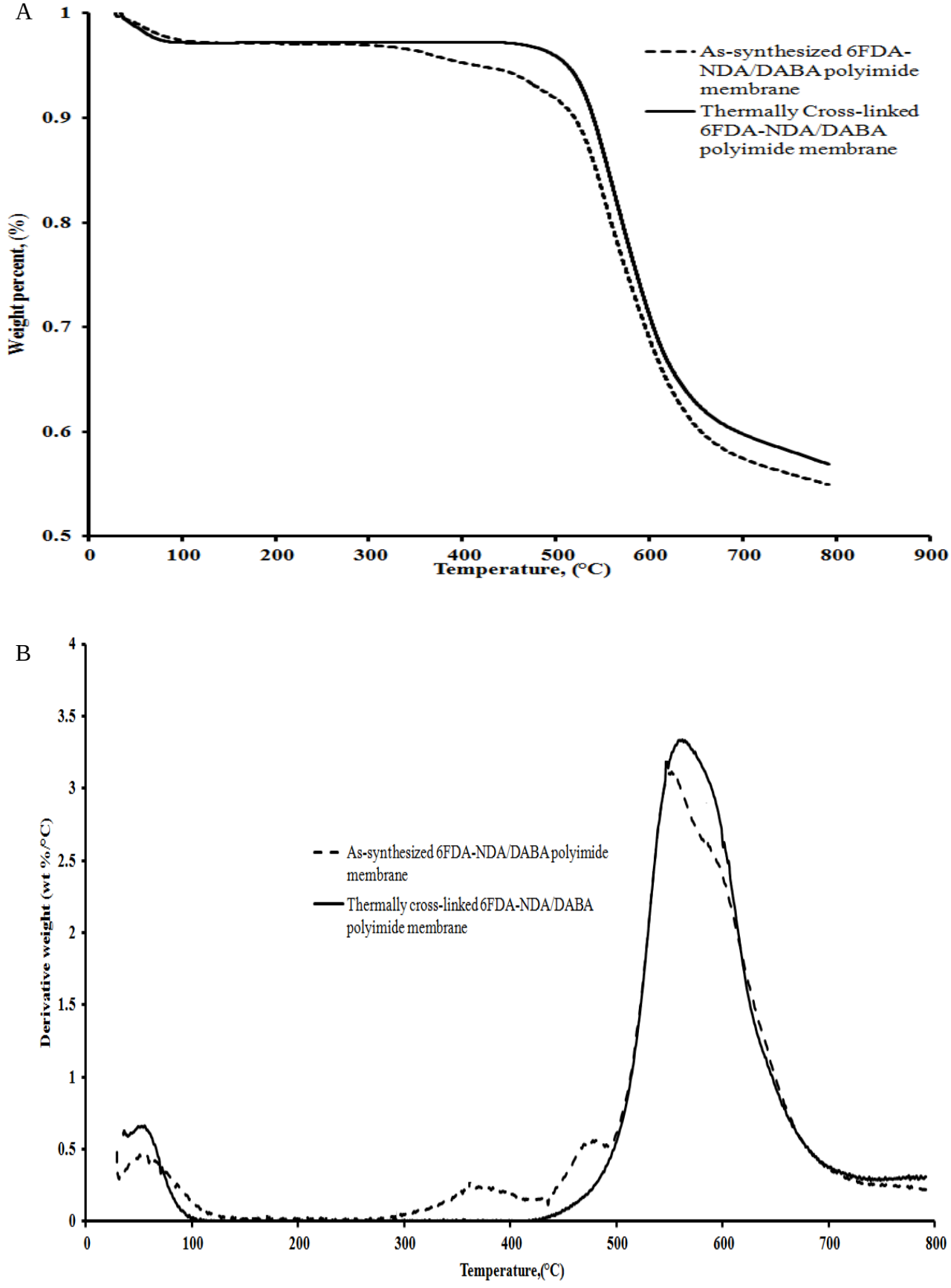

Figure 4.27: TGA analysis of A weight (wt %) B derivative weight (wt %/°C) of the as-synthesized and thermally cross-linked 6FDA-NDA/DABA polyimide membrane.

Similarly, for the thermally cross-linked polyimide membrane, weight loss in the temperature range of 30 - 100 ºC which was due to the removal of moisture. After that, the thermally cross-linked polyimide membrane was stable with negligible weight loss in the temperature between 300 and 455 ºC because all the COOH groups available in the DABA moiety had been removed during thermal cross-linking at 425 ºC. This also implied that thermal treatment at 425 ºC for 30 min was sufficient to cross-link the polyimide membrane by removing all the COOH groups via decarboxylation.

Both the as-synthesized polyimide and thermally cross-linked polyimide membrane suffered a sudden and significant weight loss after temperature 500 ºC (as shown in Figure 4.27 B) which was attributed to the degradation of the major backbone of polyimide (Le et al., 2012). As shown in Figure 4.27 B, the exact degradation temperature of the major backbone of polyimide for both the as-synthesized polyimide and thermally cross-linked polyimide membrane was 550 and 570 ºC, respectively. Based on the TGA results, the 6FDA-NDA/DABA polyimide membrane with good thermal stability is suitable to be used in the esterification of PFAD via membrane reactor at a reaction temperature of 135 °C.

4.10.3 Contact Angle Analysis

Water contact angle is an important characteristic to indicate the hydrophobicity or hydrophilicity of the synthesized polyimide membrane. Table 4.12 shows the average water contact angle of the as-synthesized 6FDA-NDA/DABA polyimide membrane and the thermally cross-linked 6FDA-NDA/DABA polyimide membrane. Generally, the surface of the material is considered to be hydrophilic, if the water contact angle is less than 90º. Meanwhile, if the water contact angle is more than 90º, the surface of the material is considered to be hydrophobic. Hydrophobicity or hydrophilicity of a surface depends on the surface energy that the material possesses in which materials with low surface energy are hydrophobic and vice versa. Materials that consist of fluorinated compound are identified to possess low surface energy (Shemper and Mathias, 2004). Therefore, the high content of fluorine groups in 6FDA moiety causing the as-synthesized polyimide membrane to be highly hydrophobic, with the contact angle of 104.8º. In addition, the hydrophobicity of the as-synthesized polyimide membrane was also due to the hydrophobic aromatic naphthalene of NDA moiety (Le et al., 2012).

Table 4.12: Water contact angle of the as-synthesized and thermally cross-linked 6FDA-NDA/DABA polyimide membrane.

Membrane	Water contact angle,(º)
As-synthesized 6FDA-NDA/DABA polyimide membrane	104.8
Thermally cross-linked 6FDA-NDA/DABA polyimide membrane	82.8

Surface roughness plays an important role in affecting the hydrophobicity and hydrophilicity of a membrane surface. The relationship between the material hydrophilicity and its surface roughness is described in the Wenzel Equation shown as below (Yoshimitsu et al., 2002):

$$\cos\theta_W = r\cos\theta_Y \tag{4.13}$$

where θ_W is the contact angle on a rough surface, θ_Y is the Young contact angle (contact angle on an ideally flat and smooth surface of the same material) and r is the roughness ratio which is the ratio of the actual area of a rough surface to the geometric projected area. Roughness ratio is always larger than 1. The Wenzel equation can be interpreted as the following:

i. For a hydrophilic surface where θ_Y is < 90 º, the value of $\cos\theta_Y$ is a positive value. Since r is > 1, the value of $\cos\theta_W$ (equals to r multiply by $\cos\theta_Y$) must be more than the value of $\cos\theta_Y$. Therefore, θ_W is smaller than θ_Y. This implied that the increase in surface roughness decrease the water contact angle of a hydrophilic surface, making the surface become more hydrophilic.

ii. For a hydrophobic surface where θ_Y is > 90 º, the value of $\cos\theta_Y$ is a negative value. Since r is > 1, the value of $\cos\theta_W$ (equals to r multiply by $\cos\theta_Y$) must be more negative than the value of $\cos\theta_Y$. Therefore, θ_W is more than θ_Y. This implied that the increase in surface roughness increase the water contact

angle of a hydrophobic surface, making the surface become more hydrophobic.

According to Wenzel Equation, in order to increase the hydrophilicity of the as-synthesized polyimide membrane which is a hydrophobic membrane (contact angle of 104.8 º), the surface roughness of the membrane must be decreased. High temperature thermal treatment which can reduce the surface roughness of a membrane (Rahimpour et al., 2009, Le et al., 2012) is one of the ways to improve the hydrophilicity of the as-synthesized polyimide membrane. As shown in Figure 4.28, the surface roughness of the membrane was significantly reduced after the as-synthesized polyimide membrane has undergone thermal treatment at temperature of 425 ºC. Annealing the membrane under high temperature caused the pores on the surface of the membrane to shrink, collapse and eventually disappear (Centeno and Fuertes, 1999), generated a smooth membrane surface. Therefore, the water contact angle of the thermally cross-linked 6FDA-NDA/DABA polyimide membrane decreased significantly from 104.8 º to 82.8 º, implying an increase in hydrophilicity of the membrane surface. Thus, high temperature thermal treatment plays two vital roles in this study, first to induce thermal cross-linking and then to improve the hydrophilicity of the membrane by reducing the membrane surface roughness.

A

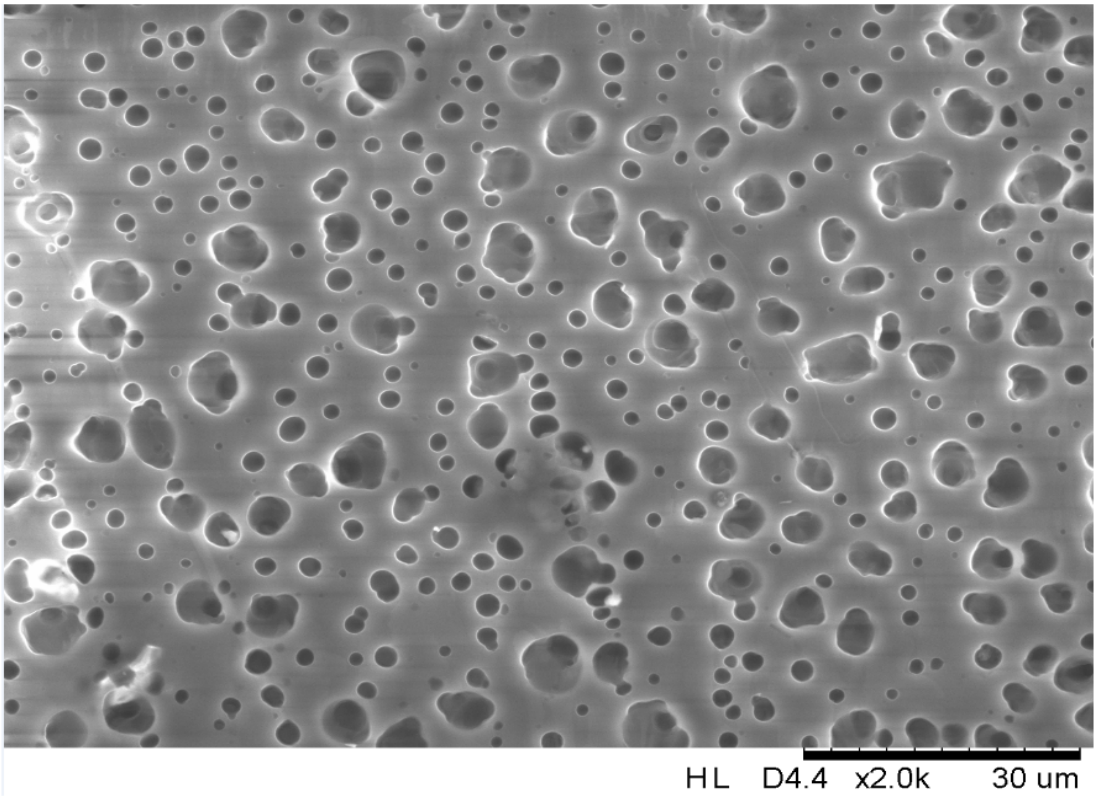

B

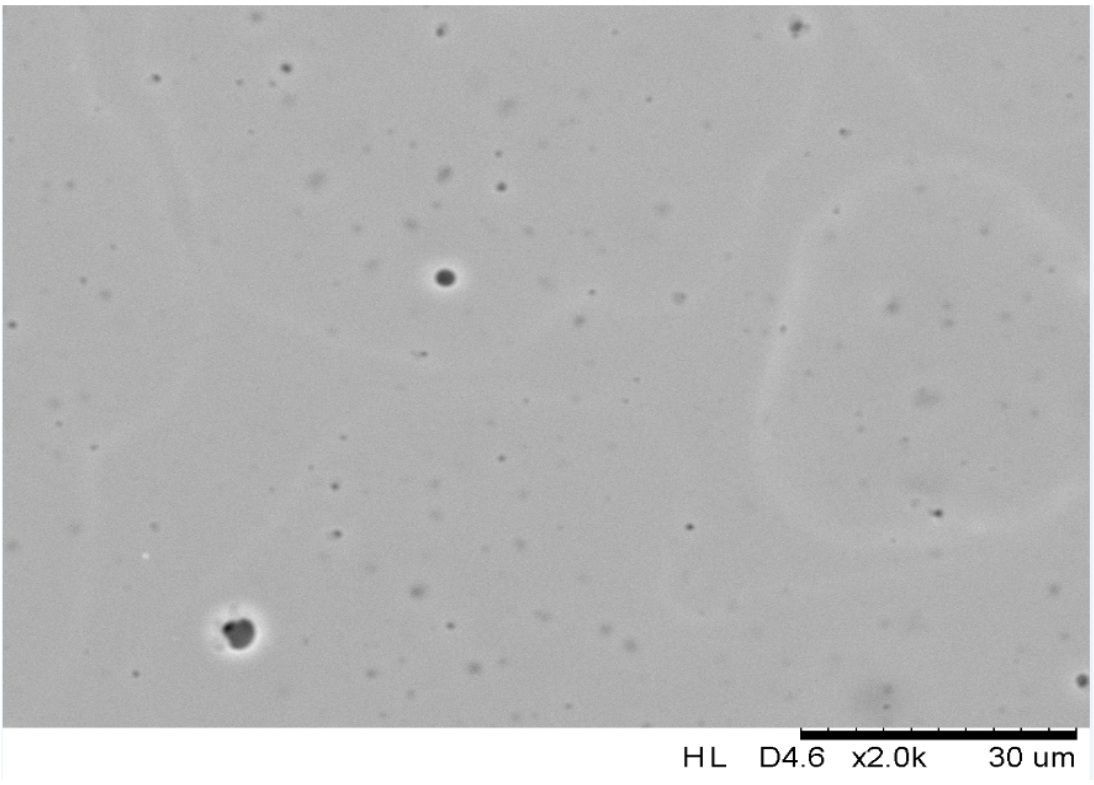

Figure 4.28: SEM images of 6FDA-NDA/DABA polyimide membrane: A as-synthesized and B thermally cross-linking.

4.10.4 X-Ray Diffraction (XRD)

XRD analysis is used to investigate the d-spacing of the membrane which is also known as the free volume of the membrane. XRD results in Table 4.13 show that high temperature thermal treatment at 425 ºC resulted in higher d-spacing in thermally cross-linked 6FDA-NDA/DABA polyimide membrane as compared to the as-synthesized polyimide membrane. In general, the thermal treatment conducted at lower temperature could reduce the free volume of the polymeric membrane. The low temperature thermal treatment of membrane can lead to the increase of chain packing density of membrane which in turn decreases the free volume of polymeric membrane (Qiu et al., 2011, Le et al., 2012). On the other hand, the thermal treatment in this study was performed at high temperature of 425 ºC caused a higher free volume of the 6FDA-NDA/DABA polyimide membrane because the average inter-chain distance of polymer was increased during decarboxylation-induced cross-linking (Qiu et al., 2011). The thermally cross-linked polyimide membrane with larger d-spacing would facilitate the diffusion of water with smaller molecules through the membrane as compared to larger molecules of methanol (ten Elshof et al., 2003).

Table 4.13: d-spacing of as-synthesized and thermally cross-linked 6FDA-NDA/DABA polyimide membrane.

Membrane	d-spacing, (Å)
As-synthesized 6FDA-NDA/DABA polyimide membrane	2.0
Thermally cross-linked 6FDA-NDA/DABA polyimide membrane	2.2

4.10.5 Membrane Swelling Analysis

The affinity of organic species (methanol, fatty acid and FAME) and water towards the membranes can be determined by membrane swelling analysis. Table 4.14 shows the degree of swelling of the as-synthesized and thermally cross-linked 6FDA-NDA/DABA polyimide membrane in different solvents involve in the esterification of PFAD via pervaporation membrane reactor. Swelling analysis indicated that the as-synthesized 6FDA-NDA/DABA polyimide membrane showed a strong swelling in methanol and weak swelling in water, FAME and PFAD. This swelling analysis further supported the observation mentioned earlier in section 4.9.3 in which the reactive separation of PFAD using as-synthesized polyimide membrane was unsuccessful due to the damage of membrane caused by membrane swelling under high reaction temperature and pressure. Since the reaction mixture of the esterification of PFAD contained high concentration of methanol, the swelling of the as-synthesized polyimide membrane in methanol was even more severe under high reaction temperature and pressure. Eventually the membrane was spoiled causing failure in the esterification of PFAD via pervaporation membrane reactor. The swelling of methanol decreased significantly for the thermally cross-linked 6FDA-NDA/DABA polyimide membrane in which the membrane swelled only 0.5 % when immersed in methanol. The results also indicated that this thermally cross-linked polyimide membrane did not swell in water, PFAD and FAME. Owing to the cross-linking modification, the polymer chain mobility of the membrane is restricted (Le et al., 2012), resulting low and insignificant degree of swelling in different reaction solvents.

Table 4.14: Degree of swelling of the as-synthesized and thermally cross-linked 6FDA-NDA/DABA polyimide membrane in different solvents involve in the esterification of PFAD via pervaporation membrane reactor.

Membranes	Degree of swelling, (%)			
	Water	Methanol	PFAD*	FAME*
As-synthesized 6FDA-NDA/DABA polyimide membrane	3.0	14.3	0.6	2.0
Thermally cross-linked 6FDA-NDA/DABA polyimide membrane	negligible	0.5	negligible	negligible

* The swelling tests of membrane in PFAD and FAME were performed at a temperature of 60 ºC to avoid solidify of PFAD.

As noticed, polyimide membranes are classified as glassy membrane (Ong et al., 2012). The major differences between glassy and rubbery membranes are their flexibility and polymeric structure. The permeation of solutes for glassy membranes depends strongly on the free volume within the rigid polymeric structure of the glassy membranes. On the other hand, in the flexible region of a rubbery membrane, the permeation of solutes depends on solute-polymer interactions. Therefore, the permeation of solutes for glassy membranes is more diffusion-controlled whereas the permeation of solutes for rubbery membranes is more sorption-controlled (Rizvi, 2010). This statement was further supported by the membrane swelling analysis in which the thermally cross-linked 6FDA-NDA/DABA polyimide membrane did not swell in water and methanol but still able to permeate both solutes through the membrane because the transport of methanol and water was govern by diffusion-controlled but not sorption-controlled.

4.10.6 Tensile Strength Analysis

Even though membrane technology is a potential technology for biodiesel production, Guerreiro et al. (2006) reported a problem of broken membrane in the transesterification of soybean oil with methanol before high conversion value can be achieved. Therefore, it is important to investigate the mechanical properties of a membrane to provide essential information for industrial application. Mechanical properties of a membrane is generally expressed in terms of tensile strength (MPa), Young's modulus (GPa) and elongation at break, (%). The mechanical properties of the as-synthesized and thermally cross-linked 6FDA-NDA/DABA polyimide membrane are presented in Table 4.15.

Table 4.15: Mechanical Properties of the as-synthesized and thermally cross-linked 6FDA-NDA/DABA polyimide membrane.

Membrane	Thickness, (μm)	Tensile strength, (MPa)	Young's modulus (GPa)	Elongation at break, (%)
As-synthesized 6FDA-NDA/DABA polyimide membrane	80	79.0	1.5	6.2
Thermally cross-linked 6FDA-NDA/DABA polyimide membrane	70	74.8	1.8	5.0

Tensile strength of a membrane is defined as the maximum stress that a membrane can withstand while being pulled or stretched before breaking. Both the as-synthesized and thermally cross-linked polyimide membrane exhibited similar tensile strength with only 5 % difference. This indicated that the thermal cross-linking did not cause any significant effect to the tensile strength of the membrane. However, the thermally cross-linked polyimide membrane showed a significant 20 % increment in Young's modulus as compared to the as-synthesized polyimide membrane. Young's modulus is defined as the ratio of stress over strain which also means the resistance of a material to deformation. The increase in Young's modulus of the thermally cross-linked polyimide membrane was due to the cross-linking of the phenyl free radicals through decarboxylation that connected the individual polymer chains to each other permanently, restricting the mobility of the polymer chains. This is the main reason that the 6FDA-NDA/DABA polyimide membrane can withstand the reaction pressure generated from the evaporation of methanol.

The elongation at break of the thermally cross-linked polyimide membrane dropped remarkably from 6.2 % to 5.0 %, which was about 20 % reduction as compared to the as-synthesized polyimide membrane. This was due to the thermally cross-linked polyimide membrane become more rigid and its fragility was increased under high temperature treatment (Le et al., 2012). In addition, elongation at break is correlated to the flexibility of the polymer. Prior to the cross-linking via high temperature decarboxylation, the as-synthesized polyimide membrane contained a lot of COOH groups, resulting the membrane to possess higher level of flexibility. Therefore, the elongation at break of the as-synthesized polyimide membrane was higher. However, the COOH groups were eliminated through high temperature

decarboxylation, causing the membrane to become rigid and less flexible. Thus, the elongation at break of the thermally cross-linked polyimide membrane dropped significantly.

CHAPTER FIVE

CONCLUSIONS AND RECOMMENDATIONS

5.1 Conclusions

MWCNTs which have been hailed as the new generation catalyst support were successfully functionalized with SO_3H group via thermal decomposition of $(NH_4)_2SO_4$ with the aid of ultrasonication treatment. The s-MWCNTs were then used to transform PFAD into FAME via esterification. It was found that s-MWCNTs with the best performance could be obtained by ultrasonicating the purified MWCNTs in a 10 wt% $(NH_4)_2SO_4$ solution for 10 min and heating at 235 °C for 30 min. UV-Vis results implied that s-MWCNTs were able to form a homogeneous solution with methanol during the esterification of PFAD which can reduce the mass transfer limitation encountered by conventional heterogeneous catalysts in biodiesel production.

A high FAME yield of 93.5 % was obtained at a methanol-to-PFAD ratio of 20, reaction temperature of 170 ºC and reaction time of 2 h using 3 wt % of s-MWCNTs loading. Besides, the s-MWCNTs also exhibited good catalytic activity, with a FAME yield higher than 75 % even after 5 repeated runs. The regeneration of the spent s-MWCNTs (after 5 runs) with H_2SO_4 was able to restore the catalytic activity to its original level. The acid sites density and the strength and thermal stability of the acid sites of the regenerated s-MWCNTs were improved significantly after acid regeneration causing the regenerated s-MWCNTs to achieve a FAME yield

of 86.2 %, even at the fifth cycle of reaction. The leaching of the SO_3H group suffered by the s-MWCNTs was not at a severe level.

A pseudo-homogeneous kinetic model for the esterification of PFAD with methanol using s-MWCNTs as a catalyst was then developed based on the experimental results. The pre-exponential factor, molar heat and activation energy for the esterification were found to be 1.9×10^2 L $mol^{-1}min^{-1}$, 84. 1 kJ mol^{-1} and 45.8 kJ mol^{-1}, respectively.

6FDA-NDA/DABA polyimide membrane was synthesized and modified via thermal cross-linking to behave as pervaporation membrane in the esterification of PFAD via reactive separation. Pervaporation membrane reactor was able to increase the FAME yield by 17.9 % as compared to the conventional batch reactor under the same reaction conditions. Moreover, it was found that the thermally cross-linked 6FDA-NDA/DABA polyimide membrane was able to remove 94.8 % of the generated water from the reaction mixture. Overall, the findings in this study have shown the potential of the esterification via pervaporation membrane reactor using s-MWCNTs as catalyst to be a noble and breakthrough technology for biodiesel production.

5.2 Recommendations

This study has shown the feasibility of pervaporation membrane reactor coupled with s-MWCNTs as catalyst in producing FAME using PFAD as oil source. The following recommendations are made for further improvement of similar research project in the future.

i. Membrane thickness is one of the main factors that control the permeation of solute molecules through non-porous dense membrane. Therefore, the effect of different thickness of 6FDA-NDA/DABA polyimide membrane towards the esterification via reactive separation can be further studied. Membrane thickness can be varied by controlling the amount of the polymer solution during membrane casting. In addition, the effect of different membrane hydrophilicity in the removal of water from the reaction mixture can be investigated by adding the 6FDA with different ratio of NDA and DABA.

ii. The process parameters study such as methanol to PFAD ratio, reaction temperature, catalyst loading and reaction time in the esterification of PFAD was performed under batch reactor. Therefore, the effect of these process parameters to the esterification of PFAD via pervaporation membrane reactor should be further studied in order to make a complete comparison in term of performance and economy feasibility.

iii. The reactive separation in this study was performed via a catalytically inert membrane in which the s-MWCNTs and the polymer membrane were separated and in a non-contact configuration. Therefore, future study should be focused on the feasibility of catalytically active membrane in reactive separation of PFAD with methanol. Catalytically active membrane can be synthesized by embedding the s-MWCNTs into the 6FDA-NDA/DABA polymer matrix.

REFERENCES

Aafaqi, R., Mohamed, A. R. & Bhatia, S. (2004) Kinetics of esterification of palmitic acid with isopropanol using p-toluene sulfonic acid and zinc ethanoate supported over silica gel as catalysts. *Journal of Chemical Technology and Biotechnology,* 79**,** 1127-1134.

Abreu, F., Lima, D., Hamú, E., Einloft, S., Rubim, J. & Suarez, P. (2003) New metal catalysts for soybean oil transesterification. *Journal of the American Oil Chemists' Society,* 80**,** 601-604.

Adams, L., Oki, A., Grady, T., McWhinney, H. & Luo, Z. (2009) Preparation and characterization of sulfonic acid-functionalized single-walled carbon nanotubes. *Physica E: Low-dimensional Systems and Nanostructures,* 41**,** 723-728.

Ahmad, A. L., Yasin, N. H. M., Derek, C. J. C. & Lim, J. K. (2011) Microalgae as a sustainable energy source for biodiesel production: A review. *Renewable and Sustainable Energy Reviews,* 15**,** 584-593.

Albrecht, W., Seifert, B., Weigel, T., Schossig, M., Holländer, A., Groth, T. & Hilke, R. (2003) Amination of poly(ether imide) membranes using di- and multivalent amines. *Macromolecular Chemistry and Physics,* 204**,** 510-521.

Albuquerque, M. C. G., Jiménez-Urbistondo, I., Santamaría-González, J., Mérida-Robles, J. M., Moreno-Tost, R., Rodríguez-Castellón, E., Jiménez-López, A., Azevedo, D. C. S., Cavalcante Jr, C. L. & Maireles-Torres, P. (2008) Cao supported on mesoporous silicas as basic catalysts for transesterification reactions. *Applied Catalysis A: General,* 334**,** 35-43.

Allouche, H., Monthioux, M. & Jacobsen, R. L. (2003) Chemical vapor deposition of pyrolytic carbon on carbon nanotubes: Part 1. Synthesis and morphology. *Carbon,* 41**,** 2897-2912.

Alonso, D. M., Mariscal, R., Moreno-Tost, R., Poves, M. D. Z. & Granados, M. L. (2007) Potassium leaching during triglyceride transesterification using k/γ-al2o3 catalysts. *Catalysis Communications,* 8**,** 2074-2080.

Andrade, J. E., Pérez, A., Sebastian, P. J. & Eapen, D. (2011) A review of bio-diesel production processes. *Biomass and Bioenergy,* 35**,** 1008-1020.

Anthamatten, M., Letts, S. A., Day, K., Cook, R. C., Gies, A. P., Hamilton, T. P. & Nonidez, W. K. (2004) Solid-state amidization and imidization reactions in vapor-deposited poly(amic acid). *Journal of Polymer Science Part A: Polymer Chemistry,* 42**,** 5999-6010.

Aranda, D. G., Santos, R. P., Tapanes, N. O., Ramos, A. & Antunes, O. (2008) Acid-catalyzed homogeneous esterification reaction for biodiesel production from palm fatty acids. *Catalysis Letters,* 122**,** 20-25.

Arzamendi, G., Arguiñarena, E., Campo, I., Zabala, S. & Gandía, L. M. (2008) Alkaline and alkaline-earth metals compounds as catalysts for the methanolysis of sunflower oil. *Catalysis Today,* 133–135**,** 305-313.

Atadashi, I. M., Aroua, M. K. & Aziz, A. A. (2011) Biodiesel separation and purification: A review. *Renewable Energy,* 36**,** 437-443.

Ataya, F., Dubé, M. A. & Ternan, M. (2006) Single-phase and two-phase base-catalyzed transesterification of canola oil to fatty acid methyl esters at ambient conditions. *Industrial and Engineering Chemistry Research,* 45**,** 5411-5417.

Bajaj, A., Lohan, P., Jha, P. N. & Mehrotra, R. (2010) Biodiesel production through lipase catalyzed transesterification: An overview. *Journal of Molecular Catalysis B: Enzymatic,* 62**,** 9-14.

Balasubramanian, K. & Burghard, M. (2005) Chemically functionalized carbon nanotubes. *Small,* 1**,** 180-192.

Barnwal, B. K. & Sharma, M. P. (2005) Prospects of biodiesel production from vegetable oils in india. *Renewable and Sustainable Energy Reviews,* 9**,** 363-378.

Baroutian, S., Aroua, M. K., Raman, A. A. A. & Sulaiman, N. M. N. (2010a) Methanol recovery during transesterification of palm oil in a tio2/al2o3 membrane reactor: Experimental study and neural network modeling. *Separation and Purification Technology,* 76**,** 58-63.

Baroutian, S., Aroua, M. K., Raman, A. A. A. & Sulaiman, N. M. N. (2010b) Potassium hydroxide catalyst supported on palm shell activated carbon for transesterification of palm oil. *Fuel Processing Technology,* 91**,** 1378-1385.

Baroutian, S., Aroua, M. K., Raman, A. A. A. & Sulaiman, N. M. N. (2011) A packed bed membrane reactor for production of biodiesel using activated carbon supported catalyst. *Bioresource Technology,* 102**,** 1095-1102.

Bart, H. J., Reidetschlager, J., Schatka, K. & Lehmann, A. (1994) Kinetics of esterification of levulinic acid with n-butanol by homogeneous catalysis. *Industrial & Engineering Chemistry Research,* 33**,** 21-25.

Bastiani, R., Zonno, I. V., Santos, I. A. V., Henriques, C. A. & Monteiro, J. L. F. (2004) Influence of thermal treatments on the basic and catalytic properties of mg,al-mixed oxides derived from hydrotalcites. *Brazilian Journal of Chemical Engineering,* 21**,** 193-202.

Berchmans, H. J. & Hirata, S. (2008) Biodiesel production from crude jatropha curcas l. Seed oil with a high content of free fatty acids. *Bioresource Technology,* 99**,** 1716-1721.

Berrios, M., Siles, J., Martín, M. A. & Martín, A. (2007) A kinetic study of the esterification of free fatty acids (ffa) in sunflower oil. *Fuel,* 86**,** 2383-2388.

Böddeker, K. W. (2008). Liquid separations with membranes, Springer.

Boey, P. L., Maniam, G. P. & Hamid, S. A. (2009) Biodiesel production via transesterification of palm olein using waste mud crab (scylla serrata) shell as a heterogeneous catalyst. *Bioresource Technology,* 100**,** 6362-6368.

Bondi, S. N., Lackey, W. J., Johnson, R. W., Wang, X. & Wang, Z. L. (2006) Laser assisted chemical vapor deposition synthesis of carbon nanotubes and their characterization. *Carbon,* 44**,** 1393-1403.

Borges, L. D., Moura, N. N., Costa, A. A., Braga, P. R. S., Dias, J. A., Dias, S. C. L., de Macedo, J. L. & Ghesti, G. F. (2013) Investigation of biodiesel production by husy and ce/husy zeolites: Influence of structural and acidity parameters. *Applied Catalysis A: General,* 450**,** 114-119.

Boucher, M. B., Unker, S. A., Hawley, K. R., Wilhite, B. A., Stuart, J. D. & Parnas, R. S. (2008) Variables affecting homogeneous acid catalyst recoverability and reuse after esterification of concentrated omega-9 polyunsaturated fatty acids in vegetable oil triglycerides. *Green Chemistry,* 10**,** 1331-1336.

Buonomenna, M. G., Choi, S. H. & Drioli, E. (2010) Catalysis in polymeric membrane reactors: The membrane role. *Asia-Pacific Journal of Chemical Engineering,* 5**,** 26-34.

Cao, P., Dubé, M. A. & Tremblay, A. Y. (2008a) High-purity fatty acid methyl ester production from canola, soybean, palm, and yellow grease lipids by means of a membrane reactor. *Biomass and Bioenergy,* 32**,** 1028-1036.

Cao, P., Dubé, M. A. & Tremblay, A. Y. (2008b) Methanol recycling in the production of biodiesel in a membrane reactor. *Fuel,* 87**,** 825-833.

Cao, P., Tremblay, A. Y., Dubé, M. A. & Morse, K. (2006) Effect of membrane pore size on the performance of a membrane reactor for biodiesel production. *Industrial and Engineering Chemistry Research,* 46**,** 52-58.

Caro, J. (2008) Catalysis in micro-structured membrane reactors with nano-designed membranes. *Chinese Journal of Catalysis,* 29**,** 1169-1177.

Castanheiro, J. E., Ramos, A. M., Fonseca, I. M. & Vital, J. (2006) Esterification of acetic acid by isoamylic alcohol over catalytic membranes of poly(vinyl alcohol) containing sulfonic acid groups. *Applied Catalysis A: General,* 311**,** 17-23.

Centeno, T. A. & Fuertes, A. B. (1999) Supported carbon molecular sieve membranes based on a phenolic resin. *Journal of Membrane Science,* 160**,** 201-211.

Chakraborty, R., Bepari, S. & Banerjee, A. (2011) Application of calcined waste fish (labeo rohita) scale as low-cost heterogeneous catalyst for biodiesel synthesis. *Bioresource Technology,* 102**,** 3610-3618.

Chapman, P. D., Oliveira, T., Livingston, A. G. & Li, K. (2008) Membranes for the dehydration of solvents by pervaporation. *Journal of Membrane Science,* 318**,** 5-37.

Chen, G. & Fang, B. (2011) Preparation of solid acid catalyst from glucose–starch mixture for biodiesel production. *Bioresource Technology,* 102**,** 2635-2640.

Chen, H., Peng, B., Wang, D. & Wang, J. (2007) Biodiesel production by the transesterification of cottonseed oil by solid acid catalysts. *Frontiers of Chemical Engineering in China,* 1**,** 11-15.

Chen, H. C., Ju, H. Y., Wu, T. T., Liu, Y. C., Lee, C. C., Chang, C., Chung, Y. L. & Shieh, C. J. (2011) Continuous production of lipase-catalyzed biodiesel in a packed-bed reactor: Optimization and enzyme reuse study. *Journal of Biomedicine and Biotechnology,* 2011**,** 6 pages.

Cho, H. J., Kim, J.-K., Cho, H.-J. & Yeo, Y.-K. (2012a) Techno-economic study of a biodiesel production from palm fatty acid distillate. *Industrial & Engineering Chemistry Research,* 52**,** 462-468.

Cho, H. J., Kim, J.-K., Hong, S. W. & Yeo, Y.-K. (2012b) Development of a novel process for biodiesel production from palm fatty acid distillate (pfad). *Fuel Processing Technology,* 104**,** 271-280.

Chorkendorff, I. & Niemantsverdriet, J. W. (eds.) 2003. *Concepts of modern catalysis and kinetics*: Wiley-VCH Verlag GmbH & Co. KGaA, Weinheim, Germany.

Chouhan, A. P. S. & Sarma, A. K. (2011) Modern heterogeneous catalysts for biodiesel production: A comprehensive review. *Renewable and Sustainable Energy Reviews,* 15**,** 4378-4399.

Cook, H. W. & McMaster, C. R. 2002. Chapter 7 fatty acid desaturation and chain elongation in eukaryotes. *New comprehensive biochemistry*. Elsevier.

D'Cruz, A., Kulkarni, M., Meher, L. & Dalai, A. (2007) Synthesis of biodiesel from canola oil using heterogeneous base catalyst. *Journal of the American Oil Chemists' Society,* 84**,** 937-943.

Dalai, A. K., Kulkarni, M. G. & Meher, L. C. Year. Biodiesel productions from vegetable oils using heterogeneous catalysts and their applications as lubricity additives. *In:* EIC Climate Change Technology, 2006 IEEE, 10-12 May 2006 2006. 1-8.

Darnoko, D. & Cheryan, M. (2000) Kinetics of palm oil transesterification in a batch reactor. *Journal of the American Oil Chemists' Society,* 77**,** 1263-1267.

de Boer, K. & Bahri, P. A. (2011) Supercritical methanol for fatty acid methyl ester production: A review. *Biomass and Bioenergy,* 35**,** 983-991.

Dehkhoda, A. M. & Ellis, N. (2013) Biochar-based catalyst for simultaneous reactions of esterification and transesterification. *Catalysis Today,* 207**,** 86-92.

Demirbas, A. (2007) Progress and recent trends in biofuels. *Progress in Energy and Combustion Science,* 33**,** 1-18.

DeRoussel, P., Khakhar, D. V. & Ottino, J. M. (2001) Mixing of viscous immiscible liquids. Part 2: Overemulsification--interpretation and use. *Chemical Engineering Science,* 56**,** 5531-5537.

Di Serio, M., Cozzolino, M., Tesser, R., Patrono, P., Pinzari, F., Bonelli, B. & Santacesaria, E. (2007) Vanadyl phosphate catalysts in biodiesel production. *Applied Catalysis A: General,* 320**,** 1-7.

Di Serio, M., Ledda, M., Cozzolino, M., Minutillo, G., Tesser, R. & Santacesaria, E. (2006) Transesterification of soybean oil to biodiesel by using heterogeneous basic catalysts. *Industrial and Engineering Chemistry Research,* 45**,** 3009-3014.

Dittmeyer, R., Svajda, K. & Reif, M. (2004) A review of catalytic membrane layers for gas/liquid reactions. *Topics in Catalysis,* 29**,** 3-27.

Donaldson, K., Aitken, R., Tran, L., Stone, V., Duffin, R., Forrest, G. & Alexander, A. (2006) Carbon nanotubes: A review of their properties in relation to pulmonary toxicology and workplace safety. *Toxicological Sciences,* 92**,** 5-22.

Dresselhaus, M. S., Dresselhaus, G., Saito, R. & Jorio, A. (2005) Raman spectroscopy of carbon nanotubes. *Physics Reports,* 409**,** 47-99.

Drioli, E., Fontananova, E., Bonchio, M., Carraro, M., Gardan, M. & Scorrano, G. (2008) Catalytic membranes and membrane reactors: An integrated approach to catalytic process with a high efficiency and a low environmental impact. *Chinese Journal of Catalysis,* 29**,** 1152-1158.

Du, C. Y., Zhao, T. S. & Liang, Z. X. (2008) Sulfonation of carbon-nanotube supported platinum catalysts for polymer electrolyte fuel cells. *Journal of Power Sources,* 176**,** 9-15.

Dubé, M. A., Tremblay, A. Y. & Liu, J. (2007) Biodiesel production using a membrane reactor. *Bioresource Technology,* 98**,** 639-647.

Ebiura, T., Echizen, T., Ishikawa, A., Murai, K. & Baba, T. (2005) Selective transesterification of triolein with methanol to methyl oleate and glycerol using alumina loaded with alkali metal salt as a solid-base catalyst. *Applied Catalysis A: General,* 283**,** 111-116.

Erickson, B. L., Asthana, H. & Drzal, L. T. (1997) Sulfonation of polymer surfaces - i. Improving adhesion of polypropylene and polystyrene to epoxy adhesives via gas phase sulfonation. *Journal of Adhesion Science and Technology,* 11**,** 1249-1267.

Ertl, H., Knozinger, H., Schuth, F. & Weitkamp, J. 2008. Catalytic membrane reactors. *Handbook of heterogeneous catalysis.* Weinheim: Wiley-VCH.

Faria, E. A., Ramalho, H. F., Marques, J. S., Suarez, P. A. Z. & Prado, A. G. S. (2008) Tetramethylguanidine covalently bonded onto silica gel surface as an efficient and reusable catalyst for transesterification of vegetable oil. *Applied Catalysis A: General,* 338**,** 72-78.

Fazal, M. A., Haseeb, A. S. M. A. & Masjuki, H. H. (2011) Biodiesel feasibility study: An evaluation of material compatibility; performance; emission and engine durability. *Renewable and Sustainable Energy Reviews,* 15**,** 1314-1324.

Figueiredo, K. C. d. S., Salim, V. M. M. & Borges, C. P. (2008) Synthesis and characterization of a catalytic membrane for pervaporation-assisted esterification reactors. *Catalysis Today,* 133-135**,** 809-814.

Fjerbaek, L., Christensen, K. V. & Norddahl, B. (2009) A review of the current state of biodiesel production using enzymatic transesterification. *Biotechnology and Bioengineering,* 102**,** 1298-1315.

Fraile, J. M., García, N., Mayoral, J. A., Pires, E. & Roldán, L. (2010) The basicity of mixed oxides and the influence of alkaline metals: The case of transesterification reactions. *Applied Catalysis A: General,* 387**,** 67-74.

Fu, Q., Gao, B., Dou, H., Hao, L., Lu, X., Sun, K., Jiang, J. & Zhang, X. (2011) Novel non-covalent sulfonated multiwalled carbon nanotubes from p-toluenesulfonic acid/glucose doped polypyrrole for electrochemical capacitors. *Synthetic Metals,* 161**,** 373-378.

Furuta, S., Matsuhashi, H. & Arata, K. (2004) Biodiesel fuel production with solid superacid catalysis in fixed bed reactor under atmospheric pressure. *Catalysis Communications,* 5**,** 721-723.

Gan, S., Ng, H. K., Chan, P. H. & Leong, F. L. (2012) Heterogeneous free fatty acids esterification in waste cooking oil using ion-exchange resins. *Fuel Processing Technology,* 102**,** 67-72.

Gomes, M. C. S., Arroyo, P. A. & Pereira, N. C. (2011) Biodiesel production from degummed soybean oil and glycerol removal using ceramic membrane. *Journal of Membrane Science,* 378**,** 453-461.

Gomes, M. C. S., Pereira, N. C. & Barros, S. T. D. d. (2010) Separation of biodiesel and glycerol using ceramic membranes. *Journal of Membrane Science,* 352**,** 271-276.

Goto, S., Tagawa, T. & Yusoff, A. (1991) Kinetics of the esterification of palmitic acid with isobutyl alcohol. *International Journal of Chemical Kinetics,* 23**,** 17-26.

Granados, M. L., Alonso, D. M., Sádaba, I., Mariscal, R. & Ocón, P. (2009) Leaching and homogeneous contribution in liquid phase reaction catalysed by solids: The case of triglycerides methanolysis using cao. *Applied Catalysis B: Environmental,* 89**,** 265-272.

Guan, G., Kusakabe, K. & Yamasaki, S. (2009) Tri-potassium phosphate as a solid catalyst for biodiesel production from waste cooking oil. *Fuel Processing Technology,* 90**,** 520-524.

Guan, H.-M., Chung, T.-S., Huang, Z., Chng, M. L. & Kulprathipanja, S. (2006) Poly(vinyl alcohol) multilayer mixed matrix membranes for the dehydration of ethanol-water mixture. *Journal of Membrane Science,* 268**,** 113-122.

Guerreiro, L., Castanheiro, J. E., Fonseca, I. M., Martin-Aranda, R. M., Ramos, A. M. & Vital, J. (2006) Transesterification of soybean oil over sulfonic acid functionalised polymeric membranes. *Catalysis Today,* 118**,** 166-171.

Guerreiro, L., Pereira, P. M., Fonseca, I. M., Martin-Aranda, R. M., Ramos, A. M., Dias, J. M. L., Oliveira, R. & Vital, J. (2010) Pva embedded hydrotalcite membranes as basic catalysts for biodiesel synthesis by soybean oil methanolysis. *Catalysis Today,* 156**,** 191-197.

Gui, M. M., Lee, K. T. & Bhatia, S. (2009) Supercritical ethanol technology for the production of biodiesel: Process optimization studies. *The Journal of Supercritical Fluids,* 49**,** 286-292.

Guo, S., He, B., Li, J., Zhao, Q. & Cheng, Y. (2014) Esterification of acetic acid and ethanol in a flow-through membrane reactor coupled with pervaporation. *Chemical Engineering & Technology,* 37**,** 478-482.

Guo, T., Nikolaev, P., Thess, A., Colbert, D. T. & Smalley, R. E. (1995) Catalytic growth of single-walled manotubes by laser vaporization. *Chemical Physics Letters,* 243**,** 49-54.

Hammond, G. P., Kallu, S. & McManus, M. C. (2008) Development of biofuels for the uk automotive market. *Applied Energy,* 85**,** 506-515.

Han, M., Yi, W., Wu, Q., Liu, Y., Hong, Y. & Wang, D. (2009) Preparation of biodiesel from waste oils catalyzed by a brønsted acidic ionic liquid. *Bioresource Technology,* 100**,** 2308-2310.

Hasheminejad, M., Tabatabaei, M., Mansourpanah, Y., far, M. K. & Javani, A. (2011) Upstream and downstream strategies to economize biodiesel production. *Bioresource Technology,* 102**,** 461-468.

Hawash, S., Kamal, N., Zaher, F., Kenawi, O. & Diwani, G. E. (2009) Biodiesel fuel from jatropha oil via non-catalytic supercritical methanol transesterification. *Fuel,* 88**,** 579-582.

He, H., Guo, X. & Zhu, S. (2006) Comparison of membrane extraction with traditional extraction methods for biodiesel production. *Journal of the American Oil Chemists' Society,* 83**,** 457-460.

Helwani, Z., Othman, M. R., Aziz, N., Kim, J. & Fernando, W. J. N. (2009) Solid heterogeneous catalysts for transesterification of triglycerides with methanol: A review. *Applied Catalysis A: General,* 363**,** 1-10.

Ho, Y. M., Liu, J. W., Qi, J. L. & Zheng, W. T. (2008) Spectroscopic investigation on carbon nanotubes coated with zno nanoparticles. *J. Phys. D: Appl. Phys.*, 41**,** 065308.

Hoekman, S. K. (2008) Biofuels in the u.S. - challenges and opportunities. *Renewable Energy,* 34**,** 14-22.

Hussain, C. M., Saridara, C. & Mitra, S. (2011) Altering the polarity of self-assembled carbon nanotubes stationary phase via covalent functionalization. *RSC Advances,* 1**,** 685-689.

IEA. (2013) *Key world energy statistic* [Online]. [Accessed 23th August 2014]. Available from World Wide Web: http://www.iea.org/publications/freepublications/publication/KeyWorld2013.pdf.

Iijima, S., Ajayan, P. M. & Ichihashi, T. (1992) Growth model for carbon nanotubes. *Physical Review Letters,* 69**,** 3100-3103.

Inframat Corporation. (2015) *Inframat advanced materials* [Online]. [Accessed 13th February 2015]. Available from World Wide Web: http://www.advancedmaterials.us/index.htm.

Ismail, A. F., Goh, P. S., Sanip, S. M. & Aziz, M. (2009) Transport and separation properties of carbon nanotube-mixed matrix membrane. *Separation and Purification Technology,* 70**,** 12-26.

Janaun, J. & Ellis, N. (2010) Perspectives on biodiesel as a sustainable fuel. *Renewable and Sustainable Energy Reviews,* 14**,** 1312-1320.

Jiang, K., Schadler, L. S., Siegel, R. W., Zhang, X., Zhang, H. & Terrones, M. (2004) Protein immobilization on carbon nanotubes via a two-step process of diimide-activated amidation. *Journal of Materials Chemistry,* 14**,** 37-39.

Jitputti, J., Kitiyanan, B., Rangsunvigit, P., Bunyakiat, K., Attanatho, L. & Jenvanitpanjakul, P. (2006) Transesterification of crude palm kernel oil and crude coconut oil by different solid catalysts. *Chemical Engineering Journal,* 116**,** 61-66.

Joelianingsih, Maeda, H., Hagiwara, S., Nabetani, H., Sagara, Y., Soerawidjaya, T. H., Tambunan, A. H. & Abdullah, K. (2008) Biodiesel fuels from palm oil via the non-catalytic transesterification in a bubble column reactor at atmospheric pressure: A kinetic study. *Renewable Energy,* 33**,** 1629-1636.

Jung, K. H., Boo, J.-H. & Hong, B. (2004) Synthesis of carbon nanotubes grown by hot filament plasma-enhanced chemical vapor deposition method. *Diamond and Related Materials,* 13**,** 299-304.

Kansedo, J. (2009). *Synthesis of biodiesel from palm oil and sea mango oil using sulfated zirconia catalyst.* Ph.D thesis, Universiti Sains Malaysia.

Kansedo, J., Lee, K. T. & Bhatia, S. (2009) Cerbera odollam (sea mango) oil as a promising non-edible feedstock for biodiesel production. *Fuel,* 88**,** 1148-1150.

Karaosmanoğlu, F., Cığızoğlu, K. B., Tüter, M. & Ertekin, S. (1996) Investigation of the refining step of biodiesel production. *Energy & Fuels,* 10**,** 890-895.

Karimi, B., Mirzaei, H. M. & Mobaraki, A. (2012) Periodic mesoporous organosilica functionalized sulfonic acids as highly efficient and recyclable catalysts in biodiesel production. *Catalysis Science & Technology,* 2**,** 828-834.

Kastner, J. R., Miller, J., Geller, D. P., Locklin, J., Keith, L. H. & Johnson, T. (2012) Catalytic esterification of fatty acids using solid acid catalysts generated from biochar and activated carbon. *Catalysis Today,* 190**,** 122-132.

Kawashima, A., Matsubara, K. & Honda, K. (2008) Development of heterogeneous base catalysts for biodiesel production. *Bioresource Technology,* 99**,** 3439-3443.

Khayet, M., Villaluenga, J. P. G., Godino, M. P., Mengual, J. I., Seoane, B., Khulbe, K. C. & Matsuura, T. (2004) Preparation and application of dense poly(phenylene oxide) membranes in pervaporation. *Journal of Colloid and Interface Science,* 278**,** 410-422.

Kim, H.-J., Kang, B.-S., Kim, M.-J., Park, Y. M., Kim, D.-K., Lee, J.-S. & Lee, K.-Y. (2004) Transesterification of vegetable oil to biodiesel using heterogeneous base catalyst. *Catalysis Today,* 93–95**,** 315-320.

Kim, K.-J., Lee, S.-B. & Han, N.-W. (1994) Kinetics of crosslinking reaction of pva membrane with glutaraldehyde. *Korean Journal of Chemical Engineering,* 11**,** 41-47.

Kim, M. J., Kim, M.-Y., Kwon, O. Z. & Seo, G. (2011) Transesterification of vegetable oils over a phosphazenium hydroxide catalyst incorporated onto silica. *Fuel Processing Technology,* 92**,** 126-131.

Kis, A., Csanyi, G., Salvetat, J. P., Lee, T.-N., Couteau, E., Kulik, A. J., Benoit, W., Brugger, J. & Forro, L. (2004) Reinforcement of single-walled carbon nanotube bundles by intertube bridging. *Nature Materials,* 3**,** 153-157.

Knothe, G., Gerpen, J. V. & Krahl, J. (2005a). The biodiesel handbook, AOCS.

Knothe, G., Van Gerpen, J. & Krahl, J. V. (2005b). The biodiesel handbook, AOCS Publication.

Köhn, R. & Fröba, M. (2003) Investigations of reactivity and magnetic properties of nanostructured iron oxide within mesoporous silica materials. *Zeitschrift fuer Anorganische und Allgemeine Chemie,* 629**,** 1673-1682.

Kouzu, M., Yamanaka, S.-y., Hidaka, J.-s. & Tsunomori, M. (2009) Heterogeneous catalysis of calcium oxide used for transesterification of soybean oil with refluxing methanol. *Applied Catalysis A: General,* 355**,** 94-99.

Kuo, C.-Y. (2009) Comparison with as-grown and microwave modified carbon nanotubes to removal aqueous bisphenol a. *Desalination,* 249**,** 976-982.

Lam, M. K. & Lee, K. T. (2011) Mixed methanol–ethanol technology to produce greener biodiesel from waste cooking oil: A breakthrough for so42−/sno2–sio2 catalyst. *Fuel Processing Technology,* 92**,** 1639-1645.

Lam, M. K., Lee, K. T. & Mohamed, A. R. (2009) Sulfated tin oxide as solid superacid catalyst for transesterification of waste cooking oil: An optimization study. *Applied Catalysis B: Environmental,* 93**,** 134-139.

Lam, M. K., Lee, K. T. & Mohamed, A. R. (2010) Homogeneous, heterogeneous and enzymatic catalysis for transesterification of high free fatty acid oil (waste cooking oil) to biodiesel: A review. *Biotechnology Advances,* 28**,** 500-518.

Le, N. L., Wang, Y. & Chung, T.-S. (2012) Synthesis, cross-linking modifications of 6fda-nda/daba polyimide membranes for ethanol dehydration via pervaporation. *Journal of Membrane Science,* 415–416**,** 109-121.

Leclercq, E., Finiels, A. & Moreau, C. (2001) Transesterification of rapeseed oil in the presence of basic zeolites and related solid catalysts. *Journal of the American Oil Chemists' Society,* 78**,** 1161-1165.

Lee, D. W., Park, Y. M. & Lee, K. Y. (2009) Heterogeneous base catalysts for transesterification in biodiesel synthesis. *Catal Surv Asia,* 13**,** 63-77.

Lee, J. S. & Saka, S. (2010) Biodiesel production by heterogeneous catalysts and supercritical technologies. *Bioresource Technology,* 101**,** 7191-7200.

Leung, D. Y. C., Wu, X. & Leung, M. K. H. (2010) A review on biodiesel production using catalyzed transesterification. *Applied Energy,* 87**,** 1083-1095.

Li, E. & Rudolph, V. (2007) Transesterification of vegetable oil to biodiesel over mgo-functionalized mesoporous catalysts†. *Energy & Fuels,* 22**,** 145-149.

Li, H. & Xie, W. (2006) Transesterification of soybean oil to biodiesel with zn/i2 catalyst. *Catalysis Letters,* 107**,** 25-30.

Li, X. & Huang, W. (2009) Synthesis of biodiesel from rap oil over sulfated titania-based solid superacid catalysts. *Energy Sources, Part A: Recovery, Utilization, and Environmental Effects,* 31**,** 1666-1672.

Li, Y.-H., Wang, S., Luan, Z., Ding, J., Xu, C. & Wu, D. (2003) Adsorption of cadmium(ii) from aqueous solution by surface oxidized carbon nanotubes. *Carbon,* 41**,** 1057-1062.

Li, Y.-H., Zhu, Y., Zhao, Y., Wu, D. & Luan, Z. (2006) Different morphologies of carbon nanotubes effect on the lead removal from aqueous solution. *Diamond and Related Materials,* 15**,** 90-94.

Li, Y., Liu, J. H.-C., Witham, C. A., Huang, W., Marcus, M. A., Fakra, S. C., Alayoglu, P., Zhu, Z., Thompson, C. M., Arjun, A., Lee, K., Gross, E., Toste, F. D. & Somorjai, G. A. (2011) A pt-cluster-based heterogeneous catalyst for homogeneous catalytic reactions: X-ray absorption spectroscopy and reaction kinetic studies of their activity and stability against leaching. *Journal of the American Chemical Society,* 133**,** 13527-13533.

Liang, X., Gong, G., Wu, H. & Yang, J. (2009) Highly efficient procedure for the synthesis of biodiesel from soybean oil using chloroaluminate ionic liquid as catalyst. *Fuel,* 88**,** 613-616.

Liang, X. & Yang, J. (2010) Synthesis of a novel multi -so3h functionalized ionic liquid and its catalytic activities for biodiesel synthesis. *Green Chemistry,* 12**,** 201-204.

Licht, F. O. (2007). World biodiesel market: The outlook to 2010, Tunbridge Wells, UK, Agra Informa.

Lin, D.-Q., Brixius, P. J., Hubbuch, J. J., Thömmes, J. & Kula, M.-R. (2003) Biomass/adsorbent electrostatic interactions in expanded bed adsorption: A zeta potential study. *Biotechnology and Bioengineering,* 83**,** 149-157.

Lin, Y.-W. & Wu, T.-M. (2009) Synthesis and characterization of externally doped sulfonated polyaniline/multi-walled carbon nanotube composites. *Composites Science and Technology,* 69**,** 2559-2565.

Lipnizki, F., Field, R. W. & Ten, P.-K. (1999a) Pervaporation-based hybrid process: A review of process design, applications and economics. *Journal of Membrane Science,* 153**,** 183-210.

Lipnizki, F., Hausmanns, S., Ten, P.-K., Field, R. W. & Laufenberg, G. (1999b) Organophilic pervaporation: Prospects and performance. *Chemical Engineering Journal,* 73**,** 113-129.

Liu, R., Wang, X., Zhao, X. & Feng, P. (2008) Sulfonated ordered mesoporous carbon for catalytic preparation of biodiesel. *Carbon,* 46**,** 1664-1669.

Liu, X., He, H., Wang, Y. & Zhu, S. (2007a) Transesterification of soybean oil to biodiesel using sro as a solid base catalyst. *Catalysis Communications,* 8**,** 1107-1111.

Liu, X., Piao, X., Wang, Y. & Zhu, S. (2010) Model study on transesterification of soybean oil to biodiesel with methanol using solid base catalyst. *The Journal of Physical Chemistry A,* 114**,** 3750-3755.

Liu, Y., Lotero, E., Goodwin Jr, J. G. & Lu, C. (2007b) Transesterification of triacetin using solid brønsted bases. *Journal of Catalysis,* 246**,** 428-433.

López, D. E., Goodwin Jr, J. G., Bruce, D. A. & Lotero, E. (2005) Transesterification of triacetin with methanol on solid acid and base catalysts. *Applied Catalysis A: General,* 295**,** 97-105.

López, D. E., Suwannakarn, K., Bruce, D. A. & Goodwin Jr, J. G. (2007) Esterification and transesterification on tungstated zirconia: Effect of calcination temperature. *Journal of Catalysis,* 247**,** 43-50.

Lotero, E., Liu, Y., Lopez, D. E., Suwannakarn, K., Bruce, D. A. & Goodwin, J. G. (2005) Synthesis of biodiesel via acid catalysis. *Industrial & Engineering Chemistry Research,* 44**,** 5353-5363.

Lu, C. & Chiu, H. (2006) Adsorption of zinc(ii) from water with purified carbon nanotubes. *Chemical Engineering Science,* 61**,** 1138-1145.

Lu, H., Liu, Y., Zhou, H., Yang, Y., Chen, M. & Liang, B. (2009) Production of biodiesel from jatropha curcas l. Oil. *Computers & Chemical Engineering,* 33**,** 1091-1096.

Mabee, W. E. (2007) Policy options to support biofuel production. *Advances in Biochemical Engineering/Biotechnology,* 108**,** 329-357.

Manafi, S. A., Amin, M. H., Rahimipour, M. R., Salahi, E. & Kazemzadeh, A. (2009) Carbon nanotubes synthesized by mechanothermal method. *New Carbon Materials,* 24**,** 39-44.

Mar, W. W. & Somsook, E. (2012) Sulfonic-functionalized carbon catalyst for esterification of high free fatty acid. *Procedia Engineering,* 32**,** 212-218.

Marchetti, J. M., Miguel, V. U. & Errazu, A. F. (2007a) Heterogeneous esterification of oil with high amount of free fatty acids. *Fuel,* 86**,** 906-910.

Marchetti, J. M., Miguel, V. U. & Errazu, A. F. (2007b) Possible methods for biodiesel production. *Renewable and Sustainable Energy Reviews,* 11**,** 1300-1311.

Mbaraka, I. & Shanks, B. (2006) Conversion of oils and fats using advanced mesoporous heterogeneous catalysts. *Journal of the American Oil Chemists' Society,* 83**,** 79-91.

Meher, L. C., Kulkarni, M. G., Dalai, A. K. & Naik, S. N. (2006) Transesterification of karanja (pongamia pinnata) oil by solid basic catalysts. *European Journal of Lipid Science and Technology,* 108**,** 389-397.

Melero, J. A., Bautista, L. F., Morales, G., Iglesias, J. & Sánchez-Vázquez, R. (2010) Biodiesel production from crude palm oil using sulfonic acid-modified mesostructured catalysts. *Chemical Engineering Journal,* 161**,** 323-331.

Melero, J. A., Iglesias, J. & Morales, G. (2009) Heterogeneous acid catalysts for biodiesel production: Current status and future challenges. *Green Chemistry,* 11**,** 1285-1308.

Miao, X., Li, R. & Yao, H. (2009) Effective acid-catalyzed transesterification for biodiesel production. *Energy Conversion and Management,* 50**,** 2680-2684.

Mo, X., López, D. E., Suwannakarn, K., Liu, Y., Lotero, E., Goodwin Jr, J. G. & Lu, C. (2008a) Activation and deactivation characteristics of sulfonated carbon catalysts. *Journal of Catalysis,* 254**,** 332-338.

Mo, X., Lotero, E., Lu, C., Liu, Y. & Goodwin, J. (2008b) A novel sulfonated carbon composite solid acid catalyst for biodiesel synthesis. *Catalysis Letters,* 123**,** 1-6.

Molaei Dehkordi, A. & Ghasemi, M. (2012) Transesterification of waste cooking oil to biodiesel using ca and zr mixed oxides as heterogeneous base catalysts. *Fuel Processing Technology,* 97**,** 45-51.

Monbiot, G. (2004) *Feeding cars, not people* [Online]. [Accessed 1st September 2013]. Available from World Wide Web: http://www.monbiot.com/archives/2004/11/23/feeding-cars-not-people/.

Monni, S. & Raes, F. (2008) Multilevel climate policy: The case of the european union, finland and helsinki. *Environmental Science and Policy,* 11**,** 743-755.

Mootabadi, H., Salamatinia, B., Bhatia, S. & Abdullah, A. Z. (2010) Ultrasonic-assisted biodiesel production process from palm oil using alkaline earth metal oxides as the heterogeneous catalysts. *Fuel,* 89**,** 1818-1825.

Mrsevic, M., Düsselberg, D. & Staudt, C. (2012) Synthesis and characterization of a novel carboxyl group containing (co)polyimide with sulfur in the polymer backbone. *Beilstein Journal of Organic Chemistry,* 8**,** 776-786.

Mukherjee, B., Santra, K., Pattnaik, G. & Ghosh, S. (2008) Preparation, characterization and in-vitro evaluation of sustained release protein-loaded nanoparticles based on biodegradable polymers. *International Journal of Nanomedicine,* 3**,** 487-496.

Muniyappa, P. R., Brammer, S. C. & Noureddini, H. (1996) Improved conversion of plant oils and animal fats into biodiesel and co-product. *Bioresource Technology,* 56**,** 19-24.

Narasimharao, K., Lee, A. & Wilson, K. (2007) Catalysts in production of biodiesel: A review. *Journal of Biobased Materials and Bioenergy,* 1**,** 19-30.

Nelson, R. G. & Schrock, M. D. (2006) Energetic and economic feasibility associated with the production, processing, and conversion of beef tallow to a substitute diesel fuel. *Biomass and Bioenergy,* 30**,** 584-591.

Ng, E.-P., Mohd Subari, S. N., Marie, O., Mukti, R. R. & Juan, J.-C. (2013) Sulfonic acid functionalized mcm-41 as solid acid catalyst for tert-butylation of hydroquinone enhanced by microwave heating. *Applied Catalysis A: General,* 450**,** 34-41.

Ng, E. P., Hadi, N., Mohd Nazlan, M. M. & Halimaton, H. (2006) Sulphated almcm-41: Mesoporous solid brønsted acid catalyst for dibenzoylation of biphenyl. *Catalysis Today,* 114**,** 257-262.

Nijhuis, T. A., van Koten, G., Kapteijn, F. & Moulijn, J. A. (2003) Separation of kinetics and mass-transport effects for a fast reaction: The selective hydrogenation of functionalized alkynes. *Catalysis Today,* 79–80**,** 315-321.

Om Tapanes, N. C., Gomes Aranda, D. A., de Mesquita Carneiro, J. W. & Ceva Antunes, O. A. (2008) Transesterification of jatropha curcas oil glycerides: Theoretical and experimental studies of biodiesel reaction. *Fuel,* 87**,** 2286-2295.

Ong, Y. K., Wang, H. & Chung, T.-S. (2012) A prospective study on the application of thermally rearranged acetate-containing polyimide membranes in dehydration of biofuels via pervaporation. *Chemical Engineering Science,* 79**,** 41-53.

Othman, R., Mohammad, A. W., Ismail, M. & Salimon, J. (2010) Application of polymeric solvent resistant nanofiltration membranes for biodiesel production. *Journal of Membrane Science,* 348**,** 287-297.

Padavan, D. T. & Wan, W. K. (2010) Synthesis and characterization of a novel versatile poly(amic acid) derived from ethylenediaminetetraacetic dianhydride. *Materials Chemistry and Physics,* 124**,** 427-433.

Pal, N., Paul, M. & Bhaumik, A. (2011) Highly ordered zn-doped mesoporous silica: An efficient catalyst for transesterification reaction. *Journal of Solid State Chemistry,* 184**,** 1805-1812.

Pangarkar, V. & Pal, S. 2008. Pervaporation. *Handbook of membrane separations.* CRC Press.

Paradise, M. & Goswami, T. (2007) Carbon nanotubes – production and industrial applications. *Materials & Design,* 28**,** 1477-1489.

Park, Y.-M., Lee, D.-W., Kim, D.-K., Lee, J.-S. & Lee, K.-Y. (2008) The heterogeneous catalyst system for the continuous conversion of free fatty acids in used vegetable oils for the production of biodiesel. *Catalysis Today,* 131**,** 238-243.

Pasias, S., Barakos, N., Alexopoulos, C. & Papayannakos, N. (2006) Heterogeneously catalyzed esterification of ffas in vegetable oils. *Chemical Engineering & Technology,* 29**,** 1365-1371.

Peña, R., Romero, R., Martínez, S. L., Ramos, M. J., Martínez, A. & Natividad, R. (2008) Transesterification of castor oil: Effect of catalyst and co-solvent. *Industrial & Engineering Chemistry Research,* 48**,** 1186-1189.

Peng, F., Zhang, L., Wang, H., Lv, P. & Yu, H. (2005) Sulfonated carbon nanotubes as a strong protonic acid catalyst. *Carbon,* 43**,** 2405-2408.

Peng, X. & Wong, S. S. (2009) Functional covalent chemistry of carbon nanotube surfaces. *Advanced Materials (Weinheim, Germany)*, 21**,** 625-642.

Pham-Huu, C., Keller, N., Ehret, G., Charbonniere, L. c. J., Ziessel, R. & Ledoux, M. J. (2001) Carbon nanofiber supported palladium catalyst for liquid-phase reactions: An active and selective catalyst for hydrogenation of cinnamaldehyde into hydrocinnamaldehyde. *Journal of Molecular Catalysis A: Chemical*, 170**,** 155-163.

Pinnarat, T. & Savage, P. E. (2008) Assessment of noncatalytic biodiesel synthesis using supercritical reaction conditions. *Industrial and Engineering Chemistry Research*, 47**,** 6801-6808.

Pu, Y., Yang, X., Zheng, H., Wang, D., Su, Y. & He, J. (2013) Adsorption and desorption of thallium(i) on multiwalled carbon nanotubes. *Chemical Engineering Journal*, 219**,** 403-410.

Qiao, X. & Chung, T.-S. (2006) Diamine modification of p84 polyimide membranes for pervaporation dehydration of isopropanol. *AIChE Journal*, 52**,** 3462-3472.

Qiu, J., Wang, G., Bao, Y., Zeng, D. & Chen, Y. (2015) Effect of oxidative modification of coal tar pitch-based mesoporous activated carbon on the adsorption of benzothiophene and dibenzothiophene. *Fuel Processing Technology*, 129**,** 85-90.

Qiu, W., Chen, C.-C., Xu, L., Cui, L., Paul, D. R. & Koros, W. J. (2011) Sub-tg cross-linking of a polyimide membrane for enhanced co2 plasticization resistance for natural gas separation. *Macromolecules,* 44**,** 6046-6056.

Quintero, R., Kim, D. Y., Hasegawa, K., Yamada, Y., Yamada, A. & Noda, S. (2014) Carbon nanotube 3d current collectors for lightweight, high performance and low cost supercapacitor electrodes. *RSC Advances,* 4**,** 8230-8237.

Rahimpour, A., Madaeni, S. S., Amirinejad, M., Mansourpanah, Y. & Zereshki, S. (2009) The effect of heat treatment of pes and pvdf ultrafiltration membranes on morphology and performance for milk filtration. *Journal of Membrane Science,* 330**,** 189-204.

Ramos, M. J., Casas, A., Rodríguez, L., Romero, R. & Pérez, Á. (2008) Transesterification of sunflower oil over zeolites using different metal loading: A case of leaching and agglomeration studies. *Applied Catalysis A: General,* 346**,** 79-85.

Ramulifho, T., Ozoemena, K. I., Modibedi, R. M., Jafta, C. J. & Mathe, M. K. (2012) Fast microwave-assisted solvothermal synthesis of metal nanoparticles (pd, ni, sn) supported on sulfonated mwcnts: Pd-based bimetallic catalysts for ethanol oxidation in alkaline medium. *Electrochimica Acta,* 59**,** 310-320.

Rashid, U. & Anwar, F. (2008) Production of biodiesel through optimized alkaline-catalyzed transesterification of rapeseed oil. *Fuel,* 87**,** 265-273.

Refaat, A. A. (2011) Biodiesel production using solid metal oxide catalysts. *International journal of Environmental Science and Technology,* 8**,** 203-221.

Rizvi, S. (2010). Separation, extraction and concentration processes in the food, beverage and nutraceutical industries, Cambridge CB21 6AH, Woodhead Publishing. 228.

Rodríguez-reinoso, F. (1998) The role of carbon materials in heterogeneous catalysis. *Carbon,* 36**,** 159-175.

Roelofs, J. C. A. A., van Dillen, A. J. & de Jong, K. P. (2000) Base-catalyzed condensation of citral and acetone at low temperature using modified hydrotalcite catalysts. *Catalysis Today,* 60**,** 297-303.

Ryoo, M. W., Chung, S. G., Kim, J. H., Song, Y. S. & Seo, G. (2003) The effect of mass transfer on the catalytic combustion of benzene and methane over palladium catalysts supported on porous materials. *Catalysis Today,* 83**,** 131-139.

Sae-Khow, O. & Mitra, S. (2010) Pervaporation in chemical analysis. *Journal of Chromatography A,* 1217**,** 2736-2746.

Sahoo, P. K., Das, L. M., Babu, M. K. G. & Naik, S. N. (2007) Biodiesel development from high acid value polanga seed oil and performance evaluation in a ci engine. *Fuel,* 86**,** 448-454.

Saleh, J., Tremblay, A. Y. & Dubé, M. A. (2010) Glycerol removal from biodiesel using membrane separation technology. *Fuel,* 89**,** 2260-2266.

Šalić, A. & Zelić, B. (2011) Microreactors-portable factories for biodiesel fuel production. *Goriva I Maziva,* 50**,** 85-110.

Samart, C., Sreetongkittikul, P. & Sookman, C. (2009) Heterogeneous catalysis of transesterification of soybean oil using ki/mesoporous silica. *Fuel Processing Technology,* 90**,** 922-925.

Sanchez Marcano, J. G. & Tsotsis, T. T. 2002. The coupling of the membrane separation process with a catalytic reaction. *Catalytic membranes and membrane reactor*. Weinheim: Wiley-VCH

Sankaranarayanan, T. M., Pandurangan, A., Banu, M. & Sivasanker, S. (2011) Transesterification of sunflower oil over moo3 supported on alumina. *Applied Catalysis A: General,* 409–410**,** 239-247.

Sarkar, B., Sridhar, S., Saravanan, K. & Kale, V. (2010) Preparation of fatty acid methyl ester through temperature gradient driven pervaporation process. *Chemical Engineering Journal,* 162**,** 609-615.

Sawangkeaw, R., Bunyakiat, K. & Ngamprasertsith, S. (2007) Effect of co-solvents on production of biodiesel via transesterification in supercritical methanol. *Green Chemistry,* 9**,** 679-685.

Sawyer, R. F. Year. Science based policy for addressing energy and environmental problems. *In:* Proc Combust Inst., 2009. 45-56.

Sdrula, N. (2010) A study using classical or membrane separation in the biodiesel process. *Desalination,* 250**,** 1070-1072.

Semwal, S., Arora, A. K., Badoni, R. P. & Tuli, D. K. (2011) Biodiesel production using heterogeneous catalysts. *Bioresource Technology,* 102**,** 2151-2161.

Serp, P. & Castillejos, E. (2010) Catalysis in carbon nanotubes. *ChemCatChem,* 2**,** 41-47.

Serp, P., Corrias, M. & Kalck, P. (2003) Carbon nanotubes and nanofibers in catalysis. *Applied Catalysis A: General,* 253**,** 337-358.

Shah, K., Parikh, J. & Maheria, K. (2014) Optimization studies and chemical kinetics of silica sulfuric acid-catalyzed biodiesel synthesis from waste cooking oil. *BioEnergy Research,* 7**,** 206-216.

Shanmugam, S., Viswanathan, B. & Varadarajan, T. K. (2004) Esterification by solid acid catalysts—a comparison. *Journal of Molecular Catalysis A: Chemical,* 223**,** 143-147.

Shao, P. & Huang, R. Y. M. (2007) Polymeric membrane pervaporation. *Journal of Membrane Science,* 287**,** 162-179.

Sharma, A., Thampi, S. P., Suggala, S. V. & Bhattacharya, P. K. (2004) Pervaporation from a dense membrane: Roles of permeant−membrane interactions, kelvin effect, and membrane swelling. *Langmuir,* 20**,** 4708-4714.

Sharma, Y. C. & Singh, B. (2009) Development of biodiesel: Current scenario. *Renewable and Sustainable Energy Reviews,* 13**,** 1646-1651.

Shemper, B. S. & Mathias, L. J. (2004) Photopolymerized low-surface-energy coatings based on a novel fluorinated ether acrylate. *Journal of Applied Polymer Science,* 91**,** 3301-3314.

Shi, W., He, B., Ding, J., Li, J., Yan, F. & Liang, X. (2010) Preparation and characterization of the organic-inorganic hybrid membrane for biodiesel production. *Bioresource Technology,* 101**,** 1501-1505.

Shu, Q., Gao, J., Nawaz, Z., Liao, Y., Wang, D. & Wang, J. (2010) Synthesis of biodiesel from waste vegetable oil with large amounts of free fatty acids using a carbon-based solid acid catalyst. *Applied Energy,* 87**,** 2589-2596.

Shu, Q., Zhang, Q., Xu, G., Nawaz, Z., Wang, D. & Wang, J. (2009a) Synthesis of biodiesel from cottonseed oil and methanol using a carbon-based solid acid catalyst. *Fuel Processing Technology,* 90**,** 1002-1008.

Shu, Q., Zhang, Q., Xu, G. & Wang, J. (2009b) Preparation of biodiesel using s-mwcnt catalysts and the coupling of reaction and separation. *Food and Bioproducts Processing,* 87**,** 164-170.

Simate, G. S., Iyuke, S. E., Ndlovu, S. & Heydenrych, M. (2012) The heterogeneous coagulation and flocculation of brewery wastewater using carbon nanotubes. *Water Research,* 46**,** 1185-1197.

Sirkar, K. K. & Ho, W. S. W. (1992). Membrane handbook, Kluwer Academic Publishers.

Sivakumar, P., Sindhanaiselvan, S., Gandhi, N. N., Devi, S. S. & Renganathan, S. (2013) Optimization and kinetic studies on biodiesel production from underutilized ceiba pentandra oil. *Fuel,* 103**,** 693-698.

Soares, O. v. S. G. P., Órfão, J. J. M. & Pereira, M. F. R. (2010) Pd−cu and pt−cu catalysts supported on carbon nanotubes for nitrate reduction in water. *Industrial & Engineering Chemistry Research,* 49**,** 7183-7192.

Stankiewicz, A. (2003) Reactive separations for process intensification: An industrial perspective. *Chemical Engineering and Processing,* 42**,** 137-144.

Su, C.-H. (2013) Kinetic study of free fatty acid esterification reaction catalyzed by recoverable and reusable hydrochloric acid. *Bioresource Technology,* 130**,** 522-528.

Su, C.-H., Fu, C.-C., Gomes, J., Chu, I. M. & Wu, W.-T. (2008) A heterogeneous acid-catalyzed process for biodiesel production from enzyme hydrolyzed fatty acids. *AIChE Journal,* 54**,** 327-336.

Su, E.-Z., Xu, W.-Q., Gao, K.-L., Zheng, Y. & Wei, D.-Z. (2007) Lipase-catalyzed in situ reactive extraction of oilseeds with short-chained alkyl acetates for fatty acid esters production. *Journal of Molecular Catalysis B: Enzymatic,* 48**,** 28-32.

Sun, Z.-P., Zhang, X.-G., Liang, Y.-Y. & Li, H.-L. (2009) A facile approach towards sulfonate functionalization of multi-walled carbon nanotubes as pd catalyst support for ethylene glycol electro-oxidation. *Journal of Power Sources,* 191**,** 366-370.

Sun, Z.-P., Zhang, X.-G., Liu, R.-L., Liang, Y.-Y. & Li, H.-L. (2008) A simple approach towards sulfonated multi-walled carbon nanotubes supported by pd catalysts for methanol electro-oxidation. *Journal of Power Sources,* 185**,** 801-806.

Suppes, G. J., Dasari, M. A., Doskocil, E. J., Mankidy, P. J. & Goff, M. J. (2004) Transesterification of soybean oil with zeolite and metal catalysts. *Applied Catalysis A: General,* 257**,** 213-223.

Taher, H., Al-Zuhair, S., Al-Marzouqi, A. H., Haik, Y. & Farid, M. M. (2011) A review of enzymatic transesterification of microalgal oil-based biodiesel using supercritical technology. *Enzyme research,* 2011**,** 468292.

Tai-Shung, N. C. (2007) Development and purification of biodiesel. *Separation and Purification Technology,* 20**,** 377-381.

Takagaki, A., Toda, M., Okamura, M., Kondo, J. N., Hayashi, S., Domen, K. & Hara, M. (2006) Esterification of higher fatty acids by a novel strong solid acid. *Catalysis Today,* 116**,** 157-161.

Tan, T., Lu, J., Nie, K., Deng, L. & Wang, F. (2010) Biodiesel production with immobilized lipase: A review. *Biotechnology Advances,* 28**,** 628-634.

ten Elshof, J. E., Abadal, C. R., Sekulić, J., Chowdhury, S. R. & Blank, D. H. A. (2003) Transport mechanisms of water and organic solvents through microporous silica in the pervaporation of binary liquids. *Microporous and Mesoporous Materials,* 65**,** 197-208.

Tesser, R., Di Serio, M., Guida, M., Nastasi, M. & Santacesaria, E. (2005) Kinetics of oleic acid esterification with methanol in the presence of triglycerides. *Industrial & Engineering Chemistry Research,* 44**,** 7978-7982.

Tessonnier, J.-P., Villa, A., Majoulet, O., Su, D. S. & Schlögl, R. (2009) Defect-mediated functionalization of carbon nanotubes as a route to design single-site basic heterogeneous catalysts for biomass conversion. *Angewandte Chemie International Edition,* 48**,** 6543-6546.

Thess, A., Lee, R., Nikolaev, P., Dai, H., Petit, P., Robert, J., Xu, C., Lee, Y. H., Kim, S. G., Rinzler, A. G., Colbert, D. T., Scuseria, G. E., Tománek, D., Fischer, J. E. & Smalley, R. E. (1996) Crystalline ropes of metallic carbon nanotubes. *Science,* 273**,** 483-487.

Tremblay, A. Y., Cao, P. & Dubé, M. A. (2008) Biodiesel production using ultralow catalyst concentrations. *Energy & Fuels,* 22**,** 2748-2755.

Tripathi, B. P., Schieda, M., Shahi, V. K. & Nunes, S. P. (2011) Nanostructured membranes and electrodes with sulfonic acid functionalized carbon nanotubes. *Journal of Power Sources,* 196**,** 911-919.

Umdu, E. S. & Seker, E. (2012) Transesterification of sunflower oil on single step sol–gel made al2o3 supported cao catalysts: Effect of basic strength and basicity on turnover frequency. *Bioresource Technology,* 106**,** 178-181.

Upare, P. P., Yoon, J.-W., Kim, M. Y., Kang, H.-Y., Hwang, D. W., Hwang, Y. K., Kung, H. H. & Chang, J.-S. (2013) Chemical conversion of biomass-derived hexose sugars to levulinic acid over sulfonic acid-functionalized graphene oxide catalysts. *Green Chemistry,* 15**,** 2935-2943.

Vankelecom, I. F. J. (2002) Polymeric membranes in catalytic reactors. *Chemical Reviews,* 102**,** 3779-3810.

Venezia, A. M., Di Carlo, G., Liotta, L. F., Pantaleo, G. & Kantcheva, M. (2011) Effect of ti(iv) loading on ch4 oxidation activity and so2 tolerance of pd catalysts supported on silica sba-15 and hms. *Applied Catalysis B: Environmental,* 106**,** 529-539.

Verziu, M., Florea, M., Simon, S., Simon, V., Filip, P., Parvulescu, V. I. & Hardacre, C. (2009) Transesterification of vegetable oils on basic large mesoporous alumina supported alkaline fluorides—evidences of the nature of the active site and catalytic performances. *Journal of Catalysis,* 263**,** 56-66.

Vicente, G., Coteron, A., Martinez, M. & Aracil, J. (1998) Application of the factorial design of experiments and response surface methodology to optimize biodiesel production. *Industrial Crops and Products,* 8**,** 29-35.

Vicente, G., Martínez, M. & Aracil, J. (2004) Integrated biodiesel production: A comparison of different homogeneous catalysts systems. *Bioresource Technology,* 92**,** 297-305.

Vicente, G., Martínez, M. & Aracil, J. (2006) Kinetics of brassica carinata oil methanolysis. *Energy & Fuels,* 20**,** 1722-1726.

Villa, A., Tessonnier, J.-P., Majoulet, O., Su, D. S. & SchlAgl, R. (2009) Amino-functionalized carbon nanotubes as solid basic catalysts for the transesterification of triglycerides. *Chemical Communications***,** 4405-4407.

Villa, A., Tessonnier, J.-P., Majoulet, O., Su, D. S. & Schlögl, R. (2010) Transesterification of triglycerides using nitrogen-functionalized carbon nanotubes. *ChemSusChem,* 3**,** 241-245.

Viriya-empikul, N., Krasae, P., Puttasawat, B., Yoosuk, B., Chollacoop, N. & Faungnawakij, K. (2010) Waste shells of mollusk and egg as biodiesel production catalysts. *Bioresource Technology,* 101**,** 3765-3767.

Vyas, A. P., Subrahmanyam, N. & Patel, P. A. (2009) Production of biodiesel through transesterification of jatropha oil using kno3/al2o3 solid catalyst. *Fuel,* 88**,** 625-628.

Wan, Z. & Hameed, B. H. (2011) Transesterification of palm oil to methyl ester on activated carbon supported calcium oxide catalyst. *Bioresource Technology,* 102**,** 2659-2664.

Wang, J., Sui, L., Wan, Q., Luo, F., Tian, L., Pan, L., Pei, X. & He, R. (2013) Effects of ultrasonic radiation intensity on the oxidation of singlewalled carbon nanotubes in a mixture of sulfuric and nitric acids. *Nano,* 08**,** 1350040.

Wang, Y. & Hsieh, Y.-L. (2010) Crosslinking of polyvinyl alcohol (pva) fibrous membranes with glutaraldehyde and peg diacylchloride. *Journal of Applied Polymer Science,* 116**,** 3249-3255.

Wang, Y., Ou, S., Liu, P., Xue, F. & Tang, S. (2006) Comparison of two different processes to synthesize biodiesel by waste cooking oil. *Journal of Molecular Catalysis A: Chemical,* 252**,** 107-112.

Wardle, D. A. (2003) Global sale of green air travel supported using biodiesel. *Renewable and Sustainable Energy Reviews,* 7**,** 1-64.

Wildgoose, G. G., Banks, C. E. & Compton, R. G. (2006) Metal nanoparticles and related materials supported on carbon nanotubes: Methods and applications. *Small,* 2**,** 182-193.

Xie, W., Huang, X. & Li, H. (2007) Soybean oil methyl esters preparation using nax zeolites loaded with koh as a heterogeneous catalyst. *Bioresource Technology,* 98**,** 936-939.

Xie, W. & Li, H. (2006) Alumina-supported potassium iodide as a heterogeneous catalyst for biodiesel production from soybean oil. *Journal of Molecular Catalysis A: Chemical,* 255**,** 1-9.

Xie, W. & Yang, D. (2011) Silica-bonded n-propyl sulfamic acid used as a heterogeneous catalyst for transesterification of soybean oil with methanol. *Bioresource Technology,* 102**,** 9818-9822.

Xu, Z., Qi, Z. & Kaufman, A. (2005) Superior catalysts for proton exchange membrane fuel cells. *Electrochemical and Solid-State Letters,* 8**,** A313-A315.

Yan, S., Kim, M., Salley, S. O. & Ng, K. Y. S. (2009) Oil transesterification over calcium oxides modified with lanthanum. *Applied Catalysis A: General,* 360**,** 163-170.

Yan, Y., Xu, L. & Dai, M. (2012) A synergetic whole-cell biocatalyst for biodiesel production. *RSC Advances,* 2**,** 6170-6173.

Yang, S., Zhang, X., Mi, H. & Ye, X. (2008) Pd nanoparticles supported on functionalized multi-walled carbon nanotubes (mwcnts) and electrooxidation for formic acid. *Journal of Power Sources,* 175**,** 26-32.

Yee, K. F., Lee, K. T., Ceccato, R. & Abdullah, A. Z. (2011a) Production of biodiesel from jatropha curcas l. Oil catalyzed by /zro2 catalyst: Effect of interaction between process variables. *Bioresource Technology,* 102**,** 4285-4289.

Yee, K. F., Wu, J. C. S. & Lee, K. T. (2011b) A green catalyst for biodiesel production from jatropha oil: Optimization study. *Biomass and Bioenergy,* 35**,** 1739-1746.

Yoshimitsu, Z., Nakajima, A., Watanabe, T. & Hashimoto, K. (2002) Effects of surface structure on the hydrophobicity and sliding behavior of water droplets. *Langmuir,* 18**,** 5818-5822.

Yu, H., Jin, Y., Li, Z., Peng, F. & Wang, H. (2008) Synthesis and characterization of sulfonated single-walled carbon nanotubes and their performance as solid acid catalyst. *Journal of Solid State Chemistry,* 181**,** 432-438.

Yu, X., Wen, Z., Li, H., Tu, S.-T. & Yan, J. (2011) Transesterification of pistacia chinensis oil for biodiesel catalyzed by cao–ceo2 mixed oxides. *Fuel,* 90**,** 1868-1874.

Yun, S., Im, H., Heo, Y. & Kim, J. (2011) Crosslinked sulfonated poly(vinyl alcohol)/sulfonated multi-walled carbon nanotubes nanocomposite membranes for direct methanol fuel cells. *Journal of Membrane Science,* 380**,** 208-215.

Zabeti, M., Wan Daud, W. M. A. & Aroua, M. K. (2009) Activity of solid catalysts for biodiesel production: A review. *Fuel Processing Technology,* 90**,** 770-777.

Zeng, J., Wang, X., Zhao, B., Sun, J. & Wang, Y. (2008) Rapid in situ transesterification of sunflower oil. *Industrial & Engineering Chemistry Research*, 48**,** 850-856.

Zeng, Q., Li, Z. & Zhou, Y. (2006) Synthesis and application of carbon nanotubes. *Journal of Natural Gas Chemistry*, 15**,** 235-246.

Zhang, B., Ren, J., Liu, X., Guo, Y., Guo, Y., Lu, G. & Wang, Y. (2010) Novel sulfonated carbonaceous materials from p-toluenesulfonic acid/glucose as a high-performance solid-acid catalyst. *Catalysis Communications,* 11**,** 629-632.

Zhang, Q., Huang, J.-Q., Qian, W.-Z., Zhang, Y.-Y. & Wei, F. (2013) The road for nanomaterials industry: A review of carbon nanotube production, post-treatment, and bulk applications for composites and energy storage. *Small,* 9**,** 1237-1265.

Zhou, H., Lu, H. & Liang, B. (2006) Solubility of multicomponent systems in the biodiesel production by transesterification of jatropha curcas l. Oil with methanol. *Journal of Chemical & Engineering Data,* 51**,** 1130-1135.

Zhou, W., Xiao, J., Chen, Y., Zeng, R., Xiao, S., Nie, H., Li, F. & Song, C. (2010) Sulfonated carbon nanotubes/sulfonated poly(ether sulfone ether ketone ketone) composites for polymer electrolyte membranes. *Polymers for Advanced Technologies,* 22**,** 1747-1752.

Zhu, H. W., Xu, C. L., Wu, D. H., Wei, B. Q., Vajtai, R. & Ajayan, P. M. (2002) Direct synthesis of long single-walled carbon nanotube strands. *Science,* 296**,** 884-886.

Zhu, M., He, B., Shi, W., Feng, Y., Ding, J., Li, J. & Zeng, F. (2010) Preparation and characterization of pssa/pva catalytic membrane for biodiesel production. *Fuel,* 89**,** 2299-2304.

Zong, M.-H., Duan, Z.-Q., Lou, W.-Y., Smith, T. J. & Wu, H. (2007) Preparation of a sugar catalyst and its use for highly efficient production of biodiesel. *Green Chemistry,* 9**,** 434-437.

APPENDICES

Calculation of Permeate Flux

Esterification of PFAD with methanol via membrane reactor under reaction temperature of 135 ºC, methanol to PFAD ratio of 20, s-MWCNTs loading of 3 wt % and 10 h of reaction time is used as sample of calculation. With the collected permeate weight of 0.65 g at 10 h and the effective membrane area of 0.0009621 m^2, the flux produced is calculated as:

$$\text{Flux, } J = \frac{Q}{A \times t} \tag{3.1}$$

$$= \frac{0.65\,\text{g}}{0.0009621\ \text{m}^2 \times 10\,\text{h}}$$

$$= 67.56\ \text{g m}^{-2}\ \text{h}^{-1}$$

Calculation of Water Removal Percentage from Reaction Mixture by 6FDA-NDA/DABA Polyimide Membrane

Esterification of PFAD with methanol via membrane reactor under reaction temperature of 135 ºC, methanol to PFAD ratio of 20, s-MWCNTs loading of 3 wt % and 10 h of reaction time is used as sample of calculation. The permeate collected at 10 h of reactive separation was 0.65 g and the water content in the permeate determined by Karl Fisher titration was 32.23 wt %. Thus, the mole of water in the collected permeate was calculated as:

$$\text{Mole of water in permeate} = 0.65\,\text{g} \times 0.3223 \times \frac{1\,\text{mol}}{18\,\text{g}}$$

$$= 0.01164\ \text{mol}$$

According to the stoichiometry equation, the mole of water available in the reaction mixture is equal to the mole of FAME produced in the esterification of PFAD. The FAME yield achieved at 10 h of reactive separation determined by GC analysis was 68.84 % which was 0.01227 mol. Thus, the mole of water produced in the esterification of PFAD via pervaporation membrane reactor at 10 h of reaction time was 0.01227 mol. Thus, the water removal percentage from the reaction mixture by the pervaporation membrane reactor was calculated as:

$$\text{Water removal percentage} = \frac{\text{Mole of water in permeate}}{\text{Mole of water produced in reaction mixture}} \times 100\,\%$$

$$= \frac{0.01164}{0.01227} \times 100\,\%$$

$$= 94.8\,\%$$

Calculation of FAME Yield

$$\text{FAME Yield (wt \%)} = \frac{\text{Weight of FAME (g)}}{\text{Weight of PFAD used (g)}} \times 100\% \quad (3.3)$$

To calculate the total weight of FAME, peak area for each methyl ester components determined by GC are needed. FAME yield produced under reaction temperature of 170 ºC, methanol to PFAD ratio of 20, s-MWCNTs loading of 3 wt % and 2 h of reaction time is used as sample of calculation.

(A) Calculate ratio area for each of the standard reference methyl esters.

$$R_f = \frac{\text{Peak area (FAME) in standard reference}}{\text{Peak area (IS) in standard reference}}$$

Table A1: Ratio area for each of standard reference methyl esters

Fatty Acid Methyl Ester	Molecular Weight (g/mole)	Ratio, R_f	Concentration (mg/mL)
Methyl myristate	242.40	0.981050687	1.00
Methyl palmitate	270.45	0.923265344	1.00
Methyl stearate	298.50	0.872421659	1.00
Methyl oleate	296.49	0.934001531	1.00
Methyl linoleate	294.47	0.896403207	1.00
Internal standard	-	1.000000000	-

(B) Calculate ratio area for each methyl esters components in the samples

$$R_s = \frac{\text{Peak area (FAME) in sample}}{\text{Peak area (IS) in sample}}$$

Table A2: Ratio area for each of sample methyl esters

Fatty Acid Methyl Ester	Molecular Weight (g/mole)	Area	Ratio, R_s
Methyl myristate	242.40	76813.19	0.22224436
Methyl palmitate	270.45	3330503.13	9.63617737
Methyl stearate	298.50	255430.63	0.73903995
Methyl oleate	296.49	2324128.80	6.72442465
Methyl linoleate	294.47	512388.65	1.48249911
Internal standard	-	345624.93	1.000000000

(C) Calculate yield for each of the methyl esters

$$\text{Weight of FAME (g)} = \frac{R_S}{R_f} \times C_{IS} \times V \times DF \qquad (3.2)$$

Dilution factor, DF = 38

Volume of upper layer formed after evaporation of the reaction filtrate, V = 12.0 mL

Concentration of internal standard used, C_{IS} = 1 mg/ml

Thus, for methyl myristate:

$$\text{Weight of methyl myristate} = \frac{0.22224436}{0.981050687} \times 38 \times 12.0\ \text{mL} \times \frac{1\,\text{mg}}{\text{mL}}$$

$$= 103.301\ \text{mg}$$

$$= 0.103301\ \text{g}$$

Table A3: Weight of each methyl ester components in the sample

Fatty Acid Methyl Ester	Weight (g)
Methyl myristate	0.103301
Methyl palmitate	4.759300
Methyl stearate	0.386284
Methyl oleate	3.283011
Methyl linoleate	0.754147
Total weight	9.286043

Total Weight = 0.103301 + 4.759300 + 0.386284 + 3.283011 + 0.754147

= 9.286043 g

(D) Calculation of FAME yield, %:

$$\text{FAME Yield (wt \%)} = \frac{9.28604\,\text{g}}{10\,\text{g}} \times 100\%$$

= 92.86 %

Calculation of Membrane d-Spacing

The average d-spacing of the thermally cross-linked 6FDA-NDA/DABA polyimide membrane is used as sample calculation. The XRD pattern of the thermally cross-linked 6FDA-NDA/DABA polyimide membrane is shown in **Figure A1**.

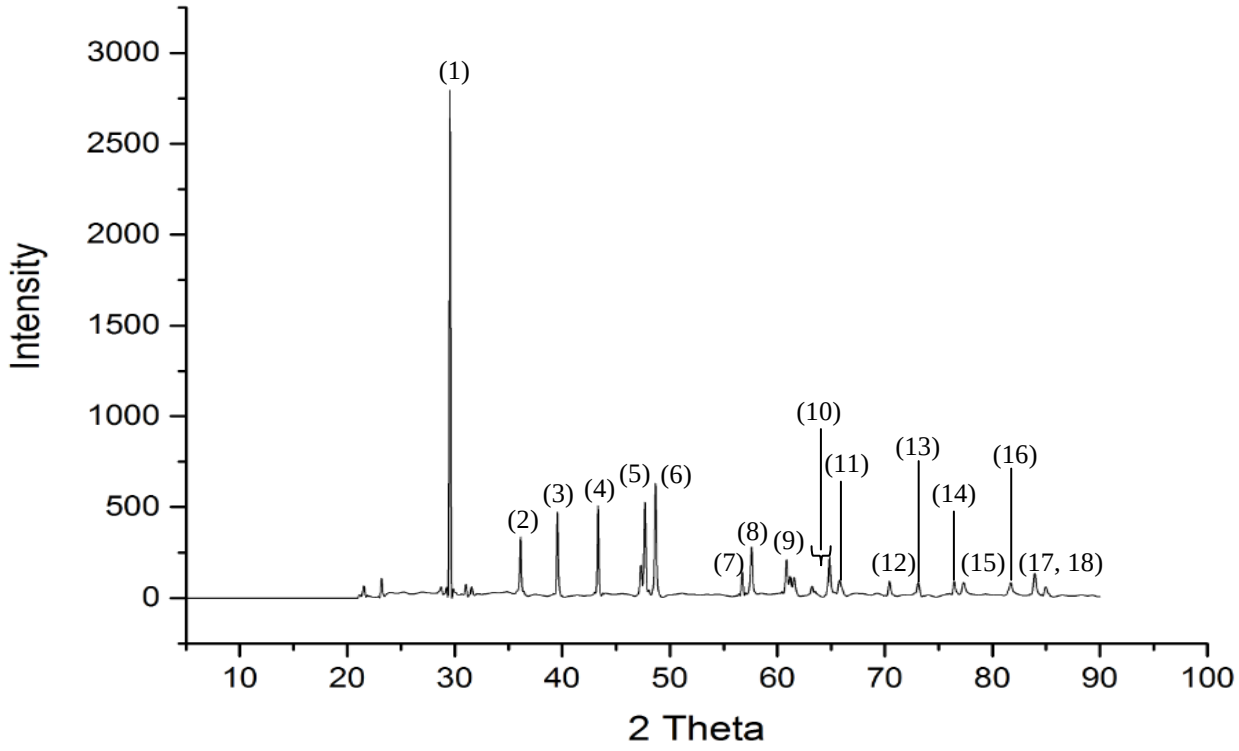

Figure A1: XRD pattern of the thermally cross-linked 6FDA-NDA/DABA polyimide membrane.

The d-spacing for each peaks labelled from 1 to 18 was determined based on Bragg's law as shown in the following:

$$n\lambda = 2d\sin\theta \tag{3.4}$$

With $n = 1$ and $\lambda = 1.5406\ \text{Å}$, the calculated d-spacing was presented in **Table A4**.

Table A4: The d-spacing for each peak in XRD pattern of the thermally cross-linked 6FDA-NDA/DABA polyimide membrane

Peak number	θ, (º)	d-spacing, (Å)	Ratio area
1	28.0	3.1841	0.27
2	36.1	2.4854	0.042
3	39.5	2.2771	0.057
4	43.3	2.0869	0.058
5	47.7	1.9067	0.11
6	48.7	1.8699	0.12
7	56.7	1.6213	0.018
8	57.6	1.5994	0.071
9	60.8	1.5216	0.071
10	64.8	1.4369	0.040
11	65.8	1.4175	0.026
12	70.4	1.3365	0.023
13	70.1	1.2937	0.029
14	76.5	1.2448	0.0075
15	77.2	1.2342	0.011
16	81.7	1.1773	0.010
17	83.9	1.1519	0.029
18	84.9	1.1409	0.019

Thus, the average d-spacing is calculated as:

$$\text{Average d - spacing} = \sum(\text{d - spacing} \times \text{ratio area}) \text{ of each peak}$$

$$= 2.2 \text{ Å}$$

LIST OF PUBLICATIONS

Journals:

Shuit, S. H., Ong, Y. T., Lee, K. T., Subhash, B. & Tan, S. H. (2012) Membrane technology as a promising alternative in biodiesel production: A review. *Biotechnology Advances,* 30**,** 1364-1380.

Shuit, S. H., Yee, K. F., Lee, K. T., Subhash, B. & Tan, S. H. (2013) Evolution towards the utilisation of functionalised carbon nanotubes as a new generation catalyst support in biodiesel production: An overview. *RSC Advances,* 3**,** 9070-9094.

Shuit, S. H. & Tan, S. H. (2014) Feasibility study of various sulphonation methods for transforming carbon nanotubes into catalysts for the esterification of palm fatty acid distillate. *Energy Conversion and Management* 88, 1283-1289.

Shuit, S. H. & Tan, S. H. (2014) Biodiesel production via esterification of palm fatty acid distillate using sulphonated multi-walled carbon nanotubes as a solid acid catalyst: Process study, catalyst reusability and kinetic study. *Bioenergy Research* (Article in Press).

Shuit, S. H. & Tan, S. H. (2014) A facile and acid-free approach towards the preparation of sulphonated multi-walled carbon nanotubes as a strong protonic acid catalyst for biodiesel production. *Journal of the Taiwan Institute of Chemical Engineers* (Article in Press).

Conference:

Shuit, S. H., Lee, K. T., Subhash, B. & Tan, S. H. (2013) Biodiesel production from palm fatty acid distillate using sulfonated multi-walled carbon nanotubes. 2nd International Symposium on Green Chemistry Renewable Carbon and Eco-Efficient Processes, 2013, La Rochelle, France.